UNIVERSITÀ DEGLI STUDI DI BRESCIA

PH.D. PROGRAM IN
MATHEMATICAL METHODS AND MODELS FOR ENGINEERING

Scientific Disciplinary Sector: ICAR/08 Mechanics of Materials and Structures

XVIII Cycle

Fracture growth in brittle and embrittled materials: variational formulations and crack tracking algorithms

---

Advisor:
Prof. Alberto Salvadori

Co-Advisor:
Prof. Derek H. Warner

Ph.D. Coordinator:
Prof. Paolo Secchi

Ph.D. Candidate:
Francesca Fantoni

To all my family, for their loving support

Acnowledgments

This work has been developed at the Department of Civil, Environmental, Architectural Engineering and Mathematics (DICATAM) of the University of Brescia during the years 2013-2015.

I am really grateful to my advisor, Prof. Alberto Salvadori, for all the teachings that he gave me during these years and for the constant support and encouragement. I wish to express my deep gratitude to him for being a patient mentor with an immeasurable enthusiasm for science, and for giving me the precious and inestimable opportunity to travel around the world. I will always remember such wonderful experiences. Nothing of this work would have been possible without him.

I wish to thank Prof. Paolo Secchi, the coordinator of the Ph.D. course and the doctoral school committee. I would like to express my sincere thanks to professors of the Mathematical Department, for offering me useful courses, with a particular mention for Prof. Lucia Gastaldi, for her precious teachings on XFEM.

Sincere thanks go to people of the group of Mechanics of Materials and Structures of the University of Brescia; first of all Prof. Angelo Carini for his help and his wise advices. Thanks to Prof. Lorenzo Bardella and Dr. Andrea Panteghini, because, even if I have never had the opportunity to work with them, they always supported and encouraged me.

Part of the present thesis has been developed at Mechanical Department of the Eindhoven University of Technology, the Netherlands, where I spent six months as visiting research fellow during fall 2014. I am greatly indebted with Dr. Joris Remmers for giving me such an opportunity, for his immense patience and for his teachings on programming languages. Thanks also for allowing me to know a wonderful country, with extremely kind people. I wish to thank all my dutch office mates with a particular mention for Emanuela and Jasna.

I am really grateful to Prof. Derek H. Warner, for co-advising this thesis and for the six months that I spent at the Civil and Environmental Department of Cornell University in Ithaca (NY) during fall 2015. I wish to thank him for discussions, teachings and the useful course on non linear FEM. I would like to thank him for making me part of his research group.
Despite the coldest winter that I have ever lived in my life, Ithaca gave me the opportunity to come into contact with special people. I would like to express my most sincere thanks to Dr. Paul Wawrzyneck for his immense knowledge on computational fracture mechanics and the consequent great help that he gave me for this thesis. Thanks for teaching me that "the purpose of computing is insight, not numbers" (quote from R. Hamming). I wish also to thank him for the hospitality, and for showing me the natural beauties of Ithaca. Thanks very much Wash (I will never learn to write your surname correctly, by the way).
A particular thank goes to Prof. Jim Jenkins for his huge kindness and helpfulness with me, even if I was not one of his students.

I wish to thank my colleagues of the University of Brescia: first of all Davide Grazioli, for his tireless assistance; Davide Catania, Alessandro Temponi, Marco Magri, Valentina Damioli, Michele Annese, and Mattia Zammarchi. In particular, I am grateful to Ornella Mattei, who started the

Ph.D. with me, simply for her precious friendship.

Thanks to my parents and all my family, to which this thesis is dedicated, for their endless support and vicinity in discouraging moments. Finally, there are no adequate words to express my deep loving thanks to Matteo, simply for everything. Thanks for one of the most special thing that a person can do: making me happy every day.

Thanks to all the people that I forgot to mention here and who contributed to this work.

Brescia, January 2015

Francesca

Abstract

The crack propagation problem for Linear Elastic Fracture Mechanics (LEFM) has been studied by several authors exploiting its analogy with standard dissipative systems theory [18, 96, 103]. From the analogy with plasticity theory, minimum theorems are derived in terms of crack tip "quasi-static velocity" for two-dimensional fracture mechanics [125]. They are reminiscent of Ceradini's [24] theorem in plasticity. Following the cornerstone work of Rice [117] on weight function theory, Leblond et al. [82, 83] proposed asymptotic expansions for Stress Intensity Factors (SIFs) in three dimensions. As formerly in 2D, expansions can be given a Colonnetti's decomposition [30, 31] interpretation. In view of the expression of the expansions proposed in [82, 83] however, symmetry of Ceradini's theorem operator is not evident and extension of the outcomes proposed in [125] not straightforward. Following a different path of reasoning, based on the physical meaning of the operator itself, minimum theorems are derived for 3D LEFM [127].

Such minimum theorems are then rephrased in terms of weight functions [129], removing in full the hypothesis of steady location of a point along the crack front assumed by several authors in previous works (among others [43, 44, 45, 117]) in order to formulate the problem in terms of Cauchy principal value. Stategies exploited to circumvent the steady location hypothesis give complete generality to the formalism for calculating the variation in the SIFs along the crack front, at the price of the purposely introduced assumption of infinite domains.
The final formalism obtained in this thesis invokes the more general concept of finite part of Hadamard of the integrals involved and shows the desirable symmetric structure. It can be applied to finite bodies, provided that an accurate approximation of weight functions, known in closed form for a very limited set of geometries, can be given. A general method to approximate weight functions for finite bodies is handled in the thesis by means of an algorithm based on the definition of weight function itself.

An implicit and effective 3D crack tracking algorithm is therefore allowed. It is based on a Newton-Raphson numerical strategy for the Griffith-Maximum Energy Release Rate (MERR) condition, which is endowed with a variational formulation at every iteration [128]. Owing to the convexity of the MERR safe equilibrium domain, the algorithm provides a finite elongation at each point of the crack front based upon the increment of the external loads as the minimum of a constrained quadratic functional, where the constraint is computationally handled by means of the penalty method. Numerical experiments show that the proposed algorithm is more accurate, and numerically stable than explicit algorithms in time, which have been formulated moving from the map of velocities of crack elongation along the crack front [130].

Finally, the obtained variational formulation of the incremental quasi-static fracture propagation problem is extended to the case of fractures in the presence of diffusion of neutral species in solids. As for example in the case of hydrogen embrittlement, species diffuse into the crack tip region because of the driving force created by the chemical potential and such a phenomenon greatly influences the subsequent fracture processes. These latter can ultimately take place in a completely embrittled environment, motivating the use of the LEFM to describe the fracture growth.

Sommario

Il problema della propagazione di una fessura per la Meccanica della Frattura Elastica Lineare (LEFM) é stato studiato da diversi autori utilizzando l'analogia con la teoria dei sistemi dissipativi standard [18, 96, 103].
Dall'analogia con la teoria della plasticitá, vengono ricavati teoremi di minimo in termini di "velocitá quasi-statica" dell'apice di fessura per la meccanica della frattura bi-dimensionale [125]. Essi costituiscono una reminiscenza del teorema di Ceradini [24] in plasticitá. Basandosi sul fondamentale lavoro di Rice [117] riguardante la teoria delle funzioni peso, Leblond e altri [82, 83] hanno proposto espansioni asintotiche per i Fattori di Intesificazione degli Sforzi (SIFs) in tre dimensioni. Come accadeva precedentemente in 2D, tali espansioni possono essere interpretate secondo la decomposizione di Colonnetti [30, 31]. Tuttavia, basandosi sull'espressione delle espansioni proposte in [82, 83], la simmetria dell'operatore di Ceradini non é evidente ed un'estensione dei risultati proposti in [125] non risulta immediata. Seguendo un tipo di ragionamento diverso, basato sul significato fisico dell'operatore stesso, vengono formulati teoremi di minimo per la LEFM 3D [127].

Tali teoremi di minimo sono poi riformulati in termini di funzioni peso [129], rimuovendo completamente l'ipotesi di stazionarietá di un punto lungo il fronte assunta da diversi autori in lavori precedenti (tra gli altri [43, 44, 45, 117]) al fine di formulare il problema in termini di valore principale di Cauchy. Le strategie utilizzate per eludere l'ipotesi di stazionarietá di un punto forniscono generalitá assoluta al formalismo usato per calcolare le variazioni degli SIFs lungo il fronte di frattura, al prezzo di introdurre volontariamente l'ipotesi di domini illimitati. Il formalismo finale ottenuto in questa tesi chiama in causa il concetto piú generale di parte finita di Hadamard degli integrali coinvolti ed esibisce la vantaggiosa struttura simmetrica. Esso puó essere applicato a mezzi limitati, a patto che possa essere fornita un'accurata approssimazione delle funzioni peso, note in forma chiusa per un insieme molto limitato di geometrie. Un metodo generale per approssimare le funzioni peso in mezzi limitati, é trattato nella tesi per mezzo di un algoritmo basato sulla definizione stessa di funzione peso.

Un algoritmo 3D di crack tracking implicito ed efficace é pertanto consentito. Esso é basato su di uno schema numerico di tipo Newton-Raphson per la condizione di Griffith di Massima Energia Rilasciata (MERR), la quale é dotata di una formulazione variazionale ad ogni iterazione [128]. Stante la convessitá del MERR dominio di non propagazione, l'algoritmo fornisce l'allungamento finito in ogni punto del fronte dovuto all'incremento dei carichi esterni come minimo di un funzionale quadratico vincolato, dove il vincolo é computazionalmente trattato con il metodo penalty. Esperimenti numerici mostrano che l'algoritmo proposto risulta essere piú accurato e numericamente piú stabile di algoritmi di tipo esplicito nel tempo, che sono stati formulati a partire dalla mappa delle velocitá dell'allungamento di frattura lungo il fronte [130].

Infine, la formulazione variazionale ottenuta del problema di propagazione incrementale quasi-statico viene estesa al caso di fratture in presenza di diffusione di speci neutre in solidi. Come ad esempio nel caso dell'infragilimento da idrogeno, le speci diffondono verso l'apice di fessura a causa della forza motrice generata dal potenziale chimico e tale fenomeno influenza notevolmente i successivi processi di frattura. Questi ultimi possono in definitiva avere luogo in un ambiente completamente infragilito, il che spiega l'utilizzo della LEFM per descrivere la propagazione della frattura.

Contents

Notation

Symbols used in the thesis have the meaning described in the following list, unless otherwise indicated in the text.

Symbols

$\mathbf{x}$	position vector in $\mathbb{R}^3$, $[x_i]_{i=1}^3$
t	time
s	curvilinear abscissa along the crack front
$\mathbf{u}(\mathbf{x},t)$	displacement vector
$\boldsymbol{\sigma}(\mathbf{x},t)$	Cauchy stress tensor
$\boldsymbol{\varepsilon}(\mathbf{x},t)$	small strains tensor
$\mathbb{C}$	Hooke tensor
$\tilde{\mathbb{K}}$	stiffness matrix
Ω	domain
$\Gamma \equiv \partial\Omega$	boundary of the domain
$\mathcal{F}$	crack front
$\mathcal{S}$	crack surface
$\{x_1, x_2, x_3\}$	local Frenet frame in each point along the crack front
$\mathbf{p}(\mathbf{x},t)$	tractions vector
$\mathbf{f}(\mathbf{x},t)$	bulk forces
$\kappa(t)$	load factor
$\theta(s,t)$	kink angle at abscissa s and time t
$l(s;t,\tau)$	curvilinear length of crack extension in the normal plane at point s
$v(s,t)$	crack front quasi-static velocity at abscissa s and time t
$\mathbf{K} = \{K_1, K_2, K_3\}$	Stress Intensity Factors vector
$\mathbf{K}^*$	zero order term of SIFs expansion
$\mathbf{K}^{(1/2)}$	1/2 order term of SIFs expansion
$\mathbf{K}^{(1)}[\cdot]$	first order term of SIFs expansion
$\mathbf{K}_0^{(1)}$	first component of $\mathbf{K}^{(1)}[\cdot]$
$\mathbf{K}_1^{(1)}$	second component of $\mathbf{K}^{(1)}[\cdot]$
$\mathbf{K}_{nl}^{(1)}$	third, non local component of $\mathbf{K}^{(1)}[\cdot]$
K_1^C	fracture toughness
$\varphi \begin{cases} = 0 \\ < 0 \end{cases}$	$\begin{cases} \text{onset of crack propagation} \\ \text{safe equilibrium domain} \end{cases}$
$\mathbf{w}(\mathbf{x},t)$	crack opening and sliding
ρ	distance from the crack front
$\mathbb{K} = [k_{ij}]$	Crack Face Weight Functions (CFWFs) matrix
$\mathbb{W}^{\mathcal{F}}$	Fundamental Kernels (FKs) matrix
G	energy release rate
G_C	fracture energy
E	Young's modulus
ν	Poisson's coefficient
μ	shear modulus
$\bar{K}$	bulk modulus
$\bar{K}^{in}$	hardening modulus
L	interstitial species

T	trapped species
$\bar{w}$	chemical reaction rate
K_{eq}	equilibrium constant of the chemical reaction
c_β	molarity of species β denoting the concentration measure
$\mathbf{h}_\beta$	mass flux of species β
μ_β	chemical potential of species β, also known as partial molar free energy
$\mathbf{q}$	heat flux vector
s_β	external supply of species β
$\bar{A}$	affinity of the chemical reaction
ω_β	chemical expansion coefficient of species β
$\mathbf{M}_L$	interstitial mobility tensor
$\mathbb{\psi}_L$	mobility
$\mathbb{D}_L$	diffusivity

Operators

$\fint$	Cauchy principal value
$\fint\!\!=$	finite part of Hadamard
$\mathcal{H}(x)$	Heaviside step function
$\mathbb{I}$	identity matrix
$\nabla[\,\cdot\,]$	gradient operator
$\nabla_s[\cdot]$	symmetric part of the gradient operator
$\mathrm{tr}[\,\cdot\,]$	trace operator
$\mathrm{div}[\,\cdot\,]$	divergence operator
$\mathrm{dev}[\,\cdot\,]$	deviatoric operator
$\mathrm{sph}[\,\cdot\,]$	volumetric part of a tensor
$\cdot$	single contraction of two vectors or two tensors
:	double contraction of two tensors
$\|\mathbf{x}\|$	norm of vector $\mathbf{x}$
$\overset{T}{}$	transpose of a tensor

Constants

$N_A = 6.02214129(27) \times 10^{23} mol^{-1}$	Avogadro's number
$R = 8.3144621 JK^{-1}mol^{-1}$	universal gas constant
$k_B = 1.38064852 \times 10^{-23} JK^{-1}$	Boltzmann constant

Chapter 1

Introduction

Fracture mechanics has been plagued by three main issues: initiation, irreversibility and path [18]. The present work treats the third of them, aiming at investigating the evolution of three dimensional fractures in brittle or embrittled materials in the context of Linear Elastic Fracture Mechanics (LEFM). Cracks can form and propagate catastrophically with very little warning in brittle materials, before any plastic deformation takes place. The copious literature of the last decades devoted to model and control the initiation and growth of fractures in brittle materials, assesses the importance of understanding and predicting the fracture pattern evolution, in order to increase the safety and improve the mechanical performance of materials and components. Modeling crack geometry and predicting crack paths has been one of the most challenging aspects of fracture mechanics, which has captured attention of many researchers.

If a body in reality is elastoplastic, LEFM is a good approximation, provided that the remote stress from the crack tip is sufficiently small with respect to the yield stress, and the calculated stresses show a square root singular behavior in a small region enclosing the crack tip [151]. In LEFM framework, the stress-strain field in the crack front vicinity is uniquely determined by the Stress Intensity Factors (SIFs), which are coefficients weighting the singularity of the stress-strain field itself [18].

Quasi-static hypothesis is assumed in this work, meaning that kinetics effects of crack growth are a priori supposed to be negligible and *time* is a positive, real parameter that merely order events. All loads are functions of such a parameter, and the cracked solid is, at each instant, in equilibrium with the loads that it supports at that time.

The variational approach to different rate independent processes has been a topic of active research in recent years; variational approach to brittle fracture in particular, has been developed in the seminal work of Francfort and Marigo [39], and further deployed with Bourdin in the past twenty years [17, 18]. The fundamental idea dates back to the energy-based Griffith's concept [49] that the crack growth is the result of a competition between bulk energy away from the crack and surface energy on the crack. In the seminal paper of Griffith [49], crack is represented by a discontinuity surface for the deformation field under investigation. Griffith's criterion can be articulated in the well known three points:

- cracking processes satisfy the irreversibility condition for which the crack can only grow
- the energy release rate, meaning the bulk energy released during an infinitesimal advance of the crack, is bounded from above by the fracture toughness
- the crack doesn't grow unless the energy release rate is critical, equating the energy that has to be spent in creating additional crack length (or area).

Bourdin, Francfort and Marigo's variational approach to fracture relies on global unilateral potential energy minimization, where potential energy consists of the stored elastic energy, the work of external forces, and the energy dissipated trough fracture growth. Evolution in time is accounted for only trough the irreversibility condition, making the formulation rate-independent. In order to take into account the high level of complexity that can derive from a minimization of the displacement field with respect to any kinematically admissible displacement and any set of crack curves, some regularization parameters are introduced to represent the crack and to define a sort of regularized energy. At each time step, minimization strategy is allowed by the separate convexity of the regularized energy with respect to the displacement field and the regularization parameter. A feature of this method is that the orientation and length of the crack are the direct outcomes of the analysis.

Such a regularized energy has been introduced as a *phase field* numerical approximation of a sharp interface problem. From the material modeling perspective, a phase field approach to fracture is conceptually linked with continuum damage mechanics models, where a scalar damage field can be interpreted as the phase field. In the context of phase field models of fracture, regularized brittle crack propagations can be considered as gradient-type damage models with particular definition of an energy function with a gradient-type regularized surface energy. A sharp crack surface topology in the solid is regularized by a diffusive crack zone governed by a scalar auxiliary variable, the phase field, that interpolates between the unbroken and the broken states of the material and the crack phase field evolution is governed through the definition of suitable convex dissipation functions (see for example the work of Hakim and Karma [52], and the works of Miehe et al. [93, 94]). Phase field methods have undergone great developments with applications in various multi-physics contexts [95], and are nowadays standard techniques to deal with the global quasi-static fracture propagation problem.

The approach introduced by Salvadori and Carini [125] for 2D LEFM, and later extended by Salvadori and Fantoni [127] for 3D LEFM, differs from Bourdin, Francfort and Marigo's variational approach to fracture and from phase-field methods, framing the problem of crack propagation in brittle materials into the theory of standard dissipative processes and ultimately leading to formulate algorithms for crack propagation that do not seek for global minima and do not require any regularization parameter.

The *global incremental quasi-static fracture propagation problem*, framed in the mechanics of standard dissipative systems [17, 18, 96, 102, 122], can be posed in the following way: given the state of stress and the history of crack propagation (if any) at each instant, express the crack propagation rate (if any) of the crack front due to a variation of the external actions as a function of the stress and of the history. As in Bourdin, Francfort and Marigo's interpretation [18], the crack length is an internal variable, and its variation induces a dissipation which must in turn satisfy the Clausius-Duhem's inequality. Enforcement of Clausius-Duhem's inequality is provided by the introduction of a convex dissipation potential. In this regard, the internal conjugate variables pair is here essentially changed with the SIFs vector after a kink, modeled as a thermodynamic force, conjugated to an internal variable related to the crack length.

Fracture elongation causes energy dissipation in the process region, in the surrounding plastic region, and eventually in the wake of the process region. In this work, infinitesimally small scale yielding is assumed to idealize the fracture process and as such, energy dissipation is considered to be localized at the crack front.
Smoothness of the latter, together with isotropic linear elasticity of the domain, are also assumed, making use of Hooke's law without limitation of stress and strain magnitudes.

In the formulation of the analogy between associated plasticity and incremental LEFM pro-

posed in [122], incipient crack growth is a difficult concept to identify and the problem is solved by a convention, likewise the determination of the elastic limit in plasticity. An *onset of crack propagation* and a *safe equilibrium domain* are governed theoretically by a local condition on SIFs, describing when the process region reaches a critical state which, in most cases of engineering interest, is independent of body, geometry and loading. This property is termed autonomy [13].

Crack propagation is here restricted to smooth in space and continuous in time growth [25, 124]. Variational formulations are stated, which characterize the three dimensional crack front quasi-static velocity as minimizer of constrained quadratic functionals. A crack tracking algorithm is formulated in order to predict point by point extension along the crack front based upon increment of external actions.

1.1 Three dimensional modeling of crack growth

One of the demanding tasks for 3D LEFM is to take into account non linearities created by the deformation of the crack front and simulations of 3D crack growth remains a significant challenge.

A viable method for this purpose is the perturbation approach, initiated after the seminal works of Bueckner [21] and Rice [116, 117] on weight function theory. An abundant literature has been devoted since then in order to provide, for different crack configurations embedded in linear elastic infinite medium, the local variation of the SIFs along the crack front resulting from some small, but otherwise arbitrary coplanar perturbation of the crack front. A non exhaustive list of authors that worked in the perturbation approach field includes Bower and Ortiz [19], Favier et al. [37], Gao and Rice [43, 44, 45], Lazarus [78, 79], Lazarus and Leblond [76, 77], Leblond and Mouchrif [81], Leblond et al. [85], Salvadori and Fantoni [129], Willis [152].
Weight function theory has been employed by several authors in order to study configurational stability problems of cracks slightly perturbed from their initial configuration.
Crack front instability in mode 1+3, leading the crack surface to deviate from planar configuration, and crack front to deviate from straight shape, has been theoretically predicted by Leblond et al. [84], analyzing the influence of fracture toughness fluctuations in [86].
Out of plane perturbations of plane crack were studied by Movchan, Gao and Willis [101], and the obtained formulae were exploited by Obrezanova, Movchan and Willis [105] in order to assess the configurational stability of a crack in plane strain conditions quasi-statically growing.

Theoretical analysis, compared with experiments, of crack front rotation and segmentation in brittle solids under mode $1 + 2 + 3$, has been performed by Lazarus et al. [74, 75], starting from the expansion of the three dimensional SIFs vector [82, 83].

Several numerical techniques exist to treat arbitrary crack paths in a three dimensional context complicated further by loading or geometric features that induce mixed mode behavior along the crack front. Finite elements, coupled with adaptative remeshing can be used to predict arbitrary, mixed-mode, non planar crack evolution [23, 92]. Crack front can be advanced in arbitrary directions and the magnitude of the elongation can be proportioned along the front based on the distribution of fracture mechanics parameters values or empirical growth laws.
Quarter-point elements have been formulated for LEFM in order to properly take into account the singularity of the stress-strain field in proximity to the crack front. Since the formulation of Barsoum [11, 12] and Henshell and Shaw [56], different authors analyzed quarter-point and higher order singular elements. To quote a few, Bank-Sills et al [6, 7, 8, 9], Freese and Tracey [40], Hibbit [57], Hussain et al. [58], Ingraffea and Manu [61], Koers [68], and Manu [90, 91].

Each time the crack front is advanced, a new finite element mesh has to be generated around

the updated front. For multiple cracks the finite element method can greatly increase the computational cost because of the need of remeshing. Furthermore, remeshing requires to map the internal variables between different meshes, which decreases accuracy for non linear problems.

Another approach that represents explicitly the crack and can handle non planar crack growth is the cohesive-zone elements approach, which places special elements governed by a traction-separation law in order to capture the behavior of the crack front. Tractions stop to be transmitted by the cohesive elements when the traction-separation function reaches its limit, creating in this way new traction-free surfaces and extending the crack [67, 108]. Cohesive elements are usually inserted at predetermined locations along the expected crack path, being computationally expensive to place such elements throughout the entire model. The crack tracking therefore results influenced by the size and locations of the cohesive elements, being the elongations of the crack restricted to follow the element boundaries.

A different finite element-based simulation technique developed to predict arbitrary shape evolution of 3D cracks subject to quasi-static loading exploits an energy-based growth formulation that relies on a first order expansion of the energy release rate. Description of the method can be found in [32] for the case of mode 1 and in [33] for the case of mixed-mode. Such a first order expansion of the energy release rate uses the Virtual Crack Extension (VCE) technique [55, 110] to extract the derivative of the energy release rate with respect to the amount of propagation along the crack front. In order to predict the shape and analyze the stability of an evolving 3D crack front in brittle fracture, the VCE method has been recently proposed by Hwang et al. in [59] for 3D cracks of arbitrary shapes that propagate under arbitrary loading conditions. It generalizes the analytical VCE method presented by Lin and Abel [89], which introduced a direct-integration technique employing a variational theory in the finite element formulation.

Alternative methods to define the crack, in the sense that they do not need a particular mesh to explicitly represent the crack front, are enrichment techniques, which are based on the decomposition of the solution in the finite element solution, and additional enrichment functions in order to inform the numerical model of the presence of the crack within the finite elements. Among them, the eXtended Finite Element Method (XFEM), that makes use of the partition of unity concept [5]. Discontinuity across crack faces and the appropriate stress fields in the vicinity of the crack front associated with a physical crack can be represented numerically bu such augmented elements [15, 97]. The XFEM representation can then be coupled with several techniques such as damage mechanics, cohesive models, and prescribed-increment methods to simulate growth. Moës et al. [98] and Gravouil et al. [48] presented a three dimensional implementation of the XFEM with application to the LEFM.

Finally, a successful technique to model crack propagation for LEFM is the Boundary Element Method (BEM) [23]. However, for the case of non linear material, the method is not well developed.

1.2 Thesis outline

Chapter 2 extends to three dimensional fracture mechanics the variational formulation of the global-incremental quasi-static fracture propagation problem derived in [122, 125] for 2D LEFM. A maximum dissipation principle at the crack front during propagation is postulated. Associated flow rule

and loading/unloading conditions in Karush-Kuhn-Tucker complementarity form descend. Consistency condition leads to the formulation of minimum theorems, which allow the evaluation of crack front quasi-static velocity driven by the increment of external actions. The starting point is the asymptotic expansion of the SIFs in powers of the crack front velocity in the normal plane to the crack front for the three dimensional case [82, 83]. Such an expansion can be put in analogy with Colonnetti's decomposition of stresses in plasticity as due to an elastic contribution and to a distorsion [30, 31]. Assuming that the Maximum Energy Release Rate (MERR) criterion models the onset of crack propagation and the safe equilibrium domain, a condition for the transition between stable and unstable propagation regimes is formulated in Section 2.5.1. This transition between stable and unstable propagation regimes is a crucial information for the safety of a structural component, assuming that unstable propagation leads to structural collapse. Minimum theorems are proved in Section 2.5.2 in the range of stable crack growth. They are reminiscent of Ceradini's theorems [24] that were proved in incremental small strain plasticity theory and characterize crack front velocity that solves the global quasi static fracture propagation problem at each instant as the unique minimizer of linearly constrained quadratic functionals. Uniqueness is a consequence of the adopted SIFs expansion and can be avoided only by using expansion for branched elongations. Proof of the minimum theorems is based on the symmetry property (with respect to the usual bilinear form) of the first-order operator of the SIFs expansion, termed $\mathbf{K}^{(1)}[\cdot]$. Such an operator relates the variation of the SIFs at a certain location along the crack front, to the first order variation of the shape of the whole crack front under fixed loading conditions. The physical meaning of the symmetry property is evident by noting that $\mathbf{K}^{(1)}[\cdot]$ is related to the energy release rate associated to elongation at constant boundary conditions. The symmetry property seems therefore quite natural if one thinks the energy release rate as the derivative of the energy. Nevertheless, it is not straightforward to envisage symmetry from definition of linear operator $\mathbf{K}^{(1)}[\cdot]$. The theoretical framework is tested in Section 2.5.3 on a simple problem, the axialsymmetric example of a circular crack subject to uniform tensile stress, confirming the potential of the proposed incremental formulation.

Chapter 3 briefly describes the methods of the finite elements (see Section 3.1) and of the extended finite elements (see Section 3.2) to include a crack in the numerical model and to properly model the singularity of the LEFM stress-strain field at the crack front. A series of techniques exploited by the fracture mechanics community to compute the SIFs is then presented in Section 3.3.

Chapter 4 arises from the need to restate the variational formulation derived in Chapter 2 in terms of weight functions. Indeed, formulation presented in Chapter 2 is complete, but the form of the third term of the SIFs expansion $\mathbf{K}^{(1)}[\cdot]$ is so involved that it obstructs the way toward the formulation of effective crack tracking algorithms.

The weight function theory for three dimensional elastic crack analysis received great attention after the work of Rice [116, 117]. Several applications have been considered since then, particularly in the context of configurational stability, crack path prediction, stress intensity factors expansions, perturbation approaches. In all cases, a specific hypothesis has been made on the variation of crack shape, in order to formulate the problem in terms of Cauchy principal value. Focusing on planar cracks that propagate in their own plane, in Section 4.1 such hypothesis is further investigated and consequences discussed. The limit to the boundary process does not lead to a Cauchy principal value interpretation of integrals involved, and the more general concept of finite part of Hadamard is invoked. While likely making the picture less simple, the obtained final formalism leads to an easy proof of the symmetry property for operator $\mathbf{K}^{(1)}[\cdot]$ and envisages an effective formulation of crack tracking algorithms provided that an accurate approximation of weight functions can be

given. A general method to approximate weight functions for finite bodies in all cases for which they are not available in closed form is described in Section 4.3. It is based on the definition of crack face weight function itself and allows an implicit in time 3D crack tracking algorithm described in detail in *Chapter 5*.

Such an implicit, Newton-Raphson based, crack tracking algorithm is endowed with a variational formulation within each iteration. Moving again from the analogy between rigid-plasticity and LEFM, a return mapping algorithm is formulated owing to the convexity of the MERR safe equilibrium domain. An *elastic trial* is set as usual by the increment of the external actions: owing to the linearity of the elastic problem, the evaluation of the trial state in terms of SIFs is trivial. The Griffith condition is tested for the computed SIFs and, if violated, a Newton-Raphson scheme is triggered off. At each iteration of the Newton-Raphson scheme a constrained minimum problem can be solved, which provides a new estimation of the crack front location. The constraint is computationally handled by means of one of the several available techniques for constrained optimization: the penalty method algorithm. The eventuality of only partial elongation of the crack front is thus captured. At such a new crack front, updated SIFs can be evaluated from the global problem. The Griffith condition is tested for the updated SIFs and, if violated, the iteration process is continued up to convergence. A remarkable difference between plasticity and fracture is that at each iteration the geometry of the crack front, and thus of the global problem, changes. The crack tracking framework is tested on the simple problem of a circular crack subject to an axial symmetric load (see Section 5.2) and to an eccentric load (see Section 5.3).

Moving from the map of velocities of crack elongation along the crack front provided by functionals of Ceradini's type described in Chapter 2, algorithms for crack advancing of the explicit type were formulated, which were driven by the increment of the external actions and allowed the step-wise approximation of crack length increment at the crack front. In their simplest formulation, those algorithms do not enforce the Griffith condition step by step and may lead to large errors in the estimation of both the critical load and configuration, measured at the transition between stable and unstable propagation regimes. The finite difference approach in particular, appears to be unreliable showing well known deficiencies associated with the selection of accurate and numerically stable finite perturbations, introducing geometric approximations and numerical truncation errors, thus leading to severe numerical cancellation issues as described in Section 5.2.1.

Finally, *Chapter 6* is devoted to describe the germinal model of fracture driven by diffusion of species in solids, coupling the LEFM problem and the diffusion problem of a neutral species in the host material. The diffusion model derives from an unpublished work of Salvadori et al. [131], which has been enhanced in this thesis with the description of fracture growth and the relative thermodynamics. Diffusing species is split into mobile and immobile, the latter being trapped by micro-structural defects of the material and not contributing to species transport, considered therefore purely interstitial. First law of thermodynamics is detailed in Section 6.2.1, while entropy imbalance is described in Section 6.2.2, assuming that the velocity of crack growth is much higher than the diffusion velocity, leading to a vanishing *entropy release rate*. Constitutive equations in Section 6.3 characterize in a thermodynamic consistent way the interstitial flux by means of Fickian diffusion model, the reaction rate of the trapping process, the Cauchy stress influenced by the swelling contribution and the plastic behavior of the host material responsible of traps formation. Substitution of constitutive equations in balance laws detailed in Section 6.1, leads to the governing equations of Section 6.3.1. Velocity of crack propagation can be still described as the minimum of the linearly constrained quadratic functionals of Chapter 2, provided that a suitable law describing the dependence of fracture energy with respect to the concentrations of the interstitial and trapped

species can be given in the framework of LEFM. Numerical validations of the model have still to be performed.

Chapter 2

Crack growth as a standard dissipative system

2.1 Notation

Consider within a three dimensional body $\Omega \in \mathbb{R}^3$ a crack of arbitrary shape as in fig. 2.1, except that both its surface $\mathcal{S}$ and front $\mathcal{F}$ are assumed to be of class C^∞, at least in the vicinity of $\mathcal{F}$ [82, 83].

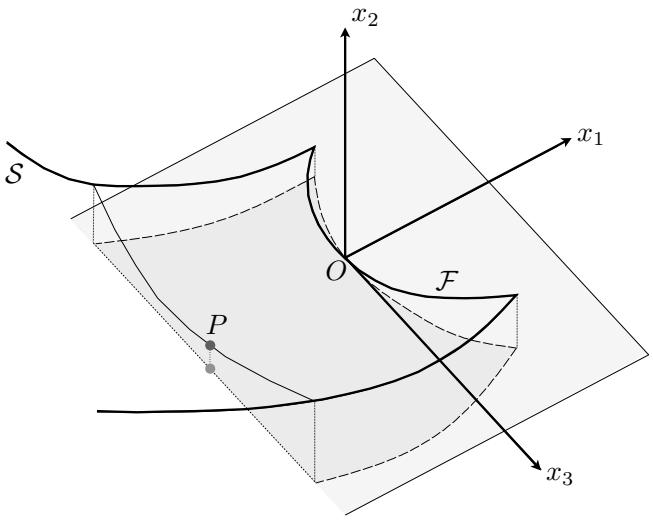

Figure 2.1: *Arbitrarily shaped crack in a three dimensional body $\Omega \in \mathbb{R}^3$. Reference $\{O, x_1, x_2, x_3\}$ is the Frenet frame at point O along the crack front $\mathcal{F}$. Dark grey shadow shows the projection of the crack surface $\mathcal{S}$ onto the tangent plane $\{O, x_1, x_3\}$ (enlighten in dark grey).*

Domain Ω is assumed to be made of an isotropic linear elastic material, with Hooke's law holding without limitations of stresses and strains. The boundary $\partial\Omega$ is the union of a Dirichlet (Γ^u) and a Neumann (Γ^p) part, with $\Gamma^u \cap \Gamma^p = \emptyset$.

The material response to the following quasi-static external actions is sought under the assumption of small strains: tractions $\mathbf{p}(\mathbf{x}, t)$ on Γ^p, displacements $\mathbf{u}(\mathbf{x}, t)$ on Γ^u, bulk forces $\mathbf{f}(\mathbf{x}, t)$ in Ω. External actions are all assumed to be proportional, in the sense that they vary only through multiplication by a time dependent scalar $\kappa(t)$, termed *load factor*, that can be conveniently assumed

to be zero at initial time[1] $t = 0$. The SIFs, denoted as usual with K_1, K_2, K_3 and collected in vector $\mathbf{K}$, determine the stress and strain fields in the crack front vicinity.

Let O denote an arbitrary point on $\mathcal{F}$. Cartesian coordinates x_1, x_2, x_3 are attached to that point with Ox_1 in the tangent plane to $\mathcal{S}$ and orthogonal to $\mathcal{F}$, Ox_2 perpendicular to $\mathcal{S}$ and Ox_3 coincident with the tangent to $\mathcal{F}$. Denote with s the curvilinear length of O on $\mathcal{F}$, and with s' that of a generic point on that curve. Denote with P a generic point on $\mathcal{S}$. The local geometry of $\mathcal{S}$ will be described with a degree of accuracy such that the distance $x_2(P)$ from P to its projection onto the tangent plane at O will be specified up to order $O(x_1^2 + x_3^2)$. This is achieved as in [82, 83] by prescribing the components C_{11}, C_{13}, C_{33} of the curvature tensor $\mathbf{C}$ of $\mathcal{S}$ at point O. The local geometry of $\mathcal{F}$ is then also described with a similar accuracy by prescribing the curvature of its projection onto the tangent plane at O. One makes the fundamental assumption that the original crack front belongs to both the old and new crack surfaces, i.e. the crack extension develops continuously and irreversibly from that original crack front. The old front will be thus denoted with $\mathcal{F}(t)$ and the new with $\mathcal{F}(\tau)$, with t and τ two instants, the latter subsequent the former. At each point s' of $\mathcal{F}(t)$, the new tangent plane at $\tau \to t^+$ is obtained by rotating the one defined at time t by an angle $\theta(s', t)$ (the *kink angle*) about the local tangent to $\mathcal{F}(t)$. Function $\theta(s', t)$ will be assumed to be of class C^∞ with respect to s'.

Consider thus an arbitrary small deviated elongation of the crack front. Denote with $l(s'; t, \tau)$ the curvilinear length of crack extension in the normal plane at point s' between $\mathcal{F}(t)$ and $\mathcal{F}(\tau)$ as in fig. 2.2. It will be assumed of class C^∞ with respect to s'. The velocity of the elongation of the crack at time t, also called *crack front quasi-static velocity*, will be denoted with:

$$v(s', t) = \lim_{\tau \to t^+} \frac{l(s'; t, \tau)}{\tau - t} \tag{2.1}$$

In view of the irreversibility hypothesis $v(s', t) \geq 0$. The value $v(s, t)$ at point O will be assumed to be non zero. This means that O will be supposed not to be an endpoint of the effectively propagating part of the front.

The *global incremental quasi-static fracture propagation problem* consists in seeking an expression of the crack front growth rate $v(s', t)$ at a generic point s' along the crack front in the presence of a variation of external loads, considered the driving force for propagation, for all the three phases of fracturing process, namely loading without crack growth, stable and unstable propagation.

2.2 SIFs expansion

It is assumed that cracks propagate irreversibly from a given front $\mathcal{F}(t)$, whereas the analysis of crack initiation is not taken into account in the present work. Crack growth is considered to be continuous in time [25], thus allowing to conveniently use SIFs expansions that were formulated in [82, 83].

SIFs vector $\mathbf{K}(s, \tau)$ at the image location of abscissa s after elongation $l(s; t, \tau)$ can be expressed in powers of $l(s; t, \tau)$. Assuming that external actions are fixed, the expansion has the form:

$$\mathbf{K}(s, \tau) = \mathbf{K}^*(s, t) + \mathbf{K}^{(1/2)}(s, t)\sqrt{l(s; t, \tau)} + \mathbf{K}^{(1)}[s, t; l(s'; t, \tau)] + O(l^{3/2}) \tag{2.2}$$

Terms $\mathbf{K}^*, \mathbf{K}^{(1/2)}$ are local factors at point s. Omitting the dependency on s and t for the sake of readability, they are given componentwise (using the Einstein summation convention) by:

$$K_i^* = \mathbb{F}_{ij}(\theta) K_j \tag{2.3}$$

[1] In what follows "time " represents any variable which monotonically increases in the physical time and merely order events; the mechanical phenomena to study are time-independent. Accordingly to the the quasi-static assumption in fact, kinetics effects are a priori assumed to be negligible.

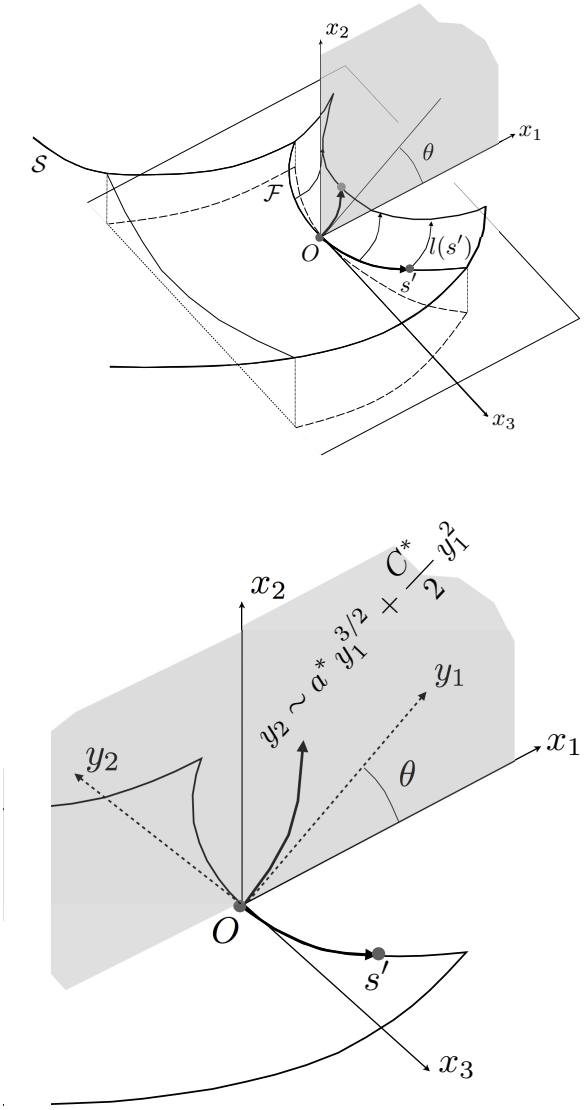

Figure 2.2: *Arbitrary crack with a small kinked and curved extension $l(s';t,\tau)$ indicated in figure as $l(s')$ without explicit time dependency. Kink angle is denoted with θ and defined in the normal plane at the abscissa s along the crack front. The normal plane at the origin is highlighted in grey. Each kink is surrounded by an unbranched, curvilinear crack path in the normal plane. In agreement with [2, 82, 83], the elongation in the normal plane is taken to be: $y_2 = a^* y_1^{3/2} + 1/2 C^* y_1^2 + O(y_1^{5/2})$ with axes $\{y_1, y_2\}$ denoting the Frenet frame right after the kink.*

$$K_i^{(1/2)} = \mathbb{G}_{ij}(\theta) T_j + a^* \mathbb{H}_{ij}(\theta) K_j \tag{2.4}$$

Symbol $\mathbf{K}^{(1)}[\cdot]$ denotes a non local operator that acts along the whole crack front $\mathcal{F}(t)$, whose expression was provided in [83] moving from the cornerstone work of Rice [117] on weight functions

theory:

$$\begin{aligned}\mathbf{K}^{(1)}[s,t;l(s';t,\tau)] &= \frac{1}{2}\left[\frac{\partial^2 K_i}{\partial(\sqrt{l})^2}\right]_{l(s')\equiv l(s)}^{C^*=0} l(s;t,\tau) + C^*\mathbb{M}_{ij}(\theta)K_j\, l(s;t,\tau) \\ &+ \mathbb{N}_{ij}(\theta)K_j\left.\frac{\partial l}{\partial s'}\right|_{s;t,\tau} + \int_{\mathcal{F}} \mathbb{Z}_{ij}(\Omega,s,s',\theta(s),\theta(s'))K_j(s')(l(s';t,\tau)-l(s;t,\tau))\,ds'\end{aligned} \tag{2.5}$$

In equations (2.3), (2.4) and (2.5), the K_js are the SIFs prior to the crack kinking, $\mathbf{T}$ is the *T-stress* vector of components T_j and a^* and C^* define the curvature of the extension. The $\mathbb{F}_{ij}s, \mathbb{G}_{ij}s, \mathbb{H}_{ij}s, \mathbb{M}_{ij}s$, and $\mathbb{N}_{ij}s$ are functions of the kink angle θ, which are termed *universal* because they obey to the autonomy concept; on the contrary the terms $\left[\frac{\partial^2 K_i}{\partial(\sqrt{l})^2}\right]_{l(s')\equiv l(s)}^{C^*=0}$ and $\mathbb{Z}_{ij}s$ depend on the geometry of body Ω. Symbol $\fint_{\mathcal{F}}$ stands for the Cauchy Principal Value along $\mathcal{F}$.

Functional $\mathbf{K}^{(1)}[\cdot]$ can be expressed as the linear combination of three different contributions:

$$\mathbf{K}^{(1)}[s,t;l(s';t,\tau)] = \mathbf{K}_0^{(1)}(s,t)l(s;t,\tau) + \mathbf{K}_1^{(1)}(s,t)\left.\frac{\partial l}{\partial s'}\right|_{s;t,\tau} + \mathbf{K}_{nl}^{(1)}[s,t;l(s';t,\tau)-l(s;t,\tau)] \tag{2.6}$$

where vector $\mathbf{K}_0^{(1)}$ accounts for the locally linear contribution of $l(s;t,\tau)$ to the variation of SIFs at s, whereas vector $\mathbf{K}_1^{(1)}$ conveys the influence of the derivative of $l(s';t,\tau)$ with respect to the abscissa s' on the crack front. Finally $\mathbf{K}_{nl}^{(1)}$ is non local and provides the contribution of the fluctuation of crack advancing at s' to SIFs at s.

2.3 Rigid-plasticity analogy

2.3.1 Onset of crack propagation and criteria for crack kinking angle evaluation

The mathematical representation of the *onset of crack propagation* at point s and time t can be given a general form:

$$\varphi(\mathbf{K}(s,t),\theta(s,t)) = \vartheta(\mathbf{K}(s,t),\theta(s,t)) - \vartheta(K_1^C,\theta^C) = 0 \tag{2.7}$$

in the normal plane of the Frenet reference defined in fig. 2.1. In eq. (2.7) K_1^C is the fracture toughness and $\theta^C = 0$ is the propagation angle in a mode 1 experimental test. $\vartheta(K_1^C,\theta^C)$ connotes the critical state. For each φ, there is a "related magnitude" ϑ which increases monotonically with the level κ of applied loads and which is supposed to obtain a critical value at the onset of crack growth [122]. Specific examples for ϑ are:

- Maximum Energy Release Rate (MERR) G incipient crack growth [49, 154]. It assumes as ϑ_{MERR} an extension of the classical Irwin formula, as detailed in eq. (2.11).
- Maximum hoop Tensile Stress (MTS) in the $r^{-1/2}$ near-tip singular field [36]. It assumes as ϑ_{MTS} the tensile stress perpendicular to any direction θ away from the crack front (the so-called hoop-stress).Here $\{r,\theta\}$ denotes a local polar coordinate system attached to the crack front.
- Maximum Shear Stress (MSS) [109]. It assumes as ϑ_{MSS} the shear stress.

- apparent Crack Extension Force (CEF) [141]. It assumes as ϑ_{CEF} the $J-$integral vector projected onto the crack growth direction.
- Strain Energy Density (SED) criterion [139].
- Maximum K_1^* ($MAXK_1^*$) criterion. It assumes as $\vartheta_{MAXK_1^*}$ the SIF K_1^* expressed in eq. (2.3).

Local Symmetry criterion (LS) [47] is the only exception to the mathematical representation of the onset of fracture in the general form (2.7).

Among the gallery of instances of crack propagation criteria, there is a part of them, widely used in the computational fracture mechanics community, namely MTS, MSS, CEF, and SED, that are represented in the SIFs space $K_1 - K_2 - K_3$ because they stem from the crack configuration at the onset of propagation. The remaining part, namely LS, MERR, $MAXK_1^*$, are grounded on the stress and strain fields in the propagated configuration as the crack elongation approaches zero from above. For them, the Amestoy-Leblond space $K_1^* - K_2^* - K_3^*$ is the natural environment.

Cracks cannot advance at time t if

$$\varphi(\mathbf{K}(s,t), \theta(s,t)) < 0 \tag{2.8}$$

The latter inequality defines the *safe equilibrium domain.* It has to be intended such that it exists a region around the origin in the SIFs space such that for all $\theta(s,t) \in \mathbb{R}$ it does not exist any vector $\mathbf{K}(s,t)$ for which $\varphi(s,t)$ vanishes, whatever the relationship between the angle of propagation $\theta(s,t)$ and the SIFs might be.

As seen in eq.(2.7) and discussed in [124], the onset of propagation is always related to a prediction of the kinking angle $\theta(s,t)$ in the eventuality of a crack elongation. The safety of a configuration at time t, no matter how far it is from the critical state, depends on the angle the crack is going to kink at the time it grows. Historically, any onset of crack propagation has been provided with a *criterion for crack kinking evaluation.* With the mere exception of the LS [47], which gives the kink angle through the equation $K_2^* = 0$, the two notions of onset of crack propagation and criteria for crack kinking evaluation correspond one another in the general formulation derived in Section 2.2 in [124]:

$$find\ \{\kappa(t), \theta(s,t)\}\ \ s.t.\ \ \varphi(s,t) = 0,\ \ \left.\frac{\partial \varphi}{\partial \theta}\right|_{s,t} = 0 \tag{2.9}$$

where the author shows that Griffith's criterion is violated in some interval by all crack propagation criteria except MERR and that the kink angle should come out from the maximality property (2.9). The onset of propagation (2.7) written as $\varphi(\kappa, \alpha, \theta) = 0$, implicitly defines a function $\kappa(\theta, \alpha)$ with α as a given parameter the expresses the mode-mixity. The actual kinking angle $\theta(s,t)$ is the one that, at any given $\alpha(s,t)$, minimizes $\kappa(t)$. Through the implicit function theorem one has:

$$\left.\frac{d\kappa}{d\theta}\right|_{\alpha} = -\left.\frac{\partial \varphi}{\partial \theta}\left(\frac{\partial \varphi}{\partial \kappa}\right)^{-1}\right|_{\alpha} = 0 \Rightarrow \left.\frac{\partial \varphi}{\partial \theta}\right|_{\alpha} = 0 \tag{2.10}$$

whence (2.9).

There are two main "streams" of literature on crack kinking criteria, that correspond to two different views.

An approach assumes that a crack propagates "as soon as it can", which means at the lowest values of external actions that allow the onset of propagation to be reached. In this view: i) formula (2.9) insures that safety is measured against the worst value of $\theta(s,t)$ for the MERR; ii) as already mentioned, it was shown in [124] that crack propagation criterion different from the MERR must

be ruled out and attempts of capturing crack growth by means of a propagation criterion different from the MERR should not be undertaken in the Griffith standpoint of fracture. This strong statement includes the LS principle at least in mixed mode. In particular, this implies that the view of kinking $K_2^*(s,t^-)=0$ by means of LS criterion is incorrect, as it requires a value for κ higher than the one predicted in (2.9). Assuming that a crack propagates at minimum external actions implies that the energy stored in the system is minimal as well. This seems to be in the line of the revisitation of brittle fracture proposed in [39], provided that the onset of propagation is reached. Moving from energy minimality principle, Chambolle et al. [25] showed that the kinking never occurs with a propagation which is continuous in time (see Property 4 in [25]). Analyses made in [124] confirm this statement in the light of formula (2.9).

On the other hand, it seems intuitive to consider a smooth in space and continuous in time crack evolution, at least after the kink. It has been proved that condition $K_2^*(s,t)=0$ is mandatory for any continuous propagation in time[2]. Therefore, denoting with t the time at which the crack kinks, a continuous propagation in time after the kink requires $K_2^*(s,t^+)=0$. Assuming that such a condition holds also at t^- (and thus a continuous in time propagation at a kink) leads to the view of LS criterion for crack kinking, which still makes use of MERR as an onset of propagation. This view is not compatible with formula (2.9), in the sense that the angle of propagation is different and also that load at which crack elongates is larger than the one required by formula (2.9). Assuming LS at a kink implies accepting that the energy inserted in the system to propagate the crack is not the minimal one. i.e. that some energy barriers must be present at a kink.

Linking conditions at t^- and $K_2^*(s,t^+)=0$ is an open, challenging problem in the fracture mechanics community. The choice made by mother nature has been not understood clearly so far. In 2D, LS and MERR criterion are so close one another that differences are far below the accuracy of experimental analysis. The scenario in 3D propagation appears to be different, as envisaged in Appendix B, so that experimental campaigns might be planned. The present work, which naturally develops in the framework of continuous propagation at kinks, will not solve the controversy. It is assumed that the load factor has no requirements apart from being non negative, $\kappa(t)\geq 0$. In other terms, $\kappa(t)$ may increase with t, decrease at some point, eventually jump so that the crack proceeds quasi-statically and continuously in time [3]. Starting from $K_2^*(s,t^+)=0$ a continuous evolution in time along a smooth crack path may proceed. The crack evolution at any $\tau>t$ is stable with respect to $\kappa(t^+)$ but not with respect to $\kappa(t^-)$ if MERR is assumed at a kink. Of course, in realistic analysis, the jump $\kappa(t^-)-\kappa(t^+)$ in the load factor is unfeasible. A dynamic evolution is therefore localized at any crack kinking, similarly to what happens in a snap through experiment. The crack length at which a quasi-statical evolution may eventually start again corresponds to a time $\tau>t$ at which $\kappa(\tau)=\kappa(t^-)$, if a unique crack evolution takes place.

2.3.2 Maximum Energy Release Rate

When cracks, idealized to small scale yielding, advance energy dissipation is concentrated at the crack fronts. Whereas in plasticity the choice of a yield function is free and the relevant amount of dissipation descends, Irwin [62] formula in the Griffith standpoint of fracture restricts the choice of

[2]See Property 3 in [25], namely: assuming the validity of the Energy Conservation and Stability Criterion, a crack cannot propagate continuously in space and time in a homogeneous, isotropic material unless it propagates in mode 1. Stability means that at each time t, the total energy, sum of the potential and surface energies, evaluated along all possible small variations of the crack from its present state, is the smallest one at that state.

[3]Obviously, an arbitrary behavior of $\kappa(t)$ may be not "realistic", in the usual sense of κ being a control parameter tuned within a laboratory. Yet, the approach is not uncommon in mechanics. Essentially, it is the same assumption that leads to model snapping and buckling problems, allowing to follow incrementally the equilibrium path after a peak [118], keeping the system at the onset of propagation (2.7).

the onset of crack propagation φ to the MERR:

$$\varphi(s,t) = \frac{1}{2}(\mathbf{K}^* \cdot \mathbf{\Lambda}\mathbf{K}^* - G_C) \tag{2.11}$$

where E is the Young modulus, ν is the Poisson's coefficient and G_C is the fracture energy, i.e. the dissipated energy per unit crack elongation and is a material characteristic. The non vanishing components of matrix $\mathbf{\Lambda} = [\Lambda_{ij}]$ in eq. (2.11) read:

$$\Lambda_{11} = \Lambda_{22} = \frac{1-\nu^2}{E}; \quad \Lambda_{33} = \frac{1+\nu}{E} \tag{2.12}$$

for an isotropic material. Note that in eq. (2.11) a factor 1/2 has been included, which will be beneficia later in the work, particularly in formula (2.26). In eq. (2.11) the expression of the energy release rate G is referred to an embedded crack in which prevails a plane strain condition in a core of the crack front. The radius of this core is a function of the distance to the free surface.

Recent investigations [26] revisited the notion of MERR in 2D and proved formula (2.11) also by means of the l'Hopital theorem [126]. Similar analyses in 3D have not been carried out and the validity of Irwin's formula (2.11) for 3D, widely accepted in the fracture mechanics community, is here assumed.

2.3.3 Phases of the fracturing process

Fracturing processes reveal three distinct phases: loading without crack growth, stable and unstable propagation. If $\varphi(s,t) < 0$ at point s and time t, a sufficiently small load increment $\delta\kappa$ between instants t and $\tau > t$ exists that does not elongate the crack:

$$\begin{aligned} &at\ any\ t\ s.t.\ \varphi(\mathbf{K}(s,t),\theta) < 0\ \ for\ all\ \theta\ it\ exists\ \ \delta\kappa = \kappa(\tau) - \kappa(t) > 0 \\ &s.t.\ \delta\mathbf{K}(s,\tau) = \frac{\mathbf{K}(s,t)}{\kappa(t)}\delta\kappa \quad and\ \ \varphi(\mathbf{K}(s,t) + \delta\mathbf{K}(s,\tau),\theta) < 0\ \ for\ all\ \theta \end{aligned} \tag{2.13}$$

Such an incremental process describes the first phase of the fracturing process, namely loading without crack growth.

When the onset of crack propagation is reached at a point s and time t, the second phase, when present, is triggered off: stable crack growth. A further increase of load $\delta\kappa$ causes crack elongation at s. Denoting with:

$$\delta\mathbf{K}(s,\tau) = \mathbf{K}(s,\tau) - \mathbf{K}(s,t^+), \ \ \delta\mathbf{K}^*(s,\tau) = \mathbf{K}^*(s,\tau) - \mathbf{K}^*(s,t^+) \tag{2.14}$$

at time t s.t. $\varphi(\mathbf{K}(s,t),\theta(s,t)) = 0$ for at least one $\theta(s,t)$, it exists $\delta\kappa = \kappa(\tau) - \kappa(t^+) > 0$ s.t.

$$\delta\mathbf{K}^*(s,\tau) = \frac{\mathbf{K}^*(s,t^+)}{\kappa(t^+)}\delta\kappa, \ \ \delta\mathbf{K}(s,\tau) = \delta\mathbf{K}^*(s,\tau) + \mathbf{K}^{(1/2)}(s,t)\sqrt{l(s;t,\tau)} + O(l) \tag{2.15}$$

Details of eq.(2.15) are discussed in Appendix A. Conceptually, it states that a quasi-static fracture extension $l(s;t,\tau)$ due to external actions requires a contemporary variation $\delta\kappa$ of external actions such that the global equilibrium is guaranteed. It is a reminiscence of Colonnetti's decomposition of stresses in plasticity[4] [30, 31], as the variation of SIFs is additively decomposed as due to an

[4]Since plastic deformations play the same role of any deformation effect of inelastic nature, Colonnetti's approach allows to consider the solution of the incremental quasi-static elastic-plastic problem as the sum of two elastic solutions: one due to the increments of the external loads and the other due to the increments of plastic deformations considered as imposed distorsions. Such an approach leads to the formulation of the elastic-plastic problem in terms of plastic multipliers solely.

elastic contribution ($\delta\mathbf{K}^*$) and to a distorsion (in fracture: crack elongation $l(s;t,\tau)$; in plasticity: plastic strain rate) which reverses itself into SIFs (stresses in plasticity) by means of a stiffness factor (in fracture: $\mathbf{K}^{(1/2)}$, in plasticity: the action of the $\mathbb{Z}$ matrix over the plastic part of the volume).
Eq. (2.15) states also implicitly that the extension $l(s;t,\tau)$ cannot be arbitrary along the crack front. Equilibrium, in the sense that $\delta\kappa$ is unique for all points s, requires $l(s;t,\tau)$ to assume a precise shape with respect to s. Such a constraint is provided in plasticity by Ceradini's functional which in fact will be extended to fracture in Section 2.5.

The third phase of crack propagation, unstable crack growth, is reached when condition $\delta\kappa > 0$ in eq. (2.15) is no longer required at some point s. A quasi-static crack growth, merely academic, can be simulated only with a decrease of external actions $\delta\kappa \leq 0$ to recover the post peak behavior, as typical in "arc length" techniques for softening materials.

2.3.4 Fracture propagation as a standard dissipative system

Several researchers have formulated the fracture propagation problem within the method of the local state of thermodynamics [18, 87, 103], eventually exploting its analogy with associated plasticity [122]. The latter work has been further developed in [125], putting fracture in analogy with a rigid-plastic model in the sense that any elastic contribution to the elongation, which would eventually be recovered after unloading, appears to be misplaced. In the Griffith theory [49] and in the light of Irwin's formula [62], propagation is governed at time t by the following conditions, reminiscence of Karush-Kuhn-Tucker conditions of plasticity:

$$\varphi(\mathbf{K}(s,t),\theta(s,t)) \leq 0, \quad v(s,t) \geq 0, \quad \varphi(\mathbf{K}(s,t),\theta(s,t))v(s,t) = 0 \tag{2.16}$$

No propagation is allowed $l(s;t,\tau) = 0$ when $\varphi(s,t) < 0$ and viceversa. In [18], the crack length is taken as a global internal variable, and its variation induces a dissipation which satisfies Clausis-Duhem's inequality through the introduction of a convex dissipation potential $\mathcal{D}$. Such an idea extends straightforwardly to three dimensional LEFM simply considering any point s along the crack front as a locus of possible dissipation. A "safe equilibrium domain" is defined as:

$$\mathbb{E}(s,t) = \{\{K_1^*(s,t), K_2^*(s,t), K_3^*(s,t)\} \in \mathbb{R}_0^+ \times \mathbb{R} \times \mathbb{R} \mid \varphi(\mathbf{K}^*(s,t)) < 0\} \tag{2.17}$$

It has a local nature at each point s of the crack front. When $\mathbf{K}^*(s,t) \in \mathbb{E}$ the material surrounding the point s experiences a purely linear elastic behavior, eventually corresponding to an elastic unloading. A curve "onset of crack propagation" $\partial\mathbb{E}$ as the boundary of the safe equilibrium domain can be defined at any point s:

$$\partial\mathbb{E}(s,t) = \{\{K_1^*(s,t), K_2^*(s,t), K_3^*(s,t)\} \in \mathbb{R}_0^+ \times \mathbb{R} \times \mathbb{R} \mid \varphi(\mathbf{K}^*(s,t)) = 0\} \tag{2.18}$$

Vectors $\mathbf{K}^*(s,t) \notin \bar{\mathbb{E}}$ are ruled out. The definitions above are reminiscent to the elastic domain and to the yield surface in the plasticity theory [53]. They implicitly label the SIFs vector $\mathbf{K}^*$ as an internal force for the LEFM problem. Consistency condition finally reads:

$$when \;\; \varphi(s,t) = 0, \;\; v(s,t) \geq 0, \;\; \left.\frac{\partial\varphi}{\partial t}\right|_{s,t} \leq 0, \;\; v(s,t) \left.\frac{\partial\varphi}{\partial t}\right|_{s,t} = 0 \tag{2.19}$$

provided that a time derivative of function $\varphi(s,t)$ can be properly defined.

2.4 Thermodynamics of fracture

Mechanical dissipation in LEFM is due to the irreversible nature of crack extension, measured in an incremental setting by the quasi-static crack front velocity vector $\mathbf{v}(s,t)$. It is defined in the Frenet frame at point s of $\mathcal{F}$ as the vector, slanted by kinking angle $\theta(s,t)$, whose norm is equal to the quasi-static crack front velocity $v(s,t)$. The power released at location s along the crack front $\mathcal{F}(t)$ during new surface creation in Griffith's approach to fracture amounts to [115]:

$$G(s,t)v(s,t)\,ds\,dt \tag{2.20}$$

It was already pointed out in defining the safe equilibrium domain $\mathbb{E}$ and the onset of crack propagation $\partial\mathbb{E}$ in equations (2.17) and (2.18) that vector $\mathbf{K}^*(s,t)$ can be viewed as a thermodynamic force. The rate of its thermodynamic conjugated variable, $\mathbf{a}^*(s,t)$, will be defined by:

$$\mathbf{K}^*(s,t)\cdot\left.\frac{\partial\mathbf{a}^*}{\partial t}\right|_{s,t} = G(s,t)v(s,t) \tag{2.21}$$

A "maximum dissipation" principle for LEFM is postulated at any point s and termed as $\mathcal{D}$-principle. It reads: at any crack front point s, for given dissipation rate vector $\left.\frac{\partial\mathbf{a}^*}{\partial t}\right|_{s,t}$ that enjoys (2.21), among all possible SIFs $\mathbf{k}^*\in\bar{\mathbb{E}}$, the function

$$\mathcal{D}\left(\mathbf{k}^*;\left.\frac{\partial\mathbf{a}^*}{\partial t}\right|_{s,t}\right) = \mathbf{k}^*\cdot\left.\frac{\partial\mathbf{a}^*}{\partial t}\right|_{s,t} \tag{2.22}$$

attains its maximum for the actual SIFs vector $\mathbf{K}^*$:

$$\mathcal{D}\left(\mathbf{K}^*;\left.\frac{\partial\mathbf{a}^*}{\partial t}\right|_{s,t}\right) = \max_{\mathbf{k}^*\in\bar{\mathbb{E}}}\ \mathcal{D}\left(\mathbf{k}^*;\left.\frac{\partial\mathbf{a}^*}{\partial t}\right|_{s,t}\right) \tag{2.23}$$

$\mathcal{D}$-principle is the counterpart of the postulate of the maximum plastic work and analogously to maximum dissipation in plasticity, $\mathcal{D}$-principle implies associative flow rule (normality law):

$$\left.\frac{\partial\mathbf{a}^*}{\partial t}\right|_{s,t} = \left.\frac{\partial\varphi}{\partial\mathbf{K}^*}\right|_{s,t}\dot{\lambda}(s,t) \tag{2.24}$$

and loading/unloading conditions in Karush-Kuhn-Tucker complementarity form at any point s along the crack front:

$$\dot{\lambda}(s,t)\geq 0,\ \ \varphi(s,t)\leq 0,\ \ \varphi(s,t)\dot{\lambda}(s,t)=0 \tag{2.25}$$

They hold at any point s along the crack front $\mathcal{F}(t)$.

Onset of propagation (2.11) shall be used into normality rule (2.24). In view of the symmetry of matrix $\mathbf{\Lambda}$ it comes out:

$$\left.\frac{\partial\mathbf{a}^*}{\partial t}\right|_{s,t} = \mathbf{\Lambda}\mathbf{K}^*(s,t)\dot{\lambda}(s,t) \tag{2.26}$$

It holds eventually:

$$\mathbf{K}^*(s,t)\cdot\left.\frac{\partial\mathbf{a}^*}{\partial t}\right|_{s,t} = \mathbf{K}^*(s,t)\cdot\left.\frac{\partial\varphi}{\partial\mathbf{K}^*}\right|_{s,t}\dot{\lambda}(s,t) = \mathbf{K}^*(s,t)\cdot\mathbf{\Lambda}\mathbf{K}^*(s,t)\dot{\lambda}(s,t) \tag{2.27}$$

The chain of identities above, in view of complementarity laws (2.25) and of positive definiteness of $\mathbf{\Lambda}$, grants that:

$$\mathbf{K}^*\cdot\left.\frac{\partial\mathbf{a}^*}{\partial t}\right|_{s,t}\geq 0 \tag{2.28}$$

that is, thermodynamic restrictions are satisfied by the pair $\mathbf{K}^*(s,t), \mathbf{a}^*(s,t)$.

Since from identities (2.27) immediately descends

$$\mathbf{K}^*(s,t) \cdot \left.\frac{\partial \mathbf{a}^*}{\partial t}\right|_{s,t} = G(s,t)\dot{\lambda}(s,t) \tag{2.29}$$

and in order to prove the equivalence (2.21), it only remains to prove that $\dot{\lambda}(s,t) = \left.\frac{\partial l}{\partial t}\right|_{s,t}$. By means of Karush-Kuhn-Tucker conditions (2.16) one writes at all points s along $\mathcal{F}(t)$ such that $\varphi(s,t) = 0$:

$$\begin{aligned}
\varphi(s,t)v(s,t) &= 0 = \quad \textit{by eq. (2.11)} \\
&= \frac{1}{2}(G(s,t)v(s,t) - G_C\, v(s,t)) = \quad \textit{by eq. (2.21)} \\
&= \frac{1}{2}(\mathbf{K}^*(s,t) \cdot \left.\frac{\partial \mathbf{a}^*}{\partial t}\right|_{s,t} - G_C\, v(s,t)) = \quad \textit{by eq. (2.29)} \\
&= \frac{1}{2}(G(s,t)\,\dot{\lambda}(s,t) - G_C\, v(s,t)) = \\
&= \varphi(s,t)\,\dot{\lambda}(s,t) - \frac{1}{2}G_C(v(s,t) - \dot{\lambda}(s,t)) = \quad \textit{by eq. (2.25)} \\
&= -\frac{1}{2}G_C(v(s,t) - \dot{\lambda}(s,t)) = \\
&= 0
\end{aligned} \tag{2.30}$$

and the thesis follows since $G_C \neq 0$.

In conclusion, vector $\left.\frac{\partial \mathbf{a}^*}{\partial t}\right|_{s,t}$ is related to the quasi-static crack front velocity vector $\left.\frac{\partial \mathbf{l}}{\partial t}\right|_{s,t}$ defined in the Frenet frame at point s of $\mathcal{F}(t)$, by eq.(2.26), namely:

$$\left.\frac{\partial \mathbf{a}^*}{\partial t}\right|_{s,t} = \mathbf{\Lambda}\mathbf{K}^*(s,t)v(s,t) \tag{2.31}$$

The maximality condition (2.23) has the meaning of maximum dissipation, as usual in standard dissipative systems, during crack propagation and Karush-Kunn-Tucker conditions (2.25), rigorously derived from (2.23), are one and the same with inequalities (2.16), which were suggested by the physics of the problem.

In thermodynamics, restrictions drive the formulation of appropriate constitutive theory usually after the specification of free energies. Thermodynamic constraint (2.28) has a sound thermodynamic origin that quite naturally leads to equation (2.31), thus providing a link between $\left.\frac{\partial \mathbf{a}^*}{\partial t}\right|_{s,t}$ and $\mathbf{K}^*$ at all points $s \in \mathcal{F}(t)$.

2.5 Minimum theorems

2.5.1 A stability condition

Assume that the front propagates continuously in time and that the elongation in the normal plane at location s amounts to $l(s;t,\tau)$. Onset of propagation $\varphi(s,t^*)$ is well defined for all $t^* \in [t,\tau]$ and if the crack front at s elongates continuously in time between t and τ then $\varphi(s,t^*) = 0$ for all $t^* \in [t,\tau]$. The time derivative of function $\varphi(s,t)$ can be properly defined as:

$$\left.\frac{\partial \varphi}{\partial t}\right|_{s,t} = \lim_{\tau \to t^+} \frac{\varphi(s,\tau) - \varphi(s,t)}{\tau - t} \tag{2.32}$$

Between instants t and τ the load factor changes as well, being the driving force of the crack growth. Assume that it changes with sufficient smoothness, so that a velocity of load increment can be properly defined:

$$\left.\frac{\partial \kappa}{\partial t}\right|_t = \lim_{\tau \to t^+} \frac{\kappa(\tau) - \kappa(t)}{\tau - t} \tag{2.33}$$

Stable crack growth requires an increase of the external loads to elongate the fracture, i.e.

$$\left.\frac{\partial \kappa}{\partial t}\right|_t > 0 \tag{2.34}$$

In view of definition (2.11) for φ, and of expansion (2.2), one writes:

$$\begin{aligned} \left.\frac{\partial \varphi}{\partial t}\right|_{s,t} &= \frac{\partial \varphi}{\partial \mathbf{K}^*} \cdot \left(\left.\frac{\partial \mathbf{K}^*}{\partial \kappa}\right|_{s,t} \left.\frac{\partial \kappa}{\partial t}\right|_t + \mathbf{K}^{(1)}[s,t;v(s',t)] \right) \overset{\varphi=0}{=} \\ &= \frac{G_C}{\kappa(t)} \left.\frac{\partial \kappa}{\partial t}\right|_t + \mathbf{\Lambda K}^*(s,t) \cdot \mathbf{K}^{(1)}[s,t;v(s',t)] \end{aligned} \tag{2.35}$$

In eq. (2.35) the linearity of operator $\mathbf{K}^{(1)}[\cdot]$ has been used to replace $l(s';t,\tau)$ with $v(s',t)$.

In Colonnetti's framework, $\left.\frac{\partial \mathbf{K}^*}{\partial \kappa}\right|_{s,t} \left.\frac{\partial \kappa}{\partial t}\right|_t$ is a mere elastic contribution to the time derivative of the SIFs vector due to the change of external loads, and $\mathbf{K}^{(1)}[s,t;v(s',t)]$ corresponds to the crack elongation rate $v(s',t)$ considered as an inelastic distorsion. Consistency condition:

$$\left.\frac{\partial \varphi}{\partial t}\right|_{s,t} v(s,t) = 0 \tag{2.36}$$

holds at all points s such that $\varphi(s,t) = 0$. Taking advantage of eq. (2.36), one writes it as:

$$\frac{G_C}{\kappa(t)} \left.\frac{\partial \kappa}{\partial t}\right|_t v(s,t) + \mathbf{\Lambda K}^*(s,t) \cdot \mathbf{K}^{(1)}[s,t;v(s',t)] v(s,t) = 0 \tag{2.37}$$

Since G_C and $\kappa(t)$ are positive scalars, the condition (2.34) for stable crack growth sets the following requirements to operator $\mathbf{K}^{(1)}[s,t;v(s',t)]$:

$$\mathbf{\Lambda K}^*(s,t) \cdot \mathbf{K}^{(1)}[s,t;v(s',t)] < 0 \;\; if \;\; v(s',t) > 0 \tag{2.38a}$$

$$\mathbf{\Lambda K}^*(s,t) \cdot \mathbf{K}^{(1)}[s,t;v(s',t)] = 0 \;\; if \; and \; only \; if \; v(s',t) = 0 \tag{2.38b}$$

at all $s \in \mathcal{F}(t)|_{\varphi=0}$. When condition (2.38a) is not met at point s, an unstable propagation may take place in a neighborhood of s. Accordingly, eq.(2.38a) is the (local) condition for the transition to the unstable phase at a point s.

2.5.2 Variational formulation

Symmetry property

Consider the affine operator $N[\cdot]$ defined as:

$$N[v] = \frac{\partial \varphi}{\partial \mathbf{K}^*} \cdot \dot{\mathbf{K}}^*(s,t) + \frac{\partial \varphi}{\partial \mathbf{K}^*} \cdot \mathbf{K}^{(1)}[s,t;v(s',t)] \tag{2.39}$$

where $\dot{\mathbf{K}}^*(s,t) = \left.\frac{\partial \mathbf{K}^*}{\partial \kappa}\right|_{s,t} \left.\frac{\partial \kappa}{\partial t}\right|_t$. The associated problem *find* $v > 0$ *s.t.* $N[v] = 0$ is equivalent to consistency condition (2.19). From theorems of variational calculus, in order to give a variational

formulation in a "restricted sense" (see [144]) to the nonlinear problem $N[v] = 0$, it is necessary that the Gateaux derivative of N, defined by virtue of $\alpha \in \mathbb{R}$:

$$N'_v[w] = \left.\frac{dN[v+\alpha w]}{d\alpha}\right|_{\alpha=0} = \frac{\partial \varphi}{\partial \mathbf{K}^*} \cdot \mathbf{K}^{(1)}[s,t;w(s',t)] \tag{2.40}$$

is symmetric with respect to the usual bilinear form, namely:

$$\int_{\mathcal{F}(t)} N'_v[w(s',t)]z(s,t)\,ds = \int_{\mathcal{F}(t)} N'_v[z(s',t)]w(s,t)\,ds \tag{2.41}$$

By noting that φ has been defined as the maximum energy release rate criterion in eq. (2.11), it turns out that $N'_v[w]$ is precisely the energy release rate associated to elongation rate w at constant boundary conditions, the term $\frac{\partial \varphi}{\partial \mathbf{K}^*} \cdot \dot{\mathbf{K}}^*$ in definition (2.39) being the variation of energy due to the variation of the external loads $\kappa(t)$.

It is not straightforward to envisage symmetry for N'_v from definition (2.5) of operator $\mathbf{K}^{(1)}[s,t;v(s',t)]$, although this property seems quite natural if one thinks the energy release rate as the derivative of the energy. On the contrary, term by term unsymmetry is apparent and one is led to erroneously conclude that a variational formulation for problem $N[v] = 0$ cannot be given. To prove symmetry for operator N'_v one must follow a different path of reasoning, based on the physical meaning of the operator itself.

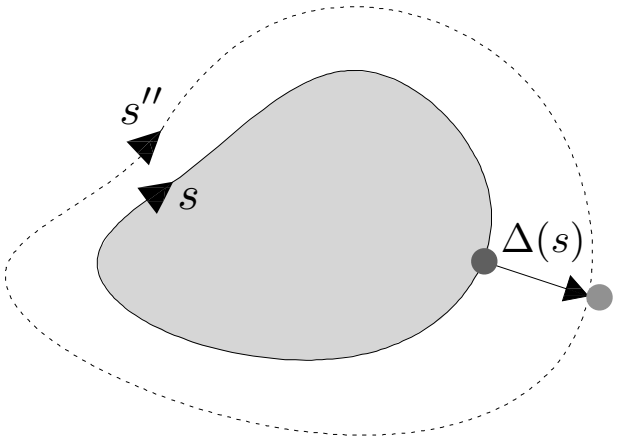

Figure 2.3: *Finite propagation length $\Delta(s)$. The shadowed area represents the crack surface before elongation.*

Consider a finite propagation length $\Delta(s;t,\tau)$ at a point s of the crack front (see figure 2.3), given by the sum of two contributions:

$$\Delta(s) = A\phi(s) + B\psi(s) \tag{2.42}$$

where time dependency has been omitted for the sake of readiness. In eq. (2.42) A and B are two positive parameters and $\phi(s)$ and $\psi(s)$ are formally two fixed and assigned non negative functions expressing the elongation of the front in the normal plane.

The total (elastic) energy of body Ω, denoted henceforth by W, is a function of the geometry,

namely of the advancing of the crack front which is uniquely defined by parameters A and B. Then $W = W(A, B)$ and apart from higher order terms one has:

$$\frac{\partial W(A,B)}{\partial A} = -\int_{\mathcal{F}} G(A,B,s)\phi(s)ds'' \tag{2.43}$$

In eq.(2.43) term $G(A, B, s)$ is the energy release rate which is function of the location of the crack front (A and B), but also of the position s along the crack front. Furthermore, if ds refers to the front before the elongation $\Delta(s)$ and ds'' to the final position of the front, it turns out:

$$ds'' = ds(1 + \gamma\Delta(s)) \tag{2.44}$$

where γ is a local corrective factor that depends upon the curvature of $\mathcal{F}$, see figure 2.4.

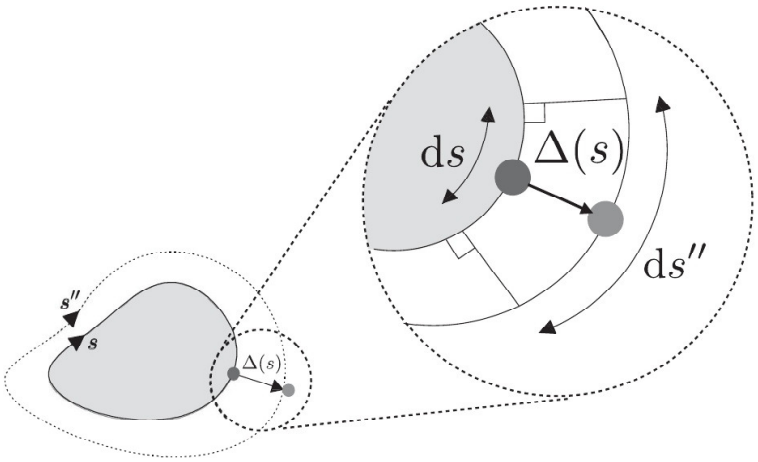

Figure 2.4: *A zoom of figure 2.3 allows to highlight the crack front length increment ds''.*

Second order terms in A and B arise during propagation, as the normal at point s changes direction at s''. Propagation in the normal plane modifies to:

$$\phi(s)\mathbf{n}(s) \cdot \mathbf{n}(s'') = \phi(s) + \textit{ second order terms} \tag{2.45}$$

For all these reasons, eq. (2.43) can be written as:

$$\frac{\partial W(A,B)}{\partial A} = -\int_{\mathcal{F}} G(A,B,s)\phi(s)[1 + \gamma(A\phi(s) + B\psi(s))]ds \tag{2.46}$$

from which:

$$\frac{\partial^2 W(A,B)}{\partial B \partial A} = -\int_{\mathcal{F}} \frac{\partial G(A,B,s)}{\partial B}\phi(s)[1 + \gamma(A\phi(s) + B\psi(s))]ds - \int_{\mathcal{F}} G(A,B,s)\phi(s)\gamma\psi(s)ds \tag{2.47}$$

Setting $A = B = 0$ the latter becomes:

$$\left.\frac{\partial^2 W}{\partial B \partial A}\right|_{A=B=0} = -\int_{\mathcal{F}} \left.\frac{\partial G(A,B,s)}{\partial B}\right|_{A=B=0} \phi(s)ds - \int_{\mathcal{F}} G(0,0,s)\phi(s)\gamma\psi(s)ds \tag{2.48}$$

Analogously one has:

$$\frac{\partial W(A,B)}{\partial B} = -\int_{\mathcal{F}} G(A,B,s)\psi(s)[1 + \gamma(A\phi(s) + B\psi(s))]ds \tag{2.49}$$

and setting $A = B = 0$ one has:

$$\left.\frac{\partial^2 W}{\partial A \partial B}\right|_{A=B=0} = -\int_{\mathcal{F}} \left.\frac{\partial G(A,B,s)}{\partial A}\right|_{A=B=0} \psi(s)ds - \int_{\mathcal{F}} G(0,0,s)\psi(s)\gamma\phi(s)ds \tag{2.50}$$

Comparing eqs. (2.48) and (2.50) one states:

$$\int_{\mathcal{F}} \frac{\partial G(s)}{\partial A}\psi(s)ds = \int_{\mathcal{F}} \frac{\partial G(s)}{\partial B}\phi(s)ds \tag{2.51}$$

Define infinitesimal increments of propagation length $l_1(s) = \delta A \cdot \phi(s)$, $l_2(s) = \delta B \cdot \psi(s)$ and the corresponding infinitesimal variations of the energy release rate $\delta_1 G(s) = \frac{\partial G(s)}{\partial A}\delta A$, $\delta_2 G(s) = \frac{\partial G(s)}{\partial B}\delta B$. It holds:

$$\int_{\mathcal{F}} \delta_1 G(s) \cdot l_2(s)ds = \delta A \delta B \int_{\mathcal{F}} \frac{\partial G(s)}{\partial A}\psi(s)ds \tag{2.52}$$

and

$$\int_{\mathcal{F}} \delta_2 G(s) \cdot l_1(s)ds = \delta A \delta B \int_{\mathcal{F}} \frac{\partial G(s)}{\partial B}\phi(s)ds \tag{2.53}$$

Owing to eq.(2.51) one concludes:

$$\int_{\mathcal{F}} \delta_1 G(s) l_2(s)ds = \int_{\mathcal{F}} \delta_2 G(s) l_1(s)ds \tag{2.54}$$

As it was pointed out that $N'_v[w]$ is precisely the energy release rate associated to elongation rate w, eq.(2.54) is nothing but the proof of symmetry property (2.41).

Variational statements

Consider the geometrical configuration at time t, namely a domain Ω that includes the fracture surface $\mathcal{S}(t)$ with its front $\mathcal{F}(t)$, in equilibrium at external actions $\kappa(t)$. Take an instant $\tau > t$ and assume that at time τ a new equilibrated configuration $\mathcal{S}(\tau)$, $\mathcal{F}(\tau)$ is achievable at $\kappa(\tau) > \kappa(t)$. The ultimate goal of any LEFM crack propagation model stands in estimating the unknown fields at the new equilibrium configuration, namely the displacements $\mathbf{u}(\mathbf{x}, t)$ and the new geometry, that is identified by the elongation in the normal plane $l(s; t, \tau)$. The problem of finding a new configuration can be set in rate form. Given the state of stress and the history of crack propagation at time t, one seeks for the crack propagation rate $v(s, t)$ in the normal plane due to a given variation of external actions $\frac{\partial \kappa}{\partial t}\big|_t$. Such a problem can be solved locally at crack front locations and it is independent upon the rate of the displacement field. Eq. (2.37) derived from consistency condition, solves the rate form problem for $v(s, t)$. In view of symmetry property (2.41), a variational formulation for eq. (2.37) can be written, whereby $v(s, t)$ is obtained as the minimum of a constrained quadratic functional, provided that the crack growth is stable. To ensure stability, in view of (2.38a), the Gateaux derivative (2.40) of operator $N[\cdot]$ has to be co-negative definite. Since $N'_v[w]$ is linear in w, the stability condition is equivalent to:

$$N'_v[w]w(s,t) < 0 \;\; \forall w(s,t) \geq 0, \;\; s \in \mathcal{F}(t) \tag{2.55}$$

In [127] two variational statements are given, that are reminiscent of Ceradini's theorem [24] for plasticity. They extend to three dimensional problems the variational formulation for the global incremental quasi-static linear elastic fracture propagation problem presented in [125] for the two-dimensional case.

Proposition 1 *Under hypothesis (2.55), the crack front velocity $v(s,t)$ that solves the global quasi-static fracture propagation problem at time t minimizes the functional:*

$$\chi[w(s,t)] = -\frac{1}{2}\int_{\mathcal{F}(t)|_{\varphi=0}} N'_v[w(s',t)]w(s,t)\,ds - \int_{\mathcal{F}(t)|_{\varphi=0}} \frac{G_C}{\kappa(t)}\left.\frac{\partial\kappa}{\partial t}\right|_t w(s,t)\,ds \tag{2.56}$$

under the constraint $w(s,t) \geq 0 \;\; \forall s \in \mathcal{F}(t)|_{\varphi=0}$.

In this proof, dependency of velocities upon s and t is not made explicit to favor readability. To prove the theorem, denote with $w = v + \delta v$. It holds:

$$\chi[w] - \chi[v] = -\frac{1}{2}\int_{\mathcal{F}|_{\varphi=0}} (N'_v[v]\delta v + N'_v[\delta v]v + N'_v[\delta v]\delta v)\,ds - \int_{\mathcal{F}|_{\varphi=0}} \frac{G_C}{\kappa(t)}\left.\frac{\partial\kappa}{\partial t}\right|_t \delta v\,ds \tag{2.57}$$

Symmetry and linearity of operator $N'_v[\cdot]$ allow writing:

$$\begin{aligned}
\chi[w] - \chi[v] &= -\int_{\mathcal{F}|_{\varphi=0}} \left(N'_v[v] + \frac{G_C}{\kappa(t)}\left.\frac{\partial\kappa}{\partial t}\right|_t\right)\delta v\,ds - \frac{1}{2}\int_{\mathcal{F}|_{\varphi=0}} N'_v[\delta v]\delta v\,ds \\
&= -\int_{\mathcal{F}|_{\varphi=0}} \frac{\partial\varphi}{\partial t}(w-v)\,ds - \frac{1}{2}\int_{\mathcal{F}|_{\varphi=0}} N'_v[\delta v]\delta v\,ds \\
&= -\int_{\mathcal{F}|_{\varphi=0}} \frac{\partial\varphi}{\partial t} w\,ds + \int_{\mathcal{F}|_{\varphi=0}} \frac{\partial\varphi}{\partial t} v\,ds - \frac{1}{2}\int_{\mathcal{F}|_{\varphi=0}} N'[\delta v]\delta v\,ds \geq 0
\end{aligned} \tag{2.58}$$

the first term is non negative , since $\frac{\partial\varphi}{\partial t} \leq 0$ in view of consistency and of the constraint $w \geq 0$. The second term vanishes in view of Karush-Kuhn-Tucker conditions (2.16). Finally, the last term is non negative under the stable crack growth assumption (2.55). The assert is thus proved.

Proposition 2 *Under hypothesis (2.55), the crack front velocity $v(s,t)$ that solves the global quasi-static fracture propagation problem at time t minimizes the functional:*

$$\omega[w(s,t)] = -\frac{1}{2}\int_{\mathcal{F}(t)|_{\varphi=0}} N'_v[w(s',t)]w(s,t)\,ds \tag{2.59}$$

under the constraint

$$N'_v[w(s',t)] + \frac{G_C}{\kappa(t)}\left.\frac{\partial\kappa}{\partial t}\right|_t \leq 0 \;\; \forall s' \in \mathcal{F}(t)|_{\varphi=0} \tag{2.60}$$

As for the proof of Proposition 1, dependencies of velocities upon s and t is not made explicit to favor readability. To prove the theorem, denote again with $w = v + \delta v$. In view of symmetry property (2.41), one writes:

$$\omega[w] - \omega[v] = -\int_{\mathcal{F}|_{\varphi=0}} N'_v[v]\delta v\,ds - \frac{1}{2}\int_{\mathcal{F}|_{\varphi=0}} N'_v[\delta v]\delta v\,ds \tag{2.61}$$

After adding and subtracting the amount

$$\int_{\mathcal{F}|_{\varphi=0}} \frac{G_C}{\kappa(t)}\left.\frac{\partial\kappa}{\partial t}\right|_t v\,ds,$$

the following algebraic passages can be straightforwardly derived:

$$\begin{aligned}\omega[w]-\omega[v] &= -\frac{1}{2}\int_{\mathcal{F}|_{\varphi=0}} N'_v[\delta v]\delta v\, ds + \int_{\mathcal{F}|_{\varphi=0}} \left(N'_v[v] + \frac{G_C}{\kappa(t)}\left.\frac{\partial\kappa}{\partial t}\right|_t\right) v\, ds \\ &- \int_{\mathcal{F}|_{\varphi=0}} \frac{G_C}{\kappa(t)}\left.\frac{\partial\kappa}{\partial t}\right|_t v\, ds - \int_{\mathcal{F}|_{\varphi=0}} N'_v[v]w\, ds \\ &= -\frac{1}{2}\int_{\mathcal{F}|_{\varphi=0}} N'_v[\delta v]\delta v\, ds + \int_{\mathcal{F}|_{\varphi=0}} \frac{\partial\varphi}{\partial t} v\, ds - \int_{\mathcal{F}|_{\varphi=0}} \left(N'_v[w] + \frac{G_C}{\kappa(t)}\left.\frac{\partial\kappa}{\partial t}\right|_t\right) v\, ds \geq 0\end{aligned} \tag{2.62}$$

in view of symmetry of operator N'_v. The first term is non negative under the stable crack growth assumption (2.55). The second term vanishes in view of Karush-Kuhn-Tucker conditions. The last term is non negative, since $v \geq 0$ and in view of constraint (2.60). The assert is thus proved.

2.5.3 Benchmark

Consider a penny shape crack with radius $a(t) > a_{imp} > 0$ embedded in a continuum body, subject to an internal pressure $p(r,t)$ that opens the crack merely acting on a concentric circle of radius a_{imp} (see figure 2.5).

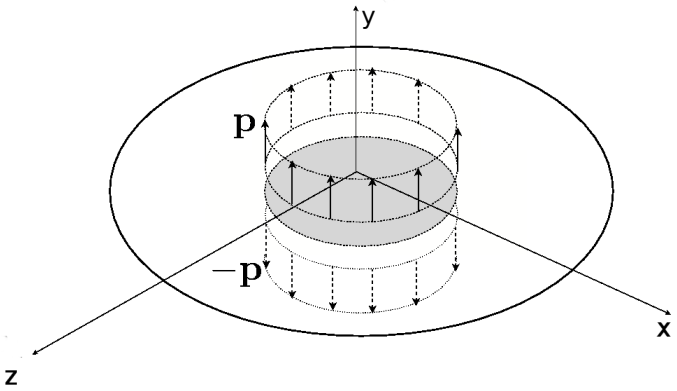

Figure 2.5: *Penny shape crack of variable radius $a(t)$ in an unbounded linear elastic medium, subject to a uniform tensile stress $\mathbf{p}(r,t) = -p(r,t)\mathbf{n}$ on a constant circular area of radius a_{imp} depicted in grey. $\mathbf{n}$ stands for the outer normal, so that $\mathbf{p}$ opens the crack.*

Pressure $p(r,t)$ has the following mathematical expression:

$$p(r,t) = \kappa(t)\mathcal{H}(a_{imp} - r) \tag{2.63}$$

$\kappa(t)$ being the load factor, as usual, and $\mathcal{H}(x)$ the Heaviside step function, namely:

$$\mathcal{H}(x) = \begin{cases} 1 \;\; if \;\; x \geq 0 \\ 0 \;\; if \;\; x < 0 \end{cases} \tag{2.64}$$

In such mode 1 condition, the crack evolution in space is smooth, without kinking. The SIFs vector has a single non vanishing component, independent on abscissa s along the crack front, that amounts to [65]:

$$K_1(a(t)) = \frac{2}{\pi}\frac{1}{\sqrt{a(t)}}\int_0^{a(t)} \frac{r\, p(r,t)}{(a(t)^2 - r^2)^{1/2}} dr \tag{2.65}$$

whence, in view of (2.63):

$$K_1(a(t)) = 2\frac{\kappa(t)}{\pi}\frac{a(t) - \sqrt{a^2(t) - a_{imp}^2}}{\sqrt{a(t)}} \tag{2.66}$$

Closed form solution (2.66) can be exploited in order to benchmark the variational framework developed in section 2.5.2.

If at instant $\tau > t$ the load factor $\kappa(\tau)$ reaches a propagation threshold so that $K_1 = K_1^C$, the onset of crack propagation is reached. Further increase of external actions allows fracture propagation and radius $a(t)$ becomes $a(t) + da(t,\tau)$. As already stressed, axial-symmetric crack growth conditions make the amount $da(t,\tau)$ independent on the abscissa s along along the crack front. Eq.(2.35) reduces to:

$$\left.\frac{\partial\varphi}{\partial t}\right|_t = \frac{G_C}{\kappa(t)}\left.\frac{\partial\kappa}{\partial t}\right|_t + \frac{\partial\varphi}{\partial\mathbf{K}^*}\cdot\mathbf{K}_0^{(1)}(t)\,\dot{a}(t) \tag{2.67}$$

where, in view of eq. (2.1),

$$\dot{a}(t) = \lim_{\tau\to t^+}\frac{da(t,\tau)}{\tau - t}$$

The closed form for scalar $K_0^{(1)}$, meaning the non vanishing component of vector $\mathbf{K}_0^{(1)}$, can be derived from the series expansion of eq. (2.66) in terms of $a(t)$:

$$\begin{aligned} K_1(a(t) + da(t,\tau)) &= K_1(a(t)) - \frac{k(t)}{\pi a(t)\sqrt{a(t)}}\frac{a(t)^2 + a_{imp}^2 - a(t)\sqrt{a(t)^2 - a_{imp}^2}}{\sqrt{a(t)^2 - a_{imp}^2}}da(t,\tau) \\ &+ O(da^2(t,\tau)) \end{aligned} \tag{2.68}$$

According to definition (2.6), operator $\mathbf{K}^{(1)}[s,t;v(s,t)] = \mathbf{K}_0^{(1)}(t)\dot{a}(t)$ and stability condition (2.38a) is satisfied. The crack growth is therefore stable, as expected again.

Functional (2.56) holds:

$$\chi[\dot{a}(t)] = -\frac{1}{2}\int_{\mathcal{F}(t)|_{\varphi=0}}\frac{\partial\varphi}{\partial\mathbf{K}^*}\cdot\mathbf{K}_0^{(1)}(t)\,\dot{a}^2(t)\,ds - \int_{\mathcal{F}(t)|_{\varphi=0}}\frac{G_C}{\kappa(t)}\left.\frac{\partial\kappa}{\partial t}\right|_t\dot{a}(t)\,ds \tag{2.69}$$

under the unilateral constraint $\dot{a}(t) \geq 0$. Consider a positive parameter α and a positive elongation rate $\dot{b}(t)$, so that the configuration $\dot{a}(t) + \alpha\,\dot{b}(t) \geq 0$ is in the set of admissible configurations for functional (2.56). Optimality implies:

$$\chi[\dot{a}(t) + \alpha\,\dot{b}(t)] \geq \chi[\dot{a}(t)] \tag{2.70}$$

or equivalently

$$\left.\frac{d}{d\alpha}\chi[\dot{a}(t) + \alpha\,\dot{b}(t)]\right|_{\alpha=0} \geq 0 \tag{2.71}$$

Crack front $\mathcal{F}(t)|_{\varphi=0}$ can be split into two parts. In the former, say $\mathcal{F}_1(t)$, $\dot{a}(t)$ is strictly positive. The complementary, say $\mathcal{F}_2(t)$, is the part of $\mathcal{F}(t)|_{\varphi=0}$ with vanishing velocity $\dot{a}(t) = 0$. Along $\mathcal{F}_1(t)$ the usual Euler-Lagrange equation $\chi'[\dot{a}(t)] = 0$ holds, whereas along $\mathcal{F}_2(t)$ the inequality $\chi'[\dot{a}(t)] \geq 0$ has to be satisfied. Accordingly, at all $s \in \mathcal{F}(t)|_{\varphi=0}$ the Karush-Kuhn-Tucker conditions hold:

$$\dot{a}(t) \geq 0, \quad \chi'[\dot{a}(t)] \geq 0, \quad \chi'[\dot{a}(t)]\dot{a}(t) = 0 \tag{2.72}$$

In view of closed form (2.68), one has:

$$\chi[\dot{a}(t)] = -\frac{1-\nu^2}{E}\dot{a}(t)\left[q[a(t)]\dot{a}(t) + 2\frac{r[a(t)]}{\kappa(t)}\left.\frac{\partial\kappa}{\partial t}\right|_t\right] \tag{2.73}$$

with:

$$\begin{aligned} q[a(t)] &= \int_0^{2\pi a(t)} K_1(a(t))\cdot K_0^{(1)}(t)\,ds \\ &= \frac{4\kappa^2(t)\left(a(t)-\sqrt{a^2(t)-a_{imp}^2}\right)\left(a^2(t)+a_{imp}^2-a(t)\sqrt{a^2(t)-a_{imp}^2}\right)}{\pi\sqrt{a^4(t)-a^2(t)a_{imp}^2}} \\ r[a(t)] &= \int_0^{2\pi a(t)} K_1^2(a(t))\,ds = \frac{8\kappa^2(t)}{\pi}\left(a(t)-\sqrt{a^2(t)-a_{imp}^2}\right)^2 \end{aligned} \tag{2.74}$$

Along $\mathcal{F}_1(t)$ the minimizer of functional (2.73) must satisfy the Euler-Lagrange equation:

$$-2\frac{1-\nu^2}{E}\left[q[a(t)]\dot{a}(t) + \frac{r[a(t)]}{\kappa(t)}\left.\frac{\partial\kappa}{\partial t}\right|_t\right] = 0 \tag{2.75}$$

By "time" integration one gets:

$$\log\frac{\kappa(t)}{\kappa_0} = \frac{1}{2}\log\frac{a(t)}{a_0} + \log\frac{a(t)+\sqrt{a^2(t)-a_{imp}^2}}{a_0+\sqrt{a_0^2-a_{imp}^2}} \tag{2.76}$$

having set $a(0)=a_0$ and $\kappa(0)=\kappa_0$. Eq. (2.76) expresses the critical load factor corresponding to the evolution of radius $a(t)$ along $\mathcal{F}_1(t)$. Due to the axial-symmetry of the problem, either $\mathcal{F}_1(t)$ coincides with the whole circular crack front or is empty. In the latter case $\dot{a}(t)=0$ and the inequality:

$$-2\frac{1-\nu^2}{E}\left[q[a(t)]\dot{a}(t) + \frac{r[a(t)]}{\kappa(t)}\left.\frac{\partial\kappa}{\partial t}\right|_t\right] \geq 0 \tag{2.77}$$

is satisfied only by $\left.\frac{\partial\kappa}{\partial t}\right|_t \leq 0$.

For example, setting $K_1(a_0) = K_1^C$ and $a_0 = a_{imp}$, from eq. (2.68) one has:

$$\kappa_0 = \frac{\pi}{2}\frac{K_1^C}{\sqrt{a_0}} \tag{2.78}$$

from which the load factor as a function of the radius follows:

$$\kappa(t) = K_1^C\pi\sqrt{a(t)}\frac{a(t)+\sqrt{a^2(t)-a_{imp}^2}}{2\,a_{imp}^2} \tag{2.79}$$

Eq. (2.79) can be inverted in terms of $a(t)$:

$$a(t) = \frac{1}{48\,\epsilon\,\kappa^2(t)\,K_1^{C2}}\left[\frac{\epsilon^2}{\pi^{2/3}} + \pi^2\epsilon\,K_1^{C4} + \pi^{2/3}K_1^{C4}\left(384\,\kappa^4(t)\,a_{imp}^2 + \pi^4K_1^{C4}\right)\right] \tag{2.80}$$

with

$$\begin{aligned} \epsilon &= \sqrt{3}K_1^{C4}\left(576\,\pi^4\kappa^4(t)\,K_1^{C4}a_{imp}^2\right. \\ &+ \left. 1536\,\kappa^6(t)\,a_{imp}^3\left(\sqrt{3}\sqrt{432\,\kappa^4(t)\,a_{imp}^2+\pi^4K_1^{C4}} + 36\,\kappa^2(t)\,a_{imp}\right) + \pi^8K_1^{C8}\right) \end{aligned} \tag{2.81}$$

Curves (2.79) and (2.80) are plotted in fig. 2.6 in the case $a_{imp}=1/2$ and $K_1^C=1$.

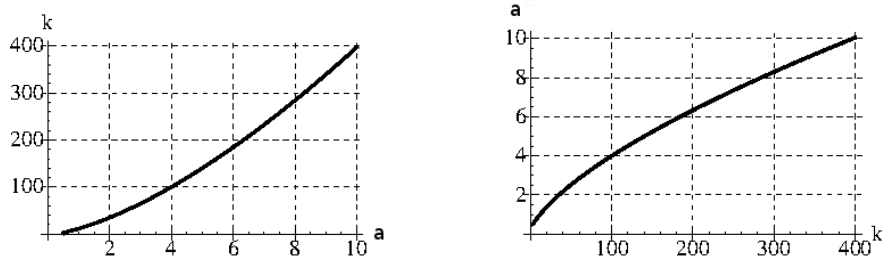

Figure 2.6: *Curves (2.79) and (2.80) in the case* $a_{imp} = 1/2$ *and* $K_1^C = 1$. *They confirm the stable nature of propagation.*

2.6 Appendix A: On the mixed mode propagation

Consider an instant t^* belonging to the time interval $]t, \tau]$ in which the crack front elongates steadily at point s. During stable crack growth, propagation is meant to be a sequence of equilibrium states. At each load $\kappa(t^*)$ a geometry configuration $l(s; t, t^*)$ corresponds which eventually evolves quasi-statically, keeping the SIFs at the onset of crack propagation $\mathbf{K}^*(s, t^*) \in \partial\mathbb{E}$. In time interval $]t, \tau]$ one has at point s:

$$\begin{aligned}\varphi(\mathbf{K}^*(s,t^*)) - \varphi(\mathbf{K}^*(s,t)) &= \frac{1}{2}\Lambda_{11}(K_1^{*2}(s,t^*) - K_1^{*2}(s,t) + K_2^{*2}(s,t^*) - K_2^{*2}(s,t)) \\ &+ \frac{1}{2}\Lambda_{33}(K_3^{*2}(s,t^*) - K_3^{*2}(s,t)) = 0 \quad t^* \in]t,\tau] \end{aligned} \tag{2.82}$$

in view of the MERR onset of propagation (2.11), where Λ_{11} and Λ_{33} are the components of matrix $\mathbf{\Lambda}$ of eq. (2.12). If the crack path in the normal plane at any $s \in \mathcal{F}$ is taken to be smooth in the time interval $]t, \tau]$, in other words along a curve at least of class C^1, then $\forall t^* \in]t, \tau]$ the kinking angle $\theta(s, t^*) = 0$ and $\mathbf{K}^*(t^*) = \mathbf{K}(t^*)$ for being $\mathbb{F} = \mathbb{I}$ in expansion (2.3), with $\mathbb{I}$ denoting the identity matrix. If furthermore one selects the Local Symmetry [47] as a kinking angle criterion, then $K_2^* = 0$ and therefore:

$$\begin{aligned}\varphi(\mathbf{K}^*(s,t^*)) - \varphi(\mathbf{K}^*(s,t)) &= \frac{1}{2}\Lambda_{11}(K_1^*(s,t^*) + K_1^*(s,t))(K_1^*(s,t^*) - K_1^*(s,t)) \\ &+ \frac{1}{2}\Lambda_{33}(K_3^*(s,t^*) + K_3^*(s,t))(K_3^*(s,t^*) - K_3^*(s,t)) = 0 \quad t^* \in]t,\tau] \end{aligned} \tag{2.83}$$

Using SIFs expansions (2.2) and (2.6) one has:

$$\begin{aligned} K_1^*(s,t^*) - K_1^*(s,t) &= \mathbf{e}_1 \cdot \left\{ \mathbf{K}^*(s,t)\frac{\kappa(t^*)}{\kappa(t)} + \mathbf{K}^{(1/2)}(s,t)\frac{\kappa(t^*)}{\kappa(t)}\sqrt{l(s;t,t^*)} \right. \\ &+ \mathbf{K}_0^{(1)}(s,t)\frac{\kappa(t^*)}{\kappa(t)}l(s;t,t^*) + \mathbf{K}_1^{(1)}(s,t)\frac{\kappa(t^*)}{\kappa(t)}\left.\frac{\partial l}{\partial s'}\right|_{s;t,t^*} \\ &+ \left. \mathbf{K}_{nl}^{(1)}[s,t;l(s';t,t^*) - l(s;t,t^*)]\frac{\kappa(t^*)}{\kappa(t)} - \mathbf{K}^*(s,t) \right\} + o(l) \\ &= \mathbf{e}_1 \cdot \left\{ \mathbf{K}^*(s,t)\frac{\delta\kappa}{\kappa(t)} + \mathbf{K}^{(1/2)}(s,t)\sqrt{l(s;t,t^*)} + \mathbf{K}_0^{(1)}(s,t)l(s;t,t^*) \right. \\ &+ \left. \mathbf{K}_1^{(1)}(s,t)\left.\frac{\partial l}{\partial s'}\right|_{s;t,t^*} + \mathbf{K}_{nl}^{(1)}[s,t;l(s';t,t^*) - l(s,t,t^*)] \right\} + o(\delta k \cdot l) \end{aligned} \tag{2.84}$$

where $\mathbf{e}_1$ denotes the unit vector in direction 1 and $\delta\kappa = \kappa(t^*) - \kappa(t)$. Analogously:

$$\begin{aligned} K_3^*(s,t^*) - K_3^*(s,t) &= \mathbf{e}_3 \cdot \left\{ \mathbf{K}^*(s,t)\frac{\delta\kappa}{\kappa(t)} + \mathbf{K}^{(1/2)}(s,t)\sqrt{l(s;t,t^*)} + \mathbf{K}_0^{(1)}(s,t)l(s;t,t^*) \right. \\ &+ \left. \mathbf{K}_1^{(1)}(s,t)\left.\frac{\partial l}{\partial s'}\right|_{s;t,t^*} + \mathbf{K}_{nl}^{(1)}[s,t;l(s';t,t^*) - l(s,t,t^*)] \right\} + o(\delta k \cdot l) \end{aligned} \tag{2.85}$$

where $\mathbf{e}_3$ denotes the unit vector in direction 3. Referring to definition of the quasi-static velocity $v(s,t)$ eq. (2.1) and of the velocity of the load increment eq. (2.33), one has for $t^* \to t^+$:

$$\begin{aligned} 0 &= (\Lambda_{11}K_1^*(s,t)\mathbf{e}_1 + \Lambda_{33}K_3^*(s,t)\mathbf{e}_3) \cdot \mathbf{K}^{(1/2)}(s,t)\sqrt{v(s,t)}\sqrt{t^*-t} \\ &+ (\Lambda_{11}K_1^*(s,t)\mathbf{e}_1 + \Lambda_{33}K_3^*(s,t)\mathbf{e}_3) \cdot \left\{ \frac{\mathbf{K}^*(s,t)}{\kappa(t)}\left.\frac{\partial\kappa}{\partial t}\right|_t + \mathbf{K}_0^{(1)}(s,t)v(s,t) \right. \\ &+ \left. \mathbf{K}_1^{(1)}(s,t)\left.\frac{\partial v}{\partial s'}\right|_{s,t} + \mathbf{K}_{nl}^{(1)}[s,t;v(s',t) - v(s,t)] \right\}(t^*-t) + o(t^*-t) \end{aligned} \tag{2.86}$$

whence the conditions:

$$\frac{\partial\varphi}{\partial\mathbf{K}^*} \cdot \mathbf{K}^{(1/2)}(s,t) = 0 \tag{2.87}$$

$$\frac{\partial\varphi}{\partial\mathbf{K}^*} \cdot \left\{ \frac{\mathbf{K}^*(s,t)}{\kappa(t)}\left.\frac{\partial\kappa}{\partial t}\right|_t + \mathbf{K}_0^{(1)}(s,t)v(s,t) + \mathbf{K}_1^{(1)}(s,t)\left.\frac{\partial v}{\partial s'}\right|_{s,t} + \mathbf{K}_{nl}^{(1)}[s,t;v(s',t) - v(s,t)] \right\} = 0 \tag{2.88}$$

at $\mathbf{K}_2^* = 0$. Equations (2.87) and (2.88) appear to be mandatory requirements for mixed mode crack propagation. Furthermore, the hypothesis of validity of LS as the criterion for crack kinking implies that parameter a^* in eq. (2.4) vanishes at time t. This proposition is easily verified: all functions $\mathbb{G}_{ij}$ vanish at $\theta = 0$ in eq. (2.4) that reduces in this case to:

$$K_i^{(1/2)} = a^*\mathbb{H}_{ij}|_{\theta=0}\, K_j \tag{2.89}$$

for all instants $t^* > t$. For being $K_2^* = K_2 = 0$, expansion (2.4) implies $K_2^{(1/2)} = a^*\mathbb{H}_{21}|_{\theta=0}K_1 = 0$. As $\mathbb{H}_{21}|_{\theta=0} = 3/4$, the geometrical restriction $a^* = 0$ comes out for all instants $t^* > t$. As a^* at time t is defined in the Frenet frame "right after the kink" and as in the limit $t^* \to t$ the Frenet frame $\{O, y_1, y_2\}$ at time t^* converges to the one at time t, so does a^*. One concludes therefore that $a^* = 0$ at time t as well. The proof of vanishing a^* at time t stems merely on the criterion of LS. Eq. (2.87) has been proved making use of the MERR onset of propagation. Onset and criterion convey separate outcomes. Typically, is not possible to obtain $a^* = 0$ via the Griffith approach, in view of the fact that (2.87) holds for all a^* if $\theta = 0$. On the other hand it has been shown that the crack front velocity at the kink must be zero, which cannot be proved by the LS criterion.

If a non smooth propagation after the kink is allowed, $\mathbb{F} \neq \mathbb{I}$ and it is not possible to use expansion (2.2) with respect to the values "before the kink" at time t.

2.7 Appendix B: MERR and LS

MERR onset of propagation uses as magnitude ϑ of eq. (2.7) the energy released during crack advance at any point along the crack front. Such a magnitude is related to stress intensity factors

after a kink via Irwin's formula, recently revisited at a kink by several authors [26, 60] in two dimensions, whence the onset of propagation reads:

$$\varphi(s,t) = \frac{1}{2}(\mathbf{K}^*(s,t)\cdot\mathbf{\Lambda}\mathbf{K}^*(s,t) - G_C) \tag{2.90}$$

It seems extremely desirable, although quite involved, an extension of [26] to the three dimensional case. As its formal derivation in the presence of kinking seems not to be available, the validity of Irwin's formula for $3D$, widely accepted in the fracture mechanics community, is here assumed.

LS and MERR share the same onset of propagation. They differ on the criteria for kinking angle prediction. The kink angle predicted by the MERR descends from the general form (2.9). It reads:

$$\frac{\partial\varphi}{\partial\theta} = \Lambda_{11}\left(K_1^*\frac{\partial K_1^*}{\partial\theta} + K_2^*\frac{\partial K_2^*}{\partial\theta}\right) + \Lambda_{33}\,K_3^*\frac{\partial K_3^*}{\partial\theta} = 0 \tag{2.91}$$

where dependency on s and t has not been made explicit and, as usual, Λ_{11} and Λ_{33} are components of matrix $\mathbf{\Lambda}$ of eq. (2.12). Matrix $\mathbb{F}$ has been defined in terms of the ratio $m = \theta/\pi$ in [82, 83] as :

$$\begin{aligned}
\mathbb{F}_{11}(m) &= 4.1m^{20} + 1.63m^{18} - 4.059m^{16} + 2.996m^{14} - 0.0925m^{12} - 2.88312m^{10} + 5.0779m^8 + \\
&\quad + \left(\frac{\pi^2}{9} - \frac{11\pi^4}{72} + \frac{119\pi^6}{15360}\right)m^6 + \left(\pi^2 - \frac{5\pi^4}{128}\right)m^4 - \frac{3\pi^2m^2}{8} + 1 \\
\mathbb{F}_{12}(m) &= 4.56m^{19} + 4.21m^{17} - 6.915m^{15} + 4.0216m^{13} + 1.5793m^{11} - 7.32433m^9 + 12.313906m^7 + \\
&\quad + \left(-2\pi - \frac{133\pi^3}{180} + \frac{59\pi^5}{1280}\right)m^5 + \left(\frac{10\pi}{3} + \frac{\pi^3}{16}\right)m^3 - \frac{3\pi m}{2} \\
\mathbb{F}_{21}(m) &= -1.32m^{19} - 3.95m^{17} + 4.684m^{15} - 2.07m^{13} - 1.534m^{11} + 4.44112m^9 - 6.176023m^7 + \\
&\quad + \left(-\frac{2\pi}{3} + \frac{13\pi^3}{30} - \frac{59\pi^5}{3840}\right)m^5 - \left(\frac{4\pi}{3} + \frac{\pi^3}{48}\right)m^3 + \frac{\pi m}{2} \\
\mathbb{F}_{22}(m) &= 12.5m^{20} + 0.25m^{18} - 7.591m^{16} + 7.28m^{14} - 1.8804m^{12} - 4.78511m^{10} + 10.58254m^8 + \\
&\quad + \left(-\frac{32}{15} - \frac{4\pi^2}{9} - \frac{1159\pi^4}{7200} + \frac{119\pi^6}{15360}\right)m^6 + \left(\frac{8}{3} + \frac{29\pi^2}{18} - \frac{5\pi^4}{128}\right)m^4 - \left(4 + \frac{3\pi^2}{8}\right)m^2 + 1 \\
\mathbb{F}_{33}(m) &= \left(\frac{1-m}{1+m}\right)^{m/2} \\
\mathbb{F}_{13}(m) &= F_{31}(m) = F_{32}(m) = F_{23}(m) = 0
\end{aligned}$$

It is straightforward to show that at $K_1 \neq 0$ eq. (2.91) is equivalent to:

$$\left[(\mathbb{F}_{11} + \alpha_2\mathbb{F}_{12})\left(\frac{\partial\mathbb{F}_{11}}{\partial\theta} + \alpha_2\frac{\partial\mathbb{F}_{21}}{\partial\theta}\right) + (\mathbb{F}_{21} + \alpha_2\mathbb{F}_{22})\left(\frac{\partial\mathbb{F}_{21}}{\partial\theta} + \alpha_2\frac{\partial\mathbb{F}_{22}}{\partial\theta}\right)\right] + \frac{1}{1-\nu}\,\alpha_3^2\,\frac{\partial\mathbb{F}_{33}}{\partial\theta} = 0 \tag{2.92}$$

where $\alpha_2 = K_2/K_1$ and $\alpha_3 = K_3/K_1$. For a given material (i.e. a given Poisson ratio) at any couple α_2, α_3 the corresponding kink angle θ_{MERR} solves eq. (2.92). At $K_1 = 0$ angle θ_{MERR} is plot as a function of ratio $\alpha_{32} = K_3/K_2$ and of Poisson ratio ν in fig. 2.7.

LS criterion is the only notable exception to the mathematical representation (2.7). It provides the kink angle θ_{LS} through the equation $K_2^* = 0$:

$$\mathbb{F}_{21} + \alpha_2\mathbb{F}_{22} = 0 \tag{2.93}$$

where $\alpha_2 = K_2/K_1$. For any α_2 eq. (2.93) provides the kink angle θ_{LS} which turns out to be independent on the mode 3 stress intensity factor.

Whereas thus in 2D the two angles θ_{MERR} and θ_{LS} differ from very small amounts [124], in $3D$ the scenario changes completely as it can be readily seen in fig. 2.8.

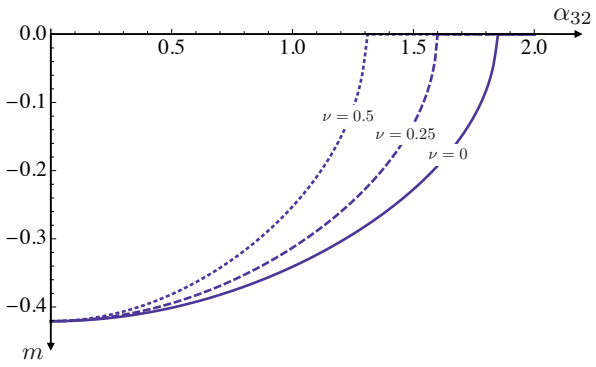

Figure 2.7: *Kink angle $\theta_{MERR} = m\pi$ as a function of the ratio $\alpha_{32} = K_3/K_2$ at $K_1 = 0$ for three different values of the Poisson coefficient ν.*

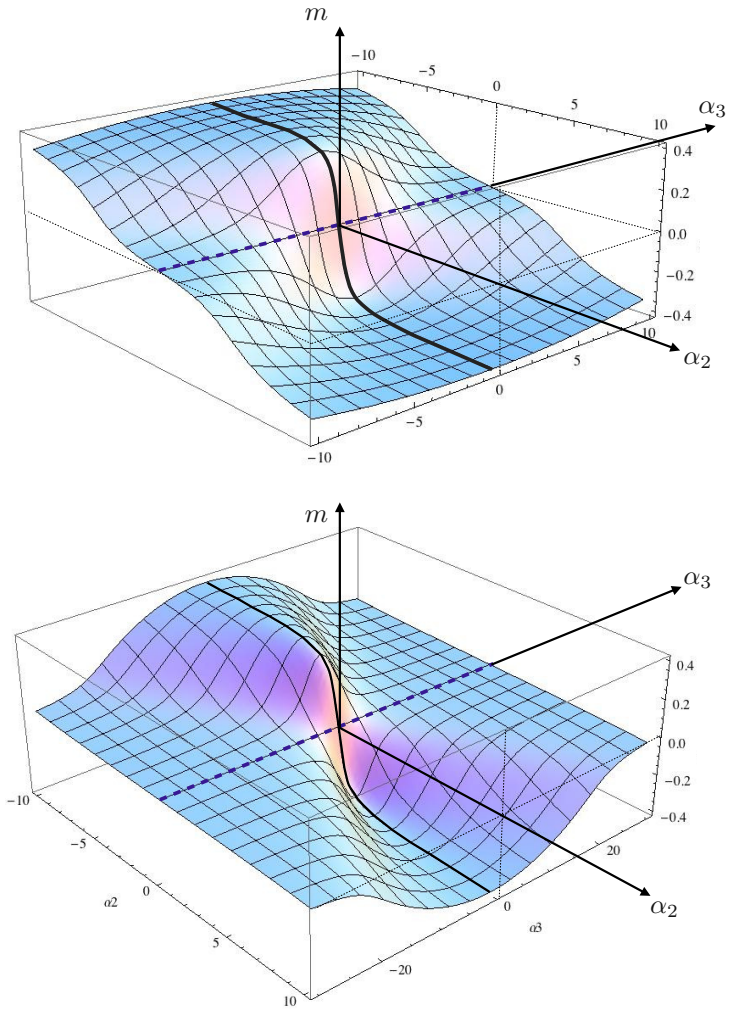

Figure 2.8: *Plot of the kink angle $\theta_{MERR} = m\pi$ as a function of the ratios $\alpha_2 = K_2/K_1$ and $\alpha_3 = K_3/K_1$. At $K_2 = 0$ (mode 1+3) the kinking angle vanishes. At $K_3 = 0$ the plane case is recovered as well as the well known curve θ versus α_2; it is here highlighted with a thick black curve. θ_{MERR} and θ_{LS} differ from very small amounts in the plane case. Accordingly, a visualization of θ_{LS} cannot be distinguished from θ_{MERR} and thus the thick curve recovers θ_{LS} as well. Noteworthy, θ_{LS} is independent upon α_3. It is then easy to envisage the surface plot of angle θ_{LS} as the cylindrical envelope of the thick curve along axis α_3. The higher the mode 3 contribution α_3 the higher the difference in the angle of propagation between LS and MERR. This evidence is clear in the bottom figure, whose axes are not in scale.*

Chapter 3

Numerical approximation of SIFs

Determination of accurate SIFs for mixed-mode loading in complex three dimensional configurations is of fundamental importance in computational linear elastic fracture mechanics.
Many finite element based techniques have been developed and used for representing a crack and consequently compute fracture mechanics parameters. Such techniques can be divided into two main categories: geometrical representations and non geometrical representations.

The first category exploits modeling techniques to explicitly represent the surfaces and the front of the crack.
The second category, on the contrary, exploits constitutive relations or kinematics methods to inform the numerical model of the presence of the crack. In the present Chapter the conventional Finite Element Method, belonging to the first category, and the eXtended Finite Element Method, belonging to the second category, are considered.

In LEFM, square-root singular stress-strain fields exist along the edge of an embedded crack. To deal with this numerical difficulty, quarter-point elements are employed within classical Finite Element Method, and asymptotic near-tip fields enhance the displacement field within the eXtended Finite Element Method. This two techniques are described in the following, together with some of the existing methods employed in the fracture mechanics community to compute SIFs, namely the displacement correlation technique, the modified crack closure integral, the virtual crack extension, and the J-integral.

3.1 Finite Element Method

The Finite Element Method (FEM) is now established as a standard tool to use for the detailed determination of stresses in engineering structures and components. The singular crack front stress and strain fields predicted by the LEFM theory cannot be represented by the polynomial basis functions used for most conventional elements [27]. Henshell and Shaw [56] and Barsoum [11] developed simultaneously and independently the quarter-point elements, which constitute a significant advancement in the FEM for LEFM. They showed that using standard quadratic isoparametric elements and moving the elements' mid-side node to the position that corresponds to one quarter of the way from the crack tip to the far end of the element, the crack front displacement, stress, and strain fields can be properly modeled. Such a milestone procedure introduces a singularity between the element parametric coordinate space and Cartesian space. Henshell and Shaw [56] described a quadrilateral quarter-point element, and Barsoum [11] suggested to collapse one edge of the element at the crack tip. Such two types of plane elements are depicted in figure 3.2-a and b, respectively. In the following Sections, 1D, 2D, and 3D quarter-points elements are briefly described. Cubic

order singular elements are also investigated, in order to analyze the behavior of the 3/2 order term, identified henceforth with Ξ_1, of the crack opening expansion in powers of the distance to the crack front. Such a term constitutes in fact a fundamental ingredient of first order expansion of the SIFs described in Chapter 4 and consequently of the crack tracking algorithm described in Chapter 5. Its accurate approximation is extremely valuable in order to correctly investigate the propagation path of fractures within the variational formulation described below.

3.1.1 1D quarter-point elements

The effect of moving the midside node of a quadratic element to the quarter-point position, is described for the case of a one dimensional element, for which the algebra is simpler than for the two- and three-dimensional elements.

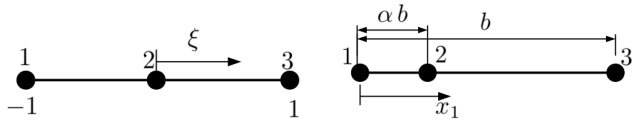

Figure 3.1: *1D quarter-point element: a) parametric coordinate ξ b) Cartesian coordinate x_1.*

Fig 3.1-a shows the parametric coordinate ξ of the element, while figure 3.1-b the Cartesian coordinate x_1, where the location of the center node is controlled by the value of the parameter α and the crack tip is located at $x_1 = 0$.

The displacement u at any point within the element is determined by interpolating the nodal displacements u_i, using standard Lagrange second order shape functions ψ_i:

$$u = \sum_{i=1}^{3} \psi_i(\xi)\, u_i = \frac{1}{2}\xi(\xi-1)u_1 + (1-\xi^2)u_2 + \frac{1}{2}\xi(\xi+1)u_3 = u_2 + \frac{1}{2}(u_3-u_1)\xi + \left(\frac{1}{2}(u_1+u_3) - u_2\right)\xi^2 \tag{3.1}$$

According to the isoparametric formulation, the same shape functions are exploited to interpolate the geometry of the element:

$$x_1 = \sum_{i=1}^{3} \psi_i(\xi)\, x_{1i} = \alpha\, b + \frac{1}{2}\, b\, \xi + b\left(\frac{1}{2} - \alpha\right)\xi^2$$

where b is the length of the element in the Cartesian space. If the center node is located at the mid-side point of the element, i.e. $\alpha = \frac{1}{2}$ and $\xi = \frac{2\,x_1}{b} - 1$, eq. (3.1) reads:

$$u = u_1 + (-3\,u_1 + 4\,u_2 - u_3)\frac{x_1}{b} + 2(u_1 - 2\,u_2 + u_3)\frac{x_1^2}{b^2} \tag{3.2}$$

Differentiating quadratic expression (3.2) with respect to x_1, one obtains the expected linear expression in x_1 for the strain ε in the element:

$$\varepsilon = \frac{du}{dx_1} = (-3\,u_1 + 4\,u_2 - u_3)\frac{1}{b} + 4(u_1 - 2\,u_2 + u_3)\frac{x_1}{b^2}$$

The stress field is also linear in x_1, being linearly related to ε according to the linear elastic condition. If the middle node is moved to the quarter-point position, for which $\alpha = \frac{1}{4}$ and $\xi = \frac{2\sqrt{b\,x_1}}{b} - 1$, eq.

(3.1) reads:

$$u = u_1 + (-3\,u_1 + 4\,u_2 - u_3)\frac{\sqrt{b\,x_1}}{b} + 2(u_1 - 2\,u_2 + u_3)\frac{x_1}{b} \tag{3.3}$$

The square root variation in x_1 of u in eq. (3.3) is the leading term in LEFM expression for the near crack tip displacement. Consequently, the strain field contains the singular term proportional to $x_1^{-1/2}$:

$$\varepsilon = \frac{du}{dx_1} = \left(-\frac{3}{2}\,u_1 + 2\,u_2 - \frac{1}{2}\,u_3\right)\frac{1}{\sqrt{b\,x_1}} + 2(u_1 - 2\,u_2 + u_3)\frac{1}{b} \tag{3.4}$$

3.1.2 2D quarter-point elements

Referring to the element of figure 3.2-a, eq. (3.4) demonstrates that the quarter-point element exhibits the desired strain (and stress) singularities along the quarter-point element edges, namely edges $1-5-2$ and $1-8-4$ in figure 3.2-a.

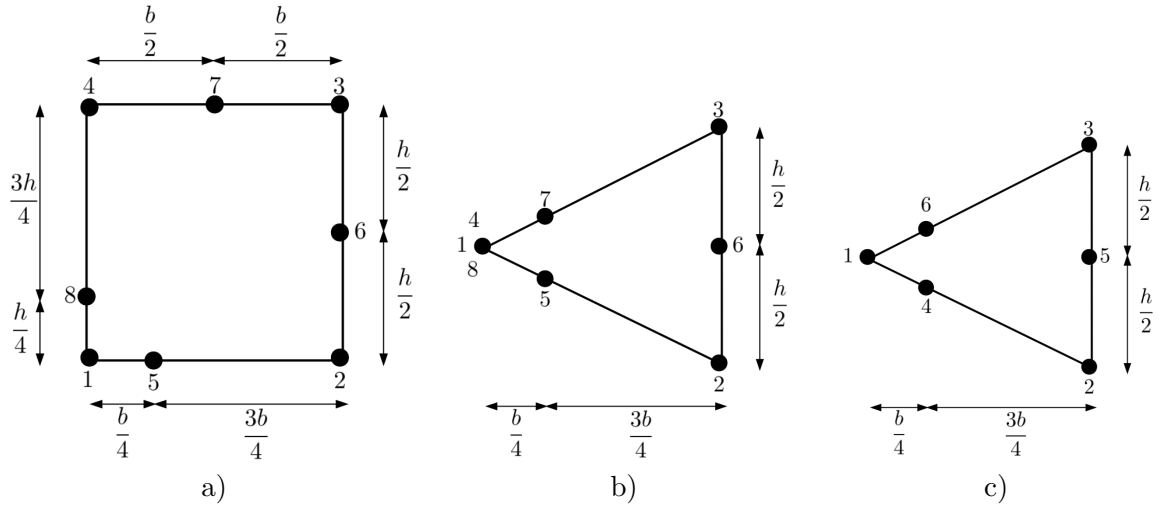

Figure 3.2: *a)Quadrilateral 2D quarter-point element [56] b)Collapsed 2D quarter-point element [11]. Nodes* $1, 4$ *and* 8 *are constrained to move together c) Natural triangular quarter-point element [40].*

However, this is not necessarily the case for all rays through the elements emanating from the crack tip. Barsoum [12] showed that for the collapsed triangular form, the proper singular expression is obtained along all rays emanating from the crack tip, provided that the side node on the edge opposite to the crack tip (node 6 in figure 3.2-b) is placed at the mid point between the two corner nodes (nodes 2 and 3 of figure 3.2-b).

Denoting with r the distance from the crack tip, Freese and Tracey [40] showed that the $r^{-1/2}$ singularity holds along paths of constant parametric coordinate η (see figure 3.3). When the opposite side node is mid-way between the corner nodes, lines of constant η map into straight rays emanating from the crack tip. When such a node is moved from the center position, lines of constant η map into quadratic curves in the Cartesian space and the $r^{-1/2}$ singularity holds along these curves, but not along straight rays.

Freese and Tracey [40] demonstrated that the so called natural triangle quarter-point element (see figure 3.2-c) reproduces the $r^{-1/2}$ singularity along all rays emanating from the crack tip regardless the position of the node opposite the crack front.

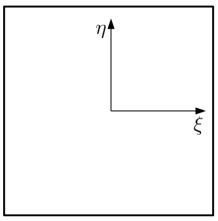

Figure 3.3: *a)Parametric coordinates ξ and η of a quadrilateral element*

Manu [91] showed that the collapsed 9-noded quarter-point element represented in figure 3.4 produces the square root behavior along all rays provided that the far side node 6 is mid way between the far corner nodes 2 and 3 and that the central node 9 is also moved to the quarter-point position.

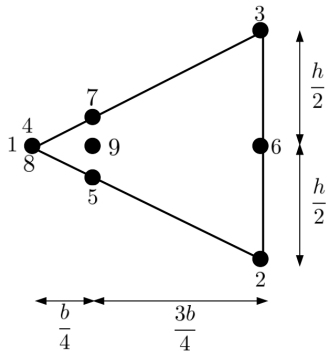

Figure 3.4: *9-noded quarter-point triangular element [91]*

The quadrilateral quarter-point element shown in figure 3.2-a has been used less frequently in practice than the triangular version and this can be partially explained by the fact that fewer of such elements can be conveniently placed around the crack tip and consequently the circumferential variation of the stress and displacement fields about a crack tip may be less accurately represented than in the triangular case. A note by Hibbitt [57] claimed that the strain energy of the quadrilateral quarter-point element of figure 3.2-a was unbounded, but Ying [156] and Bank-Sills and Bortman [6] proved that this assertion is not true. In [6], Bank-Sills and Bortman demonstrated that this element has a square root singularity along all rays emanating from the crack tip, but only if the element has a rectangular shape. Bank-Sills and Einav [7] showed that the singular stress region is slightly larger for nine-noded quadrilateral elements, provided that the central node is suitably positioned at a location on the diagonal between the crack tip and the far corner.

3.1.3 3D quarter-point elements

Three-dimensional quarter-point elements can be created by extruding the 2D forms along the crack front. Barsoum [11] discussed the use of a collapsed 20-noded brick element as the natural extension of the collapsed 8-noded quadrilateral element, considering straight-sided elements were all three element faces are rectangles, as in figure 3.5-a.

Hussain et al. [58], Manu [90], and Koers [68] considered collapsed 20-noded elements with curved crack fronts, see figure 3.5-b. Manu [90] gave constraints on node positioning that must be observed to insure the proper square root singularity on all rays emanating from the crack front.

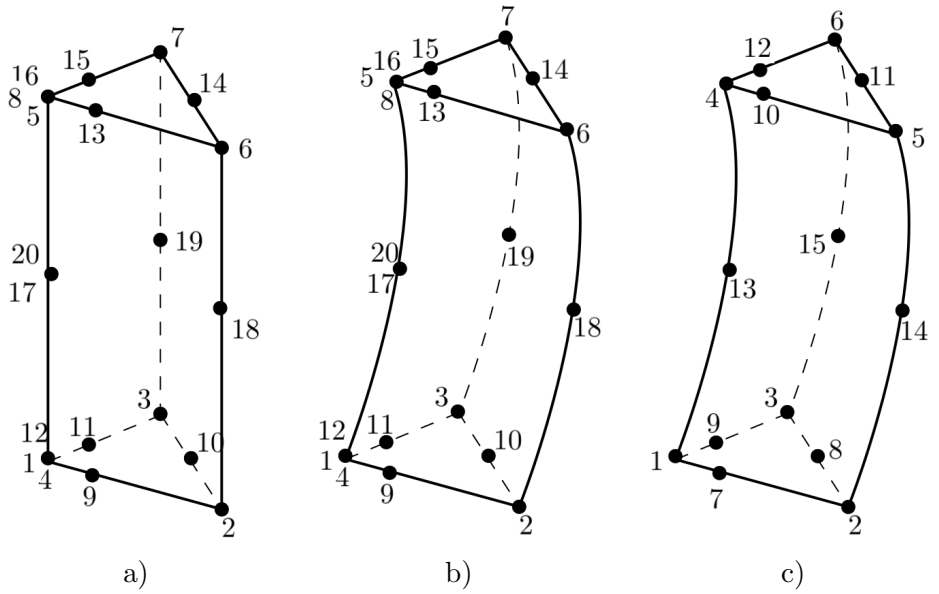

Figure 3.5: *3-dimensional 20-noded collapsed quarter-point element for straight crack fronts, figure a), and for curved crack fronts, figure b). Figure c) depicts 3-dimensional 15-noded quarter-point natural element.*

Referring to notation of figure 3.5-b the constraints that have to be enforced read:

$$\begin{array}{ccc} x_1 = x_4 = x_{12}, & x_{17} = x_{20}, & x_5 = x_8 = x_{16}, \\ x_{10} = (x_2 + x_3)/2, & x_{14} = (x_6 + x_7)/2, & x_9 = (x_1 + x_2)/4, \\ x_{11} = (x_1 + x_3)/4, & x_{13} = (x_5 + x_6)/4, & x_{15} = (x_5 + x_7)/4, \\ x_{18} = (-x_1 + x_2 - x_5 + x_6 + 2x_{17})/2, & x_{19} = (-x_1 + x_3 - x_5 + x_7 + 2x_{17})/2 & \end{array} \tag{3.5}$$

Similar conditions hold for the y and z coordinates of the nodes. The 15-noded natural wedge element represented in figure 3.5-c is of pratical interest, where placement rules similar to those in eq (3.5) have to be observed in order to show that the determinant of the Jacobian mapping matrix is singular along the crack front. Koers [68] showed that if a 20-noded element is further collapsed to a pyramid (see figure 3.6), a square root singularity is found along all rays emanating from the collapsed node.

Bank-Sills [8] and Bank-Sills and Sherman [9] showed that in the hexahedral crack-front element for a straight crack front, the square root singularity is reproduced on all rays emanating from the crack front in each cross section perpendicular to the front if the nodes of such an element are placed so that the element forms a rectangular parallelepiped. For circular crack front, they showed that the square root behavior is observed in all planes perpendicular to the crack front provided that the element edges on and parallel to the crack front are curved to form an arc of a circle.

The trapezoidal, straight-sided version of this element exhibits square root singularity only on the element faces, not on all cross sections. Similarly, for the elliptical crack fronts, if the side faces form hyperbolic surfaces locally normal to the front, then a square root singularity is observed on all hyperbolic surfaces perpendicular to the crack front.

As intuition suggests, if the size of the crack front elements is small compared to the crack front curvature, the difference in geometry between the circular and elliptical/hyperbolic elements and

the trapezoidal approximation is small. The use of the trapezoidal elements is reasonable for the more general case where an analytical description of the crack front shape is not available.

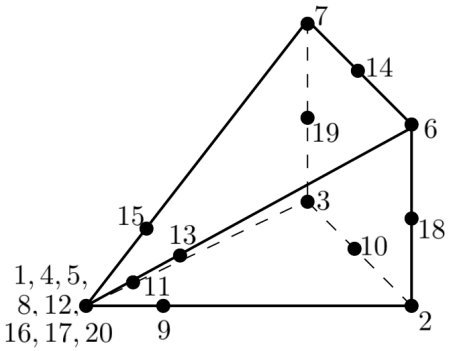

Figure 3.6: *20-noded brick element collapsed to a pyramid [68]*

3.1.4 1D cubic order singular elements

The quarter-point singular mapping can be applied to cubic order isoparametric elements with Lagrangian shape functions.

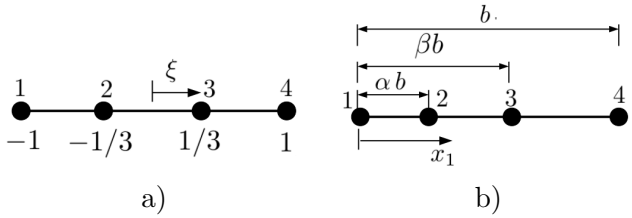

Figure 3.7: *1D cubic order element: a) parametric coordinate ξ b) Cartesian coordinate x_1.*

The expression for the displacement in a 1D element as the linear combination of shape functions $\psi_i(\xi)$ and nodal unknowns u_i results:

$$\begin{aligned} u &= \sum_{i=1}^{4} \psi_i(\xi)\, u_i = \frac{1}{16}(-1+\xi+9\xi^2-9\xi^3)u_1 + \frac{9}{16}(1-3\xi-\xi^2+3\xi^3)u_2 + \\ &+ \frac{9}{16}(1+3\xi-\xi^2-2\xi^3)u_3 + \frac{1}{16}(-1-\xi+9\xi^2+9\xi^3)u_4 \end{aligned} \tag{3.6}$$

If the locations of middle nodes are parametrized by α and β (see figure 3.7-b), the expression that interpolates geometry within the element is:

$$\begin{aligned} x_1 &= \sum_{i=1}^{4} \psi_i(\xi)\, x_{1i} = \frac{9\,\alpha\, b}{16}(1-3\xi-\xi^2+3\xi^3) + \\ &+ \frac{9\,\beta\, l}{16}(1+3\xi-\xi^2-3\xi^3) + \frac{b}{16}(-1-\xi+9\,\xi^2+9\xi^3) \end{aligned}$$

If $\alpha = \frac{1}{9}$ and $\beta = \frac{4}{9}$, such that $\xi = \frac{2\sqrt{b\,x_1}}{b} - 1$, displacement field gains a term proportional to $x_1^{3/2}$ with respect to the quadratic elements case and eq. (3.6) becomes:

$$\begin{aligned} u &= u_1 + \left(-\frac{11}{2}\,u_1 + 9\,u_2 - \frac{9}{2}\,u_3 + u_4\right)\frac{\sqrt{b\,x_1}}{b} + \\ &+ 9\left(u_1 - \frac{5}{2}\,u_2 + 2\,u_3 - \frac{1}{2}u_4\right)\frac{x_1}{b} + \frac{9}{2}\,(-u_1 + 3\,u_2 - 3\,u_3 + u_4)\,\frac{x_1\sqrt{b\,x_1}}{b^2} \end{aligned}$$

Consequently, the strain field gains a term proportional to $x_1^{1/2}$ and has the following expression:

$$\begin{aligned} \varepsilon &= \frac{du}{dx_1} = \frac{1}{2}\left(-\frac{11}{2}\,u_1 + 9\,u_2 - \frac{9}{2}\,u_3 + u_4\right)\frac{1}{\sqrt{b\,x_1}} + \\ &+ 9\left(u_1 - \frac{5}{2}\,u_2 + 2\,u_3 - \frac{1}{2}\,u_4\right)\frac{1}{b} + \frac{27}{4}(-u_1 + 3\,u_2 - 3\,u_3 + u_4)\frac{x_1}{b\sqrt{b\,x_1}} \end{aligned}$$

The near crack tip strain field admits the following series expansion in powers of x_1:

$$\varepsilon = \frac{B_1}{\sqrt{x_1}} + \sum_{i=1}^{+\infty} B_i\, x_1^{(i-1)/2} \tag{3.7}$$

and additional terms in expansion (3.7) can be obtained using elements with higher order basis functions.

3.1.5 2D cubic order singular elements

Consider the parametric and Cartesian description of a cubic 10-noded triangular element shown in figure 3.8.

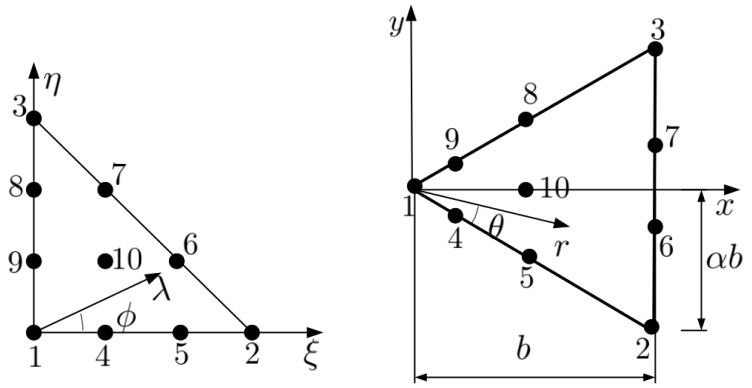

a) b)

Figure 3.8: *10-noded two dimensional element: a) parametric coordinates b) Cartesian coordinates.*

The corresponding nodal coordinates are given in table 3.1.

In order to demonstrate that element depicted in figure 3.8-b is capable of representing a radial displacement variation of the form:

$$\mathbf{u}(r) = \sum_{i=0}^{3} a_i\, r^{i/2} \tag{3.8}$$

Node	ξ	η	x	y
1	0	0	0	0
2	1	0	b	-α b
3	0	1	b	α b
4	1/3	0	b/9	-α b/9
5	2/3	0	4 b/9	-α 4 b/9
6	2/3	1/3	b	-α b/3
7	1/3	2/3	b	α b/3
8	0	2/3	4 b/9	α 4b/9
9	0	1/3	b/9	α b/9
10	1/3	1/3	4 b/9	0

Table 3.1: *Parametric and Cartesian coordinates of 10-noded two dimensional triangular element*

the Cartesian realization of the element is chosen to be symmetric about the x axis. This simplifies subsequent expressions without losing the generality of the results. The shape functions for this element are:

$$\begin{aligned}
\psi_1 &= 1 - \frac{11}{2}\,\xi - \frac{11}{2}\eta + 9\,\xi^2 + 18\,\xi\,\eta + 9\,\eta^2 - \frac{9}{2}\xi^3 - \frac{27}{2}\,\xi^2\,\eta - \frac{27}{2}\,\xi\,\eta^2 - \frac{9}{2}\eta^3,\\
\psi_2 &= \xi - \frac{9}{2}\,\xi^2 + \frac{9}{2}\,\xi^3,\\
\psi_3 &= \eta - \frac{9}{2}\,\eta^2 + \frac{9}{2}\,\eta^3,\\
\psi_4 &= 9\,\xi - \frac{45}{2}\,\xi^2 - \frac{45}{2}\,\xi\,\eta + \frac{27}{2}\,\xi^3 + 27\,\xi^2\,\eta + \frac{27}{2}\,\xi\,\eta^2,\\
\psi_5 &= -\frac{9}{2}\,\xi + 18\,\xi^2 + \frac{9}{2}\,\xi\,\eta - \frac{27}{2}\,\xi^3 - \frac{27}{2}\,\xi^2\,\eta,\\
\psi_6 &= -\frac{9}{2}\,\xi\,\eta + \frac{27}{2}\,\xi^2\,\eta,\\
\psi_7 &= -\frac{9}{2}\,\xi\,\eta + \frac{27}{2}\,\xi\,\eta^2,\\
\psi_8 &= -\frac{9}{2}\,\eta + \frac{9}{2}\,\xi\,\eta + 18\,\eta^2 - \frac{27}{2}\,\xi\,\eta^2 - \frac{27}{2}\eta^3,\\
\psi_9 &= 9\,\eta - \frac{45}{2}\,\xi\,\eta - \frac{45}{2}\,\eta^2 + \frac{27}{2}\,\xi^2\,\eta + 27\,\xi\,\eta^2 + \frac{27}{2}\,\eta^3,\\
\psi_{10} &= 27(\xi\,\eta - \xi^2\,\eta - \xi\,\eta^2)
\end{aligned} \tag{3.9}$$

Consider for example a ray starting at node 1 and extending along the bottom of the element where $\lambda = 0$ and $\theta = \tan^{-1}(-\alpha)$. The distance r can be expressed as:

$$r = \sqrt{x^2 + y^2} \tag{3.10}$$

with

$$\begin{aligned}
x &= \sum_{i=1}^{10} \psi_i(\xi,\eta)\, x_i,\\
y &= \sum_{i=1}^{10} \psi_i(\xi,\eta)\, y_i
\end{aligned} \tag{3.11}$$

Substituting $\xi = \lambda$ and $\eta = 0$ into eq. (3.11) along with the x and y nodal coordinates from table 3.1, yields expressions for x and y in terms of λ. Eq. (3.10) becomes:

$$r = \lambda^2 \, b \, \sqrt{1 + \alpha^2}$$

whence

$$\lambda = \sqrt{\frac{r}{b\sqrt{1+\alpha^2}}} \tag{3.12}$$

The general expression for the interpolated displacement $\mathbf{u}$ in the element:

$$\mathbf{u} = \sum_{i=1}^{10} \psi_i(\xi, \eta) \, \mathbf{u}_i$$

becomes

$$\mathbf{u}(\lambda) = \sum_{i=1}^{10} \psi_i(\lambda, 0) \, \mathbf{u}_i \tag{3.13}$$

along the ray under consideration. Substitution of eq. (3.12) into (3.13), and evaluation of the resulting shape functions (3.9) gives:

$$\begin{aligned} \mathbf{u}(r) &= \mathbf{u}_1 + \frac{1}{2}\sqrt{\frac{r}{b\sqrt{1+\alpha^2}}}\,(-22\,\mathbf{u_1} + 2\,\mathbf{u}_2 + 18\,\mathbf{u}_4 - 9\,\mathbf{u}_5) + \\ &+ \frac{1}{2}\frac{r}{b\sqrt{1+\alpha^2}}\,(18\,\mathbf{u_1} - 9\mathbf{u}_2 - 45\,\mathbf{u}_4 + 36\,\mathbf{u}_5) + \\ &+ \frac{1}{2}\left(\frac{r}{b\sqrt{1+\alpha^2}}\right)^{3/2}(-9\,\mathbf{u}_1 + 9\,\mathbf{u}_2 + 27\,\mathbf{u}_4 - 27\,\mathbf{u}_5) \end{aligned}$$

The same procedure can be adopted to demonstrate the behavior of displacement field of type (3.8) for each ray emanating from the crack tip. Similar results hold for non-symmetric geometries of the element with respect to the x axis, but the resulting expressions for $\mathbf{u}(r)$ become more complicated.

3.1.6 3D cubic order singular elements

A three dimensional triangular prism shaped cubic order element is represented in figure 3.9. The element has 30 nodes, as it implements cubic order displacement variations within triangular cross sections and quadratic order displacement variations along the axis of the element. Four of the nodes on quadrilateral face away from the crack front are constrained and statically condensed in order to make the element compatible with contiguous quadratic order hexahedral elements. Parametric and Cartesian coordinates of such an element are detailed in table 3.2. Referring to figure 3.9-a the element is comprised of three "layers" of 10-nodes in a triangular arrangement. The shape functions for any triangular layer are [133]:

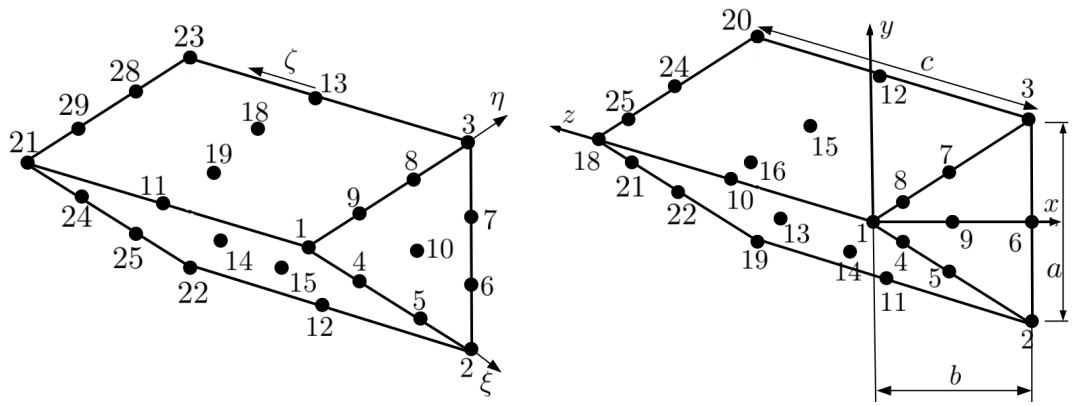

Figure 3.9: *30-noded three dimensional element: a) parametric coordinates b) Cartesian coordinates.*

$$
\begin{aligned}
L_1 &= 1 - \frac{11}{2}(\xi - \eta) + 9(\xi^2 + \eta^2) + 18\xi\eta - \frac{9}{2}(\xi^3 + \eta^3) - \frac{27}{2}(\xi^2\eta + \xi\eta^2),\\
L_2 &= \xi - \frac{9}{2}(\xi^2 + \xi^3),\\
L_3 &= \eta - \frac{9}{2}(\eta^2 + \eta^3),\\
L_4 &= 9\xi - \frac{45}{2}(\xi^2 + \xi\eta) + \frac{27}{2}(\xi^3 + \xi\eta^2) + 27\xi^2\eta,\\
L_5 &= \frac{9}{2}(-\xi + \xi\eta) + 18\xi^2 - \frac{27}{2}(\xi^3 + \xi^2\eta),\\
L_6 &= -\frac{9}{2}\xi\eta + \frac{27}{2}\xi^2\eta,\\
L_7 &= -\frac{9}{2}\xi\eta + \frac{27}{2}\xi\eta^2,\\
L_8 &= \frac{9}{2}(-\eta + \xi\eta) + 18\eta^2 - \frac{27}{2}(\xi\eta^2 + \eta^3),\\
L_9 &= 9\eta - \frac{45}{2}(\xi\eta + \eta^2) + \frac{27}{2}(\xi^2\eta + \eta^3) + 27\xi\eta^2,\\
L_{10} &= 27(\xi\eta - \xi^2\eta - \xi\eta^2)
\end{aligned}
$$

The triangular shape functions are multiplied by quadratic Lagrange polynomials to obtain the 3D shape functions:

$$\psi_i = \frac{1}{2}L_i(\zeta^2 - \zeta), \qquad \psi_{i+10} = L_i(1 - \zeta^2), \qquad \psi_{i+20} = \frac{1}{2}L_i(\zeta^2 + \zeta), \qquad i = 1, ..., 10$$

To make the element compatible with conventional quadratic order elements, the following relationships between the displacements $\mathbf{u}$ of nodes in figure 3.9-a and displacements $\bar{\mathbf{u}}$ of nodes in

Node	ξ	η	ζ	x	y	z
1	0	0	-1	0	0	0
2	1	0	-1	b	-1/2 a	0
3	0	1	-1	b	1/2 a	0
4	1/3	0	-1	1/9 b	-1/18 a	0
5	2/3	0	-1	4/9 b	-2/9 a	0
6	2/3	1/3	-1	b	0	0
7	1/3	2/3	-1	4/9 b	2/9 a	0
8	0	2/3	-1	1/9 b	1/18 a	0
9	0	1/3	-1	4/9 b	0	0
10	1/3	1/3	-1	0	0	1/2 c
11	0	0	0	b	-1/2 a	1/2 c
12	1	0	0	b	1/2 a	1/2 c
13	0	1	0	1/9 b	-1/18 a	1/2 c
14	1/3	0	0	4/9 b	-2/9 a	1/2 c
15	2/3	0	0	4/9 b	2/9 a	1/2 c
16	2/3	1/3	0	1/9 b	1/18 a	1/2 c
17	1/3	2/3	0	4/9 b	0	1/2 c
18	0	2/3	0	0	0	c
19	0	1/3	0	b	-1/2 a	c
20	1/3	1/3	0	b	1/2 a	c
21	0	0	1	1/9 b	-1/18 a	c
22	1	0	1	4/9 b	-2/9 a	c
23	0	1	1	b	0	c
24	1/3	0	1	4/9 b	2/9 a	c
25	2/3	0	1	a/9 b	1/18 a	c
26	2/3	1/3	1	4/9 b	0	c
27	1/3	2/3	1	-	-	-
28	0	2/3	1	-	-	-
29	0	1/3	1	-	-	-
30	1/3	1/3	1	-	-	-

Table 3.2: *Parametric and Cartesian coordinates of 30-noded three dimensional element of figure 3.9*

figure 3.9-b, are written:

$$\begin{array}{cccc}
\mathbf{u}_1 = \bar{\mathbf{u}}_1, & \mathbf{u}_2 = \bar{\mathbf{u}}_2, & \mathbf{u}_3 = \bar{\mathbf{u}}_3, & \mathbf{u}_4 = \bar{\mathbf{u}}_4, \\
\mathbf{u}_5 = \bar{\mathbf{u}}_5, & \mathbf{u}_8 = \bar{\mathbf{u}}_7, & \mathbf{u}_9 = \bar{\mathbf{u}}_8, & \mathbf{u}_{10} = \bar{\mathbf{u}}_9, \\
\mathbf{u}_{11} = \bar{\mathbf{u}}_{10}, & \mathbf{u}_{12} = \bar{\mathbf{u}}_{11}, & \mathbf{u}_{13} = \bar{\mathbf{u}}_{12}, & \mathbf{u}_{14} = \bar{\mathbf{u}}_{13}, \\
\mathbf{u}_{15} = \bar{\mathbf{u}}_{14}, & \mathbf{u}_{18} = \bar{\mathbf{u}}_{15}, & \mathbf{u}_{19} = \bar{\mathbf{u}}_{16}, & \mathbf{u}_{20} = \bar{\mathbf{u}}_{17}, \\
\mathbf{u}_{21} = \bar{\mathbf{u}}_{18}, & \mathbf{u}_{22} = \bar{\mathbf{u}}_{19}, & \mathbf{u}_{23} = \bar{\mathbf{u}}_{20}, & \mathbf{u}_{24} = \bar{\mathbf{u}}_{21}, \\
\mathbf{u}_{25} = \bar{\mathbf{u}}_{22}, & \mathbf{u}_{28} = \bar{\mathbf{u}}_{24}, & \mathbf{u}_{29} = \bar{\mathbf{u}}_{25}, & \mathbf{u}_{30} = \bar{\mathbf{u}}_{26},
\end{array}$$

$$
\begin{aligned}
\mathbf{u}_6 &= \frac{2}{9}\bar{\mathbf{u}}_2 - \frac{1}{9}\bar{\mathbf{u}}_3 + \frac{8}{9}\bar{\mathbf{u}}_6, \\
\mathbf{u}_7 &= -\frac{1}{9}\bar{\mathbf{u}}_2 + \frac{2}{9}\bar{\mathbf{u}}_3 + \frac{8}{9}\bar{\mathbf{u}}_6, \\
\mathbf{u}_{16} &= \frac{2}{9}(\bar{\mathbf{u}}_2 + \bar{\mathbf{u}}_3 + \bar{\mathbf{u}}_{19} + \bar{\mathbf{u}}_{20}) + \frac{4}{9}(\bar{\mathbf{u}}_6 + \bar{\mathbf{u}}_{23}) + \frac{2}{3}\bar{\mathbf{u}}_{11} + \frac{1}{3}\bar{\mathbf{u}}_{12}, \\
\mathbf{u}_{17} &= \frac{2}{9}(\bar{\mathbf{u}}_2 + \bar{\mathbf{u}}_3 + \bar{\mathbf{u}}_{19} + \bar{\mathbf{u}}_{20}) + \frac{4}{9}(\bar{\mathbf{u}}_6 + \bar{\mathbf{u}}_{23}) + \frac{1}{3}\bar{\mathbf{u}}_{11} + \frac{2}{3}\bar{\mathbf{u}}_{12}, \\
\mathbf{u}_{26} &= \frac{2}{9}\bar{\mathbf{u}}_{19} - \frac{1}{9}\bar{\mathbf{u}}_{20} + \frac{8}{9}\bar{\mathbf{u}}_{23}, \\
\mathbf{u}_{27} &= -\frac{1}{9}\bar{\mathbf{u}}_{19} + \frac{2}{9}\bar{\mathbf{u}}_{20} + \frac{8}{9}\bar{\mathbf{u}}_{23}
\end{aligned}
$$

Numerical computation of the 3/2 order term of the crack opening and sliding expansion
Geometrical description of a crack accounts for two boundaries $\mathcal{S}^+$, $\mathcal{S}^-$ which model the lips of the crack (see figure 3.10).

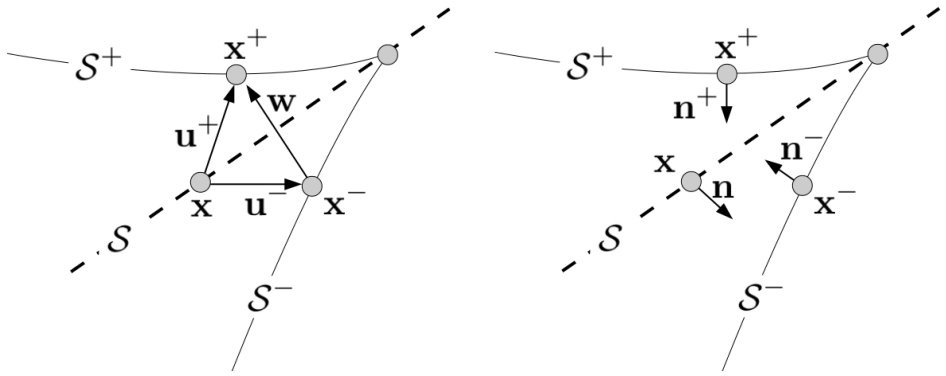

a) Geometry b) Static

Figure 3.10: *Definitions*

At each "time" t, two one-to-one applications $\mathbf{u}^+$, $\mathbf{u}^-$ between the reference surface $\mathcal{S}$ and $\mathcal{S}^+$, $\mathcal{S}^-$ are set, such that:

$$
\begin{aligned}
\forall \mathbf{x}^+(t) \in \mathcal{S}^+ \; \exists ! \, \mathbf{x} \in \mathcal{S} \; : \; \mathbf{u}^+(t) = \mathbf{x}^+(t) - \mathbf{x} \\
\forall \mathbf{x}^-(t) \in \mathcal{S}^- \; \exists ! \, \mathbf{x} \in \mathcal{S} \; : \; \mathbf{u}^-(t) = \mathbf{x}^-(t) - \mathbf{x}
\end{aligned}
$$

with the property that at initial time $t = 0$:

$$\mathbf{u}^+(0) = \mathbf{u}^-(0) = 0$$

The displacement discontinuity $\mathbf{w}(\mathbf{x}, t)$, also referred as "relative opening and sliding", is defined as:

$$\mathbf{w}(\mathbf{x}, t) = \mathbf{u}^+(t) - \mathbf{u}^-(t) \tag{3.14}$$

On both $\mathcal{S}^+$, $\mathcal{S}^-$ outwards normals, say $\mathbf{n}^+$, $\mathbf{n}^-$ are well defined. The hypothesis of small displacements implies:

$$\mathbf{n}^+ = -\mathbf{n}^-$$

In each point $\mathbf{x}$ of the crack surface $\mathcal{S}$, the normal component of crack opening defined as in eq. (3.14) at time t, indicated with $w(\mathbf{x}, t)$, admits an expansion in the normal plane in terms of the distance to the crack front r [54]:

$$w(\mathbf{x}, t) = \sum_{n=0}^{+\infty} \Xi_n(s, t)\, r^n \sqrt{r} \tag{3.15}$$

where s indicates as usual the curvilinear abscissa along the crack front $\mathcal{F}$.

3D cubic order singular elements depicted in figure 3.9 have been implemented in a finite element code in order to test the accuracy in the computation of the $\Xi_1(s, t)$ term defined in eq. (3.15).

Consider the benchmark of a circular crack with radius $a = 10$ in an infinite domain (such an approximation has been obtained in the finite element framework embedding the circular crack in a cylindrical domain with radius 10 times greater than a and height 20 times greater than a), subject to uniform tractions applied over the full crack faces with magnitude equal to the load factor κ, chosen with a unit value, as in figure 3.11.

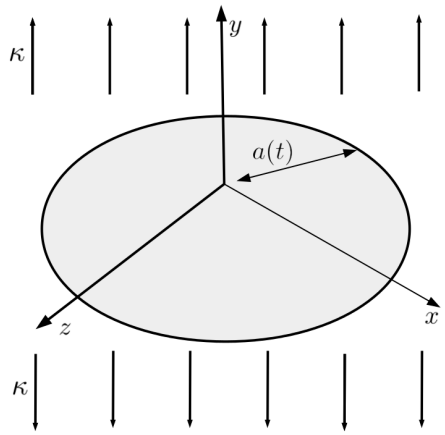

Figure 3.11: *Penny shape crack of radius $a(t)$ in an infinite linear elastic homogeneous domain subject to uniform tractions κ.*

Analytical solution of the crack opening $w(\mathbf{x}, t)$ for the problem at hand reads [54]:

$$w(\mathbf{x}, t) = \frac{4(1-\nu)}{\mu\,\pi} \kappa \sqrt{a^2(t) - (a(t) - r(\mathbf{x}, t))^2} \tag{3.16}$$

whence

$$\Xi_0(t) = \frac{4\,\kappa\,\sqrt{2\,a(t)}(1-\nu)}{\mu\,\pi}, \qquad \Xi_1(t) = -\frac{\kappa\sqrt{2}(1-\nu)}{\sqrt{a(t)}\,\mu\,\pi} \tag{3.17}$$

where ν is the Poisson's ratio and μ is the shear modulus of the bulk material. Considering fictitious values for material parameters, namely Young's modulus $E = 100$ and $\nu = 0.3$, graph 3.12 represents the obtained results for $w(\mathbf{x}, t)$, where $FE\,min$, $FE\,max$, and $FE\,mean$ refer to the minimum, to the maximum, and to the average value, respectively, obtained along the crack front in the finite element analysis.

Assume that the crack opening w is:

$$w(\mathbf{x}, t) = a_1 \sqrt{\frac{r}{b}} + a_2 \frac{r}{b} + a_3 \frac{r}{b} \sqrt{\frac{r}{b}} \tag{3.18}$$

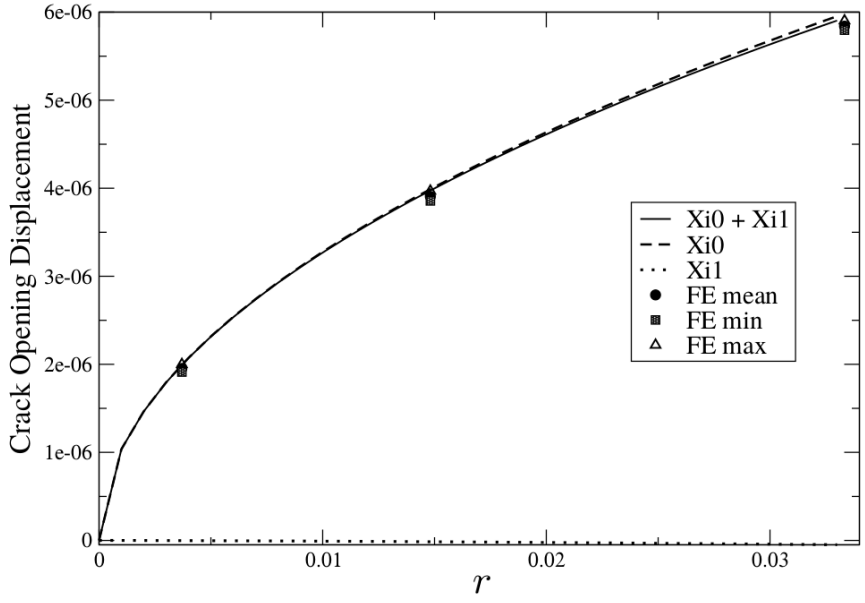

Figure 3.12: *Crack opening $w(\mathbf{x}, t)$ with respect to the distance from the crack front r. Continuous and dashed lines refer to the analytical values for Ξ_0 and Ξ_1 (3.17). Symbols refer to the finite element analysis results, exploiting cubic order 3D elements represented in figure 3.9.*

where b is the crack front element size (see figure 3.9-b), equal to $1/3$ in this finite element analysis. Evaluating (3.18) at the two side nodes and one corner node location, the following system is obtained:

$$\begin{Bmatrix} 1/3 & 1/9 & 1/27 \\ 2/3 & 4/9 & 8/27 \\ 1 & 1 & 1 \end{Bmatrix} \begin{Bmatrix} a_1 \\ a_2 \\ a_3 \end{Bmatrix} = \begin{Bmatrix} w_1 \\ w_2 \\ w_3 \end{Bmatrix}$$

which gives coefficients:

	$FE\,min$	$FE\,max$	$FE\,mean$
a_1	$5.65E-05$	$6.02E-05$	$5.84E-05$
a_2	$2.90E-06$	$-1.25E-06$	$7.87E-07$
a_3	$-1.45E-06$	$-1.03E-07$	$-7.97E-07$

and correspondent percentage errors on values of Ξ_0 and Ξ_1 with respect to the analytical values (3.17):

	$\%(Analytical - FE\,min)$	$\%(Analytical - FE\,max)$	$\%(Analytical - FE\,mean)$
Ξ_0	5.61	-0.59	2.39
Ξ_1	-30.38	90.80	28.49

Even if all the values of the crack opening w computed with the FEM are within a small percentage of error (5%) with respect to the analytical solution (3.16), and the Ξ_0 values determined from

fitting the FE displacements show similar level of accuracy, the errors in the Ξ_1 values are almost one order of magnitude greater. In addition, values of Ξ_1 result much more sensitive with respect to the values of Ξ_0 to small variations in the FE displacements, being orders of magnitude smaller than Ξ_0. The near crack front crack opening behavior is dominated by the square root term Ξ_0, as proved in figure 3.12. Consequently it appears that extracting high quality Ξ_1 terms is not possible exploiting displacements from the crack front elements only, at least for models where the ratio between the crack front elements size and the crack radius b/a is of order 1/10 (in the presented analysis $b/a = 1/30$). Larger crack front elements might increase the significance of the 3/2 term, but the quality of the computed SIFs would likely decrease.

Pursuing the idea to not exploit crack front elements only, consider the component u_y of theoretical near front displacement field expressed as the Williams expansion [66]:

$$u_y = \sum_{n=1}^{+\infty} \frac{r^{n/2}}{2\,\mu}\, a_n \left[\left(3 - 4\nu - \frac{n}{2} - (-1)^n\right) \sin\frac{n\theta}{2} - \frac{n}{2} \sin\left(\frac{n}{2} - 2\right)\theta \right] \tag{3.19}$$

where $\{r, \theta\}$ are, as usual, the local polar coordinates in each point along the crack front. Matching eq.(3.19) and (3.15) for the 1/2 and 3/2 terms, one obtains:

$$\begin{aligned} u_y(n = 1, \theta = \pi) &= \frac{r^{1/2}}{2\,\mu} a_1 (4 - 4\,\nu) = \Xi_0\, r^{1/2} \\ u_y(n = 3, \theta = \pi) &= \frac{r^{3/2}}{2\,\mu} a_3 (-4 + 4\,\nu) = \Xi_1\, r^{3/2} \end{aligned}$$

whence

$$\Xi_0 = a_1 \frac{2(1-\nu)}{\mu}, \qquad \Xi_1 = a_3 \frac{2(\nu - 1)}{\mu}$$

Extracting displacements from the crack front cubic-order singular wedge elements and two rings of brick elements surrounding the crack front, and deriving coefficients a_1 and a_3 of eq. (3.19) using a least square fit, one obtains:

	$\%(Analytical - FE\,min)$	$\%(Analytical - FE\,max)$	$\%(Analytical - FE\,mean)$
Ξ_0	1.42	2.39	2.01
Ξ_1	18.40	1.29	2.58

Numerical approximation of the 3/2 order coefficient Ξ_1 of the crack opening expansion (3.15) reaches a percentage difference with respect to the analytical solution (3.17) less then 3% for the mean value. The same procedure using standard quarter-point wedge elements represented in figure 3.5 leads to the following results:

	$\%(Analytical - FE\,min)$	$\%(Analytical - FE\,max)$	$\%(Analytical - FE\,mean)$
Ξ_0	5.61	−0.59	2.39
Ξ_1	−10.21	3.49	7.67

3.2 eXtended Finite Element Method

The use of singular elements described in Section 3.1 forces to reconstruct a new finite element mesh each time a crack is propagated in order to match the geometry of the discontinuity. The eXtended Finite Element Method (XFEM) avoids such remeshing operations enhancing the displacement field by means of additional degrees of freedom which are added to the existing nodes of the finite element

mesh. A crack can therefore be extended during the simulation at any time and in any direction by adding new degrees of freedom leaving the number of nodes and elements within the mesh unaltered, as well as their mutual connectivity. The method exploits a property of the standard finite element shape functions that has been acknowledged in the seminal paper of Babuška and Melenk [5], in conjunction with a discontinuous mode and the near-tip asymptotic fields incorporated at the element level presented by Moës et al. [97]. The method is briefly described in the following Sections for a 2D crack. Specifically, the case of an internal line across which the displacement filed may be discontinuous is considered. Moës et al. [98] applied the method for fractures in three-dimensional specimens.

3.2.1 Problem formulation

Consider the domain $\Omega \in \mathbb{R}^2$ bounded by $\Gamma \equiv \partial\Omega$. The boundary Γ is composed by Γ^u , Γ^p, and $\mathcal{S}$, such that $\Gamma = \Gamma^u + \Gamma^p + \mathcal{S}$. The domain is crossed by the discontinuity $\mathcal{S}$ and the two resulting part of the domain are denoted by Ω^+ and Ω^- as depicted in figure 3.13. Prescribed displacements $\bar{\mathbf{u}}$ are imposed on Γ^u while tractions $\bar{\mathbf{p}}$ are imposed on Γ^p. The crack surface $\mathcal{S}$ is assumed to be traction-free.

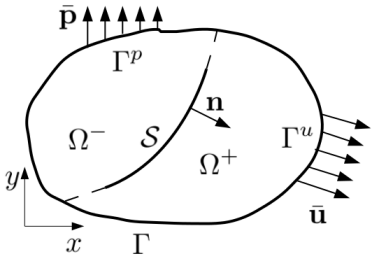

Figure 3.13: *A domain Ω is crossed by a discontinuity $\mathcal{S}$ that divides the domain in two parts denoted with Ω^+ and Ω^-, respectively.*

The equilibrium equations and boundary conditions are:

$$\begin{aligned} \operatorname{div}[\boldsymbol{\sigma}] + \mathbf{f} &= \mathbf{0} \quad in \quad \Omega \\ \boldsymbol{\sigma}\,\mathbf{n} &= \bar{\mathbf{p}} \quad on \quad \Gamma^p \end{aligned} \tag{3.20a}$$

Since the discontinuity $\mathcal{S}$ can be considered as an internal boundary, the following traction-free conditions can be added to equations (3.20a):

$$\begin{aligned} \boldsymbol{\sigma}\,\mathbf{n} &= \mathbf{0} \quad on \quad \mathcal{S}^+ \\ \boldsymbol{\sigma}\,\mathbf{n} &= \mathbf{0} \quad on \quad \mathcal{S}^- \end{aligned} \tag{3.20b}$$

where $\boldsymbol{\sigma}$ is the Cauchy stress, $\mathbf{f}$ is the body force vector per unit volume and $\mathbf{n}$ is the outward normal pointing into Ω^+, see figure 3.13. In the hypothesis of small strains and displacements, the kinematics equations consist of the strain displacement relation:

$$\boldsymbol{\varepsilon} = \boldsymbol{\varepsilon}(\mathbf{u}) = \nabla_s \mathbf{u} \tag{3.20c}$$

where ∇_s is the symmetric part of the gradient operator, and the boundary condition:

$$\mathbf{u} = \bar{\mathbf{u}} \;\; on \;\; \Gamma^u \tag{3.20d}$$

The constitutive equation is given by the Hooke's law:

$$\boldsymbol{\sigma} = \mathbb{C} : \boldsymbol{\varepsilon} \tag{3.20e}$$

where $\mathbb{C}$ is the Hooke tensor.

Weak form
In order to write the weak form of the problem formulation (3.20), the space of admissible displacement fields is defined by:

$$\mathscr{U} = \{\mathbf{v} \in \mathscr{V} \ : \ \mathbf{v} = \bar{\mathbf{u}} \ \textit{on} \ \Gamma^u, \ \ \mathbf{v} \ \textit{discontinuous on} \ \mathcal{S}\} \tag{3.21}$$

where the space $\mathscr{V}$ is related to the regularity of the solution. It suffices to point out here that it allows for discontinuous functions across the crack line. The test function space is similarly defined as :

$$\mathscr{U}_0 = \{\delta\mathbf{u} \in \mathscr{V} : \delta\mathbf{u} = 0 \ \textit{on} \ \Gamma^u, \ \ \delta\mathbf{u} \ \textit{discontinuous on} \ \mathcal{S}\} \tag{3.22}$$

The weak form of the equilibrium equations is given by:

$$\int_\Omega \boldsymbol{\sigma} : \boldsymbol{\varepsilon}(\delta\mathbf{u}) \, d\Omega = \int_\Omega \mathbf{f} \cdot \delta\mathbf{u} \, d\Omega + \int_{\Gamma^p} \bar{\mathbf{p}} \cdot \delta\mathbf{u} \, d\Gamma \ \ \forall \delta\mathbf{u} \in \mathscr{U}_0 \tag{3.23}$$

By means of the constitutive relation (3.20e) and the kinematics constraints in the weak form, the problem is to find $\mathbf{u} \in \mathscr{U}$ such that:

$$\int_\Omega \boldsymbol{\varepsilon}(\mathbf{u}) \ : \ \mathbb{C} \ : \ \boldsymbol{\varepsilon}(\delta\mathbf{u}) \, d\Omega = \int_\Omega \mathbf{f} \cdot \delta\mathbf{u} \, d\Omega + \int_{\Gamma^p} \bar{\mathbf{p}} \cdot \delta\mathbf{u} \, d\Gamma \ \ \forall \delta\mathbf{u} \in \mathscr{U}_0 \tag{3.24}$$

It is shown in [15] that eq. (3.24) is equivalent to strong form (3.20a), if one includes the traction-free conditions (3.20b) on the two crack faces.

Enrichment of the displacement field
Incorporating the displacement jump in the analytical displacement field before performing the spatial discretization of the model, makes the discontinuity truly a part of the boundary value problem and avoids mesh dependent solutions. A way to introduce a discontinuity in a continuous and smooth displacement field is presented by Belytschko and Black [15] and consists in adding a second displacement field multiplied by a step function to the existing displacement field. Furthermore, as described by Moës et al. [97], the near-tip asymptotic fields are incorporated in the displacement field in order to properly take into account the presence of a crack tip in the LEFM framework. The total displacements field $\mathbf{u}$ consists of a continuous regular field $\hat{\mathbf{u}}$ and two additional continuous displacements fields $\breve{\mathbf{u}}$ and $\tilde{\mathbf{u}}$ multiplied by the step function and by the near-tip asymptotic fields, respectively:

$$\mathbf{u}(\mathbf{x}, t) = \hat{\mathbf{u}}(\mathbf{x}, t) + \mathcal{H}_\mathcal{S}(\mathbf{x}) \, \breve{\mathbf{u}}(\mathbf{x}, t) + \mathbf{F}(\mathbf{x}) \, \tilde{\mathbf{u}}(\mathbf{x}, t) \tag{3.25}$$

$\mathcal{H}_\mathcal{S}$ is a function which is constant on either side of the discontinuity:

$$\mathcal{H}_\mathcal{S} = \begin{cases} \mathcal{H}^+ & if \quad \mathbf{x} \in \Omega^+ \\ \mathcal{H}^- & if \quad \mathbf{x} \in \Omega^- \end{cases} \tag{3.26}$$

The magnitude of the displacement jump h is equal to the magnitude of the additional field $\breve{\mathbf{u}}$ exactly at the discontinuity:

$$h = \mathcal{H}^+ - \mathcal{H}^- \tag{3.27}$$

Jump function	$\mathcal{H}^+$	$\mathcal{H}^-$	h
Heaviside	1	0	1
Symmetric	1/2	-1/2	1
Unit Symmetric	1	-1	2

Table 3.3: *An overview of different step functions $\mathcal{H}_{\mathcal{S}}$ that can be used to create a jump in the displacement field.*

An overview of possible step functions is given in table 3.3.

Matrix $\mathbf{F}$ in eq.(3.25) contains the asymptotic near-tip fields defined as:

$$\{F_l(r,\theta)\} = \left\{\sqrt{r}sin\left(\frac{\theta}{2}\right), \sqrt{r}cos\left(\frac{\theta}{2}\right), \sqrt{r}sin\left(\frac{\theta}{2}\right)sin(\theta), \sqrt{r}cos\left(\frac{\theta}{2}\right)sin(\theta)\right\} \tag{3.28}$$

where $\{r,\theta\}$ are the local polar coordinates at the crack tip. Note that the first function in (3.28), namely $\sqrt{r}sin\,(\theta/2)$, is discontinuous across the crack faces whereas the last three functions are continuous. The strain field is found by taking the derivative of the displacement field (3.25) with respect to the position in the body $\mathbf{x}$:

$$\boldsymbol{\varepsilon}(\mathbf{x},t) = \nabla_s\hat{\mathbf{u}}(\mathbf{x},t) + \mathcal{H}_{\mathcal{S}}\nabla_s\breve{\mathbf{u}}(\mathbf{x},t) + \nabla_s(\mathbf{F}(\mathbf{x})\tilde{\mathbf{u}}(\mathbf{x},t)) \quad \mathbf{x} \notin \mathcal{S} \tag{3.29}$$

Assuming zero body forces, weak form (3.23) becomes:

$$\begin{aligned}\int_\Omega \boldsymbol{\sigma} : \nabla_s\hat{\mathbf{u}}\, d\Omega \;\; + \;\; \int_\Omega \mathcal{H}_{\mathcal{S}}\,\boldsymbol{\sigma} : \nabla_s\breve{\mathbf{u}}\, d\Omega + \int_\Omega \boldsymbol{\sigma} : \nabla_s(\mathbf{F}\tilde{\mathbf{u}})\, d\Omega = \\ \int_{\Gamma^p} \bar{\mathbf{p}}\cdot\hat{\mathbf{u}}\, d\Gamma \;\; + \;\; \int_{\Gamma^p} \mathcal{H}_{\mathcal{S}}\,\bar{\mathbf{p}}\cdot\breve{\mathbf{u}}\, d\Gamma + \int_{\Gamma^p} \bar{\mathbf{p}}\cdot\mathbf{F}\tilde{\mathbf{u}}\, d\Gamma\end{aligned} \tag{3.30}$$

where the first term on the left hand side of equation (3.30) describes the internal forces in the body due to the regular displacement field, whereas the second and the third term represent the internal forces due to the additional displacement fields. The right hand side of the equation contains terms related to prescribed tractions imposed on the external boundary of the domain.

3.2.2 Finite element formulation

As usual in the finite element formulation, the domain Ω is divided into a number of elements with finite volume ω, which are supported by nodes as depicted in figure 3.14.

It was shown in [5] that when a field $f(\mathbf{x},t)$ is not continuous, it can be still discretized using the finite element shape functions $\psi_i(\mathbf{x})$ in combination with an enhanced basis function exploiting the partition of unity property of the finite element shape functions, namely:

$$f(\mathbf{x},t) = \sum_{i=1}^{n_{nod}} \psi_i(\mathbf{x}) \left(a_i(t) + \sum_{j=1}^{m} \gamma_j(\mathbf{x})\, b_{ij}(t) \right) \tag{3.31}$$

where n_{nod} is the number of the mesh nodes, $a_i(t)$ are the regular degrees of freedom, $\gamma_j(\mathbf{x})$ is an enhanced basis with m orthogonal terms and $b_{ij}(t)$ are the additional nodal degrees of freedom that support the enhanced basis functions. Shape function associated with node i is equal to 1 in node i and 0 in all other nodes; additionally the set of shape functions possesses the already mentioned

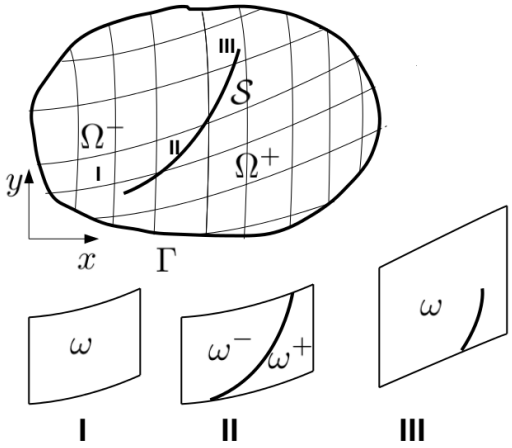

Figure 3.14: *Subdivision of the domain Ω into finite elements supported by n_{nod} nodes. Element I is a regular element with integration volume ω. Element II is crossed by a discontinuity, which can be considered as an internal boundary S_ω. The integration domain is split into two parts: ω^+ and ω^-. Element III contains the crack tip.*

partition of unity property, which implies that the sum of all shape functions in an arbitrary point $\mathbf{x}$ of the domain is equal to 1:

$$\sum_{i=1}^{n_{nod}} \psi_i(\mathbf{x}) = 1 \qquad \forall \mathbf{x} \in \Omega$$

The part of the domain for which the magnitude of the shape function of node i is non zero is called the support of the node. In the case of standard isoparametric shape functions, the support of a node is identical to the compact set of elements attached to that node. Number m of enhanced basis functions may be different for each node i in the model. However, in order to avoid linear dependency, the enhanced basis γ_j and the shape functions ψ_i may not originate from the same span of functions.

In this case of a single discontinuity in LEFM framework, the discrete displacement field $\mathbf{u}^h$ becomes:

$$\mathbf{u}^h(\mathbf{x},t) = \sum_{i=1}^{n_{nod}} \psi_i(\mathbf{x}) \left(a_i(t) + \mathcal{H}_\mathcal{S}(\mathbf{x}) b_i(t) + \sum_{l=1}^{4} F_l(\mathbf{x})\, c_i^l(t) \right) \tag{3.32}$$

where $a_i(t)$ are the regular degrees of freedom, while $b_i(t)$ and $c_i^l(t)$ are the additional degrees of freedom of node i. Alternatively, the discrete displacement field $\mathbf{u}^h$ in (3.32) can be cast in the following matrix form for a single element:

$$\mathbf{u}^h = \mathbf{N}\,\mathbf{a} + \mathcal{H}_\mathcal{S}\mathbf{N}\,\mathbf{b} + \mathbf{N}\,\mathbf{F}\,\mathbf{c} \tag{3.33}$$

where matrix $\mathbf{N}$ contains the shape functions for all the nodes that support this element, and $\mathbf{a}, \mathbf{b}$ and $\mathbf{c}$ are the vectors of the regular and additional degrees of freedom.

The strain field in matrix form, obtained by differentiating the discrete displacement field (3.33) with respect to $\mathbf{x}$, reads:

$$\boldsymbol{\varepsilon}^h = \mathbf{B}\,\mathbf{a} + \mathcal{H}_\mathcal{S}\,\mathbf{B}\,\mathbf{b} + \mathbf{G}\,\mathbf{c} \quad \mathbf{x} \notin S \tag{3.34}$$

where:

$$\begin{aligned} \mathbf{B} &= \nabla_s \mathbf{N} \\ \mathbf{G} &= \nabla_s (\mathbf{N}\,\mathbf{F}) \end{aligned} \tag{3.35}$$

Admissible test functions $\delta\mathbf{u}$ can be decomposed in a regular and additional fields as the actual displacement field (3.25):

$$\delta\mathbf{u}(\mathbf{x}) = \delta\hat{\mathbf{u}} + \mathcal{H}_{\mathcal{S}}\,\delta\breve{\mathbf{u}} + \mathbf{F}\delta\tilde{\mathbf{u}}$$

According to discretization (3.33):

$$\begin{aligned} \delta\hat{\mathbf{u}}^h &= \mathbf{N}\,\delta\mathbf{a}; \quad \delta\breve{\mathbf{u}}^h = \mathbf{N}\,\delta\mathbf{b}; \quad \mathbf{F}\,\delta\tilde{\mathbf{u}}^h = \mathbf{N}\,\mathbf{F}\,\delta\mathbf{c}; \\ \nabla_s\delta\hat{\mathbf{u}}^h &= \mathbf{B}\,\delta\mathbf{a}; \quad \nabla_s\delta\breve{\mathbf{u}}^h = \mathbf{B}\,\delta\mathbf{b}; \quad \nabla_s(\mathbf{F}\,\delta\tilde{\mathbf{u}}^h) = \mathbf{G}\,\delta\mathbf{c}; \end{aligned} \tag{3.36}$$

Inserting these relations into equilibrium equation (3.30), yields the discetized equilibrium equation in weak form for a single element:

$$\begin{aligned} \int_\omega (\mathbf{B}\,\delta\mathbf{a})^T\boldsymbol{\sigma}\,d\omega &+ \int_\omega \mathcal{H}_{\mathcal{S}}\,(\mathbf{B}\,\delta\mathbf{b})^T\boldsymbol{\sigma}\,d\omega + \int_\omega (\mathbf{G}\,\delta\mathbf{c})^T\boldsymbol{\sigma}\,d\omega = \\ \int_{\gamma^p} (\mathbf{N}\,\delta\mathbf{a})^T\,\bar{\mathbf{p}}\,d\gamma &+ \int_{\gamma^p} \mathcal{H}_{\mathcal{S}}(\mathbf{N}\,\delta\mathbf{b})^T\bar{\mathbf{p}}\,d\gamma + \int_{\gamma^p} (\mathbf{N}\,\mathbf{F}\delta\mathbf{c})^T\bar{\mathbf{p}}\,d\gamma \end{aligned} \tag{3.37}$$

where γ^p is the Neumann elemental boundary. By taking one of the admissible variations $\delta\mathbf{a}$, $\delta\mathbf{b}$, and $\delta\mathbf{c}$ at the time, the weak form of the equilibrium can be separated into three sets of equations:

$$\begin{aligned} \int_\omega \mathbf{B}^T\boldsymbol{\sigma}\,d\omega &= \int_{\gamma^p} \mathbf{N}^T\bar{\mathbf{p}}\,d\gamma \\ \int_\omega \mathcal{H}_{\mathcal{S}}\mathbf{B}^T\boldsymbol{\sigma}\,d\omega &= \int_{\gamma^p} \mathcal{H}_{\mathcal{S}}\,\mathbf{N}^T\,\bar{\mathbf{p}}\,d\gamma \\ \int_\omega \mathbf{G}^T\,\boldsymbol{\sigma}\,d\omega &= \int_{\gamma^p} (\mathbf{N}\,\mathbf{F})^T\bar{\mathbf{p}}\,d\gamma \end{aligned} \tag{3.38}$$

The first equation is related to the regular degrees of freedom of the element, which is identical to the equilibrium equation for an element without a discontinuity. As a result, it is possible to add a discontinuity to an element during the calculations by adding the additional equilibrium relations and the corresponding degrees of freedom $\mathbf{b}$ or $\mathbf{c}$.

Assume a linear elastic and rate independent constitutive relation for the material[1], namely:

$$\boldsymbol{\sigma} = \mathbb{C}\boldsymbol{\varepsilon} = \mathbb{C}(\mathbf{B}\,\mathbf{a} + \mathcal{H}_{\mathcal{S}}\,\mathbf{B}\,\mathbf{b} + \mathbf{G}\,\mathbf{c}) \tag{3.39}$$

Differentiating system (3.38) with respect to the displacement variables $\mathbf{a}$, $\mathbf{b}$, and $\mathbf{c}$, in the small strain formulation only the stress field in the bulk material $\boldsymbol{\sigma}$ is a function of the discrete displacement terms, according to:

$$\frac{\partial\boldsymbol{\sigma}}{\partial\mathbf{a}} = \mathbb{C}\,\mathbf{B}, \quad \frac{\partial\boldsymbol{\sigma}}{\partial\mathbf{b}} = \mathcal{H}_{\mathcal{S}}\,\mathbb{C}\,\mathbf{B}, \quad \frac{\partial\boldsymbol{\sigma}}{\partial\mathbf{c}} = \mathbb{C}\,\mathbf{G} \tag{3.40}$$

[1]This is not a limitation of the formulation and in general any material law can be used to model the behavior of the bulk material.

Using relations (3.40), the system of equations (3.38) reads:

$$\begin{bmatrix} \tilde{\mathbb{K}}_{aa} & \tilde{\mathbb{K}}_{ab} & \tilde{\mathbb{K}}_{ac} \\ \tilde{\mathbb{K}}_{ba} & \tilde{\mathbb{K}}_{bb} & \tilde{\mathbb{K}}_{bc} \\ \tilde{\mathbb{K}}_{ca} & \tilde{\mathbb{K}}_{cb} & \tilde{\mathbb{K}}_{cc} \end{bmatrix} \begin{bmatrix} \mathbf{a} \\ \mathbf{b} \\ \mathbf{c} \end{bmatrix} = \begin{bmatrix} \mathbf{f}_a^{ext} \\ \mathbf{f}_b^{ext} \\ \mathbf{f}_c^{ext} \end{bmatrix} \tag{3.41}$$

where the terms in the elemental stiffness matrix are:

$$\begin{aligned} \tilde{\mathbb{K}}_{aa} &= \int_\omega \mathbf{B}^T \mathbb{C}\, \mathbf{B}\, d\omega \\ \tilde{\mathbb{K}}_{ab} = \tilde{\mathbb{K}}_{ba} &= \int_\omega \mathcal{H}_\mathcal{S}\, \mathbf{B}^T \mathbb{C}\, \mathbf{B}\, d\omega \\ \tilde{\mathbb{K}}_{bb} &= \int_\omega \mathcal{H}_\mathcal{S}\, \mathcal{H}_\mathcal{S}\, \mathbf{B}^T \mathbb{C}\, \mathbf{B}\, d\omega \\ \tilde{\mathbb{K}}_{ac} = \tilde{\mathbb{K}}_{ca}^T &= \int_\omega \mathbf{B}^T \mathbb{C}\, \mathbf{G}\, d\omega \\ \tilde{\mathbb{K}}_{bc} = \tilde{\mathbb{K}}_{cb}^T &= \int_\omega \mathcal{H}_\mathcal{S} \mathbf{B}^T \mathbb{C}\, \mathbf{G}\, d\omega \\ \tilde{\mathbb{K}}_{cc} &= \int_\omega \mathbf{G}^T \mathbb{C}\, \mathbf{G}\, d\omega \end{aligned} \tag{3.42}$$

Note that if the tangent matrix $\mathbb{C}$ is symmetric, symmetry of the submatrices $\tilde{\mathbb{K}}_{aa}$, $\tilde{\mathbb{K}}_{ab}$, $\tilde{\mathbb{K}}_{bb}$, $\tilde{\mathbb{K}}_{ac}$, $\tilde{\mathbb{K}}_{bc}$ and $\tilde{\mathbb{K}}_{cc}$ is preserved. Consequently, the total stiffness matrix also remains symmetric. Finally, the expression of the elemental external forces is:

$$\begin{aligned} \mathbf{f}_a^{ext} &= \int_{\gamma^p} \mathbf{N}^T \bar{\mathbf{p}}\, d\gamma \\ \mathbf{f}_b^{ext} &= \int_{\gamma^p} \mathcal{H}_\mathcal{S}\, \mathbf{N}^T \bar{\mathbf{p}}\, d\gamma \\ \mathbf{f}_c^{ext} &= \int_{\gamma^p} (\mathbf{N}\, \mathbf{F})^T \bar{\mathbf{p}}\, d\gamma \end{aligned} \tag{3.43}$$

Governing equations (3.42) and (3.43) have been derived in the most general way and can be implemented in any kind of continuum element as long as the underlying shape functions obey the partition of unity property. The partition of unity also has the desirable feature that the finite element equations retain the sparsity properties of the original mesh.

Implementation aspects

The XFEM treats the crack as a completely separate geometric entity and the only interaction with the mesh occurs in the selection of the enriched nodes and the quadrature of the weak form. In the following, criteria for selecting the enriched nodes for an arbitrary mesh and crack geometry are given. In terms of enrichment with the jump function $\mathcal{H}_\mathcal{S}$, the following convention is adopted: a node is enriched if its support is cut by the crack into two disjoint pieces. In fact, when the support of a node is not crossed by the discontinuity, the enhancement function is constant and belong to the same span of functions as the finite element shape functions. This is in violation with the requirement of the partition of unity method that the shape function and the enhanced base must be linear independent [5].

In the general case where the crack tip doesn't coincide with an element edge, the nodes whose support contains the crack tip are enriched with the near tip asymptotic functions $\{F_l(\mathbf{x})\}$ (3.28).

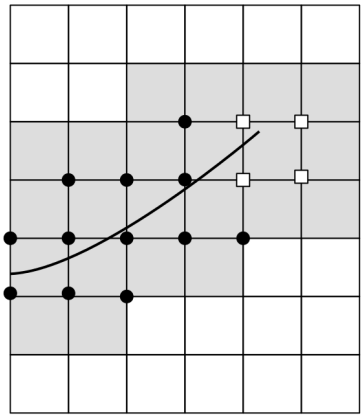

Figure 3.15: *2D crack (bold line) in a uniform mesh. The circled black nodes are enriched by the jump function $\mathcal{H}_{\mathcal{S}}$, while the squared white nodes are enriched by the crack tip functions. Grey elements contains additional terms in the stiffness matrix.*

Different kinds of enrichment are represented in figure 3.15. Therefore any node whose support is intersected by the crack is enriched by a discontinuous function, either of type $\mathcal{H}_{\mathcal{S}}$ or of type $\{F_l(\mathbf{x})\}$ such that the displacement is allowed to be discontinuous along the full extent of the crack. Sets of nodes enriched with the $\{F_l(\mathbf{x})\}$ functions can be enlarged in order to include all nodes within a characteristic distance from the associated crack tip, in which region the asymptotic near tip fields are assumed to dominate the solution. In this regard, one can distinguish between a topological and a geometrical enrichment. In the topological enrichment only the nodes whose support is touching the crack tip are enriched. As a matter of fact, the topological enrichment is active over an area which vanishes to zero as the mesh size goes to zero. In the geometrical enrichment instead, all nodes located within a given distance to the crack tip are enriched, leading to higher order of convergence between exact $(\boldsymbol{\sigma}, \mathbf{u})$ and approximate $(\boldsymbol{\sigma}^h, \mathbf{u}^h)$ fields.

For what regards the numerical integration of the weak form (3.30), for elements cut by the crack and enriched with the jump function $\mathcal{H}_{\mathcal{S}}$, a modification of the element quadrature routine is necessary in order to accurately assemble the contribution to the weak from on both sides of the discontinuity where the integrated field is continuous. As the crack is allowed to be arbitrarily oriented in an element, the use of standard Gauss quadrature may not adequately integrate the discontinuous field. For elements cut by the crack, the element domain ω is defined as the sum of a set of subpolygons ω_s whose boundaries align with the crack geometry, see figure 3.16:

$$\omega = \sum_s \omega_s$$

Such subpolygons are only necessary for integration purposes, no additional degrees of freedom are associated with their construction.

3.3 Numerical approximation of SIFs

As already stressed, extraction of accurate SIFs $\mathbf{K} = \{K_1, K_2, K_3\}$ from the finite element results is of primary relevance in LEFM for evaluation of displacement, stress, and strain fields in the near crack front region. Techniques for extracting SIFs can be divided into two categories: direct approaches, which directly relate the SIFs with results of the finite element analysis, and energetic

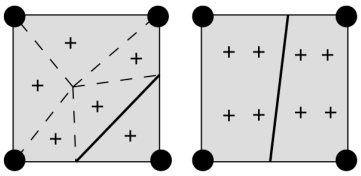

Figure 3.16: *Numerical integration scheme of quadrilateral elements crossed by the crack (bold line). Sample points are denoted with +. The element on the left is split into a sub-element with five vertices and one with three vertices. The first part is triangulated into five parts, denoted by dashed lines. Each triangle can be integrated using a standard 1 point Gauss integration scheme. The element on the right is split into two quadrilateral sub-elements and each of them can be integrated with a standard* 2×2 *Gauss integration scheme.*

approaches, generally more accurate than the direct ones, for which computation of the energy release rate is demanded. In the following, four different techniques to compute SIFs are described: displacement correlation technique, which has to be classified as a direct approach, and virtual crack extension method, modified crack closure integral and J-integral (and the relative interaction integral version), which on the contrary have to be classified as energetic approaches. Some of them rely on William's solution [150] for stress and displacement fields in the vicinity of each point along the crack front, that, referring to a local Frenet frame $\{x_1, x_2, x_3\}$ and a polar coordinate system $\{r, \theta\}$ as the ones in figure 3.17, have the form:

$$\begin{Bmatrix} \sigma_{11} \\ \sigma_{22} \\ \sigma_{12} \\ \sigma_{13} \\ \sigma_{23} \end{Bmatrix} = \frac{1}{\sqrt{2\pi\, r}} K_1 \cos\frac{\theta}{2} \begin{Bmatrix} \left(1 - \sin\frac{\theta}{2}\sin\frac{3\theta}{2}\right) \\ \left(1 + \sin\frac{\theta}{2}\sin\frac{3\theta}{2}\right) \\ \sin\frac{\theta}{2}\cos\frac{3\theta}{2} \\ 0 \\ 0 \end{Bmatrix} + \frac{1}{\sqrt{2\pi\, r}} K_2 \begin{Bmatrix} -\sin\frac{\theta}{2}\left(2 + \cos\frac{\theta}{2}\cos\frac{3\theta}{2}\right) \\ \sin\frac{\theta}{2}\cos\frac{\theta}{2}\cos\frac{3\theta}{2} \\ \cos\frac{\theta}{2}\left(1 - \sin\frac{\theta}{2}\sin\frac{3\theta}{2}\right) \\ 0 \\ 0 \end{Bmatrix} + \frac{1}{\sqrt{2\pi\, r}} K_3 \begin{Bmatrix} 0 \\ 0 \\ 0 \\ -\sin\frac{\theta}{2} \\ \cos\frac{\theta}{2} \end{Bmatrix} \tag{3.44}$$

and

$$\sigma_{33} = \begin{cases} \nu(\sigma_{11} + \sigma_{22}) & \textit{plane strain} \\ 0 & \textit{plane stress} \end{cases}$$

$$\begin{Bmatrix} u_1 \\ u_2 \\ u_3 \end{Bmatrix} = \frac{K_1}{\mu}\sqrt{\frac{r}{2\pi}}\frac{1}{4} \begin{Bmatrix} (2k-1)\cos\frac{\theta}{2} - \cos\frac{3\theta}{2} \\ (2k+1)\sin\frac{\theta}{2} - sin\frac{3\theta}{2} \\ 0 \end{Bmatrix} + \frac{K_2}{\mu}\sqrt{\frac{r}{2\pi}}\frac{1}{4} \begin{Bmatrix} (2k+3)\sin\frac{\theta}{2} + \sin\frac{3\theta}{2} \\ -(2k-3)\cos\frac{\theta}{2} - \cos\frac{3\theta}{2} \\ 0 \end{Bmatrix} + \frac{K_3}{\mu}\sqrt{\frac{2\,r}{\pi}} \begin{Bmatrix} 0 \\ 0 \\ \sin\frac{\theta}{2} \end{Bmatrix} \tag{3.45}$$

where μ is the shear modulus and $k = 3 - 4\nu$ for plane strain and $k = (3-\nu)/(1+\nu)$ for plane stress, being ν the Poisson's ratio.

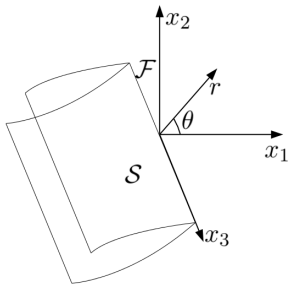

Figure 3.17: *Local Frenet frame* $\{x_1, x_2, x_3\}$ *and polar coordinate system* $\{r, \theta\}$ *in each point along the crack front* $\mathcal{F}$ *of a three dimensional crack.*

3.3.1 Displacement correlation technique

Displacement correlation technique is one of the simplest method used to extract SIFs from finite element results [27]. It relies on the form of the theoretical asymptotic displacement field $\mathbf{u} = \{u_1; u_2; u_3\}$ (3.45). Referring to the two dimensional representation of figure 3.18-a, the finite element displacements for one point in the mesh, that usually is selected to be a node on the crack face, are substituted directly into the analytical expression (3.45), after subtracting the displacements of the crack tip, obtaining the following expression for SIFs:

$$\begin{aligned} K_1 &= \frac{2\,\mu\sqrt{2\pi}(u_2(B) - u_2(A))}{\sqrt{r(B)}(k+1)} \\ K_2 &= \frac{2\,\mu\sqrt{2\pi}(u_1(B) - u_1(A))}{\sqrt{r(B)}(k+1)} \\ K_3 &= \frac{\mu\sqrt{\pi}(u_3(B) - u_3(A))}{\sqrt{2r(B)}} \end{aligned}$$

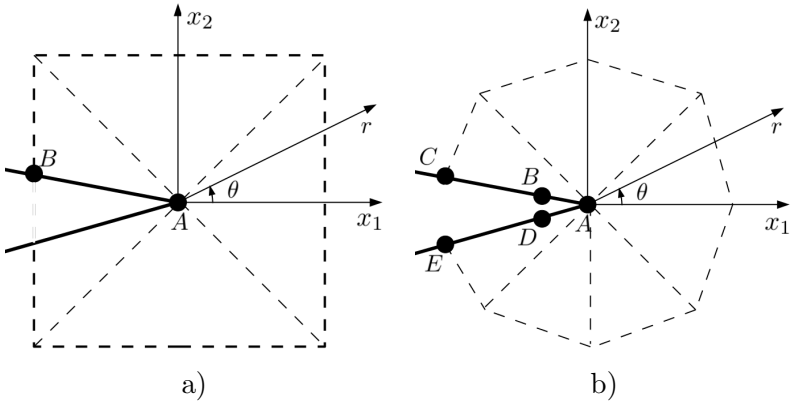

Figure 3.18: *Displacement correlation technique: correlation points location for a non singular element (a), and for quarter-point element (b).*

Despite its simplicity and inherent separation of SIFs, accuracy of the displacement correlation technique depends on the choice of the correlation point B which needs to be selected in the zone

where the **K** fields dominate and for this purpose highly refined meshes are usually required around the crack front.

For the 2D case, using the quarter-point crack tip elements described in Section 3.1.2, the finite element crack opening displacement along the crack face deriving from the quarter-point element interpolation (3.3) are (see figure 3.18-b):

$$\begin{aligned} u_2^{upper} - u_2^{lower} &= [\,4(u_2(B) - u_2(D)) + u_2(E) - u_2(C)\,]\sqrt{\frac{r}{b}} + \\ &+ [\,4(u_2(B) - u_2(D)) + 2(u_2(C) - u_2(E))\,]\frac{r}{b} \\ u_1^{upper} - u_1^{lower} &= [\,4(u_1(B) - u_1(D)) + u_1(E) - u_1(C)\,]\sqrt{\frac{r}{b}} + \\ &+ [\,4(u_1(B) - u_1(D)) + 2(u_1(C) - u_1(E))\,]\frac{r}{b} \end{aligned}$$

The square root term of the finite element crack opening displacement has then to be substituted into the analytical crack tip displacement field (3.45) to yield:

$$\begin{aligned} K_1 &= \frac{\mu\sqrt{2\pi}}{\sqrt{b}(k+1)}[\,4(u_2(B) - u_2(D)) + u_2(E) - u_2(C)] \\ K_2 &= \frac{\mu\sqrt{2\pi}}{\sqrt{b}(k+1)}[\,4(u_1(B) - u_1(D)) + u_1(E) - u_1(C)] \end{aligned}$$

Similar expressions are given by Ingraffea and Manu [61] for 3D configurations.

3.3.2 Modified crack closure integral technique

The modified crack closure integral was originally proposed by Rybicki and Kanninen for the 2D case [113] exploiting Irwin's crack closure integral that relates the energy release rate to the crack tip stress and displacement fields for a small crack increment Δl (see figure 3.19-a). Irwin's crack closure integral means that if a crack extends by a small amount Δl, the energy absorbed in the process is equal to the work required to close the crack to its original length:

$$\begin{aligned} G_1 &= \lim_{\Delta l \to 0} \frac{1}{2\Delta l} \int_0^{\Delta l} \sigma_{22}(r = x_1, \theta = 0)\, u_2(r = \Delta l - x_1, \theta = \pi)\, dr \\ G_2 &= \lim_{\Delta l \to 0} \frac{1}{2\Delta l} \int_0^{\Delta l} \sigma_{12}(r = x_1, \theta = 0)\, u_1(r = \Delta l - x_1, \theta = \pi)\, dr \end{aligned} \tag{3.46}$$

Finite element equations can be used to relate the crack tip stress to the internal finite element forces near the crack tip, so that eq. (3.46) can be expressed in terms of nodal forces and displacements. Linear displacement finite elements are used in the case discussed by Rybicki and Kanninen [113] for which the expression for the energy release rate G is very simple. Referring to notation used in figure 3.19-b, one analysis can be performed to compute the internal nodal force at the crack tip $f_2(C)$. The crack is then extended and a second analysis yields nodal displacements $\mathbf{u}(C)$ and $\mathbf{u}(D)$ reducing eq. (3.46) to:

$$G_1 = \frac{1}{2\Delta l} f_2(C)(u_2(C) - u_2(D)), \qquad G_2 = \frac{1}{2\Delta l} f_1(C)(u_1(C) - u_1(D))$$

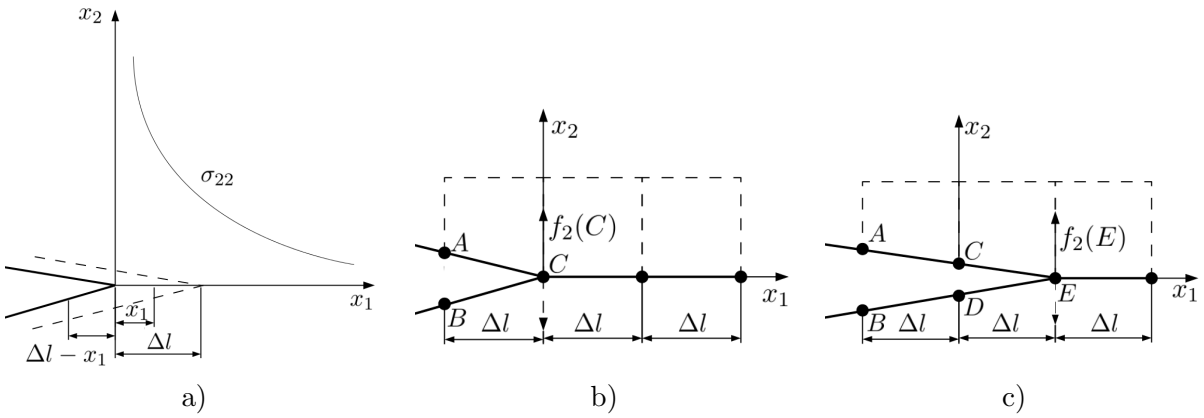

Figure 3.19: *a) Crack closure integral notation. Local mesh configuration exploited in the modified crack closure integral technique: first analysis before elongation (b), and second analysis after elongation (c).*

Nevertheless, if Δl is sufficiently small, displacements at nodes C and D in figure 3.19-c can be approximated by those at nodes A and B of figure 3.19-b avoiding the necessity of a second finite elements analysis, leading to the following expression for the energy release rate:

$$G_1 = \frac{1}{2\Delta l} f_2(C)(u_2(A) - u_2(B)), \qquad G_2 = \frac{1}{2\Delta l} f_1(C)(u_1(A) - u_1(B))$$

SIFs can then be computed from Irwin's formula [62]:

$$K_1 = \sqrt{G_1\, E}, \qquad K_2 = \sqrt{G_2\, E} \tag{3.47a}$$

for plane stress and

$$K_1 = \sqrt{\frac{G_1\, E}{(1-\nu^2)}}, \qquad K_2 = \sqrt{\frac{G_2\, E}{(1-\nu^2)}} \tag{3.47b}$$

for plane strain case.

The modified crack closure integral procedure has been extended for the higher order element case. Its formulation for quarter-point elements [111] leads to the expression of the crack tip displacement and stress fields in terms of second order polynomials that are consistent with the quarter-point behavior. Referring to the notation of figure 3.20, the resulting expression for G after integration of eq. (3.46) reads:

$$\begin{aligned}
G_1 &= \frac{1}{2\Delta l}\left[(c_{11}f_2(E) + c_{12}f_2(F) + c_{13}f_2(G))(u_2(C) - u_2(D)) + \right. \\
&+ \left. (c_{21}f_2(E) + c_{22}f_2(F) + c_{23}f_2(G))(u_2(A) - u_2(B))\right] \\
G_2 &= \frac{1}{2\Delta l}\left[(c_{11}f_1(E) + c_{12}f_1(F) + c_{13}f_1(G))(u_1(C) - u_1(D)) + \right. \\
&+ \left. (c_{21}f_1(E) + c_{22}f_1(F) + c_{23}f_1(G))(u_1(A) - u_1(B))\right]
\end{aligned}$$

with

$$\begin{aligned} c_{11} &= \frac{33\pi}{2} - 52, \quad c_{12} = 17 - \frac{21\pi}{4}, \quad c_{13} = \frac{21\pi}{2} - 32, \\ c_{21} &= 14 - \frac{33\pi}{8}, \quad c_{22} = \frac{21\pi}{16} - \frac{7}{2}, \quad c_{23} = 8 - \frac{21\pi}{8} \end{aligned}$$

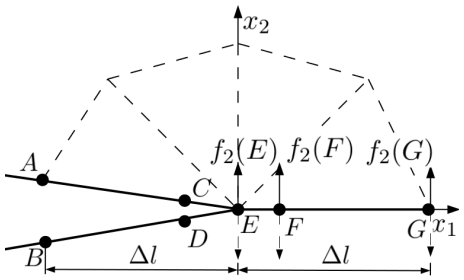

Figure 3.20: *Local mesh configuration used for the modified crack closure integral technique for the case of 2D quarter-point elements*

Formulas for a number of additional element types are presented in [112]. For the same mesh, the modified crack closure integral technique provides more accurate SIFs than the displacement correlation one, but less accurate than the J-integral approach described in Section 3.3.4, requiring displacements and nodal forces only. The presence of crack face tractions requires additional terms with respect to those in eq (3.46).

3.3.3 Virtual crack extension technique

The Virtual Crack Extension (VCE) method was proposed by Parks [110] and Hellen [55] as an energy approach that computes the rate of change of the total potential energy of a system for a small (virtual) extension of the crack that is equal to the energy release rate in the LEFM framework. In the absence of body forces, the total potential energy Π of a finite element system is

$$\Pi = \frac{1}{2}\mathbf{u}^T \tilde{\mathbb{K}}\, \mathbf{u} - \mathbf{u}^T \mathbf{f} \tag{3.48}$$

where $\mathbf{u}, \tilde{\mathbb{K}}$ and $\mathbf{f}$ are the nodal displacement vector, the stiffness matrix and the applied nodal force vector, respectively. The energy release rate for a small (virtual) crack extension δl in a direction normal to the original crack front is related to the change in the potential energy by the following integral along the crack front $\mathcal{F}$:

$$-\delta\Pi = \int_{\mathcal{F}} G(s)\, \delta l(s)\, ds = -\frac{1}{2}\mathbf{u}^T \delta\tilde{\mathbb{K}}\, \mathbf{u} + \mathbf{u}^T \delta\mathbf{f} \tag{3.49}$$

where $\delta\tilde{\mathbb{K}}$ and $\delta\mathbf{f}$ are the variations of the stiffness matrix and load vector, respectively, due to the virtual crack front advance $\delta l(s)$. As originally proposed, the virtual crack extension method provides only a total energy release rate G, without separation for the three modes of fractures. Decomposition of displacement field as described in the next Section 3.3.4 can overcome this shortcoming.

The VCE method proposed by Hwang et al. in [59] provides the integral form of stiffness derivatives for 3D finite elements in order to compute $\delta\tilde{\mathbb{K}}$ in eq. (3.49), avoiding the need to specify a finite

length for crack extension to simulate a VCE. Such an approach allows to overcome the drawbacks of geometric approximations and numerical truncation errors deriving from a finite perturbation of the finite element meshes in order to approximate the stiffness derivative by subtracting two stiffness matrices. With the subtraction of two stiffness matrices, the difference of the stiffness divided by the finite crack increment should converge to the stiffness derivative as the increment approaches zero, but the change of the mesh configuration can affect the solution accuracy. This is due to the fact that if the perturbations are too large relative to the finite element mesh, the difference approximation is inaccurate, while if the perturbations are too small, numerical truncation errors may become significant.

Different types of virtual crack extensions are feasible in order to compute the energy release rate along the crack front. Among them, Bank-Sills [10] showed that a crack extension $\delta l(s)$ that varies linearly with crack curvilinear abscissa s leads to the most accurate results. The VCE method provides a tool to obtain accurate numerical results for energy release rate and its derivatives, thus for the second variations of the potential energy. In the form presented in [59], it allows to take into account the interactions between virtual crack extensions at different positions along the crack front in case of overlapping areas perturbed at adjacent positions, and the influence of the local curvature of the curved crack front.

3.3.4 J-integral

The J-integral is a well known fracture mechanics parameter [20, 114]. The J-integral is equivalent to the energy release rate G under linear elastic material assumption, and in its original formulation it relates G of a two-dimensional body to a contour integral.

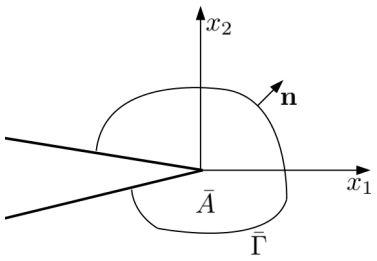

Figure 3.21: *2D J-integral: notation*

Referring to the Frenet frame at the crack tip, where, as usual, x_1 axis is tangential to the crack and the x_2 axis is perpendicular to the crack as in figure 3.21, the J-integral is defined as:

$$J = \lim_{\bar{\Gamma}\to 0} \int_{\bar{\Gamma}} \bar{W}\, n_1 - \sigma_{ij}\, \frac{\partial u_i}{\partial x_1}\, n_j \, d\Gamma \tag{3.50}$$

where $\bar{W} = \frac{1}{2}\sigma_{ij}\,\varepsilon_{ij}$ is the strain energy density, $\boldsymbol{\sigma}$ is the Cauchy stress tensor, $\mathbf{n}$ is the unit outward normal to the contour $\bar{\Gamma}$ and $\mathbf{u}$ is, as usual, the displacement vector. Summation convention is exploited over identical indices. In the case of elastic material behavior in the absence of body forces inside the integration area, and of tractions on the crack surface, the contour integral (3.50) is proved to be path-independent. Additional terms are required in eq. (3.50) to prove path-independency in the presence of body forces or crack face tractions. Early use of the J-integral within FEM focused on a direct evaluation of eq. (3.50) along a contour in the finite element mesh, usually selected to pass trough element Gauss integration points, where stresses are expected to be most accurately evaluated. Unfortunately, such an implementation rarely exhibits path independence of

the integral and ad hoc procedures must be adopted to obtain an objective value for J. Furthermore, the limiting definition (3.50) of the contour $\bar{\Gamma}$ requires extensive mesh refinement near the crack tip to obtain meaningful numerical results. Li et al. [88] showed how the contour J-integral can be transformed to an equivalent area integral, which has been show to be objective with respect to the domain of integration and to be naturally suited for finite element models. The area form of the integral (3.50) reads:

$$\bar{J} = \int_{\bar{A}} \left[\sigma_{ij} \frac{\partial u_i}{\partial x_1} - \bar{W} \delta_{1j} \right] \frac{\partial q}{\partial x_j} \, dA \tag{3.51}$$

where δ_{ij} is the Kronecher delta and q is a weighting function defined over the domain $\bar{A}$ of integration that can be physically thought as the displacement field due to a virtual crack extension.

Function q is defined by prescribing nodal values that are interpolated over elements in the domain using standard shape functions ψ_i:

$$q = \sum_i \psi_i \, q_i, \qquad \frac{\partial q}{\partial x_j} = \sum_i \frac{\partial \psi_i}{\partial x_j} \, q_i$$

Domain of integration $\bar{A}$ can be either an annular region that surrounds the crack tip, or the inner contour of such annular region can be shrunk to the crack tip. The q function should have a unit value on the inner contour of the domain $\bar{A}$ and a zero value on the outer contour. A linear spatial variation is usually assumed between the two contours.

The J-integral as defined in eq. (3.50) provides the total energy release rate G for the crack under consideration, namely:

$$\bar{J} = G = \begin{cases} \frac{1-\nu^2}{E}(K_1^2 + K_2^2) & \textit{plane strain} \\ \\ \frac{1}{E}(K_1^2 + K_2^2) & \textit{plane stress} \end{cases}$$

An effective technique for separating the SIFs of different fracture modes was introduced by Ishikawa [63] and independently by Bui [22]. Separation of modes is allowed by a decomposition of the near crack-tip displacement fields into a symmetric $\mathbf{u}^I$ and a skew-symmetric $\mathbf{u}^{II}$ part with respect to the x_1 axis. Considering the notation of figure 3.21, one has:

$$\mathbf{u} = \mathbf{u}^I + \mathbf{u}^{II} = \frac{1}{2} \begin{Bmatrix} u_1 + \bar{u}_1 \\ u_2 - \bar{u}_2 \end{Bmatrix} + \frac{1}{2} \begin{Bmatrix} u_1 - \bar{u}_1 \\ u_2 + \bar{u}_2 \end{Bmatrix} \tag{3.52}$$

with $\bar{\mathbf{u}}(x_1, x_2) = \mathbf{u}(x_1, -x_2)$. A similar decomposition can be used for the stress field:

$$\boldsymbol{\sigma} = \boldsymbol{\sigma}^I + \boldsymbol{\sigma}^{II} = \frac{1}{2} \begin{bmatrix} \sigma_{11} + \bar{\sigma}_{11} & \sigma_{12} - \bar{\sigma}_{12} \\ \sigma_{12} - \bar{\sigma}_{12} & \sigma_{22} + \bar{\sigma}_{22} \end{bmatrix} + \frac{1}{2} \begin{bmatrix} \sigma_{11} - \bar{\sigma}_{11} & \sigma_{12} + \bar{\sigma}_{12} \\ \sigma_{12} + \bar{\sigma}_{12} & \sigma_{22} - \bar{\sigma}_{22} \end{bmatrix} \tag{3.53}$$

Exploiting decomposition of displacement and stress fields (3.52) and (3.53), the mode-separated J-integral values can be computed from eq. (3.51):

$$G_1 = \bar{J}_1 = \bar{J}(\mathbf{u}^I), \qquad G_2 = \bar{J}_2 = \bar{J}(\mathbf{u}^{II}) \tag{3.54}$$

and SIFs arise from eq. (3.47). Modal decomposition (3.54) can be simply implemented in a mesh that is symmetric about the crack plane in the domain of evaluation $\bar{A}$, but such a condition is not necessary and interpolation can be used to find displacements and stresses for non symmetric meshes.

For what regards the three dimensional case, a local value of the J-integral, at each point s along the crack front $\mathcal{F}$ is given by:

$$J(s) = \lim_{\bar{\Gamma}\to 0} \int_{\bar{\Gamma}} \bar{W}\, n_1 - \sigma_{ij} \frac{\partial u_i}{\partial x_1}\, n_j \, d\Gamma \tag{3.55}$$

where $\bar{\Gamma}$ lies in the plane orthogonal to the crack front and all quantities are expressed in the local Frenet frame depicted in figure 3.22. Unlike the global path independence of the 2D version eq. (3.50), eq. (3.55) is path independent only in a local sense as $\bar{\Gamma} \to 0$ [99]. As in the 2D case, eq. (3.55) shows difficulties in being directly evaluated in a finite element context, because of the need to define a path $\bar{\Gamma}$ that passes through integration points. Consequently, the 3D J-integral (3.55) can be transformed into a volume integral, introducing a weighting function q [104].

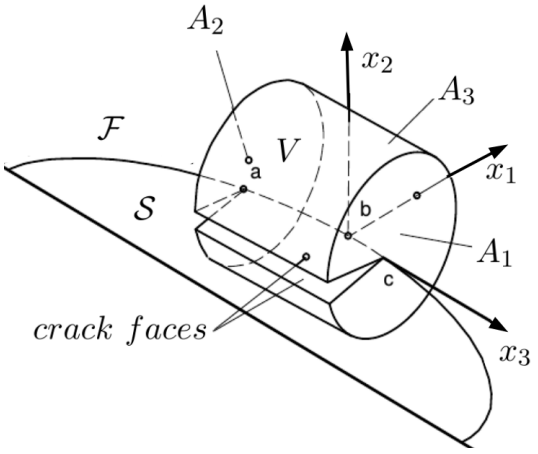

Figure 3.22: *3D J-integral: notation.*

Referring to figure 3.22, for an elastic, homogeneous material, under quasi-static, isothermal loading, with no body forces within the contour and traction-free crack faces, the J-integral reads [147]:

$$\bar{J} = \int_V \left[\sigma_{ij} \frac{\partial u_i}{\partial x_1} - \bar{W}\, \delta_{1j} \right] \frac{\partial q}{\partial x_j}\, dV \tag{3.56}$$

Eq. (3.56) assumes that the crack front curvature is negligible within the domain of integration V and if this hypothesis is not realistic for the case at hand, an additional volume integral appears in (3.56).

The scalar weight function q varies smoothly within V. A simple form for q assigns it a smooth variation from zero on surfaces A_1, A_2 and A_3 of figure 3.22 to a value of 1 on the crack front $\mathcal{F}$. All material over which the q-function and its derivative are non-zero must be included in the volume integral (3.56).

As for the 2D case, the q-function can be interpreted as virtual displacement of a material point due to the virtual extension of the crack front. Nikishkov and Atluri [104] presented different candidates for the q-function for quadratic order elements and Bank-Sills and Sherman [9] analyzed three of them in details. In particular they showed that a linear variation of $q(s)$ along the crack front leads to most accurate results than the functions naturally derived from the use of quadratic order shape functions. Eq. (3.56) is the total energy release rate over the domain of integration V for the virtual crack extension q. An approximate local value $J(s_b)$ can be obtained by normalizing

the integral with respect to the area of the virtual crack extension:

$$J(s_b) \approx \frac{\int_{s_a}^{s_c} J(s)\, q(s)\, ds}{\int_{s_a}^{s_c} q(s)\, ds} \tag{3.57}$$

where s_a, s_b, and s_c are the curvilinear abscissas of points a, b, and c of figure 3.22, respectively. Analogously to what done for the 2D case, a modal decomposition of displacement field leads to:

$$\mathbf{u} = \mathbf{u}^I + \mathbf{u}^{II} + \mathbf{u}^{III} = \frac{1}{2}\begin{Bmatrix} u_1 + \bar{u}_1 \\ u_2 - \bar{u}_2 \\ u_3 + \bar{u}_3 \end{Bmatrix} + \frac{1}{2}\begin{Bmatrix} u_1 - \bar{u}_1 \\ u_2 + \bar{u}_2 \\ 0 \end{Bmatrix} + \frac{1}{2}\begin{Bmatrix} 0 \\ 0 \\ u_3 - \bar{u}_3 \end{Bmatrix}$$

with $\bar{\mathbf{u}}(x_1, x_2, x_3) = \mathbf{u}(x_1, -x_2, x_3)$, and the corresponding decomposition of the stress field is:

$$\boldsymbol{\sigma} = \boldsymbol{\sigma}^I + \boldsymbol{\sigma}^{II} + \boldsymbol{\sigma}^{III} = \frac{1}{2}\begin{Bmatrix} \sigma_{11} + \bar{\sigma}_{11} \\ \sigma_{22} + \bar{\sigma}_{22} \\ \sigma_{33} + \bar{\sigma}_{33} \\ \sigma_{12} - \bar{\sigma}_{12} \\ \sigma_{23} - \bar{\sigma}_{23} \\ \sigma_{31} - \bar{\sigma}_{31} \end{Bmatrix} + \frac{1}{2}\begin{Bmatrix} \sigma_{11} - \bar{\sigma}_{11} \\ \sigma_{22} - \bar{\sigma}_{22} \\ 0 \\ \sigma_{12} + \bar{\sigma}_{12} \\ 0 \\ 0 \end{Bmatrix} + \frac{1}{2}\begin{Bmatrix} 0 \\ 0 \\ \sigma_{33} - \bar{\sigma}_{33} \\ 0 \\ \sigma_{23} + \bar{\sigma}_{23} \\ \sigma_{31} + \bar{\sigma}_{31} \end{Bmatrix}$$

M-Integral

In the present Section, the domain form of the M-Integral, or Interaction Integral, is presented [138, 155], as a technique for extracting SIFs from numerical results as accurate as the J-Integral, but providing directly separated K_1, K_2 and K_3 values.

Consider two states of a cracked body: state (1), indicated with $(\sigma_{ij}^{(1)}, \varepsilon_{ij}^{(1)}, u_i^{(1)})$, that corresponds to the present state, and state (2), indicated with $(\sigma_{ij}^{(2)}, \varepsilon_{ij}^{(2)}, u_i^{(2)})$, that is an auxiliary state which is chosen as the asymptotic fields either for mode 1, or mode 2, or mode 3. Exploiting additive decomposition of displacement, stress and strain fields valid in linear analysis, one has:

$$u_i = u_i^{(1)} + u_i^{(2)}, \qquad \sigma_{ij} = \sigma_{ij}^{(1)} + \sigma_{ij}^{(2)}, \qquad \varepsilon_{ij} = \varepsilon_{ij}^{(1)} + \varepsilon_{ij}^{(2)}$$

The J-integral (3.56) for the sum of the two states is:

$$\begin{aligned} \bar{J}^{(1+2)} &= \int_V \left[\sigma_{ij}^{(1)} \frac{\partial u_i^{(1)}}{\partial x_1} + \sigma_{ij}^{(1)} \frac{\partial u_i^{(2)}}{\partial x_1} + \sigma_{ij}^{(2)} \frac{\partial u_i^{(1)}}{\partial x_1} + \sigma_{ij}^{(2)} \frac{\partial u_i^{(2)}}{\partial x_1} + \right. \\ &- \left. \bar{W}^{(1)} \delta_{1j} - \bar{W}^{(2)} \delta_{1j} - \bar{W}^{(1,2)} \delta_{1j} \right] \frac{\partial q}{\partial x_j}\, dV \end{aligned}$$

where the interaction strain energy is: $\bar{W}^{(1,2)} = \sigma_{ij}^{(1)} \varepsilon_{ij}^{(2)} = \sigma_{ij}^{(2)} \varepsilon_{ij}^{(1)}$ assuming that the same constitutive tensor couples state (1) and state (2) stress and state (1) and state (2) strain. Rearranging terms gives:

$$\bar{J}^{(1+2)} = \bar{J}^{(1)} + \bar{J}^{(2)} + \bar{M}^{(1,2)} \tag{3.58}$$

where $\bar{J}^{(1)}$ equals eq. (3.56) for state (1), $\bar{J}^{(2)}$ equals eq. (3.56) for state (2), and $\bar{M}^{(1,2)}$ is the interaction integral for states (1) and (2) that reads:

$$\bar{M}^{(1,2)} = \int_V \left[\sigma_{ij}^{(1)} \frac{\partial u_i^{(2)}}{\partial x_1} + \sigma_{ij}^{(2)} \frac{\partial u_i^{(1)}}{\partial x_1} - \bar{W}^{(1,2)} \delta 1 j \right] \frac{\partial q}{\partial x_j}\, dV \tag{3.59}$$

According to (3.57) a pointwise value of the interaction integral at location s_b, see figure 3.22, along a 3D crack front is:

$$\bar{M}^{(1,2)}(s_b) = \frac{\bar{M}^{(1,2)}(s)}{\int_{s_a}^{s_c} q(s)\, ds}$$

The additive decomposition of SIFs:

$$K_1 = K_1^{(1)} + K_1^{(2)}, \qquad K_2 = K_2^{(1)} + K_2^{(2)}, \qquad K_3 = K_3^{(1)} + K_3^{(2)}$$

and Irwin's formula [62]:

$$G = \Lambda_{11}(K_1^2 + K_2^2) + \Lambda_{33}\, K_3^2$$

with components of matrix $\mathbf{\Lambda}$ expressed in eq. (2.12), leads to:

$$\begin{aligned} \bar{J}^{(1+2)} &= \Lambda_{11}(K_1^{(1)2} + K_2^{(1)2}) + \Lambda_{33}\, K_3^{(1)2} + \Lambda_{11}(K_1^{(2)2} + K_2^{(2)2}) + \Lambda_{33}\, K_3^{(2)2} + \\ &+ 2\,\Lambda_{11}\, K_1^{(1)} K_1^{(2)} + 2\,\Lambda_{11}\, K_2^{(1)} K_2^{(2)} + 2\,\Lambda_{33}\, K_3^{(1)} K_3^{(2)} \end{aligned} \tag{3.60}$$

Equating eq. (3.58) with eq. (3.60) leads to the following relationship:

$$\bar{M}^{(1,2)} = 2\,\Lambda_{11}(K_1^{(1)} K_1^{(2)} + K_2^{(1)} K_2^{(2)}) + 2\,\Lambda_{33}\, K_3^{(1)} K_3^{(2)} \tag{3.61}$$

From the two definitions of the interaction integral (3.59) and (3.61) one has:

$$\int_V \left[\sigma_{ij}^{(1)} \frac{\partial u_i^{(2)}}{\partial x_1} + \sigma_{ij}^{(2)} \frac{\partial u_i^{(1)}}{\partial x_1} - \bar{W}^{(1,2)} \delta_{1j} \right] \frac{\partial q}{\partial x_j} dV = 2\,\Lambda_{11}\,(K_1^{(1)} K_1^{(2)} + K_2^{(1)} K_2^{(2)}) + 2\,\Lambda_{33}\, K_3^{(1)} K_3^{(2)}$$

Making the judicious choice of auxiliary state (2) as the pure mode 1 (state $(2a)$), or pure mode 2 (state $(2b)$) or pure mode 3 (state $(2c)$) asymptotic fields, namely:

	K_1	K_2	K_3
$2a$	1.0	0.0	0.0
$2b$	0.0	1.0	0.0
$2c$	0.0	0.0	1.0

and state (1) as the solution of finite element analysis, leads to the following linear system:

$$\begin{Bmatrix} 2\Lambda_{11} & 0 & 0 \\ 0 & 2\Lambda_{11} & 0 \\ 0 & 0 & 2\Lambda_{33} \end{Bmatrix} \begin{Bmatrix} K_1^{(1)} \\ K_2^{(1)} \\ K_3^{(1)} \end{Bmatrix} = \begin{Bmatrix} \bar{M}^{(1,2a)} \\ \bar{M}^{(1,2b)} \\ \bar{M}^{(1,2c)} \end{Bmatrix}$$

which provides the values of the SIFs.

Chapter 4

Weight function theory

In this Chapter the weight function theory for three-dimensional LEFM is briefly reviewed and some results regarding the first order variation of the SIFs reformulated. The main reason for these derivations, presented for the first time in [129], resides in the fact that, although the variational formulation detailed in Chapter 2 is complete, the form (2.6) of operator $\mathbf{K}^{(1)}[\cdot]$ is so involved that an effective implementation of crack tracking strategies may reveal not straightforward. Furthermore, having at hand the symmetric operator $\mathbf{K}^{(1)}[\cdot]$ and being merely capable to express it as the sum (2.6) of unsymmetric factors is quite disappointing and compel to seek for alternative forms. The two evidences above inspire the present formulation.

Introduction of the weight function theory is ascribable to Bueckner in 1970 [21] for two dimensional elastic crack analysis and it is a milestone in fracture mechanics. Weight function theory for the three dimensional counterpart was introduced by Rice in 1985 [116]. In [116], Rice pointed out the relation between three-dimensional weight function concepts and the determination of mode 1 SIFs along crack fronts whose locations are slightly perturbed from some simple reference geometry in an unbounded domain and quasi-static crack growth conditions. In particular Rice applied the method to half plane cracks with slightly wavy front subjected to mode 1 loading. The work was extended afterwards by Gao and Rice [43] to the case of mode 2 and mode 3 loading and to internal circular cracks [44] and external circular cracks [45]. Weight function theory for three dimensional elastic crack analysis was exhaustively discussed by Rice in the cornerstone work of 1989 [117], where weight functions approach provided fundamental theoretical results as well as numerical estimations. Since then, it has been used largely in three dimensional elastic crack analyses, in the context of configurational stability, crack growth and trapping prediction, SIFs expansion, perturbation approaches, interactions with dislocations and other defects.

Weight functions are displacements solutions of the linear elastic fracture mechanics boundary value problem in a *distributional sense*. Nine components $h_{ij}(P, s)$ provide the mode i SIF at location s along the crack front induced by a unit Dirac delta body force in direction j located at an arbitrary point P of the body, with $i = 1, 2, 3$ and $j = 1, 2, 3$. As such, the work-like product of an arbitrary set of body forces with the weight functions gives the crack front SIFs induced by those forces. With the aim to agree with mode number designation for the SIFs, index 1, attributed to weight functions and related quantities, indicates the direction orthogonal to the crack plane, index 2 indicates the direction orthogonal to the crack front $\mathcal{F}$ and oriented in the same direction of propagation, and index 3 indicates the direction tangent to $\mathcal{F}$ and oriented as the curvilinear abscissa s along $\mathcal{F}$.

The present work simplifies the picture, dealing only with cracks that lie in a plane x, z. For

its purposes the knowledge of weight functions h_{ij} is not mandatory. Referring to the cornerstone work of Rice of 1989 [117], it suffices to know their jump across the crack at point $P \in \mathcal{S}(t)$ of application of the load, that is the so called *crack face weight function* k_{ij} (shortened henceforth in CFWF), defined thus by:

$$k_{ij}(P,s) = \lim_{\epsilon \to 0^+} [h_{ij}(P + \epsilon\, e_y, s) - h_{ij}(P - \epsilon\, e_y, s)] \tag{4.1}$$

e_y being the unit vector of axis y. CFWFs, collected in matrix $\mathbb{K} = [k_{ij}]$, are endowed with analogous properties of h_{ij}. In particular, for a crack of arbitrary shape with surface $\mathcal{S}(t)$ and front $\mathcal{F}(t)$ pressurized by tractions $\mathbf{t}$ at point $P = (x, z)$ as depicted in figure 4.1, the SIFs along the crack front can be evaluated by integral:

$$K_i(s,t) = \int_{\mathcal{S}(t)} k_{ij}(P,s)\, t_j(P)\, dx\, dz \tag{4.2}$$

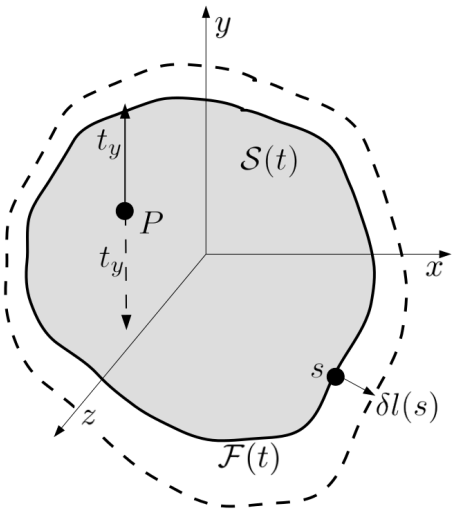

Figure 4.1: *A plane crack of arbitrary shape is pressurized by tractions t_y at point P: notation*

Formula (4.2) acts as definition of CFWF $k_{ij}(P,s)$ as the i-th SIF at point s of the crack front $\mathcal{F}(t)$ resulting from the application of a pair of opposite unit point forces equal to $\pm\, e_j$ on the upper $(+)$ and lower $(-)$ crack surfaces at point P.

Consider that, under fixed loading conditions, the crack front is extended *normal to itself* [117] by a smooth variation $\delta l(s)$, treated as infinitesimal, where the time dependency will be omitted henceforth for the sake of readability. Then, the variation $\delta\mathbf{w}$ of the displacement jump $\mathbf{w}(x,z)$ across the crack faces (i.e. the opening and sliding relative displacement) reads:

$$\delta\mathbf{w}(x,z) = 2 \int_{\mathcal{F}(t)} \mathbb{K}(P,s)\mathbf{\Lambda}\mathbf{K}(s)\delta l(s) ds \tag{4.3}$$

to the first order in $\delta l(s)$. where components of matrix $\mathbf{\Lambda}$ are defined in eq. (2.12) for an isotropic material. A similar formula holds for an arbitrary anisotropic medium, but the matrix $\mathbf{\Lambda}$ is then no longer diagonal.

Outcomes (4.2) and (4.3) can be attributed to Rice [117] (see formulas (5) and (6) of the celebrated

paper).

Consider two locations s and s' along the crack front $\mathcal{F}$. Place on $\mathcal{S}$ a point P by moving into the crack zone a small perpendicular distance ρ from s as depicted in figure 4.2.

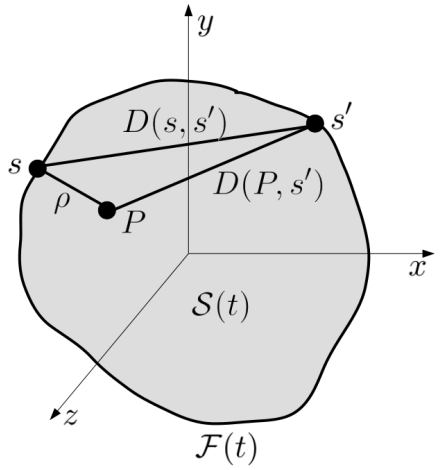

Figure 4.2: *Distances: ρ from point P on crack surface $\mathcal{S}(t)$ and its projection s to the crack front $\mathcal{F}(t)$; $D(P, s')$ from point P and a point s' along $\mathcal{F}(t)$, and $D(s, s')$ from s to s'. When $\rho \to 0$, $D(P, s') \to D(s, s')$.*

The ratio:

$$\frac{\mathbb{K}(P, s')}{\sqrt{\rho}} \tag{4.4}$$

has a well defined limit as $\rho \to 0$. A representation formula for the CFWFs holds (see for instance Lazarus [79]):

$$\mathbb{K}(P, s') = \frac{\sqrt{2\rho}}{\pi\sqrt{\pi}} \frac{1}{D^2(P, s')} \mathbb{W}^{\mathcal{S}}(P, s') \tag{4.5}$$

where $D(P, s')$ stands for the distance between point P and location s' along the crack front (see figure 4.2). Since tensile and shear problems are uncoupled for a planar crack in an infinite body, components of matrix $\mathbb{W}^{\mathcal{S}} = [W_{ij}^{\mathcal{S}}]$ are such that:

$$W_{12}^{\mathcal{S}} = W_{13}^{\mathcal{S}} = W_{21}^{\mathcal{S}} = W_{31}^{\mathcal{S}} = 0 \tag{4.6}$$

whatever the shape of the crack front. Such a property reflects on CFWFs in view of property (4.5).

Consider the well-defined limit [83]:

$$\mathbb{W}^{\mathcal{F}}(s, s') = \lim_{\rho \to 0} \mathbb{W}^{\mathcal{S}}(P, s') \tag{4.7}$$

Components $W_{ij}^{\mathcal{F}}(s, s')$ of matrix $\mathbb{W}^{\mathcal{F}}(s, s')$ are termed *fundamental kernels* (shortened in FKs). They depend on the crack front shape. The CFWFs are positively homogeneous of degree $-3/2$ meaning that if all distances are multiplied by some positive factor α, the CFWFs are multiplied by $\alpha^{-3/2}$. Eqs. (4.5) and (4.7) implie that FKs are positively homogeneous of degree 0:

$$\mathbb{W}^{\mathcal{F}}(\alpha s, \alpha s') = \mathbb{W}^{\mathcal{F}}(s, s') \quad \forall \alpha > 0 \tag{4.8}$$

Considering two problems, one with point forces equal to $\pm e_i$ exerted on the crack faces at a distance ρ from s, and one with point forces equal to $\pm e_j$ exerted on the crack faces at a distance ρ' from s', applying Betti's theorem, and using formulas (4.3) and (4.7), the following "symmetry" property arises for fundamental kernels and isotropic materials:

$$\mathbf{\Lambda}\mathbb{W}^{\mathcal{F}}(s,s')\mathbf{\Lambda}^{-T} = \mathbb{W}^{\mathcal{F}}(s',s) \tag{4.9}$$

Leblond and coworkers [82, 83] have shown that the limit of $\mathbb{W}^{\mathcal{F}}$ when $s' \to s$ is universal, in the sense that $\mathbb{W}^{\mathcal{F}}(s,s)$ does not depend on the geometry. It depends on the behavior of weight functions when the point of application of the load tends towards the point of observation of the SIF, which is a local property independent on the far geometry. This limit has values:

$$\begin{cases} \lim_{s'\to s} W_{11}^{\mathcal{F}}(s,s') = 1, \\ \lim_{s'\to s} W_{22}^{\mathcal{F}}(s,s') = \frac{2-3\nu}{2-\nu}, \\ \lim_{s'\to s} W_{33}^{\mathcal{F}}(s,s') = \frac{2+\nu}{2-\nu}, \\ \lim_{s'\to s} W_{23}^{\mathcal{F}}(s,s') = 0 \end{cases} \tag{4.10}$$

Fundamental kernels $\mathbb{W}^{\mathcal{F}}(s,s')$ for particular crack front shapes

FKs are known in closed form only for some particular crack front geometries and they will be detailed below for the case of circular and half plane cracks, as accurately reviewed by Lazarus in [79]:

- *Circular cracks*

for internal circular cracks with $\Gamma^u = \emptyset$, loaded by remote stresses, the values of non zero components of FKs are [44, 65]:

$$\begin{cases} W_{11}^{\mathcal{F}}(\phi_0,\phi_1) = 1 \\ W_{22}^{\mathcal{F}}(\phi_0,\phi_1) = \frac{2cos(\phi_0-\phi_1)-3\nu}{2-\nu} \\ W_{33}^{\mathcal{F}}(\phi_0,\phi_1) = \frac{2(1-\nu)cos(\phi_0-\phi_1)+3\nu}{2-\nu} \\ W_{23}^{\mathcal{F}}(\phi_0,\phi_1) = \frac{1}{1-\nu}W_{32}^{\mathcal{F}}(\phi_1,\phi_0) = \frac{2sin(\theta_0-\theta_1)}{2-\nu} \end{cases}$$

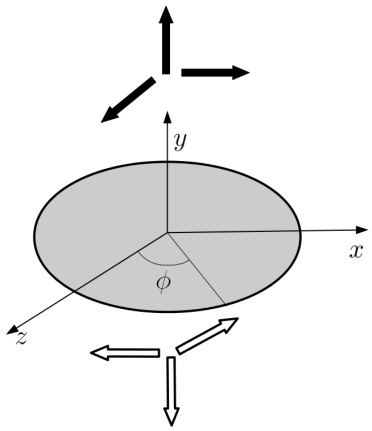

for external circular cracks loaded by remote stresses, only the component $W_{11}^{\mathcal{F}}$ is known for several cases of remote boundary conditions [45, 117]:
- remote points are clamped (vanishing displacements and rotations)

$$W_{11}^{\mathcal{F}}(\phi_0, \phi_1) = 1$$

- remote points are allowed to move in the direction orthogonal to the crack plane, but cannot rotate

$$W_{11}^{\mathcal{F}}(\phi_0, \phi_1) = 1 + 4\,\sin^2\left(\frac{\phi_0 - \phi_1}{2}\right)$$

- remote points can rotate, but cannot move in the direction orthogonal to the crack plane

$$W_{11}^{\mathcal{F}}(\phi_0, \phi_1) = 1 + 24\,\sin^2\left(\frac{\phi_0 - \phi_1}{2}\right)\cos(\phi_0 - \phi_1)$$

- remote points are constrained against any motion (vanishing force and momentum)

$$W_{11}^{\mathcal{F}}(\phi_0, \phi_1) = 1 + 4\,\sin^2\left(\frac{\phi_0 - \phi_1}{2}\right)[1 + 6\,\cos(\phi_0 - \phi_1)]$$

- *Half plane cracks*

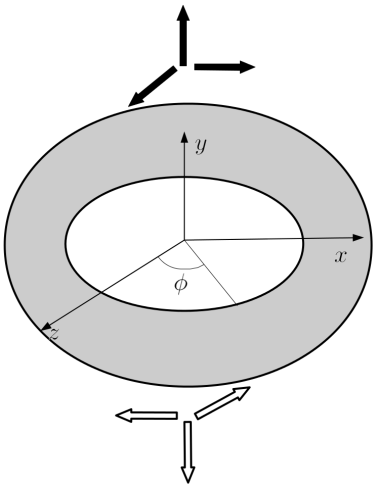

for half plane cracks with $\Gamma^u = \emptyset$ loaded by remote stresses (fig. a), or line traction (fig. b), or surface traction (fig c) the values of non zero components of FKs are:

$$\begin{cases} W_{11}^{\mathcal{F}}(z_1, z_0) = 1 \\ W_{22}^{\mathcal{F}}(z_1, z_0) = \frac{2-3\nu}{2-\nu} \\ W_{33}^{\mathcal{F}}(z_1, z_0) = \frac{2+\nu}{2-\nu} \\ W_{23}^{\mathcal{F}}(z_1, z_0) = 0 \end{cases}$$

The simple case of half plane crack has been extended to the case of the tunnel crack in order to introduce a length scale into the model, which is in fact missing for the half plane crack case (see Leblond and Mouchrif work for mode 1 [81], and Lazarus and Leblond works for shear loading [76, 77]).

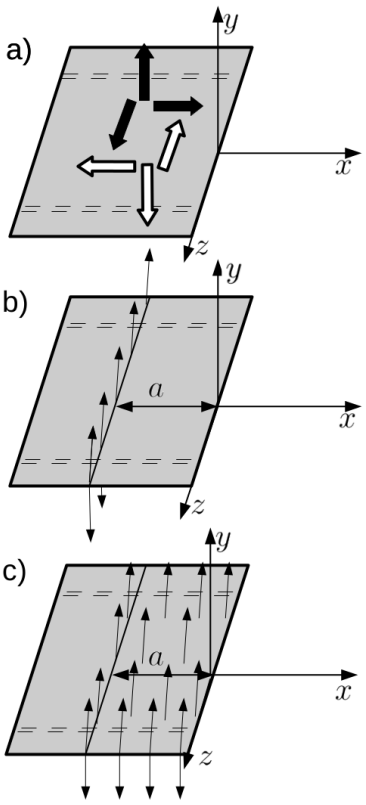

4.1 First order variation of the SIFs

Consider that an arbitrary three dimensional crack advances quasi-statically, under constant loading, by $\delta l(s)$ within its plane in the direction perpendicular to its front. The complex form (2.6) of operator $\mathbf{K}^{(1)}[\cdot]$ originates from a fundamental hypothesis about weight functions theory that was made in the seminal paper of Rice [117]. In setting up the formalism for calculating variations in the SIFs along a crack front to the first order accuracy in the advance $\delta l(s)$, a location along the crack front (say s_1) has been assumed to be steady, i.e. ($\delta l(s_1) = 0$). Focusing on planar cracks that propagate in their own plane so that kink angle $\theta(s)$ vanishes for all points along the crack front (as for delamination for instance), from expansion (2.2) one has:

$$\delta K_1(s) = K_1^{(1)}[s; \delta l(s')] \tag{4.11}$$

that relates the variation of SIF at location s to the first order variation $\delta l(s')$ of the whole crack front $\mathcal{F}$ under fixed loading conditions. The non locality of formula (4.11) is due to long range elastic interactions.

In such pure mode 1 conditions, quantities w_y for the crack opening displacement, $W_{11}^{\mathcal{S}}$ and $W_{11}^{\mathcal{F}}$ will be simply denoted henceforth as $w, W^{\mathcal{S}}$ and $W^{\mathcal{F}}$, respectively, in order to lighten the notation. Consider a point (x_1, z_1) at distance ρ_1 from s_1. From equations (2.12), (4.3) and (4.5), one can derive:

$$\delta w(x_1, z_1) = 2\Lambda_{11} \frac{\sqrt{2\rho_1}}{\pi\sqrt{\pi}} \int_{\mathcal{F}(t)} \frac{W^{\mathcal{S}}((x_1, z_1), s)}{D^2((x_1, z_1), s)} K_1(s)\, \delta l(s)\, ds \tag{4.12}$$

Diving both sides of eq. (4.12) by $\sqrt{\rho_1}$ and letting $\rho_1 \to 0$ one has [37, 117]:

$$\delta K_1(s_1) = \frac{1}{2\pi} \int_{\mathcal{F}} \frac{W^{\mathcal{F}}(s_1, s)}{D^2(s_1, s)} K_1(s)\, \delta l(s)\, ds \tag{4.13}$$

Condition $\delta l(s_1) = 0$ ensures the existence of the principal value integral along the crack front $\int_{\mathcal{F}}$ in eq. (4.13). Eq. (4.13) is exactly the same as eq. (2.5) (see [83]) with:

$$\frac{1}{2\pi} \frac{\mathbb{W}^{\mathcal{F}}(s_1, s)}{D^2(s_1, s)} = \mathbb{Z}(\Omega, s_1, s, \theta(s_1), \theta(s))$$

in the special case of a planar crack with a coplanar extension and $\delta l(s_1) = 0$. For completeness, it is shown the extension of eq. (4.13) to the case of mixed mode, due to Favier et al. [37], namely:

$$\delta \mathbf{K}(s_1) = \mathbb{N}(\theta)\, \mathbf{K}(s_1) \left.\frac{\partial \delta l}{\partial s'}\right|_{s_1} + \frac{1}{2\pi} \int_{\mathcal{F}} \frac{\mathbb{W}^{\mathcal{F}}(s_1, s)}{D^2(s_1, s)} \mathbf{K}(s)\, \delta l(s)\, ds \tag{4.14}$$

where matrix $\mathbb{N}(\theta)$ is the matrix defined in expansion (2.5), that in the case of vanishing kink angle reads:

$$\mathbb{N}(0) = \frac{2}{2-\nu} \begin{bmatrix} 0 & 0 & 0 \\ 0 & 0 & -1 \\ 0 & 1-\nu & 0 \end{bmatrix} \tag{4.15}$$

The drawbacks of hypothesis $\delta l(s_1) = 0$ have been circumvented by means of two different strategies (accurately reviewed by Lazarus in [79] in the general case of mixed mode propagation). The first one [117] consists of decomposing an arbitrary elongation of the crack front $\delta l(s)$ into two parts:
- a translatory motion of displacement vector $\delta l(s_1)\, e_2(s_1)$, where e_2 is the axis of the local Frenet frame orthogonal to $\mathcal{F}$ and oriented in the direction of propagation. This motion brings the point s_1 to its correct final position leaving the crack front shape unchanged. The corresponding normal advance $\delta l_*(s)$ is given, to the first order in $\delta l(s)$, by:

$$\delta l_*(s) = \delta l(s_1)\, e_2(s_1) \cdot\, e_2(s) \tag{4.16}$$

The associated variation of SIF $K_1(s)$ will be denoted by $\delta_* K_1(s)$.
- a motion with normal advance $\delta l(s) - \delta l_*(s)$ which vanishes at s_1. $\delta K_1(s_1)$ is therefore given by eq. (4.13).
The sum of the two motions leads to the final expression of the first order variation of the SIF in $\delta l(s)$:

$$\delta K_1(s_1) = \delta_* K_1(s_1) + \frac{1}{2\pi} \int_{\mathcal{F}} \frac{W^{\mathcal{F}}(s_1, s)}{D^2(s_1, s)} K_1(s)[\delta l(s) - \delta l_*(s)] ds \tag{4.17}$$

Provided that the quantity $\delta_* K_1(s_1)$ can be computed, eq. (4.17) allows to update the SIF from the initial values of the SIF and of the FK. For example, $\delta_* K_1(s_1)$ vanishes if the translatory motion $\delta l(s_1)\, e_2(s_1)$ do not change the problem, as in the case of a crack far from any boundary, so that the body can be assumed to be infinite submitted to remote stress loading.

The second strategy consists in decomposing the normal advance into a uniform advance $\delta l(s_1)$ and the advance $\delta l(s) - \delta l(s_1)$ for which eq. (4.13) can be used. This procedure leads to the following final expression:

$$\delta K_1(s_1) = [\delta K_1(s_1)]_{\delta l(s) \equiv \delta l(s_1)} + \frac{1}{2\pi} \int_{\mathcal{F}} \frac{W^{\mathcal{F}}(s_1, s)}{D^2(s_1, s)} K_1(s)[\delta l(s) - \delta l(s_1)]\, ds \tag{4.18}$$

provided that $[\delta K_1(s_1)]_{\delta l(s)\equiv\delta l(s_1)}$ can be computed, as for instance for circular, straight half-plane or tunnel cracks where the uniform advance $\delta l(s) \equiv \delta l(s_1)$ does not change the geometry of the problem.
The two approaches just described give complete generality to the formalism for calculating variations in the SIFs along a crack front, at the price of the purposely introduced assumption of infinite domain. When finite domain and associated boundary conditions have to be considered, the increase of the SIFs due to an additional motion pertaining to the two strategies described above may be of the same order of the one due to the change in the shape of the crack front. In [129], a different approach is pursued and the hypothesis of steady location, and consequently the ones introduced at a later stage to circumvent the resulting limitations, are removed in full. In this case the limit to the boundary process does not lead to a Cauchy principal value interpretation of integrals involved anymore, and the general concept of finite part of Hadamard is invoked. With the aim of intelligibility, the general path of reasoning of this new approach is firstly illustrated for the straightforward case of a semi infinite plane crack loaded by a pair of equal and opposite normal forces applied on the crack surfaces at a distance a from the crack front. The procedure is then detailed and further extended to the case of generic plane cracks under mode 1 loading.

4.1.1 Semi infinite plane crack

Consider the semi infinite plane crack loaded by unit point forces $t_y(P)$ applied on the crack surfaces at a distance a from the crack front as depicted in figure 4.3.

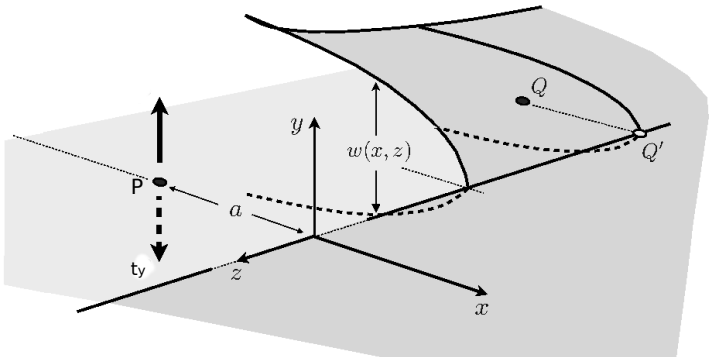

Figure 4.3: *Semi infinite plane crack loaded by a pair of equal and opposite normal forces $t_y(P)$ applied to the crack surfaces at point P at a distance a from the crack front. Field point Q is defined at coordinates $\{x, 0, z\}$ whereas Q' is the orthogonal projection of point Q onto the crack front.*

Such a mode 1 loading problem has been solved analytically [65, 140]. The opening $w(Q)$ at point $Q(x, z)$ for any $x < 0$ reads:

$$w(Q;a) = 2\,\frac{1-\nu}{\mu}\,\frac{t_y}{\pi^2}\,\frac{1}{\sqrt{(x+a)^2+z^2}}\arctan\left[\frac{2\sqrt{a|x|}}{\sqrt{(x+a)^2+z^2}}\right] \tag{4.19}$$

where ν is the Poisson's coefficient and μ is the shear modulus of the material. $w(Q;a)$ admits the following expansion about the crack front for $x < 0$:

$$w(Q;a) = \frac{(1-\nu)t_y}{\pi^2\mu}\left[\frac{4\sqrt{a}}{(a^2+z^2)}\sqrt{|x|} - \frac{8a^{3/2}}{3\,(a^2+z^2)^2}|x|^{3/2}\right] + O(|x|^{\frac{5}{2}}) \tag{4.20}$$

which is a truncation of the classical expansion [54] in the normal plane:

$$w(Q;a) = \sum_{n=0}^{\infty} \Xi_n(z,a)|x|^n\sqrt{|x|} \tag{4.21}$$

The outline of the opening is plot in figure 4.4. Owing to the well known relationship:

$$\Xi_0(z,a) = \frac{1-\nu}{\mu}\,\frac{4}{\sqrt{2\pi}}\,K_1(z) \tag{4.22}$$

the first order term in expansion (4.20) leads to the identity

$$K_1(z) = \frac{\sqrt{2}}{\pi\sqrt{\pi}}\frac{\sqrt{a}}{a^2+z^2}\,t_y \tag{4.23}$$

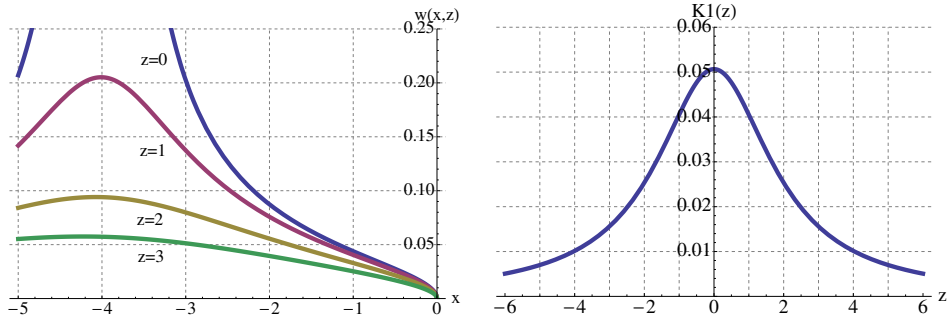

Figure 4.4: *a) Upper half of the opened semi infinite plane crack under mode 1 point force loading acting at $a = 4, z = 0$. As expected, opening is not bounded under the point load. b) $K_1(z)$ along the crack front.*

The crack remains plane during its propagation, even if the shape of its front will change from the straight initial configuration. Nevertheless this scenario will not be considered here, taking into account only an "unrealistic" but uniform propagation of the front in order to extend Rice's approach in the simplest case. On the contrary, interest is focused on a *z-independent propagation of the whole crack front* as if the distance a becomes $a + \delta l(z)$ for all abscissae z along the crack front. In view of the z-independency, the crack front elongation $\delta l(z)$ will be denoted simply as δl henceforth in this example. Bearing in mind that the amount $x + a$ remains unchanged at any point Q, it is straightforward to show that

$$\delta w(Q;a) = w(Q;a+\delta l) - w(Q;a) = 2\frac{1-\nu}{\mu}\,\frac{t_y}{\pi^2}\,\frac{a-x}{(x+a)^2+z^2}\,\frac{1}{\sqrt{a|x|}}\delta l + o(\delta l) \tag{4.24}$$

at any $x < 0$.

By means of the crack-face weight function

$$k_{11}((x,z),s') = \frac{\sqrt{2|x|}}{\pi\sqrt{\pi}}\,\frac{1}{x^2+(s'-z)^2} \tag{4.25}$$

which is available for the straightforward crack front shape at hand - see [117] formula (36), outcome (4.24) is obtained from integral (4.3):

$$\delta w(Q;a) = \frac{1-\nu}{\mu}\int_{-\infty}^{+\infty} k_{11}((x,z),s')\;K_1(s')\;\delta l(s')\,\mathrm{d}s' \tag{4.26}$$

to the first order in δl. The term $\Xi_0(z,a)$ was used by Rice in formula (61) of [117] to express the first order variation

$$\delta w(Q;a) = 4\frac{1-\nu}{\mu}\,\frac{1}{\sqrt{2\pi}}\,\sqrt{|x|}\,\delta K_1(z)$$

under the assumption that $\delta l(Q') = 0$, with Q' orthogonal projection of point Q along the crack front - see figure 4.3. Such an assumption, that is not inborn in the integral formulation (4.26), cannot be pursued in the present example however, as distance $|x|$ from the crack front becomes $|x| + \delta l$ and linear terms in δl come into play from the higher order terms of the expansion (4.21):

$$\begin{aligned} w(Q;a+\delta l) &= \sum_{n=0}^{\infty} \Xi_n(z,a+\delta l)(|x|+\delta l)^n\sqrt{|x|+\delta l} \qquad (4.27)\\ &= \sum_{n=0}^{\infty}\sum_{k=0}^{n}\left(\begin{array}{c} n \\ k \end{array}\right)|x|^{n-k}\delta l^k\left(\Xi_n(z,a) + \left.\frac{\partial \Xi_n}{\partial a}\right|_a \delta l\right)\left(\sqrt{|x|} - \frac{\sqrt{|x|}}{2x}\delta l\right) + o(\delta l) \end{aligned}$$

whence:

$$\begin{aligned} \delta w(Q;a) &= \sqrt{|x|}\left\{-\frac{\Xi_0(z,a)}{2x} + \left.\frac{\partial \Xi_0}{\partial a}\right|_a + \frac{3}{2}\Xi_1(z,a)\right\}\delta l + \qquad (4.28)\\ &\quad |x|\sqrt{|x|}\left\{\left.\frac{\partial \Xi_1}{\partial a}\right|_a + \sum_{n=2}^{\infty}\left[-\Xi_n(z,a)\left(\frac{|x|^{n-1}}{2x} + n|x|^{n-2}\right) + \left.\frac{\partial \Xi_n}{\partial a}\right|_a |x|^{n-1}\right]\right\}\delta l + o(\delta l) \end{aligned}$$

By comparing the latter with (4.26), after dividing both sides by $\sqrt{|x|}$ and taking the limit $x \to 0^-$, it comes out:

$$\left.\frac{\partial \Xi_0}{\partial a}\right|_a (z,a) = \lim_{x\to 0^-}\left[\frac{\Xi_0(z,a)}{2x} - \frac{3}{2}\Xi_1(z,a) + \frac{1-\nu}{\mu}\,\frac{1}{\sqrt{|x|}}\int_{-\infty}^{+\infty} k_{11}((x,z),s')\,K_1(s')\mathrm{d}s'\right] \qquad (4.29)$$

i.e., in view of (4.22), (4.25):

$$\delta K_1(z) = \left\{\lim_{x\to 0^-}\left[\frac{K_1(z)}{2x} + \frac{\sqrt{2\pi}}{4}\int_{-\infty}^{+\infty}\frac{k_{11}((x,z),s')}{\sqrt{|x|}}\,K_1(s')\mathrm{d}s'\right] - \frac{\mu}{1-\nu}\,\frac{\sqrt{2\pi}}{4}\,\frac{3}{2}\Xi_1(z,a)\right\}\,\delta l \qquad (4.30)$$

According to representation formula (4.5) and limit (4.7), the FK $W^{\mathcal{F}}(z,s')$ has the form [79]:

$$W^{\mathcal{F}}(z,s') = \pi\sqrt{\frac{\pi}{2}}D^2(z,s')\lim_{x\to 0^-}\frac{k_{11}((x,z),s')}{\sqrt{|x|}} \qquad (4.31)$$

where $D(z,s')$ denotes the cartesian distance between locations z and s' along the crack front. $W^{\mathcal{F}}(z,s')$ is known to be finite in general and in particular for the semi infinite plane crack under mode 1 loading because of (4.25). Furthermore, one has:

$$\begin{aligned} &\lim_{x\to 0^-}\int_{-\infty}^{+\infty}\frac{k_{11}((x,z),s')}{\sqrt{|x|}}\,K_1(s')\,\mathrm{d}s' = \qquad (4.32)\\ &\quad \frac{\sqrt{2}}{\pi\sqrt{\pi}}\int_{-\infty}^{+\infty}\frac{W^{\mathcal{F}}(z,s')}{D^2(z,s')}\left(K_1(s') - K_1(z) - \left.\frac{\partial K_1}{\partial s'}\right|_z (s'-z)\right)\mathrm{d}s' + \\ &\quad\quad K_1(z)\lim_{x\to 0^-}\int_{-\infty}^{+\infty}\frac{k_{11}((x,z),s')}{\sqrt{|x|}}\,\mathrm{d}s' + \left.\frac{\partial K_1}{\partial s'}\right|_z \lim_{x\to 0^-}\int_{-\infty}^{+\infty}\frac{k_{11}((x,z),s')}{\sqrt{|x|}}\,(s'-z)\mathrm{d}s' \end{aligned}$$

In view of (4.25) one has for the case at hand:

$$\int_{-\infty}^{+\infty} \frac{k_{11}((x,z),s')}{\sqrt{|x|}}\,\mathrm{d}s' = -\frac{\sqrt{2}}{\sqrt{\pi}}\,\frac{1}{x}\,, \qquad \int_{-\infty}^{+\infty} \frac{k_{11}((x,z),s')}{\sqrt{|x|}}\,(s'-z)\mathrm{d}s' = 0$$

and (4.30) turns out to be:

$$\delta K_1(z) = \left[\frac{1}{2\pi}\int_{-\infty}^{+\infty} \frac{W^{\mathcal{F}}(s',z)}{D^2(s',z)}\,\left(K_1(s') - K_1(z) - \left.\frac{\partial K_1}{\partial s'}\right|_z (s'-z)\right)\mathrm{d}s' - \frac{\mu}{1-\nu}\,\frac{3\sqrt{2\pi}}{8}\,\Xi_1(z,a)\right]\,\delta l \tag{4.33}$$

Direct substitution provides:

$$\delta K_1(z) = \frac{\mathsf{t_y}}{\sqrt{2a}}\,\frac{1}{\pi\sqrt{\pi}}\,\frac{z^2-3a^2}{(a^2+z^2)^2}\,\delta l \tag{4.34}$$

that confirms the outcome derived directly from (4.23). In the easy case of semi infinite plane crack under mode 1 loadings, equations (4.30) and (4.33) extend, in the sense that the steady location hypothesis has been removed, Rice's formula (63) in [117], namely:

$$\delta K_1(z) = \frac{1}{2\pi}\,\fint_{-\infty}^{+\infty} \frac{W^{\mathcal{F}}(z,s')}{D^2(z,s')} K_1(s')\,\delta l(s')\,ds' \tag{4.35}$$

Outcome (4.30) can be formulated in terms of the finite part of Hadamard. Such an interpretation shows the intimate nature of the limit process established in [117] in the general case, i.e. when the hypothesis of steady location has not made recourse to.

To this aim, the finite part of Hadamard is firstly defined as follows. Let $\varepsilon_0 > 0$, $\varepsilon \to I(\varepsilon)$ denote a complex-valued function which is continuous in $]0,\varepsilon_0]$ and assume that

$$I(\varepsilon) = I_0 + I_1\log(\varepsilon) + \sum_{j=2}^{m} I_j\,\varepsilon^{1-j} + o(1); \qquad \varepsilon \to 0 \tag{4.36}$$

where $I_j \in \mathbb{C}$. Then I_0 is called the *Hadamard's finite part* of $I(\varepsilon)$. In dealing with integrals, the finite part I_0 of a usually divergent integral $\int_{-\infty}^{+\infty} f(t)\,dt$ is denoted by the symbol $\fint_{-\infty}^{+\infty} f(t)\,dt$.

Applying the definition above to formula (4.30), it holds:

$$\begin{aligned} I(\varepsilon) = \lim_{\varepsilon\to 0^+}\left[\int_{-\infty}^{z-\varepsilon} \frac{W^{\mathcal{F}}(z,s')}{D^2(z,s')}\,K_1(s')\mathrm{d}s' + \int_{z+\varepsilon}^{+\infty} \frac{W^{\mathcal{F}}(z,s')}{D^2(z,s')}\,K_1(s')\mathrm{d}s'\right] = \\ \int_{-\infty}^{+\infty} \frac{W^{\mathcal{F}}(z,s')}{D^2(z,s')}\,\left(K_1(s') - K_1(z) - \left.\frac{\partial K_1}{\partial s'}\right|_z (s'-z)\right)\mathrm{d}s' + \\ K_1(z)\lim_{\varepsilon\to 0^+}\left[\int_{-\infty}^{z-\varepsilon} \frac{W^{\mathcal{F}}(z,s')}{D^2(z,s')}\,\mathrm{d}s' + \int_{z+\varepsilon}^{+\infty} \frac{W^{\mathcal{F}}(z,s')}{D^2(z,s')}\,\mathrm{d}s'\right] + \\ \left.\frac{\partial K_1}{\partial s'}\right|_z \lim_{\varepsilon\to 0^+}\left[\int_{-\infty}^{z-\varepsilon} \frac{W^{\mathcal{F}}(z,s')}{D^2(z,s')}\,(s'-z)\mathrm{d}s' + \int_{z+\varepsilon}^{+\infty} \frac{W^{\mathcal{F}}(z,s')}{D^2(z,s')}\,(s'-z)\mathrm{d}s'\right] = \\ \int_{-\infty}^{+\infty} \frac{W^{\mathcal{F}}(z,s')}{D^2(z,s')}\,\left(K_1(s') - K_1(z) - \left.\frac{\partial K_1}{\partial s'}\right|_z (s'-z)\right)\mathrm{d}s' + K_1(z)\lim_{\varepsilon\to 0^+}\frac{2}{\varepsilon} \end{aligned} \tag{4.37}$$

Accordingly, eq. (4.33) can be rephrased as:

$$\delta K_1(z) = \frac{1}{2\pi} \fint_{-\infty}^{+\infty} \frac{W^{\mathcal{F}}(z,s')}{D^2(z,s')} K_1(s')\, \delta l(s')\, \mathrm{d}s' - \frac{\mu}{1-\nu} \frac{3\sqrt{2\pi}}{8} \Xi_1(z,a)\, \delta l \tag{4.38}$$

Identifying z with s, eq. (4.38) can be compared with (4.11) and operator $K_1^{(1)}$ stated as:

$$K_1^{(1)}[z;\delta l(z')] = \frac{1}{2\pi} \fint_{-\infty}^{+\infty} \frac{W^{\mathcal{F}}(z,s')}{D^2(z,s')} K_1(s')\, \delta l(s')\, \mathrm{d}s' - \frac{\mu}{1-\nu} \frac{3\sqrt{2\pi}}{8} \Xi_1(z,a) \delta l \tag{4.39}$$

Recalling the definition of the Gateaux derivative of the affine operator $N[\cdot]$ detailed in eq. (2.40), it can be expressed for this case in the form:

$$N_v'[w] = \frac{1-\nu^2}{E} K_1(z) \left[\frac{1}{2\pi} \fint_{-\infty}^{+\infty} \frac{W^{\mathcal{F}}(z,s')}{D^2(z,s')} K_1(s') w(s') ds' - \frac{\mu}{1-\nu} \frac{3\sqrt{2\pi}}{8} \Xi_1(z,a) w(z) \right] \tag{4.40}$$

The obtained final formalism leads to an easy proof of the symmetry property of Gateaux derivative of $N[\cdot]$ (2.41) that has been demonstrated in Section 2.5.2 relying on the physical meaning of the operator itself. Eq. (2.41) has the form:

$$\begin{aligned} \int_{-\infty}^{+\infty} K_1(z) v(z) \fint_{-\infty}^{+\infty} \frac{W^{\mathcal{F}}(z,s')}{D^2(z,s')} K_1(s')\, w(s') \mathrm{d}s' \mathrm{d}z = \\ \int_{-\infty}^{+\infty} K_1(z) w(z) \fint_{-\infty}^{+\infty} \frac{W^{\mathcal{F}}(z,s')}{D^2(z,s')} K_1(s')\, v(s') \mathrm{d}s' \mathrm{d}z \end{aligned} \tag{4.41}$$

In a nutshell thus operator $N_v'[\cdot]$ inherits symmetry from the fundamental kernel matrix $\mathbb{W}^{\mathcal{F}}$. The proof of symmetry property (2.41) in the form (4.41) allows to restate variational formulations presented in [127] and described in Section 2.5.2 in terms of weight functions. Discrete part of such variational statements leads to an effective numerical scheme for the approximation of the quasi-static velocity of the crack front.

4.1.2 Arbitrary plane cracks under mode 1 loading

Outcomes (4.30), (4.38) and (4.41), straightforwardly derived for the case of a semi infinite plane crack, are now extended to generic plane cracks under mode 1 loading. Consider thus a plane crack configuration, under the assumption that it propagates in its own plane and in pure mode 1 (see figure 4.5).

Choose two locations s and s' along the front $\mathcal{F}$ at time t. Locate on $\mathcal{S}(t)$ a point P by moving from $\mathcal{F}(t)$ into the crack zone a small perpendicular distance ρ from s, and a point Q by moving a small distance ρ' from s'. Analogously to eq. (4.21), the opening at point P and time t, denoted by $w(P;t)$, admits an expansion [54] in the normal plane in terms of ρ:

$$w(P;t) = \sum_{n=0}^{\infty} \Xi_n(s)\, \rho^n \sqrt{\rho} \tag{4.42}$$

At time $t + \delta t > t$ the crack front reshapes, moving to curve $\mathcal{F}(t+\delta t)$. At location s along $\mathcal{F}(t)$ an (always positive) infinitesimal elongation $\delta l(s;t,t+\delta t) > 0$, indicated henceforth simply with $\delta l(s)$, takes place in the normal plane. The opening at point P and time $t+\delta t$ changes, and will be denoted either by $w(P;t+\delta t)$ or by $w(P;\delta l(s))$. Expansion (4.27) applies to $w(P;\delta l(s))$, if a

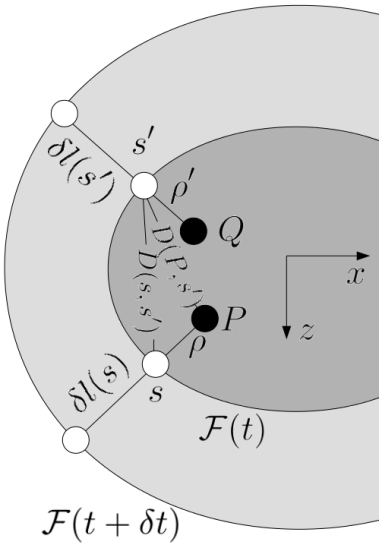

Figure 4.5: *An arbitrary plane crack, under the assumption that it evolves merely in its own plane and in pure mode 1: notation.*

proper definition of $\frac{\partial \Xi_n}{\partial a}\big|_a \delta l(s)$ is set, in order to take into account the variation of the crack front with time, where a is in this case a characteristic length of the crack at time t that locates the position of $\mathcal{F}$ at time t.

The first order variation $\frac{\partial \Xi_n}{\partial a}\big|_a \delta l(s)$ is here defined, in accordance with [82, 83], in the Gateaux differential sense for Ξ_n. To this aim, the $\delta l(s)$ is assumed to be the product of a given non-negative function (say $\eta(s) > 0$) by a small positive real parameter α. The following notation will be used:

$$\left.\frac{\partial \Xi_n}{\partial a}\right|_a \delta l(s) = \left.\frac{\partial \Xi_n}{\partial \alpha}(s, \alpha\, \eta(s))\right|_{\alpha=0} \alpha \tag{4.43}$$

The parameter α can be thought of as some kinematic time and the function $\eta(s)$ as the corresponding rate of propagation of the crack front. Equation (4.28) can be extended in the following terms:

$$\delta w(P;a) \;=\; \sqrt{\rho}\left\{\frac{\Xi_0(s)}{2\rho} + \left.\frac{\partial \Xi_0}{\partial a}\right|_a + \frac{3}{2}\Xi_1(s)\right\}\delta l(s) + \rho\,\sqrt{\rho}\; h(s;\rho;\mathcal{F})\; \delta l(s) + o(\delta l) \tag{4.44}$$

with $h(s;\rho;\mathcal{F})$ bounded at $\rho \to 0^+$.

One may make the influence of the crack front $\mathcal{F}$ at time t on $\Xi_n(s)$ explicitly in writing $\Xi_n(s, \mathcal{F}(t))$. After the elongation by $\delta l(s)$, at time $t + \delta t > t$, the normal plane at abscissa s can be different from the one before the elongation at time t. This difference impacts on $\Xi_n(s, \mathcal{F}(t+\delta t))$ and ultimately on $w(P; a + \delta l)$. The perpendicular to the new crack front at location s no longer passes trough point P, but misses it by a distance $(\rho + \delta l(s))\delta\phi$ measured parallel to $\mathcal{F}(t+\delta t)$ where $\delta\phi = d[\delta l(s)]/da\, \delta s$. This effect, as noted already by Rice in [117], may be included in the analysis, recognizing that $\delta w(P;a)$ should be strictly replaced by its value plus $(\rho + \delta l(s))\delta\phi$ times the gradient of δw in the direction parallel to $\mathcal{F}(t+\delta t)$. However, that modification gives a term of order $\rho\sqrt{\rho}\;\delta\phi$, that can be included in $h(s;\rho;\mathcal{F})\delta l(s)$ in equation (4.44).

In view of equation (4.22) that still holds, equation (4.44) becomes:

$$\begin{aligned}\delta w(P;a) &= \sqrt{\rho}\left\{\frac{1-\nu}{\mu}\,\frac{4}{\sqrt{2\pi}}\left[\frac{K_1(s)}{2\rho}+\left.\frac{\partial K_1}{\partial a}\right|_a\right]+\frac{3}{2}\Xi_1(s)\right\}\delta l(s)\\ &+ \rho\sqrt{\rho}\,h(s;\rho;\mathcal{F})\,\delta l(s)+o(\delta l)\end{aligned} \tag{4.45}$$

with $\left.\frac{\partial K_1}{\partial a}\right|_a$ defined analogously to $\left.\frac{\partial \Xi_n}{\partial a}\right|_a$ in (4.43). After dividing both sides by $\sqrt{\rho}$ and taking the limit $\rho\to 0^+$, one has from (4.26) and (4.45):

$$\begin{aligned}\delta K_1(s) &= \lim_{\rho\to 0^+}\left[-\frac{K_1(s)}{2\rho}\,\delta l(s)+\frac{\sqrt{2\pi}}{4}\int_{\mathcal{F}(t)}\frac{k_{11}((x,z),s')}{\sqrt{\rho}}\,K_1(s')\,\delta l(s')\,\mathrm{d}s'\right]\\ &- \frac{\mu}{1-\nu}\,\frac{3\sqrt{2\pi}}{8}\,\Xi_1(s)\,\delta l(s)\end{aligned} \tag{4.46}$$

where $\frac{k_{11}((x,z),s')}{\sqrt{\rho}}$ has a well defined limit as $\rho\to 0^+$ as already stressed. By means of representation formula (4.5), the former equation reads

$$\begin{aligned}\delta K_1(s) &= \lim_{\rho\to 0^+}\left[-\frac{K_1(s)}{2\rho}\,\delta l(s)+\frac{1}{2\pi}\int_{\mathcal{F}(t)}\frac{W^{\mathcal{S}}(P,s')\,K_1(s')\,\delta l(s')}{D^2(P,s')}\,\mathrm{d}s'\right]\\ &- \frac{\mu}{1-\nu}\,\frac{3\sqrt{2\pi}}{8}\,\Xi_1(s)\,\delta l(s)\end{aligned} \tag{4.47}$$

that extends Rice's formula (63) in [117] to the case at hand.

Denoting with

$$\Upsilon(\rho,s;s')=W^{\mathcal{S}}(P,s')\,K_1(s')\,\delta l(s')$$

equation (4.47) holds:

$$\begin{aligned}\delta K_1(s) &= \frac{1}{2\pi}\lim_{\rho\to 0^+}\int_{\mathcal{F}(t)}\frac{\Upsilon(\rho,s;s')-\Upsilon(\rho,s;s)-\left.\frac{\partial\Upsilon}{\partial s'}\right|_s(s'-s)}{D^2(P,s')}\,\mathrm{d}s'\\ &+ \lim_{\rho\to 0^+}\left[\frac{1}{2\pi}W^{\mathcal{S}}(P,s)\int_{\mathcal{F}(t)}\frac{1}{D^2(P,s')}ds'-\frac{1}{2\rho}\right]K_1(s)\delta l(s)\\ &+ \lim_{\rho\to 0^+}\frac{1}{2\pi}\left.\frac{\partial\Upsilon}{\partial s'}\right|_s\int_{\mathcal{F}(t)}\frac{s'-s}{D^2(P,s')}ds'-\frac{\mu}{1-\nu}\frac{3\sqrt{2\pi}}{8}\Xi_1(s)\delta l(s)\end{aligned} \tag{4.48}$$

As it will be proven in appendix A, the following asymptotics hold:

$$\int_{\mathcal{F}(t)}\frac{1}{D^2(P,s')}ds'=\frac{\pi}{\rho}-c\pi+\fint_{\mathcal{F}(t)}\frac{1}{D^2(s,s')}ds'+o(\rho) \tag{4.49}$$

$$\int_{\mathcal{F}(t)}\frac{s'-s}{D^2(P,s')}ds'=\fint_{\mathcal{F}(t)}\frac{s'-s}{D^2(s,s')}ds'+o(\rho) \tag{4.50}$$

where c is the local curvature of the crack front at point s. Furthermore, $\mathbb{W}^{\mathcal{S}}$ will be taken sufficiently smooth with respect to ρ to be expanded in Taylor series as:

$$\mathbb{W}^{\mathcal{S}}(P,s)=\mathbb{W}^{\mathcal{F}}(s,s)+\left.\frac{\partial\mathbb{W}^{\mathcal{S}}}{\partial\rho}\right|_{s,s}\rho+o(\rho)=1+\left.\frac{\partial\mathbb{W}^{\mathcal{S}}}{\partial\rho}\right|_{s,s}\rho+o(\rho) \tag{4.51}$$

in view of property (4.10). As a consequence, singularities cancel out and one finally has

$$\begin{aligned}\delta K_1(s) &= \frac{1}{2\pi}\int_{\mathcal{F}(t)} \frac{\Upsilon(0,s;s') - \Upsilon(0,s;s) - \frac{\partial \Upsilon}{\partial s'}\big|_s (s'-s)}{D^2(s,s')}\,\mathrm{d}s' \\ &+ \frac{1}{2\pi}\left.\frac{\partial \Upsilon}{\partial s'}\right|_s \int_{\mathcal{F}(t)} \frac{s'-s}{D^2(s,s')}\,\mathrm{d}s' \\ &+ \left[\frac{1}{2\pi}\,\fint_{\mathcal{F}(t)} \frac{1}{D^2(s,s')} ds' - \frac{c}{2} + \frac{1}{2}\left.\frac{\partial W^{\mathcal{S}}}{\partial \rho}\right|_{s,s}\right] K_1(s)\delta l(s) \\ &- \frac{\mu}{1-\nu}\frac{3\sqrt{2\pi}}{8}\,\Xi_1(s)\,\delta l(s)\end{aligned} \tag{4.52}$$

It seems of interest to investigate if formula (4.52) may be given a significance in terms of finite part of Hadamard as for equation (4.38). In view of the outcome:

$$\begin{aligned}\fint_{\mathcal{F}(t)} \frac{\Upsilon(0,s;s')}{D^2(s,s')}\,\mathrm{d}s' &= \int_{\mathcal{F}(t)} \frac{\Upsilon(0,s;s') - \Upsilon(0,s;s) - \frac{\partial \Upsilon}{\partial s'}\big|_s (s'-s)}{D^2(s,s')}\,\mathrm{d}s' \\ &+ \Upsilon(0,s;s)\ \fint_{\mathcal{F}(t)} \frac{1}{D^2(s,s')}\,\mathrm{d}s' + \left.\frac{\partial \Upsilon}{\partial s'}\right|_s \int_{\mathcal{F}(t)} \frac{s'-s}{D^2(s,s')}\,\mathrm{d}s'\end{aligned}$$

it holds

$$\begin{aligned}\delta K_1(s) &= \frac{1}{2\pi}\,\fint_{\mathcal{F}(t)} \frac{W^{\mathcal{F}}(s,s')\,K_1(s')\,\delta l(s')}{D^2(s,s')}\,\mathrm{d}s' + \left[\frac{1}{2}\left.\frac{\partial W^{\mathcal{S}}}{\partial \rho}\right|_{s,s} - \frac{c}{2}\right] K_1(s)\,\delta l(s) \\ &- \frac{\mu}{1-\nu}\frac{3\sqrt{2\pi}}{8}\,\Xi_1(s)\,\delta l(s)\end{aligned} \tag{4.53}$$

Formula (4.53) identifies four alternative basic constituents of operator $K_1^{(1)}[\cdot]$, besides the SIFs of course, with respect to the operator $\mathbb{Z}$ of eq. (2.5) detailed in [83]. Such constituents are: the non universal FK $\mathbb{W}^{\mathcal{F}}$, the derivative $\frac{\partial \mathbb{W}^{\mathcal{S}}}{\partial \rho}$, the *geometrical term* c, and the 3/2 order term Ξ_1 of the crack opening expansion (4.42).
In this regard, several open issues need to be dealt with. The estimation of Ξ_1 requires high order special elements along the crack front, together with the deployment of effective algorithms for its identification, as described in Section 3.1.6. Quantities $\mathbb{W}^{\mathcal{S}}$ are not known for general configurations of cracks, particularly in finite bodies, in which they depend on the definition of Dirichlet and Neumann boundary conditions. Intuition suggests that $\left.\frac{\partial \mathbb{W}^{\mathcal{S}}}{\partial \rho}\right|_{s,s}$ has a universal character, but such a feature has not been proved yet.

In the general case of plane cracks under pure mode 1 loading, symmetry property (2.41) of operator $N_v'[\cdot]$ can be written in terms of weight functions. Gateaux derivative of operator $N[\cdot]$ (2.40) holds:

$$\begin{aligned}N_v'[w] &= \frac{1-\nu^2}{E} K_1(s)\left[\frac{1}{2\pi}\,\fint_{\mathcal{F}(t)} \frac{W^{\mathcal{F}}(s,s')K_1(s')w(s')}{D^2(s,s')} ds' \right. \\ &+ \left.\left(\frac{1}{2}\left.\frac{\partial W^{\mathcal{S}}}{\partial \rho}\right|_{s,s} - \frac{c}{2}\right) K_1(s)w(s) - \frac{\mu}{1-\nu}\frac{3\sqrt{2\pi}}{8}\Xi_1(s)w(s)\right]\end{aligned} \tag{4.54}$$

and symmetry property (2.41) has the form

$$\int_{\mathcal{F}(t)} K_1(s)\, v(s) \fint_{\mathcal{F}(t)} \frac{W^{\mathcal{F}}(s,s')\, K_1(s')\, w(s')}{D^2(s,s')}\, \mathrm{d}s'\, \mathrm{d}s = \int_{\mathcal{F}(t)} K_1(s) w(s) \fint_{\mathcal{F}(t)} \frac{W^{\mathcal{F}}(s,s')\; K_1(s')\; v(s')}{D^2(s,s')} \mathrm{d}s'\, \mathrm{d}s \tag{4.55}$$

that is a sound extension of property (4.41).

4.2 Internal circular crack

4.2.1 Closed form of the first order variation of K_1

In the following benchmark, the closed form of the first order variation of SIF K_1 (4.53) is derived for the case of an internal circular crack.

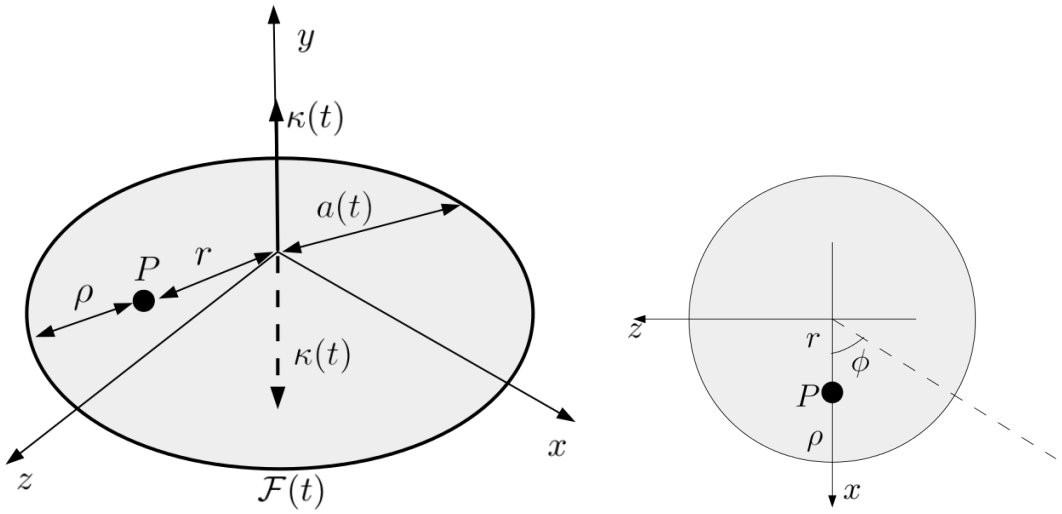

Figure 4.6: *a) Penny shape crack of variable radius $a(t)$ in an unbounded linear elastic media, subject to two point load forces $-\kappa(t)\mathbf{n}$ in its center, where $\kappa(t)$ stands for the load factor and $\mathbf{n}$ stands for the outer normal, so they open the crack. b) Notation about a circular crack front*

Consider a penny shape crack (see figure 4.6) with radius $a(t) \geq a(0) > 0$ embedded in a continuum body, subject to two point-loads of magnitude $\mathbf{t} = -\kappa(t)\mathbf{n}$ acting in the centers of the upper and lower crack surfaces which are directed away from the crack faces, so to open the crack. At each t, the solution in terms of SIFs can be found in [65] and reads:

$$K_1(a(t)) = \frac{\kappa(t)}{\pi a(t)} \frac{1}{\sqrt{\pi a(t)}} \tag{4.56}$$

independently on abscissa s along the crack front. The solution

$$w(\rho) = \frac{1-\nu}{\mu}\, \frac{2}{\pi^2}\, \frac{\kappa}{r}\, \arccos\left(\frac{r}{a}\right) = \frac{1-\nu}{\mu}\, \frac{\kappa}{\pi^2}\, \frac{\sqrt{\rho}}{a\sqrt{a}} \left(2\sqrt{2} + \frac{13}{3\sqrt{2}} \frac{\rho}{a}\right) + o(\rho^{3/2}) \tag{4.57}$$

in terms of the crack opening w can be obtained by the Fourier-Hankel transform, with $\rho = a - r > 0$ (see figure 4.6). By virtue of (4.42):

$$\Xi_0(a) = \frac{2\sqrt{2}}{\pi^2}\,\frac{1-\nu}{\mu}\,\frac{\kappa}{a\sqrt{a}} \qquad \Xi_1(a) = \frac{13}{3\sqrt{2}}\,\frac{1-\nu}{\mu}\,\frac{\kappa}{\pi^2}\,\frac{1}{a^2\sqrt{a}} \tag{4.58}$$

Assuming an homothetic infinitesimal expansion δa about the center, one notes that r does not change with δa and gets the counterpart of (4.44) as:

$$\begin{aligned}\delta w &= 2\,\frac{1-\nu}{\mu}\,\frac{1}{\pi^2}\,\frac{\kappa}{a}\,\frac{1}{\sqrt{2a-\rho}}\,\frac{1}{\sqrt{\rho}}\,\delta a + o(\delta a)\\ &= \frac{\sqrt{2}}{\pi^2}\frac{1-\nu}{\mu}\frac{\kappa}{a\sqrt{a}}\left[\frac{1}{\sqrt{\rho}} + \frac{1}{4a}\sqrt{\rho}\right]\delta a + O(\rho\,\sqrt{\rho}\,\delta a) + o(\delta a)\end{aligned} \tag{4.59}$$

The latter can be recovered via crack-face weight functions from integral (4.3), by taking into account (4.56) and:

$$k_{11}((x,z),s') = \frac{\sqrt{\rho(2a-\rho)}}{\pi\sqrt{\pi a}}\,\frac{1}{D^2((x,z),s')} \tag{4.60}$$

that is provided in [117]. In view of the outcome (4.56), one immediately obtains for a constant elongation $\delta a(s) = \delta a$

$$\delta K_1 = -\frac{3}{2}\frac{\kappa}{\pi a^2}\frac{1}{\sqrt{\pi a}}\delta a \tag{4.61}$$

The same result can be derived from the procedure described in Section 4.1. As first, it can be deduced from the limit process (4.48). For a circular crack of radius a it holds:

$$D^2(P,s') = a^2 + r^2 - 2\,a\,r\cos(\phi); \qquad D^2(s,s') = 2a^2(1-\cos(\phi)) \tag{4.62}$$

whence

$$\int_{\mathcal{F}(t)} \frac{1}{D^2(P,s')}\,\mathrm{d}s' = \int_{-\pi}^{\pi} \frac{a}{a^2 + r^2 - 2\,a\,r\cos(\phi)}\,\mathrm{d}\phi = \frac{2\,a\,\pi}{a^2 - r^2} \tag{4.63}$$

$$\int_{\mathcal{F}(t)} \frac{s'-s}{D^2(P,s')}\,\mathrm{d}s' = \int_{-\pi}^{\pi} \frac{a^2\phi}{a^2 + r^2 - 2\,a\,r\cos(\phi)}\,\mathrm{d}\phi = 0 \tag{4.64}$$

With regard to the finite part of Hadamard one has:

$$\begin{aligned}I(\varepsilon) &= \lim_{\varepsilon\to 0^+}\left[\int_{-\pi}^{-\varepsilon}\frac{1}{D^2(s,s')}ds' + \int_{\varepsilon}^{\pi}\frac{1}{D^2(s,s')}ds'\right]\\ &= \frac{2}{a\varepsilon} - \frac{\varepsilon}{6a} + o(\varepsilon)\end{aligned} \tag{4.65}$$

whence

$$⨍_{-\pi}^{\pi} \frac{1}{D^2(s,s')}\,\mathrm{d}s' = 0 \tag{4.66}$$

Integral (4.49) at $\rho \to 0^+$ reads:

$$\int_{\mathcal{F}(t)} \frac{1}{D^2(P,s')}\,\mathrm{d}s' = \frac{2\,a\,\pi}{2a-\rho}\,\frac{1}{\rho} = \frac{\pi}{\rho} + \frac{\pi}{2a} + o(1) \tag{4.67}$$

thus the curvature $c = -1/(2a)$ in view of (4.49) and (4.67). Moreover, as from representation formula (4.5) and (4.60) the weight function reads

$$W^{\mathcal{S}}(P,s) = \sqrt{\frac{2a-\rho}{2a}}, \tag{4.68}$$

it also holds:

$$\left.\frac{\partial W^{\mathcal{S}}}{\partial \rho}\right|_{s,s} = -\frac{1}{4a} \tag{4.69}$$

Outcome (4.61) comes out immediately from (4.52) in view of (4.58), (4.64), (4.66), and the identity:

$$\int_{\mathcal{F}(t)} \frac{\Upsilon(0,s;s') - \Upsilon(0,s;s) - \left.\frac{\partial \Upsilon}{\partial s'}\right|_s (s'-s)}{D^2(s,s')} ds' = 0 \tag{4.70}$$

Outcome (4.61) can be deduced from the finite part of Hadamard concept as in (4.48), rather trivially. In view of the axial symmetry of the problem at hand, identity (4.66) implies:

$$\fint_{\mathcal{F}} \frac{W^{\mathcal{F}}(s,s')\, K_1(s')\, \delta a(s')}{D^2(s,s')}\, \mathrm{d}s' = 0 \tag{4.71}$$

Accordingly, eq. (4.48) reads:

$$\begin{aligned} \delta K_1 &= \left(\frac{1}{2} \left.\frac{\partial W^{\mathcal{S}}}{\partial \rho}\right|_{s,s} - \frac{c}{2} \right) K_1\, \delta a - \frac{\mu}{1-\nu} \frac{3\sqrt{2\pi}}{8}\, \Xi_1(a)\, \delta a \\ &= \left(\frac{K_1}{8a} - \frac{\mu}{1-\nu} \frac{3\sqrt{2\pi}}{8}\, \Xi_1(a) \right) \delta a = -\frac{3}{2}\, \frac{\kappa}{\pi\, a^2}\, \frac{1}{\sqrt{\pi\, a}}\, \delta a \end{aligned} \tag{4.72}$$

as in eq. (4.61).

4.2.2 Incremental formulation

The incremental picture described in Chapter 2 is here rephrased for the circular crack loaded in an axial symmetric way depicted in figure 4.6-a. According to the closed form solution for the SIF K_1 (4.56), when the load factor $\kappa(a(t))$ reaches the threshold:

$$\kappa(a(t)) = K_1^C \pi a(t) \sqrt{\pi a(t)} \tag{4.73}$$

the onset of crack propagation is reached. A further increase of external actions $\delta\kappa$ allows fracture to propagate. In this axial-symmetric crack growth condition, the radius increment δa is independent on the abscissa s along the crack front. Operator $\mathbf{K}^{(1)}[s,t;\delta a(t)]$ in eq. (2.6) simplifies for being scalar and " local", i.e. $K^{(1)}[s,t;\delta a(t)] = K^{(1)}\delta a(t)$ and expressed in closed form in equation (4.61). Analogously $\mathbf{K}^*(s,t) = K_1(t)$. As stability condition (2.38a) is trivially satisfied, the crack growth is stable, as expected. Functional (2.56) simplifies in a quadratic function that holds:

$$\chi[w(t)] = -\frac{1}{2} \int_{\mathcal{F}(t)|_{\varphi=0}} \Lambda_{11} K_1(t) K^{(1)}(t)\, ds\, w^2(t) - \int_{\mathcal{F}(t)|_{\varphi=0}} \frac{G_C}{\kappa(t)} \left.\frac{\partial \kappa}{\partial t}\right|_t ds\, w(t) \tag{4.74}$$

under the unilateral constraint $w(t) \geq 0$. In view of the closed form (4.61), functional $\chi[w(t)]$ becomes:

$$\chi[w(t)] = -\frac{1-\nu^2}{E} \frac{\kappa^2(t)}{\pi^3} \frac{w(t)}{a^2(t)} \left[-\frac{3}{a(t)} w(t) + \frac{4}{\kappa(t)} \left.\frac{\partial \kappa}{\partial t}\right|_t \right]$$

Consider a positive parameter α and a positive elongation rate $\delta b(t)$, so that the configuration $w(t) = \delta a(t) + \alpha\,\delta b(t)$ is in the set of admissible configurations for functional (4.74). Optimality implies that

$$\chi[\delta a(t) + \alpha\delta b(t)] \geq \chi[\delta a(t)]$$

or equivalently

$$\frac{d}{d\alpha}\chi[\delta a(t) + \alpha\,\delta b(t)]\Big|_{\alpha=0} = 0$$

In the event $\delta a(t) > 0$, the Euler-Lagrange equation

$$\chi'[\delta a(t)] = -\frac{1-\nu^2}{E}\frac{2}{\pi^3}\frac{\kappa^2(t)}{a^2(t)}\left[-\frac{3}{a(t)}\delta a(t) + \frac{2}{\kappa(t)}\left.\frac{\partial\kappa}{\partial t}\right|_t\right] = 0 \tag{4.75}$$

holds, whereas the inequality $\chi'[\delta a(t)] \geq 0$ has to be generally satisfied. Accordingly, at all $s \in \mathcal{F}(t)|_{\varphi=0}$ the Karush-Kuhn-Tucker conditions hold:

$$\delta a(t) \geq 0, \quad \chi'[\delta a(t)] \geq 0, \quad \chi'[\delta a(t)]\delta a(t) = 0$$

By " time" integration of (4.75) one gets:

$$\log\frac{\kappa(t)}{\kappa_0} = \frac{3}{2}\log\frac{a(t)}{a_0} \tag{4.76}$$

having set $a(0) = a_0$, $\kappa(0) = \kappa_0$. The benchmark eq. (4.73) immediately follows from setting $K_1(a_0) = K_1^C$, $\kappa_0 = K_1^C\pi^2 a_0^{3/2}$. Equation (4.76) expresses the critical load factor corresponding to the evolution of radius $a(t)$. In the event $\delta a(t) = 0$, the inequality $\chi'[\delta a(t)] \geq 0$ reads:

$$-\frac{1-\nu^2}{E}\frac{2}{\pi^3}\frac{\kappa^2(t)}{a^2(t)}\frac{2}{\kappa(t)}\left.\frac{\partial\kappa}{\partial t}\right|_t \geq 0$$

and is satisfied only by $\left.\frac{\partial\kappa}{\partial t}\right|_t \leq 0$, i.e. only by unloading conditions as expected.

4.2.3 Discretization

Let $h > 0$ be a parameter and let δa^h be a discrete approximation of the unknown field $\delta a(t)$. The approximation δa^h is taken to belong to a finite dimensional subspace V_h such that:

$$\forall\delta a, \inf_{\delta a^h \in V_h} \|\delta a - \delta a^h\| \to 0 \;\; as \;\; h \to 0 \tag{4.77}$$

Denote with $\{\psi_j | j = 1, ..., N_h\}$ a basis of space V_h of finite dimension N_h. The discrete solution is the linear combination of shape functions $\psi_j(s)$ and nodal unknowns δa_j:

$$\delta a^h(t) = \sum_{j=1}^{N_h}\psi_j(s)\delta a_j \tag{4.78}$$

where $\psi_j(s_j) = 1$ and $\psi_i(s_j) = 0$ if $i \neq j$. After collecting nodal unknowns δa_j in vector $\boldsymbol{\delta a}$ the discrete form of functional (4.74) reads:

$$\begin{aligned}\chi[\boldsymbol{\delta a}] &= -\frac{1}{2}\sum_{i=1}^{N_h}\sum_{j=1}^{N_h}\int_{\mathcal{F}(t)} N'_{\mathcal{F}}[\psi_j(s)]\,\psi_i(s)\,ds\,\delta a_i\,\delta a_j \\ &- \sum_{i=1}^{N_h}\int_{\mathcal{F}(t)}\frac{G_C}{\kappa(t)}\left.\frac{\partial\kappa}{\partial t}\right|_t\psi_i(s)ds\end{aligned} \tag{4.79}$$

with linear operator $N'_{\mathcal{F}}[\cdot]$ defined as (see eq.(4.43)):

$$N'_{\mathcal{F}}[\psi_j(s)] = \frac{1-\nu^2}{E} K_1(s) \left[\frac{1}{2\pi} \fint_{\mathcal{F}(t)} \frac{W^{\mathcal{F}}(s,s') K_1(s')}{D^2(s,s')} \psi_j(s')\, ds' + \right.$$
$$\left. + \left(\frac{1}{2} \left. \frac{\partial W^{\mathcal{S}}}{\partial \rho} \right|_{s,s} - \frac{c}{2} \right) K_1(s)\psi_j(s) - \frac{\mu}{1-\nu} \frac{3\sqrt{2\pi}}{8} \Xi_1(s)\psi_j(s) \right] \tag{4.80}$$

The stationary point for $\chi[\boldsymbol{\delta a}]$ is the solution of the linear system

$$\mathbb{A}\, \boldsymbol{\delta a} = \mathbf{b} \tag{4.81}$$

with

$$\mathbb{A}_{ij} = -\int_{\mathcal{F}(t)} N'_{\mathcal{F}}[\psi_j(s)]\psi_i(s)\, ds \tag{4.82}$$

$$b_i = \int_{\mathcal{F}(t)} \frac{G_C}{\kappa(t)} \left. \frac{\partial \kappa}{\partial t} \right|_t \psi_i(s)\, ds \tag{4.83}$$

For the penny shape crack at hand the crack front $\mathcal{F}(t)$ is a circumference of radius $a(t)$. The positive integer N_h that defines the dimension of space V_h is here taken as the number of subdivisions of the crack front. Each arc of the subdivision is enclosed by the center angle $\bar{\phi} = 2\pi N_h^{-1}$ and has a length $h = a(t)\bar{\phi}$. As usual in the language of approximation method it is termed " element". The element length h seems to be the most suitable choice for the discretization parameter in (4.77). The implicit assumption of uniform decomposition is a natural consequence of the axial-symmetry of the problem.

The " smooth" elongation δa of the crack front normal to itself is approximated via the linear combination (4.78). Denoting with $s = a(t)\phi$ the curvilinear abscissa along the front, shape functions $\psi_j(s)$ are taken to be linear in ϕ (see figure 4.7) and once for all it is assumed that $0 \le \phi \le 2\pi$.

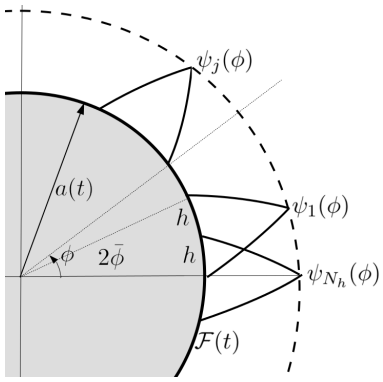

Figure 4.7: *A plot of shape functions along the crack front $\mathcal{F}(t)$. Even tough they are linear in ϕ their plot is not straight because of the curvature of the crack front. As the "smooth" elongation δa of the crack front is normal to itself [117], shape functions increment the radius locally for the penny shape crack at hand.*

The characteristic function $\mathcal{H}_j[\phi]$ on element $j = 1, 2, ..., N_h$ is a step function that is vanishing outside element j. It is formally defined as

$$\mathcal{H}_j[\phi] = \begin{cases} 1 \;\; if \;\; (j_m - 1)\bar{\phi} \le \phi \le j_m\, \bar{\phi} \\ 0 \;\; otherwise \end{cases}$$

with $j_m = jmoduloN_h$ standing for the remainder of the division between integers j and N_h. Characteristic functions are used to define the support of shape functions $\psi_j(\phi)$. They read:

$$\psi_j(\phi) = \left(1 - j + \frac{\phi}{\bar{\phi}}\right) \mathcal{H}_j[\phi] + \left(1 - \frac{\phi - j\bar{\phi}}{\bar{\phi}}\right) \mathcal{H}_{j+1}[\phi] \quad j = 1, 2, ..., N_h$$

By writing $jmoduloN_h$ it is ensured that shape function $\psi_{N_h}(\phi)$ is defined partially on the last element and partially on the first. The support of each shape function is thus made of two consecutive elements - see also figure 4.7.

According to eq. (4.80) operator $N'_{\mathcal{F}}[\cdot]$ has local and non local contributions. The former amounts to:

$$N'^{loc}_{\mathcal{F}}[\psi_j(s)] = \frac{1-\nu^2}{E} K_1(s) \left[\left(\frac{1}{2} \left. \frac{\partial W^{\mathcal{S}}}{\partial \rho} \right|_{s,s} - \frac{c}{2} \right) K_1(s) - \frac{\mu}{1-\nu} \frac{3\sqrt{2\pi}}{8} \Xi_1(s) \right] \psi_j(s) \tag{4.84}$$

whereas the non-local contribution is the counterpart of eq. (4.80). Taking into account closed forms (4.56) for the SIF K_1, (4.58) for the coefficient Ξ_1 of the crack opening expansion and (4.69) for the derivative of $W^{\mathcal{S}}$ with respect to ρ, $N'^{loc}_{\mathcal{F}}[\cdot]$ holds:

$$N'^{loc}_{\mathcal{F}}[\psi_j(s)] = -\frac{1-\nu^2}{E} \frac{\kappa^2}{(\pi a)^3} \frac{3}{2a} \psi_j(s)$$

Such a local operator provides a sparse contribution to matrix $\mathbb{A}$ of linear system (4.81). It is essentially the so-called mass matrix:

$$\mathbb{A}^{loc}_{ij} = \frac{1-\nu^2}{E} \frac{\kappa^2}{(\pi a)^3} \frac{3}{2} \int_0^{2\pi} \psi_i(\phi)\psi_j(\phi)\, d\phi \tag{4.85}$$

which is vanishing when shape functions do not overlap, namely when $supp(\psi_i) \cap supp(\psi_j) = \emptyset$.

The remaining part of operator $N'_{\mathcal{F}}[\cdot]$ leads to the following non local contribution to matrix $\mathbb{A}$.

$$\begin{aligned} \mathbb{A}^{nl}_{ij} &= -\frac{1-\nu^2}{E} \frac{1}{2\pi} \int_{\mathcal{F}(t)} K_1(s)\psi_i(s) \, \Xint=_{\mathcal{F}(t)} \frac{W^{\mathcal{F}}(s,s')K_1(s')\psi_j(s')}{D^2(s,s')} \, ds' \, ds = \\ &= -\frac{1-\nu^2}{E} \frac{\kappa^2}{(\pi a)^3} \frac{1}{4\pi} \int_{supp(\psi_i)} \psi_i(\phi) \, \Xint=_{supp(\psi_j)} \frac{\psi_j(\phi')}{1 - cos(\phi' - \phi)} \, d\phi' \, d\phi \end{aligned} \tag{4.86}$$

Even for not overlapping shape function supports $supp(\psi_i) \cap supp(\psi_j) = \emptyset$, the corresponding matrix entry $\mathbb{A}^{nl}_{ij}$ is not vanishing. The system matrix $\mathbb{A}$ is thus fully populated, as usual in the approximation methods based on integral equations as for instance BEM (Boundary Element Methods) [29]. Nevertheless, when $supp(\psi_i) \cap supp(\psi_j) = \emptyset$, the finite part of Hadamard in eq. (4.86) coincides with a standard Riemann integral and usual Gaussian quadrature rules allow an effective evaluation of entries $\mathbb{A}_{ij}$. When shape function supports overlap, finite parts of Hadamard have to be evaluated analytically. This approach is quite standard in BEM (see for instance [120, 121, 123]) and will be detailed below. Evaluation of given terms (4.83) shows no difficulties and is obviously local in nature:

$$b_i = \frac{G_C}{\kappa(t)} \left. \frac{\partial \kappa}{\partial t} \right|_t a(t) \int_0^{2\pi} \psi_i(\phi)\, d\phi \tag{4.87}$$

Matrix $\mathbb{A}$ and vector $\mathbf{b}$ have the following properties:

$$\mathbb{A}_{ij} = \mathbb{A}_{lm} \;\; \forall\, 1 \leq i,j,l,m \leq N_h \;\; s.t. \;\; l - i = m - j \tag{4.88a}$$

$$b_i = b_k \;\; \forall\, 1 \leq i,k \leq N_h \tag{4.88b}$$

in view of the selected discretization. As a consequence, the system solution is such that

$$\delta a_i = \delta a_k \;\; \forall\, 1 \leq i,k \leq N_h$$

as desirable in view of the axial symmetry of the problem at hand. In order to compare the accuracy of the solution with the given benchmark, it is useful to restate $\mathbb{A}_{ij}$ and b_i in the following way:

$$\mathbb{A}_{ij} = -\frac{1-\nu^2}{E}\frac{\kappa^2}{(\pi\, a)^3}\, A_{ij}, \qquad b_i = \frac{G_C}{\kappa(t)}\, \frac{\partial \kappa}{\partial t}\bigg|_t \bar{b}_i \tag{4.89}$$

where

$$A_{ij} = \frac{1}{4\pi}\int_0^{2\pi} \psi_i(\phi) \fint_0^{2\pi} \frac{\psi_j(\phi')}{1-\cos(\phi'-\phi)}\, d\phi'\, d\phi - \frac{3}{2}\int_0^{2\pi} \psi_i(\phi)\psi_j(\phi)\, d\phi \tag{4.90}$$

$$\bar{b}_i = \int_0^{2\pi} \phi_i(\phi)\, d\phi \tag{4.91}$$

Obviously matrix $\mathbf{A}$ and vector $\bar{\mathbf{b}}$ enjoy the properties (4.88a, 4.88b) as well. It comes out immediately

$$\delta a_i = -(\mathbf{A}^{-1}\mathbf{b})_i\, \frac{a(t)}{\kappa(t)}\, \frac{\partial \kappa}{\partial t}\bigg|_t \tag{4.92}$$

to be compared with Euler-Lagrange equation (4.75), i.e.

$$\delta a = +\frac{2}{3}\frac{a(t)}{\kappa(t)}\, \frac{\partial \kappa}{\partial t}\bigg|_t$$

The scalar $-(\mathbf{A}^{-1}\mathbf{b})_i$, which is in fact independent on i, can then be compared with $2/3$ in order to benchmark the accuracy of the proposed variational strategy for the selected example. Table 4.1 collects the results of the benchmark. Evidences show that the rate of convergence[1]

$$p = log_2 \frac{\varepsilon_n}{\varepsilon_{n+1}}$$

with $\varepsilon_n = |-(\mathbf{A}^{-1}\mathbf{b})_i - 2/3|$, is clearly linear.

Matrix $\mathbf{A}$ shows a distinctive behavior that reflects some mathematical properties of the weight functions. As illustrated in figures 4.8 and 4.9, the diagonal terms A_{ii} are negative, differently from all non diagonal entries. In absolute value the diagonal terms are much higher than all other counterparts, which in fact become closer and closer to zero when the distance between the shape functions supports increases.

[1] A sequence x_n is said to converge to L with order p if there exists a constant C such that $|x_n - L| < Cn^{-p}\, \forall\, n$.

N_h	$(\mathbf{A}^{-1}\mathbf{b})_i$	Error Abs. $\varepsilon_n = \lvert -(\mathbf{A}^{-1}\mathbf{b})_i - 2/3\rvert$	Rel. (%) $100\,3/2\,\varepsilon_n$	Convergence p
8	-0.67142	0.0047618	0.71428	-
16	-0.66900	0.0023350	0.35024	1.02813
32	-0.66783	0.0011609	0.17414	1.00814
64	-0.66725	0.00057939	0.086909	1.00265
128	-0.66696	0.00028950	0.043425	1.00098
256	-0.66681	0.00014471	0.021706	1.00040

Table 4.1: *Accuracy of the variational strategy for the selected penny shape example.*

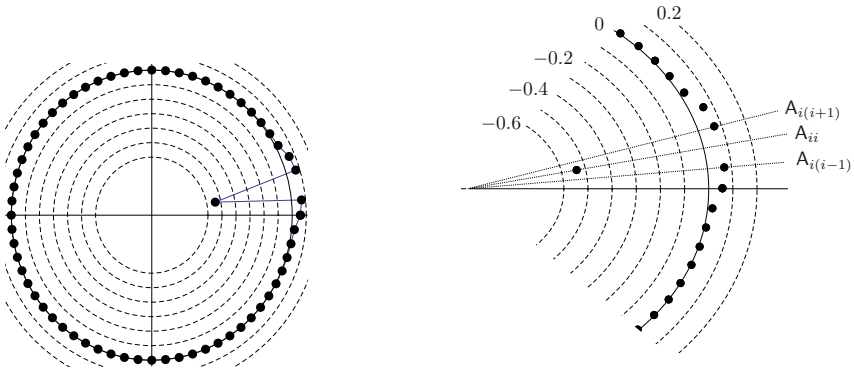

Figure 4.8: *The picture visualizes the values of the entries of matrix* $\mathbf{A}$ *in eq. (4.90) for parameter* $N_h = 64$. *The values of a row of* $\mathbf{A}$ *are depicted on the left, and zoomed on the right. Diagonal terms* A_{ii} *are negative and much higher in absolute value. The higher the distance between the supports of the shape functions the closer to zero the value of* A_{ij}

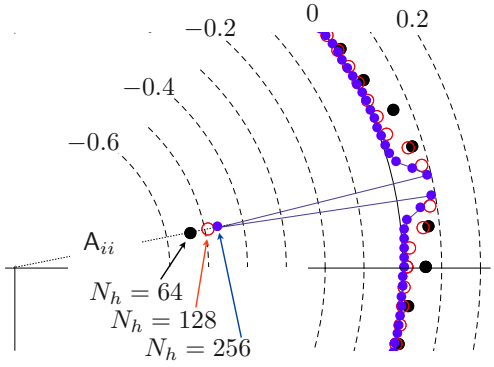

Figure 4.9: *The picture is a zoom of the values of the entries of matrix* $\mathbf{A}$ *in eq. (4.90) for parameters* $N_h = 64$, $N_h = 128$ *and* $N_h = 256$.

4.2.4 Finite part of Hadamard evaluation along a circle

The final part of this section is dedicated to elucidate the evaluation of integrals in equation (4.90).

Consider as first the item of coincident supports and take $i = j = 1$ for the sake of simplicity.

Apart from factor $1/4\pi$ the non local part of matrix $\mathbf{A}$ in eq. (4.90) in its expanded form reads:

$$\begin{aligned} A_{11}^{nl} &= \frac{1}{\bar{\phi}^2}\int_0^{\bar{\phi}} \phi \left[\not\int_0^{\bar{\phi}} \frac{\phi'}{1-\cos(\phi'-\phi)}\,d\phi' + \int_{\bar{\phi}}^{2\bar{\phi}} \frac{2\bar{\phi}-\phi'}{1-\cos(\phi'-\phi)}\,d\phi' \right] d\phi \\ &+ \frac{1}{\bar{\phi}^2}\int_{\bar{\phi}}^{2\bar{\phi}} (2\bar{\phi}-\phi) \left[\int_0^{\bar{\phi}} \frac{\phi'}{1-\cos(\phi'-\phi)}\,d\phi' + \not\int_{\bar{\phi}}^{2\bar{\phi}} \frac{2\bar{\phi}-\phi'}{1-\cos(\phi'-\phi)}\,d\phi' \right] d\phi \end{aligned}$$

with angle $\bar{\phi} = 2\pi/N_h$. It comes out:

$$\begin{aligned} \not\int_0^{\bar{\phi}} \frac{\phi'}{1-\cos(\phi'-\phi)}\,d\phi' &= \frac{1}{\bar{\phi}}\left\{ \log\left[\sin^2\left(\frac{\phi-\bar{\phi}}{2}\right)\right] - \log\left[\sin^2\left(\frac{\phi}{2}\right)\right]\right\} \\ &- \cot\left(\frac{\bar{\phi}-\phi}{2}\right) \end{aligned}$$

$$\begin{aligned} \not\int_{\bar{\phi}}^{2\bar{\phi}} \frac{2\bar{\phi}-\phi'}{1-\cos(\phi'-\phi)}\,d\phi' &= \frac{1}{\bar{\phi}}\left\{ \log\left[\sin^2\left(\frac{\phi-\bar{\phi}}{2}\right)\right] - \log\left[\sin^2\left(\frac{\phi-2\bar{\phi}}{2}\right)\right]\right\} \\ &+ \cot\left(\frac{\bar{\phi}-\phi}{2}\right) \end{aligned}$$

From identities above it turns out that the two external integrals in ϕ:

$$\int_0^{\bar{\phi}} \phi \not\int_0^{\bar{\phi}} \frac{\phi'}{1-\cos(\phi'-\phi)}\,d\phi'\,d\phi$$

$$\int_0^{\bar{\phi}} \phi \int_{\bar{\phi}}^{2\bar{\phi}} \frac{2\bar{\phi}-\phi'}{1-\cos(\phi'-\phi)}\,d\phi'\,d\phi$$

are not well defined separately. Nevertheless, the singularity of the kind $2/(\phi-\bar{\phi})$ is present in both integrals and cancels out in the sum. Accordingly, integral

$$\int_0^{\bar{\phi}} \phi \left[\not\int_0^{\bar{\phi}} \frac{\phi'}{1-\cos(\phi'-\phi)}\,d\phi' + \int_{\bar{\phi}}^{2\bar{\phi}} \frac{2\bar{\phi}-\phi'}{1-\cos(\phi'-\phi)}\,d\phi' \right] d\phi$$

is a well defined Riemann integral in ϕ. Integral

$$\int_{\bar{\phi}}^{2\bar{\phi}} (2\bar{\phi}-\phi) \left[\int_0^{\bar{\phi}} \frac{\phi'}{1-\cos(\phi'-\phi)}\,d\phi' + \not\int_{\bar{\phi}}^{2\bar{\phi}} \frac{2\bar{\phi}-\phi'}{1-\cos(\phi'-\phi)}\,d\phi' \right] d\phi$$

shows analogous peculiarities, therefore the analysis of the item of coincident supports is completed.

The item of adjacent supports merely remains. Again for the sake of simplicity take $i=1$, $j=2$. Non local part of eq. (4.90) in its expanded form reads:

$$\begin{aligned} A_{12}^{nl} &= \frac{1}{\bar{\phi}^2}\int_0^{\bar{\phi}} \phi \left[\int_{\bar{\phi}}^{2\bar{\phi}} \frac{\phi'-\bar{\phi}}{1-\cos(\phi'-\phi)}\,d\phi' + \int_{2\bar{\phi}}^{3\bar{\phi}} \frac{3\bar{\phi}-\phi'}{1-\cos(\phi'-\phi)}\,d\phi' \right] d\phi \\ &+ \frac{1}{\bar{\phi}^2}\int_{\bar{\phi}}^{2\bar{\phi}} (2\bar{\phi}-\phi) \left[\not\int_{\bar{\phi}}^{2\bar{\phi}} \frac{\phi'-\bar{\phi}}{1-\cos(\phi'-\phi)}d\phi' + \int_{2\bar{\phi}}^{3\bar{\phi}} \frac{3\bar{\phi}-\phi'}{1-\cos(\phi'-\phi)}\,d\phi' \right] d\phi \end{aligned}$$

It comes out:

$$\begin{aligned}\int_{\bar\phi}^{2\bar\phi} \frac{\phi'-\bar\phi}{1-\cos(\phi'-\phi)}\,d\phi' &= \frac{1}{\bar\phi}\left\{\log\left[\sin^2\left(\frac{\phi-2\bar\phi}{2}\right)\right]-\log\left[\sin^2\left(\frac{\phi-\bar\phi}{2}\right)\right]\right\}\\ &- \cot\left(\bar\phi-\frac{\phi}{2}\right)\end{aligned}$$

$$\begin{aligned}\int_{2\bar\phi}^{3\bar\phi} \frac{3\bar\phi-\phi'}{1-\cos(\phi'-\phi)}\,d\phi' &= \frac{1}{\bar\phi}\left\{\log\left[\sin^2\left(\frac{\phi-2\bar\phi}{2}\right)\right]-\log\left[\sin^2\left(\frac{\phi-3\bar\phi}{2}\right)\right]\right\}\\ &+ \cot\left(\bar\phi-\frac{\phi}{2}\right)\end{aligned}$$

The outer integral in ϕ is a well defined Riemann integral in this case. Furthermore, it holds:

$$\fint_{\bar\phi}^{2\bar\phi} \frac{\phi-\bar\phi}{1-\cos(\phi'-\phi)}\,d\phi' = \int_{\bar\phi}^{2\bar\phi} \frac{\phi-\bar\phi}{1-\cos(\phi'-\phi)}\,d\phi'$$

whence the evaluation of A_{12}^{nl} shows no further issues.

4.3 Weight functions update

Following the same path of reasoning of Rice [117], equation (4.13), or its relatives (4.17) and (4.18), provides the first order variation of the SIF $K_1(s_1)$ when the FK $W^{\mathcal{F}}(s_1,s)$ is known. A procedure for computing the evolution of $W^{\mathcal{F}}$ has to be given in order to provide a δK_1 distribution, associated with infinitesimal elongation $\delta l(s)$, which can be integrated over a sequence of successive crack fronts, starting at a simple one, in order to give K_1 for a general shape. At this point it is necessary to introduce the assumption that two points along the crack front, say s_1 and s_2, are stationary (i.e. $\delta l(s_1)=0$ and $\delta l(s_2)=0$), for which the FK $W^{\mathcal{F}}(s_1,s_2)$ is known. In view of representation formula (4.5), applying two point forces in the y-direction on the crack faces at point (x_2,z_2) at a distance ρ_2 from s_2, the CFWF $k_{11}((x_2,z_2),s)$ holds:

$$k_{11}((x_2,z_2),s) = \frac{\sqrt{2\,\rho_2}\,W^{\mathcal{S}}((x_2,z_2),s)}{D^2((x_2,z_2),s)} \tag{4.93}$$

In such loadings conditions, SIF $K_1(s_1)$ becomes $k_{11}((x_2,z_2),s_1)$ in eq.(4.13), namely:

$$\delta k_{11}((x_2,z_2),s_1) = \frac{1}{2\pi}\fint_{\mathcal{F}} \frac{W^{\mathcal{F}}(s_1,s)}{D^2(s_1,s)} k_{11}((x_2,z_2),s)\,\delta l(s)\,ds \tag{4.94}$$

Dividing both sides of eq. (4.94) by $\sqrt{\rho_2}$ and letting $\rho_2\to 0$, one can obtain the variation of the FK $W^{\mathcal{F}}(s_1,s_2)$ to the first order in $\delta l(s)$, in the case of $\delta l(s_1)=\delta l(s_2)=0$:

$$\delta W^{\mathcal{F}}(s_1,s_2) = \frac{D^2(s_2,s_1)}{2\pi}\fint_{\mathcal{F}} \frac{W^{\mathcal{F}}(s_1,s)W^{\mathcal{F}}(s_2,s)}{D^2(s_1,s)D^2(s_2,s)}\,\delta l(s)\,ds \tag{4.95}$$

Equation (4.95) provides the first order variation of the FK $\delta W^{\mathcal{F}}(s_1,s_2)$ when $W^{\mathcal{F}}(s_1,s)$ and $W^{\mathcal{F}}(s_2,s)$ are known along the crack front. In the case of mixed mode, eq. (4.95) is extended by

Favier et al. [37] to:

$$\begin{aligned}\delta\mathbb{W}^{\mathcal{F}}(s_1,s_2) &= \mathbb{N}(\theta)\mathbb{W}^{\mathcal{F}}(s_1,s_2)\left.\frac{\partial l}{\partial s'}\right|_{s_1} - \mathbb{W}^{\mathcal{F}}(s_1,s_2)\mathbb{N}(\theta)\left.\frac{\partial l}{\partial s'}\right|_{s_2} + \\ &+ \frac{D^2(s_1,s_2)}{2\pi}\int_{\mathcal{F}}\frac{\mathbb{W}^{\mathcal{F}}(s_1,s)\mathbb{W}^{\mathcal{F}}(s_2,s)}{D^2(s_1,s)D^2(s_2,s)}\delta l(s)\,ds \end{aligned} \tag{4.96}$$

with $\mathbb{N}(\theta)$ defined in expansion (2.5).

Focusing once again on the pure mode 1 case, in order to get rid of conditions $\delta l(s_1) = \delta l(s_2) = 0$, one has to introduce a motion $\delta l_{**}(s)$ such that $\delta l_{**}(s_1) = \delta l(s_1)$ and $\delta l_{**}(s_2) = \delta l(s_2)$. Denoting with $\delta W^{\mathcal{F}}_{**}(s_1,s_2)$ the corresponding first order variation of the FK, eq. (4.95) becomes:

$$\delta W^{\mathcal{F}}(s_1,s_2) = \delta W^{\mathcal{F}}_{**}(s_2,s_1) + \frac{D^2(s_1,s_2)}{2\pi}\int_{\mathcal{F}}\frac{W^{\mathcal{F}}(s_1,s)W^{\mathcal{F}}(s_2,s)}{D^2(s_1,s)D^2(s_2,s)}\left[\delta l(s) - \delta l_{**}(s)\right]ds \tag{4.97}$$

Drawback of such an approach is the necessity to define $\delta l_{**}(s)$ such that $\delta W^{\mathcal{F}}_{**}(s_1,s_2)$ can be computed, and it has not been solved at present in the general case. As remarked in [79], in case of infinite domains loaded at infinity, it is always possible to find a combination of a translatory motion, a homothetical expansion and a rotation that brings the two points s_1 and s_2 from any initial position to any final position, while leaving the kernel unaffected so that $\delta W^{\mathcal{F}}_{**}(s_1,s_2) = 0$. Formulas (4.13) and (4.95) that express the first order variation of the SIF and of the FK, respectively, establish the bases of the perturbation approach, briefly described in Chapter 5. The latter has been applied merely to infinite bodies so far, because of the steady locations assumption. Removing in full the hypothesis of steady locations, and consequently the ones introduced to circumvent the resulting limitations, an algorithm to approximate weight functions for all cases for which they are not available in closed form is needed and is described below.

Formulation of the algorithm is based on the definition of the weight functions itself and allows estimation of FKs for the general case of finite domains and general crack front shapes. Such an algorithm is grounded on the classical Finite Element Method (FEM) and does not provide an analytical expression of the first order variation of the FKs as the counterpart of eq. (4.95), as done on the contrary in [129], where eq. (4.53) can be considered an extension of Rice's result eq. (4.13) for the first order variation of SIFs. In view of equation (4.2), the mode 1 CFWF $k_{11}(P,s')$ can be estimated by the application of two point forces $\mathbf{t} = -\delta(P)\mathbf{n}$ in the outward normal direction to the crack surface, where $\delta(P)$ stands for Dirac delta applied at point P, whose distance from the crack front point s amounts to ρ. As pointed out by Rice [116], it is convenient to regard these forces $\mathbf{t}$ as being distributed uniformly over a disk of arbitrary small radius centered on $P = (x,z)$. The corresponding SIF $K_1(\delta(P);s')$ at curvilinear abscissa s' is therefore:

$$K_1(\delta(P);s') = \int_{\mathcal{S}(t)} k_{11}(P,s')\delta(P)\,dx\,dz = \frac{\sqrt{2\rho}}{\pi\sqrt{\pi}}\frac{1}{D^2(P,s')}W^{\mathcal{S}}(P,s') \tag{4.98}$$

in view of representation formula (4.5). Inserting Taylor series expansion of $W^{\mathcal{S}}(P,s')$ with respect to ρ:

$$W^{\mathcal{S}}(P,s') = W^{\mathcal{F}}(s,s') + \left.\frac{\partial W^{\mathcal{S}}}{\partial\rho}\right|_{s,s}\rho + o(\rho) \tag{4.99}$$

into (4.98), the following estimates for the FK $W^{\mathcal{F}}(s,s')$ eventually come out:

$$W^{\mathcal{F}}(s,s') = K_1(\delta(P);s')\frac{\pi\sqrt{\pi}}{\sqrt{2\rho}}D^2(P,s') + o(1) \tag{4.100a}$$

$$W^{\mathcal{F}}(s,s') = K_1(\delta(P);s')\frac{\pi\sqrt{\pi}}{\sqrt{2\rho}}D^2(P,s') - \left.\frac{\partial W^{\mathcal{S}}}{\partial\rho}\right|_{s,s}\rho + o(\rho) \tag{4.100b}$$

Eq. (4.100b) is a linear approximation of FK $W^{\mathcal{F}}(s,s')$ in ρ that takes into account the role of the derivative of $W^{\mathcal{S}}$ with respect to ρ.

In order to investigate the accuracy of formulas (4.100a) and (4.100b) a circular crack of unit radius $a(t)=1$ immersed in an unbounded linear elastic isotropic domain has been considered.

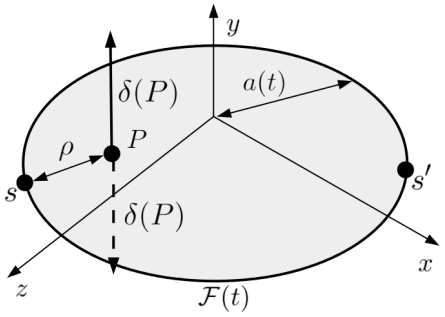

Figure 4.10: *Penny shape crack with radius $a(t)$ embedded in an infinite body subject to two point forces with magnitude $-\delta(P)\mathbf{n}$ at point P at a distance ρ from the crack front $\mathcal{F}(t)$, where $\delta(P)$ is a Dirac delta at point P and $\mathbf{n}$ is the outward unit normal, so they open the crack.*

Closed forms are available for the crack geometry at hand loaded by two point forces at point $P=(x,z)$ so to open the crack lips, see figure 4.10. CFWF $k_{11}(P,s')$, $W^{\mathcal{S}}(P,s')$ are expressed by formulas (4.60)and (4.68), respectively. FK is therefore

$$W^{\mathcal{F}}(s,s') = 1 \tag{4.101}$$

in view of definition (4.7). Thus having at hand the closed form solution for the SIF $K_1(\delta(P);s')$ along curvilinear abscissa s' of the crack front (see eq. (4.98)), the right hand side of equations (4.100) can be easily computed and the FK compared with the analytical solution (4.101). The outcomes are reported in figure 4.11.

FK $W^{\mathcal{F}}(s,s')$ is a map between a two dimensional space in $\mathbb{R}$, $W^{\mathcal{F}}:\mathbb{R}\times\mathbb{R}\to\mathbb{R}$. Equations (4.100) therefore shall be considered in a two-dimensional perspective, without being blurred from the observation that the crack front is a curve, i.e. a one-dimensional entity. The FK $W^{\mathcal{F}}(s,s')$ could be approximated via a linear combination of unknowns W_j and standard interpolatory shape functions $\psi_j(\mathbf{x})$ with $\mathbf{x}=\{s,s'\}\in\mathbb{R}\times\mathbb{R}$ as:

$$W^{\mathcal{F}}(\mathbf{x}) \approx \sum_{n=1}^{N} W_n\psi_n(\mathbf{x}) + \sum_{m=1}^{M} W_m\psi_m(\mathbf{x}) \tag{4.102}$$

In the approximation above, W_ns are the N nodal unknowns for $W^{\mathcal{F}}$ at points for which $s'\neq s$. In view of identities (4.10), in pure mode 1 one has $W^{\mathcal{F}}(s,s)=1$, and the M nodal unknowns W_m at

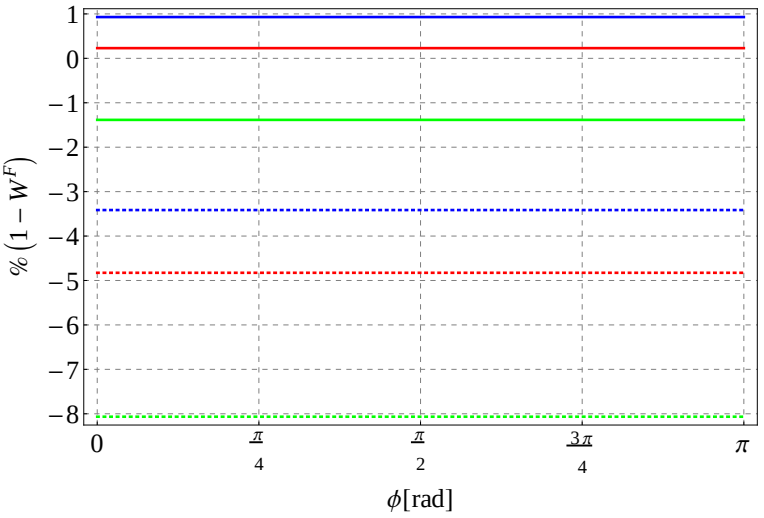

Figure 4.11: *A representation of the error in approximating FK $W^{\mathcal{F}}(s,s')$ along a circle of unit radius loaded in mode 1. The ordinate depicts the relative error in percentage in a logarithmic scale. Center angle ϕ is plot between 0 and π, for the sake of symmetry. Continuous lines refer to approximation (4.100a) and dotted lines to the first order approximation (4.100b). Blue lines refer to a value of $\rho = 0.1$, red lines to a value of $\rho = 0.05$ and green lines to a value of $\rho = 0.01$.*

locations $s = s'$ may be enforced to take equal to a unit amount. Equations (4.100) are therefore of the form:

$$\sum_{n=1}^{N} W_n \psi_n(\mathbf{x}) = f(\mathbf{x}) - \sum_{m=1}^{M} \psi_m(\mathbf{x}) \tag{4.103}$$

and they can be numerically approximated in several ways. The easiest is perhaps by collocation, i.e. collocating eq. (4.103) at the N points $\mathbf{x}_i$:

$$\sum_{n=1}^{N} W_n \psi_n(\mathbf{x}_i) = f(\mathbf{x}_i) - \sum_{m=1}^{M} \psi_m(\mathbf{x}_i), \qquad i = 1, 2, ..., N \tag{4.104}$$

Collocation approach is easy and small time consuming, but it is influenced from the arbitrary location of collocation points.

Alternatively, a Galerkin approach can be established as usual, by multiplying with a test function of the same functional space as the shape functions and performing an integration over bidimensional domain Q depicted in figure 4.12.

$$\sum_{n=1}^{N} \int_Q \psi_n(\mathbf{x}) \psi_j(\mathbf{x})\, ds\, ds' W_n = \int_Q \psi_j(\mathbf{x}) f(\mathbf{x})\, ds\, ds' - \sum_{m=1}^{M} \int_Q \psi_m(\mathbf{x}) \psi_j(\mathbf{x})\, ds\, ds', \qquad j = 1, 2, ..., N \tag{4.105}$$

4.3.1 Implementation

The circular crack of unit radius represented in figure 4.10 is the selected model problem. Different subdivisions of the crack front have been considered; in particular the crack front has been divided

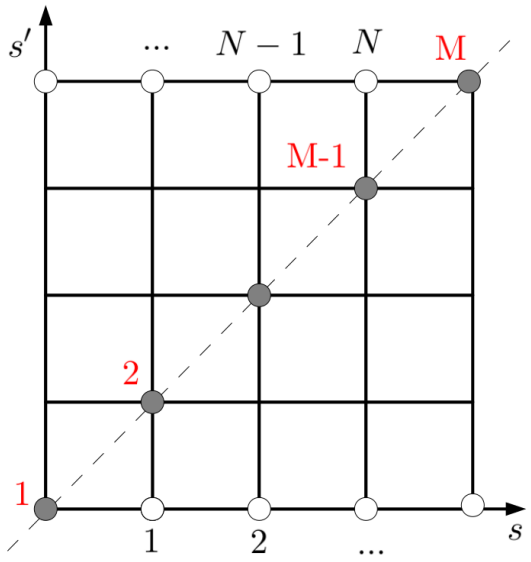

Figure 4.12: *A representation of two dimensional domain Q for the problem (4.103). N points filled in white are such that $s \neq s'$ and W_n is unknown $\forall\, n = 1, 2, ..., N$, while M points filled in grey are such that $s = s'$ and $W_m = 1$ in view of identity (4.10) $\forall m = 1, 2, ..., M$.*

into $8, 16, 32, 64$, and 128 elements.

Standard linear shape functions have been considered for each element i of the 2D domain Q depicted in figure 4.12. The shape function vector has the form:

$$\boldsymbol{\psi}(s, s') = \left\{ \frac{(s - s_{2i})(s' - s'_{4i})}{(s_{1i} - s_{2i})(s'_{1i} - s'_{4i})}; \frac{(s - s_{1i})(s' - s'_{4i})}{(s_{2i} - s_{1i})(s'_{2i} - s'_{4i})}; \frac{(s - s_{4i})(s' - s'_{2i})}{(s_{3i} - s_{4i})(s'_{3i} - s'_{2i})}; \frac{(s - s_{3i})(s' - s'_{1i})}{(s_{4i} - s_{3i})(s'_{4i} - s'_{1i})} \right\} \tag{4.106}$$

where s_{ji} and s'_{ki} are the j^{th} abscissa and the k^{th} ordinate of nodes of element i, with $1 \leq j, k \leq 4$.

For what regards the collocation technique, collocation nodes have been placed at small distances to the left and to the right of each node, as plotted in figure 4.13-a for the case of 8 elements, since the nodes of the discretization are locations where the definition of the SIFs is ill-posed for insufficient smoothness of the discretized crack front. Such a distance has been chosen to be equal to $1/10$ of the element length.

Accordingly to this choice, for the 8 elements case, 16 collocation points are placed along the circular crack front and making reference to the 2D representation of domain Q of figure 4.12, $M = 8$ and $N = 56$. Since collocation nodes do not coincide with element's vertices, two collocation nodes correspond to each vertex along the circumference and four collocation nodes $\mathbf{x}_i^c$ correspond to each of the N points $\mathbf{x}_i$ of 2D domain Q as depicted in figure 4.13-b with $i = 1, 2, ..., N$ and $c = 1, 2, 3, 4$. Eq. (4.104) is thus evaluated at each of the four collocation nodes and averaged thereafter, i.e. it has been implemented in the form:

$$\frac{1}{4} \sum_{c=1}^{4} \sum_{n=1}^{N} W_n \psi_n(\mathbf{x}_i^c) = \frac{1}{4} \sum_{c=1}^{4} \left[f(\mathbf{x}_i^c) - \sum_{m=1}^{M} \psi_m(\mathbf{x}_i^c) \right], \qquad i = 1, 2, ..., N \tag{4.107}$$

Approximation of FK $W^{\mathcal{F}}(\mathbf{x})$ by means of Galerkin approach, as expressed in eq. (4.105), has

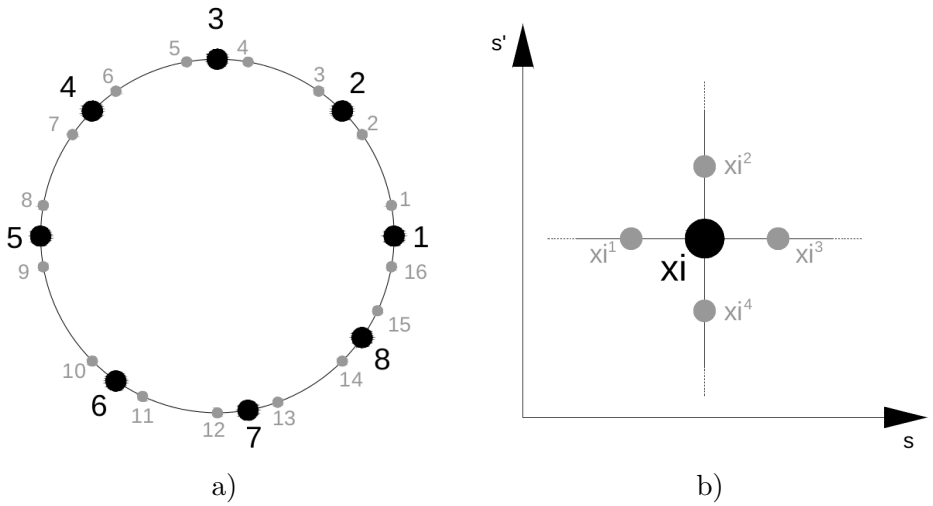

Figure 4.13: *a) Circular crack front divided into* 8 *elements. The corresponding* 8 *nodes are represented by black dots. Collocation points are placed at a small distance to the left and to the right of each node. The resulting* 16 *collocation nodes are represented with grey dots. b) In the 2D domain* Q*,* 4 *collocation points* $\mathbf{x}_i^c$*, represented by grey dots, correspond to each node* $\mathbf{x}_i$ *represented by the back dot, with* $i = 1, 2, ..., N$ *and* $c = 1, 2, 3, 4$*.*

been implemented exploiting the usual Gaussian quadrature rule in order to perform integrations over 2D domain Q.

After computing the N coefficients W_n of system (4.103), the fundamental kernel $W^{\mathcal{F}}(\mathbf{x}_i)$ has been approximated by means of equation (4.102). SIFs $K_1(\delta(P); s')$ at curvilinear abscissa s' along the crack front have been evaluated numerically by the software FRANC3D (FRacture ANalysis Code 3D), developed at Cornell University (Ithaca, NY). It is designed to be used as a companion to a general Finite Element (FE) package (ABAQUS in this case). The uncracked FE mesh is created using standard tools available in the FE package, the crack geometry and location are then prescribed with FRANC3D and the model is remeshed. The analysis is perfomed by the FE package and the resulting displacements are read back into FRANC3D which computes the SIFs along the crack front exploiting either the calculation of the M-integral or alternatively the Displacement Correlation Technique. In FRANC3D, for an accurate SIFs computation, a pattern or template of elements with controlled sizes and shapes is placed about the crack front. Such a template takes the form of generalized cylindrical tubes of elements, whose dimension is controlled by a parameter called *template radius (tr)*, with the crack front serving as the axis of the cylinder, as plotted in figure 4.14-b. Wedge shaped 15-noded quarter-point elements, as the ones depicted in figure 3.5-c, are placed immediately adjacent to the crack front forming the first ring of elements of figure 4.14-b. These elements are surrounded by other two rings of 20-noded brick elements. Tetrahedral 10-noded elements are used for the bulk of the volume mesh, and pyramidal 13-noded elements enforce compatibility between bricks and tetrahedral elements.

Referring to the model problem of figure (4.10), a circular crack with unit radius has been inserted into a cylinder whose dimensions and boundary conditions are reported in figure 4.15-a, considering a fictitious brittle material with Young's modulus $E = 1$, and Poisson's ratio $\nu = 0.3$.

Figure 4.15-b shows SIFs $K_1(\delta(P); s')$ at point s' along the crack front, numerically computed in FRANC3D for three different values of the template radius $tr = 0.2$, $tr = 0.1$ and $tr = 0.05$ and a position of the point forces $\rho = 0.3$. All of the three curves show a good agreement with the

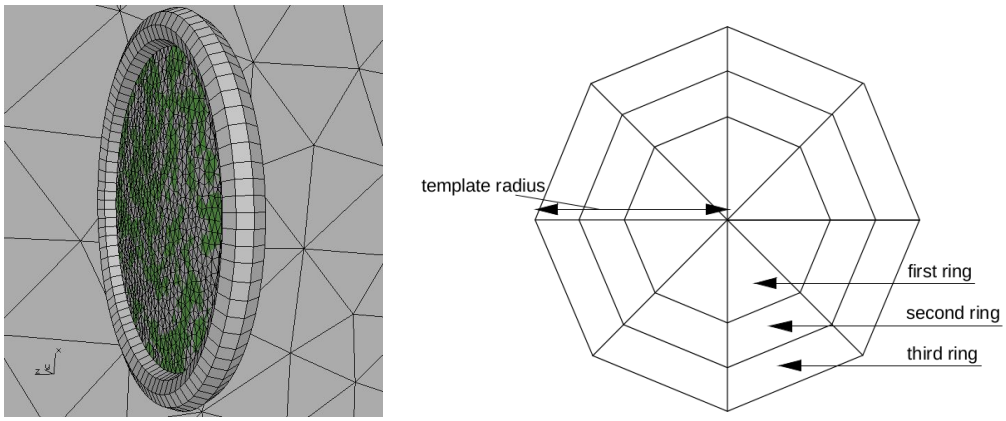

a) b)

Figure 4.14: *a) Three dimensional representation of the template of elements surrounding the crack front of the circular crack with unit radius $a = 1$ in the software FRANC3D b) Cross section of the template of elements that surround any crack front in FRANC3D, forming a cylindrical tube of elements with the crack front serving as the axis of the cylinder. Dimensions of such rings is controlled by the parameter template radius tr.*

analytical solution formula (4.60).

According to eq. (4.101), in the case of an internal circular crack loaded in pure mode 1, the FK $W^F(s, s')$ has to be equal to 1 in all points s' along the crack front.

Figure 4.16 shows the results obtained from the implementation of the FK approximation algorithm (4.102) described above, exploiting SIFs $K_1(\delta(P); s')$ computed in FRANC3D with three different values of template radius ($tr = 0.2, tr = 0.1$ and $tr = 0.05$). Results are compared with the solution obtained exploiting the analytical solution for the SIFs $K_1(\delta(P); s')$ formula (4.60). Figure 4.16 refers to the particular case of an eccentricity of the load $\rho = 0.3$ and a number of elements $N_h = 32$ along $\mathcal{F}$. Behavior of the curves with respect to s' is exactly the same, whatever subdivion of the crack front in N_h element is considered.
Figure 4.16-a corresponds to approximation (4.100a), while figure 4.16-b corresponds to the first order approximation (4.100b). Furthermore collocation technique (4.104) and Galerkin approach (4.105) reveal equivalent for the FK approximation algorithm, leading to the same results. Both using approximation (4.100a) and approximation (4.100b), contrarily to what intuition suggests, smaller template radii do not lead to better approximation of $W^{\mathcal{F}}$, as one can envisage from figure 4.16 where the green curves corresponding to $tr = 0.05$ provide higher values of the error with respect to the other two corresponding to the case $tr = 0.1$ and $tr = 0.05$. There is no an assured explanation for this phenomenon, but performed numerical analyses suggest that the reason lies on the dimension of the elements along the boundary of the cylindrical domain plotted in figure 4.15-a. In other words, the greater the uniformity of elements' size in the bulk, the better the approximation of $W^{\mathcal{F}}(s, s')$.

As expected, first order approximation (4.100b), that involves the derivative of $W^{\mathcal{S}}(P, s')$ with respect to ρ, leads to smaller values of the percentage error on the FK approximation- always less that 3%- with respect to approximation (4.100a) that exceeds 10% in certain points along $\mathcal{F}$.

In view of definition (4.7), the smaller the value of ρ, the better the $W^{\mathcal{F}}(s, s')$ approximation, but too small values of ρ can compromise the accuracy in the computation of SIFs in FRANC3D because of the proximity of the point load to the crack front, as confirmed by figure 4.17, that refers

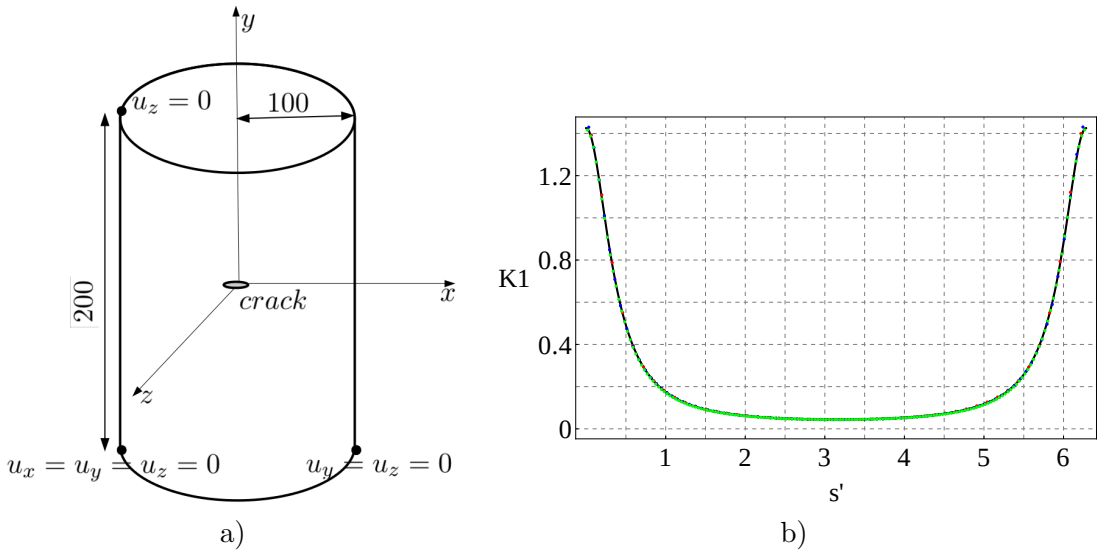

Figure 4.15: *a) Schematic representation of the cylindrical domain containing the circular crack of unit radius* $a = 1$*, exploited to compute SIFs in FRANC3D, with material parameters* $E = 1$ *and* $\nu = 0.3$*. In order to reach the condition of a crack in an infinite medium the cylinder has a radius 100 times the crack radius and a height 200 times the crack radius. Boundary conditions are detailed as well. b) SIFs* $K_1(\delta(P); s')$ *with respect to the curvilinear abscissa* s' *along the crack front computed in FRANC3D with three different values of the template radius (*$tr = 0.2$ *(red dots),* $tr = 0.1$ *(blue dots), and* $tr = 0.05$ *(green dots)) when two point forces are applied at a distance* $\rho = 0.3$ *from the crack front. The three curves match the analytical solution formula (4.60) represented by the continuous black curve.*

to a value of $\rho = 0.1$.

Supported by these results, it is planned to extend the formulation of the approximation of the fundamental kernels also to modes 2 and 3. Finally, the analytical counterpart of the first order variation of FKs eq. (4.95) is extremely desirable in the case of general crack front shapes in finite domains, as first order variation of SIFs formula (4.53) is the counterpart of Rice's result equation (4.13).

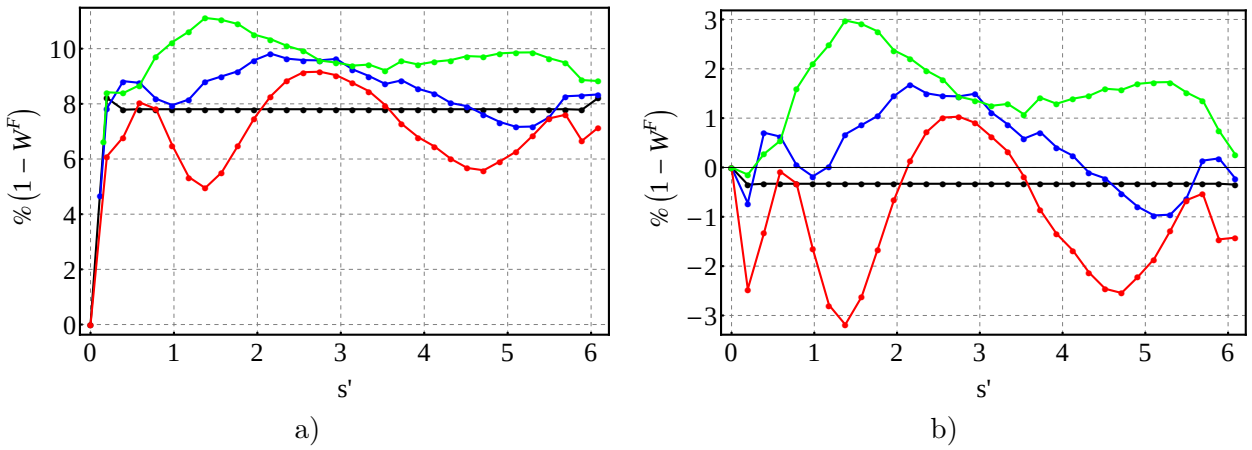

Figure 4.16: *Implementation of the FK $W^{\mathcal{F}}(s,s')$ approximation formulas (4.100) on a circular crack with unit radius embedded in the linear elastic and homogeneous cylindrical domain represented in figure 4.15-a. The graphs shows the percentage error on the approximation of $W^{\mathcal{F}}(s,s')$ along the curvilinear abscissa s' with respect to the analytical solution for the FK, namely $W^{\mathcal{F}}(s,s') = 1 \quad \forall s' \in \mathcal{F}$. Three different values of the template radius are considered in the software FRANC3D, namely $tr = 0.2$ (red curves), $tr = 0.1$ (blue curves) and $tr = 0.05$ (green curves). Black curves refer to the use of the analytical solution for $K_1(\delta(P);s')$ eq. (4.60) in the FK approximation algorithm. The point forces are applied at a distance $\rho = 0.3$ from the crack front $\mathcal{F}$. a) Results for approximation (4.100a). b) Results for the first order approximation (4.100b).*

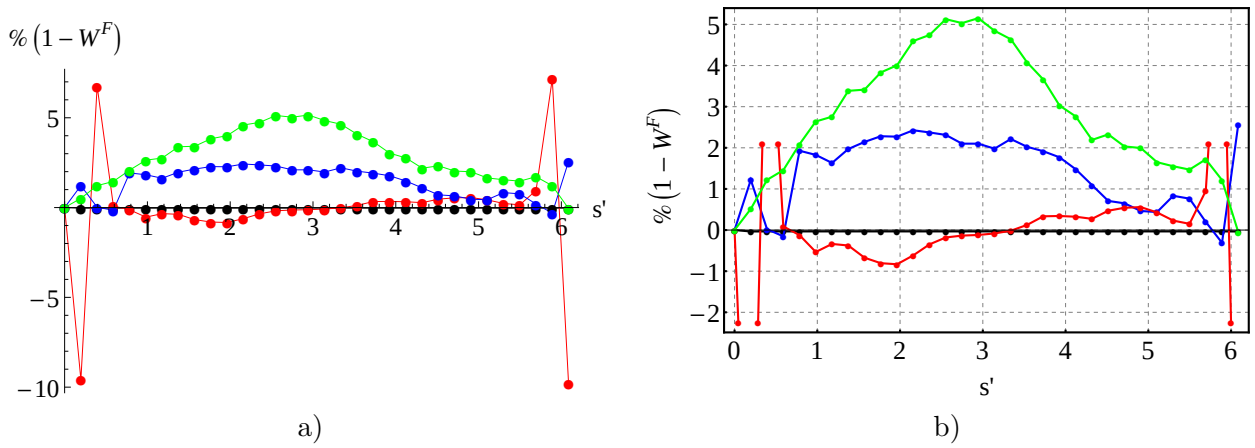

Figure 4.17: *a) Percentage error on the FK $W^{\mathcal{F}}(s,s')$ approximation by means of the first order formula (4.100b) with respect to the analytical solution (4.101). The model problem is a circular crack with unit radius embedded in the linear elastic and homogeneous cylindrical domain represented in figure 4.15-a. The point loads $\delta(P)$ are applied at a distance $\rho = 0.1$ from the crack front and SIFs $K_1(\delta(P);s')$ are computed in FRANC3D exploiting three different values of the template radius tr, namely $tr = 0.2$ (red curves), $tr = 0.1$ (blue curves), and $tr = 0.05$ (green curves). A direct comparison with figure 4.16-b, which refers to a value of $\rho = 0.3$, shows that, despite FK definition (see eq. (4.7)) predicts better approximation of $W^{\mathcal{F}}(s,s')$ for smaller values of rho (compare black curves that refer to the analytical solution for $K_1(\delta(P);s')$ eq. (4.60)), the accuracy in the computation of SIFs in FRANC3D can be compromised by the vicinity of the point loads to the crack front. For example, for $tr = 0.2$, in the nodes closest to the point loads, it is reached an error almost equal to 10% in absolute value on the approximation of $W^{\mathcal{F}}(s,s')$. b) Zoom of figure a.*

4.4 Appendix A: Finite part of Hadamard and limit to the boundary of the squared distance

Elliptic crack fronts

In the present appendix details on the computation of integral (4.49), namely:

$$\lim_{\rho\to 0^+}\int_{\mathcal{F}(t)}\frac{1}{D^2(P,s')}\,ds' \tag{4.108}$$

are firstly shown in the case of elliptic crack front and then extended to the case of general crack front shapes.

For an elliptic crack front of major semi-axis a and minor one b, with the notation of figure 4.18, the radius $\overline{OQ}=R(\phi_Q)$ holds:

$$R(\phi_Q)=\frac{ab}{\sqrt{b^2\cos^2(\phi_Q)+a^2\sin^2(\phi_Q)}}$$

whence the distance between points P and Q, the latter being located at the generic abscissa s', reads:

$$D^2(P,s')=[\,\cos(\phi_P)\,(-\rho+R(\phi_P))-\cos(\phi_Q)R(\phi_Q)\,]^2+[\,\sin(\phi_P)\,(-\rho+R(\phi_P))-\sin(\phi_Q)R(\phi_Q)\,]^2$$

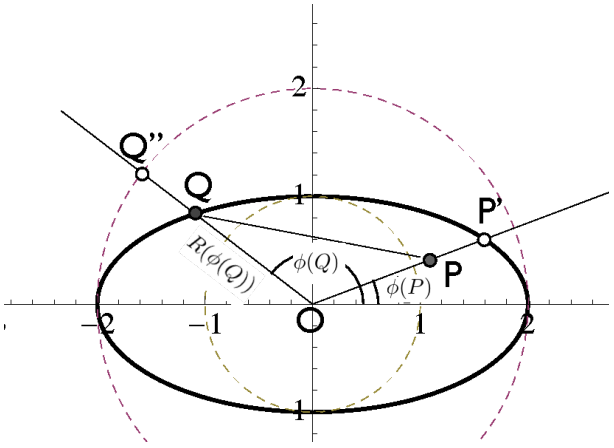

Figure 4.18: *Notation about an elliptic crack front with* $a=2$ *and* $b=1$.

Even for easy configurations as $\phi_P=0$, such that $R(\phi_P)=a$, the squared distance function

$$D^2(P,s')\big|_{\phi_P=0}=(a-\rho)^2-2\cos(\phi_Q)R(\phi_Q)\,(a-\rho)+R(\phi_Q)^2$$

appears to be too much involved to lead to a closed form for integral (4.108). The main features of limit (4.108) will thus be studied by making recourse to a different approach, assuming $\phi_P=0$. With the notation of figure 4.19 and $\phi_Q=\phi$, it holds in fact:

$$\begin{aligned}\lim_{\rho\to 0^+}\int_{\mathcal{F}(t)}\frac{1}{D^2(P,s')}\,\mathrm{d}s' &= \int_{\mathcal{F}(t)/[-\overline{\phi},\overline{\phi}]}\frac{j(\phi)}{a^2-2\cos(\phi)R(\phi)\,a+R(\phi)^2}\,\mathrm{d}\phi \\ &+ \lim_{\rho\to 0^+}\int_{-\alpha}^{\alpha}\frac{\sqrt{1+[y_2'(y_1)]^2}}{(\rho+y_2(y_1))^2+y_1^2}\mathrm{d}y_1\end{aligned} \tag{4.109}$$

having defined with $\alpha = R(\bar{\phi})\sin(\bar{\phi})$ and with $j(\phi) = \sqrt{R(\phi)^2 + R'(\phi)^2}$ the Jacobian determinant of the variable transformation. Having set $\phi_P = 0$, it turns out

$$[y_2'(y_1)]^2 = \frac{a^2 - (y_2 + a)^2}{b^2 - y_1^2} \tag{4.110}$$

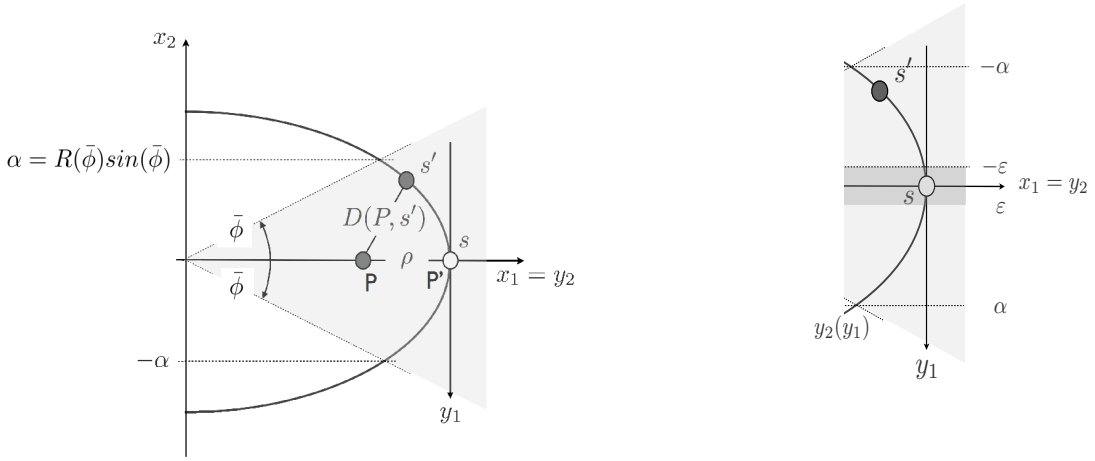

a) b)

Figure 4.19: *Notation about an elliptic crack used in: a) the limit process $\rho \to 0^+$; b) the finite part of Hadamard. By defining α in a more general way, the notation applies to a generic smooth crack front. Accordingly, the crack front curve $\mathcal{F}$ can be split as $\mathcal{F}_0 \cup \mathcal{F}_1$. Curve $\mathcal{F}_1$ is defined as in b). Consider the Frenet frame at s and an interval of size $[-\alpha, \alpha]$ about the origin of the tangent axis, here denoted as y_1. Denote locally the (smooth) crack front curve $\mathcal{F}$ as $y_2(y_1)$. The curve $\mathcal{F}_1$ is the subset of $\mathcal{F}$ such that $-\alpha \leq y_1 \leq \alpha$ and $\mathcal{F}_0$ the complementary part $\mathcal{F}_0 = \mathcal{F} \backslash \mathcal{F}_1$.*

The integrand function

$$\frac{\sqrt{1 + [y_2'(y_1)]^2}}{(\rho + y_2(y_1))^2 + y_1^2} = \frac{1}{(\rho + y_2)^2 + y_1^2} \sqrt{1 + \frac{a^2 - (y_2 + a)^2}{b^2 - y_1^2}}$$

is sufficiently smooth to admit a series expansion about $y_2 = 0$. In fact, having assumed $\{y_1, y_2\}$ as to coincide with the Frenet frame, at $y_1 = 0$ it holds $y_2 = y_2' = 0$. The expansion reads

$$\frac{\sqrt{1 + [y_2'(y_1)]^2}}{(\rho + y_2(y_1))^2 + y_1^2} = \frac{1}{\rho^2 + y_1^2} - \frac{2\rho}{(\rho^2 + y_1^2)^2}\, y_2 + h(\rho; y_1, y_2(y_1)) \tag{4.111}$$

with $h(\rho; y_1, y_2(y_1))$ such that

$$\lim_{\rho \to 0^+} \int_{-\alpha}^{\alpha} h(\rho; y_1, y_2(y_1)) \mathrm{d}y_1 = \int_{-\alpha}^{\alpha} h(0; y_1, y_2(y_1)) \mathrm{d}y_1$$

Accordingly, in integral (4.109) one is left with

$$\lim_{\rho \to 0^+} \int_{-\alpha}^{\alpha} \frac{1}{\rho^2 + y_1^2}\, \mathrm{d}y_1 - \lim_{\rho \to 0^+} \int_{-\alpha}^{\alpha} \frac{2\rho}{(\rho^2 + y_1^2)^2}\, y_2\, \mathrm{d}y_1$$

The former limit is not bounded:

$$\lim_{\rho\to 0^+}\int_{-\alpha}^{\alpha}\frac{1}{\rho^2+y_1^2}\mathrm{d}y_1=\frac{\pi}{\rho}-\frac{2}{\alpha} \tag{4.112}$$

The integrand function in the second integral vanishes at $\rho=0$ but in the limit process the second integral is known to generate a so called "free term". Denoting with c the curvature at point P', i.e. $y_2=c\,y_1^2+o(y_1^2)$, it holds:

$$\lim_{\rho\to 0^+}\int_{-\alpha}^{\alpha}\frac{2\rho}{(\rho^2+y_1^2)^2}\,y_2\,\mathrm{d}y_1=c\,\pi \tag{4.113}$$

In conclusion therefore,

$$\begin{aligned}\lim_{\rho\to 0^+}\int_{\mathcal{F}(t)}\frac{1}{D^2(P,s')}\,\mathrm{d}s' &= \int_{\mathcal{F}(t)/[-\overline{\phi},\overline{\phi}]}\frac{j(\phi)}{a^2-2\cos(\phi)R(\phi)\;a+R(\phi)^2}\,\mathrm{d}\phi \\ &+ \frac{\pi}{\rho}-\frac{2}{\alpha}-c\,\pi+\int_{-\alpha}^{\alpha}h(0;y_1,y_2(y_1))\mathrm{d}y_1\end{aligned} \tag{4.114}$$

With regard to the finite part of Hadamard, one has:

$$\begin{aligned}I(\varepsilon) &= \lim_{\varepsilon\to 0^+}\int_{\mathcal{F}(t)/[-\varepsilon,\varepsilon]}\frac{1}{D^2(s,s')}\,\mathrm{d}s'=\int_{\mathcal{F}(t)/[-\overline{\phi},\overline{\phi}]}\frac{1}{D^2(s,s')}\,\mathrm{d}s'+\lim_{\varepsilon\to 0^+}\int_{[-\overline{\phi},\overline{\phi}]/[-\varepsilon,\varepsilon]}\frac{1}{D^2(s,s')}\,\mathrm{d}s' \\ &= \int_{\mathcal{F}(t)/[-\overline{\phi},\overline{\phi}]}\frac{j(\phi)}{a^2-2\cos(\phi)R(\phi)\;a+R(\phi)^2}\,\mathrm{d}\phi+\lim_{\varepsilon\to 0^+}\int_{[-\overline{\phi},\overline{\phi}]/[-\varepsilon,\varepsilon]}\frac{\sqrt{1+[y_2'(y_1)]^2}}{y_2^2+y_1^2}\mathrm{d}y_1\end{aligned}$$

and in view of property (4.110) and expansion (4.111)

$$\begin{aligned}I(\varepsilon) &= \int_{\mathcal{F}(t)/[-\overline{\phi},\overline{\phi}]}\frac{j(\phi)}{a^2-2\cos(\phi)R(\phi)\;a+R(\phi)^2}\,\mathrm{d}\phi+\lim_{\varepsilon\to 0^+}\int_{[-\overline{\phi},\overline{\phi}]/[-\varepsilon,\varepsilon]}\frac{1}{y_1^2}+h(0;y_1,y_2(y_1))\mathrm{d}y_1 \\ &= \int_{\mathcal{F}(t)/[-\overline{\phi},\overline{\phi}]}\frac{j(\phi)}{a^2-2\cos(\phi)R(\phi)\;a+R(\phi)^2}\,\mathrm{d}\phi+\frac{2}{\varepsilon}-\frac{2}{\alpha}+\int_{-\alpha}^{\alpha}h(0;y_1,y_2(y_1))\mathrm{d}y_1\end{aligned} \tag{4.115}$$

By comparing the latter with limit (4.114) the basic identity

$$\lim_{\rho\to 0^+}\int_{\mathcal{F}(t)}\frac{1}{D^2(P,s')}\,\mathrm{d}s'=\frac{\pi}{\rho}-c\,\pi+\fint_{\mathcal{F}(t)}\frac{1}{D^2(s,s')}\,\mathrm{d}s' \tag{4.116}$$

comes immediately out. It has a general validity, as it will be proven below.

General crack fronts

In order to perform integral (4.49) and the limit thereafter the crack front curve $\mathcal{F}(t)$ can be split as $\mathcal{F}_0(t)\cup\mathcal{F}_1(t)$. Curve $\mathcal{F}_1(t)$ is defined as follows - see also figure 4.19-b. Consider the Frenet frame at s and an interval of size $[-\alpha,\alpha]$ about the origin on the tangent axis, here denoted with y_1. Denote locally the (smooth) crack front curve $\mathcal{F}(t)$ as $y_2(y1)$. The curve $\mathcal{F}_1(t)$ is the subset of $\mathcal{F}(t)$ such that $-\alpha\le y_1\le\alpha$ and $\mathcal{F}_0(t)$ the complementary part $\mathcal{F}_0(t)=\mathcal{F}(t)\backslash\mathcal{F}_1(t)$. Accordingly, curve $\mathcal{F}_0(t)$ does not contain s and the limit $\rho\to 0^+$ is trivial for the integral along $\mathcal{F}_0(t)$.

Denote with

$$s'-s=\psi(y_1)=\int_0^{y_1}\sqrt{1+\left(y_2'(y_1)\right)^2}\,\mathrm{d}y_1=y_1+o(y_1)$$

along $\mathcal{F}_1(t)$ and consider integrals

$$\lim_{\rho\to 0^+}\int_{\mathcal{F}_1(t)}\frac{1}{D^2(P,s')}\,\mathrm{d}s' = \lim_{\rho\to 0^+}\int_{-\alpha}^{\alpha}\frac{\sqrt{1+(y_2'(y_1))^2}}{(\rho+y_2(y_1))^2+y_1^2}\,\mathrm{d}y_1 \tag{4.117}$$

$$\lim_{\rho\to 0^+}\int_{\mathcal{F}_1(t)}\frac{s'-s}{D^2(P,s')}\,\mathrm{d}s' = \lim_{\rho\to 0^+}\int_{-\alpha}^{\alpha}\psi(y_1)\frac{\sqrt{1+(y_2'(y_1))^2}}{(\rho+y_2(y_1))^2+y_1^2}\,\mathrm{d}y_1 \tag{4.118}$$

If $\mathcal{F}_1(t)$ is sufficiently smooth, it holds about $y_2 = 0$

$$\sqrt{1+(y_2'(y_1))^2} = 1+\sum_{n=1}^{+\infty}(-1)^n\frac{1}{4^n}\frac{(2n)!}{(1-2n)(n!)^2}\,\gamma_n\,y_1^{2n} \tag{4.119}$$

$$\begin{aligned}\frac{1}{(\rho+y_2(y_1))^2+y_1^2} &= \frac{1}{\rho^2+y_1^2}-\frac{2\,\rho}{(\rho^2+y_1^2)^2}\,y_2\\ &+ \sum_{n=2}^{+\infty}(-1)^n\left(\frac{y_2}{\rho^2+y_1^2}\right)^n\sum_{k=0}^{n\div 2}\beta_{kn}\,\frac{\rho^{n-2k}\,y_1^{2k}}{\rho^2+y_1^2}\end{aligned} \tag{4.120}$$

with $\beta_{kn},\gamma_n\in\mathbb{R}$. The expansion can thus be written again as in equation (4.111)

$$\frac{\sqrt{1+(y_2'(y_1))^2}}{(\rho+y_2(y_1))^2+y_1^2} = \frac{1}{\rho^2+y_1^2}-\frac{2\rho}{(\rho^2+y_1^2)^2}\,y_2+h(\rho;y_1,y_2(y_1)) \tag{4.121}$$

with $h(\rho;y_1,y_2(y_1))$ bounded about $\rho=0$ for all $y_1\in[-\alpha,\alpha]$ so such that

$$\lim_{\rho\to 0^+}\int_{-\alpha}^{\alpha}h(\rho;y_1,y_2(y_1))\mathrm{d}y_1 = \int_{-\alpha}^{\alpha}h(0;y_1,y_2(y_1))\mathrm{d}y_1$$

thus leading to formula (4.114) again:

$$\lim_{\rho\to 0^+}\int_{\mathcal{F}(t)}\frac{1}{D^2(P,s')}\,\mathrm{d}s' = \int_{\mathcal{F}_0(t)}\frac{1}{D^2(P,s')}\,\mathrm{d}s'+\frac{\pi}{\rho}-\frac{2}{\alpha}-c\,\pi+\int_{-\alpha}^{\alpha}h(0;y_1,y_2(y_1))\mathrm{d}y_1 \tag{4.122}$$

In order to characterize limit (4.117) in terms of the finite part of Hadamard one writes:

$$\begin{aligned}I(\varepsilon) &= \lim_{\varepsilon\to 0^+}\int_{\mathcal{F}(t)/[-\varepsilon,\varepsilon]}\frac{1}{D^2(s,s')}\,\mathrm{d}s' = \int_{\mathcal{F}_0(t)}\frac{1}{D^2(s,s')}\,\mathrm{d}s'\\ &+ \lim_{\varepsilon\to 0^+}\int_{\mathcal{F}_1(t)/[-\varepsilon,\varepsilon]}\frac{\sqrt{1+[y_2'(y_1)]^2}}{y_2^2+y_1^2}\mathrm{d}y_1\end{aligned}$$

and in view of expansion (4.121)

$$\begin{aligned}I(\varepsilon) &= \int_{\mathcal{F}_0(t)}\frac{1}{D^2(s,s')}\,\mathrm{d}s'+\lim_{\varepsilon\to 0^+}\int_{\mathcal{F}_1(t)/[-\varepsilon,\varepsilon]}\frac{1}{y_1^2}+h(0;y_1,y_2(y_1))\mathrm{d}y_1\\ &= \int_{\mathcal{F}_0(t)}\frac{1}{D^2(s,s')}\,\mathrm{d}s'+\frac{2}{\varepsilon}-\frac{2}{\alpha}+\int_{-\alpha}^{\alpha}h(0;y_1,y_2(y_1))\mathrm{d}y_1\end{aligned} \tag{4.123}$$

By comparing the latter with limit (4.122) the basic identity (4.116) is recovered for a generic crack front.

The same path of reasoning leads to:

$$\begin{aligned}\lim_{\rho\to 0^+}\int_{\mathcal{F}(t)}\frac{s'-s}{D^2(P,s')}\,\mathrm{d}s' &= \int_{\mathcal{F}_0(t)}\frac{s'-s}{D^2(s,s')}\,\mathrm{d}s' + \lim_{\rho\to 0^+}\int_{-\alpha}^{\alpha}\frac{y_1}{\rho^2+y_1^2}\,\mathrm{d}y_1 + O(1) = \\ &= \fint_{\mathcal{F}(t)}\frac{s'-s}{D^2(s,s')}\,\mathrm{d}s' \end{aligned} \tag{4.124}$$

as

$$\lim_{\rho\to 0^+}\int_{-\alpha}^{\alpha}\frac{y_1}{\rho^2+y_1^2}\,\mathrm{d}y_1 = 0$$

Chapter 5

Crack tracking algorithms

One of the challenging aspect of LEFM is to take into account non linearities induced by crack front deformations. A suitable approach for this is the crack front perturbation method based on successive iterations of the three dimensional weight function theory derived by Rice [116, 117] and briefly reviewed in Chapter 4. It was first adapted for numerical purposes by Bower and Ortiz [19] that extended the method of Gao and Rice [44, 45] to arbitrary large deformations of the crack front, leading the way to numerical resolution of complex three dimensional crack problems in the context of perturbation approaches.

With these latter, three dimensional weight function theory is applied numerically to a succession of small perturbations of the crack front resulting in arbitrary large ones. In [19], Bower and Ortiz investigated the propagation paths of semi-infinite tensile cracks in heterogeneous media, in both fatigue and brittle fracture. A simplified numerical implementation of perturbation approaches was later presented by Lazarus [78] for the case of arbitrary plane cracks, loaded in mode 1, embedded in an infinite elastic body, and extended afterwards to mixed mode (2+3) shear loadings by Favier and coworkers [37], where propagation was supposed to be channeled along some weak planar layer in order to remain coplanar. Extension of Favier et al. [37] is notably heavier than the original for mode 1 [78], because of the inevitably coupling of modes 2 and 3.

The procedure describing perturbation approaches can be divided into two steps. The first step regards the determination of the SIFs and FKs $\mathbb{W}^{\mathcal{F}}$ along some arbitrary crack front, starting from some crack shape, as close as possible to the front studied, for which they are known.
Then one has to construct a succession of intermediate cracks, very close to each other, between the initial crack front and the final desired one. Applying iteratively equations (4.13) for $\delta K_1(s)$, or its relative (4.14) for $\delta\mathbf{K}(s)$, and (4.95) for $W^{\mathcal{F}}(s,s')$, or its relative (4.96) for $\mathbb{W}^{\mathcal{F}}(s,s')$, one can finally obtain the SIFs and the FKs along the desired front.

The second step of the procedure regards the determination path of any arbitrary crack, the initial crack being that corresponding to the end of step 1. A suitable propagation law has to be provided in order to compute the elongation $\delta l(s)$ along the crack front and to update its position consequently. Again, formulas (4.13), or (4.14), and (4.95), or (4.96), update the SIFs and the FKs along the new configuration. Repeating, as many times as required, the two preceding operations to the new fronts obtained, one can study the propagation path of fractures only meshing the one dimensional crack front because only one dimensional integrals along the crack front are involved, avoiding the 3D meshing of the whole body.

In homogeneous materials loaded in mode 1 Lazarus [78], starting from elliptical, rectangular and heart shaped cracks, showed that cracks become circular after a certain time, while in the case of mixed mode Favier et al. [37] found that the cracks reach an almost elliptical shape in all cases,

deriving ultimately an approximate, but accurate, analytic formula for the ratio of the axes of this stable shape.

In Section 5.1, a different crack tracking algorithm is presented [128, 130]. It is grounded on an implicit Newton-Raphson based scheme which is endowed with a variational formulation. It exploits general formula (4.53) for the first order variation of the SIFs $K_1(s)$ and the weight function update algorithm described in Section 4.3 at each iteration of the crack tracking scheme.

5.1 A variationally based crack tracking algorithm

The incremental framework depicted in Chapter 2 allows to find the crack front quasi static velocity $v(s,t)$ of a point s of the crack front $\mathcal{F}(t)$. Explicit algorithms in time (as Forward Euler, Heun or Explicit Runge-Kutta) could then be conveniently deployed, following the usual implementations for ordinary differential equations.
In [128] a different kind of crack tracking algorithm has been developed. Unlike the explicit techniques mentioned above, it satisfies the Karush-Kuhn-Tucker conditions (2.16) at all times, which is an essential feature of stable crack growth. Such an algorithm is expected to be more accurate, robust, and numerically stable than explicit methods.

To build an implicit in time crack tracking algorithm, a finite elongation $l(s;t,\tau)$ in the normal plane has to be modeled from an initial time t, in which the domain Ω contains the fracture surface $\mathcal{S}(t)$ with its front $\mathcal{F}(t)$ in equilibrium at external actions $\kappa(t)$, to a final time $\tau > t$ in which a new equilibrated configuration $\mathcal{S}(\tau), \mathcal{F}(\tau)$ is achievable at $\kappa(\tau) > \kappa(t)$. It is assumed that, at time t, $\varphi(s,t) \leq 0 \ \forall s \in \mathcal{F}(t)$ and $\varphi(s,t) = 0$ in a subregion $\mathcal{F}^0(t)$. As the elongation is solely modeled, the constraint that the crack surface at time τ includes the one at time t is a priori satisfied. The driving force for the crack growth is considered here a finite change in the external actions $\delta\kappa = \kappa(\tau) - \kappa(t)$. The supposed unique crack elongation $l(s;t,\tau)$ that guarantees $\varphi(s,\tau) \leq 0$ (see eq. (2.7)) for all s along the new crack front $\mathcal{F}(\tau)$ will be recovered iteratively.

In the assumption made of smooth crack path (i.e. $t \equiv t^+$), Leblond's expansion (2.2) applies to the first order in $l(s;t,\tau)$ and an iterative algorithm is developed in analogy with elasto-plasticity [122].

A sequence of numerical crack fronts are generated and denoted with $\mathcal{F}_{[n]}(\tau)$, with $n \in \mathbb{N}$ standing for a counter of the iterations of the crack tracking scheme. According to this notation and expansion (2.2), SIFs vector at step n is defined as $\mathbf{K}^*_{[n]}(s,\tau)$. Assuming that the fronts $\mathcal{F}_{[n]}(\tau)$ converge to a finite configuration at $n \to +\infty$, the limit configuration for the front and the SIFs vector will be denoted by $\mathcal{F}(\tau)$ and $\mathbf{K}^*(s,\tau)$, respectively.

The algorithm moves from an *elastic trial* - the step "0"- at the configuration $\mathcal{F}_{[0]}(\tau) = \mathcal{F}(t)$:

$$\mathbf{K}^*_{[0]}(s,\tau) = \mathbf{K}^*(s,t)\frac{\kappa(\tau)}{\kappa(t)} \tag{5.1}$$

The onset of fracture (2.11) at the elastic trial yields:

$$\varphi_{[0]}(s,\tau) = \frac{1}{2}\left(\mathbf{K}^*_{[0]}(s,\tau)\cdot\mathbf{\Lambda}\mathbf{K}^*_{[0]}(s,\tau) - G_C\right) \tag{5.2}$$

Two alternatives are allowed, the first of which:

$$\varphi_{[0]}(s,\tau) < 0 \quad \forall s \in \mathcal{F}_{[0]}(\tau) \tag{5.3}$$

is typically expected for unloading, i.e. $\delta\kappa < 0$. When condition (5.3) is satisfied, the points along the crack front $\mathcal{F}_{[0]}(\tau)$ stand in the safe equilibrium domain and no crack extension is possible. It

is by far more interesting when condition above is not satisfied at some locations along the crack front. Those locations will define the part $\bar{\mathcal{F}}^o_{[0]}(\tau) \subset \mathcal{F}_{[0]}(\tau)$, that from now on will be taken to be a closed interval. It is defined by the following inequality:

$$\bar{\mathcal{F}}^o_{[0]}(\tau) = \{s \in \mathcal{F}_{[0]}(\tau) \;\; s.t. \;\; \varphi_{[0]}(s,\tau) \geq 0\} \tag{5.4}$$

As $\bar{\mathcal{F}}^0_{[0]}(\tau)$ is defined in terms of $\mathbf{K}^*_{[0]}(s,\tau)$, its size depends on $\delta\kappa$. When $\delta\kappa = 0$ then $\bar{\mathcal{F}}^o_{[0]}(\tau) = \mathcal{F}^o(t)$, as obvious, noting however that the sets might be empty. For increasing loads $\delta\kappa > 0$, $\bar{\mathcal{F}}^o_{[0]}(\tau)$ cannot be smaller than $\mathcal{F}^o(t)$ because of the linearity of the problem that leads to the elastic trial (5.1). Denoting with $\bar{\mathcal{F}}_{[0]}(\tau)$ the subset of $\bar{\mathcal{F}}^o_{[0]}(\tau)$ in which inequality $\varphi(s,\tau) > 0$ holds strictly, the inclusion chain $\bar{\mathcal{F}}^o_{[0]}(\tau) \supseteq \bar{\mathcal{F}}_{[0]}(\tau) \supseteq \mathcal{F}^o(t)$ comes out.
A new configuration for the crack front $\mathcal{F}(\tau)$ must be sought such that $\varphi(s,\tau) \leq 0$ for all $s \in \mathcal{F}(\tau)$: it will be the converging solution of a Newton-Raphson scheme. In view of Gateaux derivative (2.40) of the affine operator $N[\cdot]$, an operator $N'_{\mathcal{F}_{[0]}}$ is defined as follows:

$$N'_{\mathcal{F}_{[0]}}[\delta l_{[1]}] = \mathbf{\Lambda}\mathbf{K}^*_{[0]}(s,\tau) \cdot \mathbf{K}^{(1)}_{[0]}[s,t;\delta l_{[1]}(s';t,\tau)] \tag{5.5}$$

with $\delta l_{[1]}(s';t,\tau)$ standing for the approximation of $l(s';t,\tau)$ at the first iteration ($n = 1$) of the crack tracking scheme. Operator $\mathbf{K}^{(1)}[\cdot]$ obtains the subscript $_{[0]}$, meaning that $\mathbf{K}^{(1)}_{[0]}[\cdot]$ is defined (according to equation (4.53)) by means of an integral over front $\mathcal{F}_{[0]}(\tau)$. The sum:

$$\bar{\varphi}_{[0]}(s,\tau,\delta l_{[1]}) = \varphi_{[0]}(s,\tau) + N'_{\mathcal{F}_{[0]}}[\delta l_{[1]}] \tag{5.6}$$

is the first order approximation of the onset of fracture at configuration $\mathcal{F}_{[0]}(\tau)$ with respect to the crack elongation, noting that the load was incremented before the trial and is not subjected to change before the successive elastic trial. Definition (5.6) includes the case $\varphi_{[0]}(s,\tau) < 0$ since in such a case $\delta l_{[1]}(s;t,\tau) = 0$ for all $s \in \mathcal{F}_{[0]}(\tau)$ and it holds:

$$\bar{\varphi}_{[0]}(s,\tau,\delta l_{[1]}) = \varphi_{[0]}(s,\tau)$$

Karush-Kuhn-Tucker inequalities are enforced on $\bar{\varphi}_{[0]}$:

$$\bar{\varphi}_{[0]}(s,\tau,\delta l_{[1]}) \leq 0, \quad \delta l_{[1]}(s;t,\tau) \geq 0, \quad \bar{\varphi}_{[0]}(s,\tau,\delta l_{[1]})\delta l_{[1]}(s;t,\tau) = 0, \quad \forall s \in \mathcal{F}_{[0]}(\tau) \tag{5.7}$$

Equation $\bar{\varphi}_{[0]}(s,\tau,\delta l_{[1]}) = 0$ can be numerically approximated in several ways. The most natural in the light of the remarks above is a weak form along $\mathcal{F}_{[0]}(\tau)$, by means of test functions $\delta\hat{l}$ that belong to the same space of $\delta l(s;t,\tau)$ namely:

$$-\int_{\mathcal{F}_{[0]}(\tau)} N'_{\mathcal{F}_{[0]}}[\delta l_{[1]}]\,\delta\hat{l}\,ds - \int_{\mathcal{F}_{[0]}(\tau)} \varphi_{[0]}(s,\tau)\,\delta\hat{l}\,ds = 0 \tag{5.8}$$

Equation (5.8) is the Euler-Lagrange equation whose solutions are the functions for which the following functional is stationary:

Proposition 3
Under hypothesis of stable crack growth:

$$N'_{\mathcal{F}_{[0]}}[\delta w]\,\delta w \leq 0, \quad N'_{\mathcal{F}_{[0]}}[\delta w] = 0 \, if \, and \, only \, if \, \delta w = 0 \tag{5.9}$$

the crack front increment $\delta l_{[1]}(s;t,\tau)$ that solves the problem (5.7) at iteration $n=0$ minimizes the functional:

$$\chi_{[0]}[\delta w(s;t,\tau)] = -\frac{1}{2}\int_{\mathcal{F}_{[0]}(\tau)} N'_{\mathcal{F}_{[0]}}[\delta w(s';t,\tau)]\,\delta w(s;t,\tau)\,ds - \int_{\mathcal{F}_{[0]}(\tau)} \varphi_{[0]}(s,\tau)\,\delta w(s;t,\tau)\,ds \quad (5.10)$$

under the constraint $\delta w(s;t,\tau) \geq 0\, \forall s \in \mathcal{F}_{[0]}(\tau)$.

Once the crack elongation $\delta l_{[1]}(s;t,\tau)$ has been evaluated, a new crack front $\mathcal{F}_{[1]}(\tau)$ arises. As the geometry changes, a new global analysis is required to estimate SIFs $\mathbf{K}^*_{[1]}(s,\tau)$ at all points along $\mathcal{F}_{[1]}(\tau)$. Two alternatives are again allowed, either

$$\varphi_{[1]}(s,\tau) = \frac{1}{2}\left(\mathbf{K}^*_{[1]}(s,\tau)\cdot\mathbf{\Lambda}\mathbf{K}^*_{[1]}(s,\tau) - G_C\right) < 0 \quad \forall s \in \mathcal{F}_{[1]}(\tau) \quad (5.11)$$

or the latter is not satisfied at some point along $\mathcal{F}_{[1]}(\tau)$. When condition (5.11) is satisfied, the points along the crack front $\mathcal{F}_{[1]}(\tau)$ stand in the safe equilibrium domain, thus $\mathcal{F}_{[1]}(\tau)$ is the approximation of the new crack front $\mathcal{F}(\tau)$. If condition (5.11) is not satisfied at some locations:

$$\varphi_{[1]}(s,\tau) = \frac{1}{2}\left(\mathbf{K}^*_{[1]}(s,\tau)\cdot\mathbf{\Lambda}\mathbf{K}^*_{[1]}(s,\tau) - G_C\right) \geq 0 \quad s \in \bar{\mathcal{F}}^o_{[1]}(\tau)$$

then Proposition 3 can be exploited to estimate a new elongation and an approximation $\mathcal{F}_{[2]}(\tau)$. To this aim, Proposition 3 can be easily written and proved with reference to the generic step n of the Newton- Raphson scheme as follows.

Proposition 3b
Under hypothesis of stable crack growth:

$$N'_{\mathcal{F}_{[n]}}[\delta w]\,\delta w \leq 0, \qquad N'_{\mathcal{F}_{[n]}}[\delta w] = 0 \; if\, and\, only\, if \; \delta w = 0 \quad (5.12)$$

the crack front increment $\delta l_{[n+1]}(s;t,\tau)$ that solves the problem (5.7) at iteration n minimizes the functional:

$$\chi_{[n]}[\delta w(s;t,\tau)] = -\frac{1}{2}\int_{\mathcal{F}_{[n]}(\tau)} N'_{\mathcal{F}_{[n]}}[\delta w(s';t,\tau)]\,\delta w(s;t,\tau)\,ds - \int_{\mathcal{F}_{[n]}(\tau)} \varphi_{[n]}(s,\tau)\,\delta w(s;t,\tau)\,ds \quad (5.13)$$

under the constraint $\delta w(s;t,\tau) \geq 0\, \forall s \in \mathcal{F}_{[n]}(\tau)$.

In this proof dependency of increments δw upon s and t is not made explicit to favor readability. Denote with $\delta w = \delta l_{[n+1]} + \Delta l_{[n+1]}$. Taking advantage of symmetry and linearity of operator $N'_{\mathcal{F}_{[n]}}$, it holds:

$$\begin{aligned}
&\chi_{[n]}[\,\delta w\,] - \chi_{[n]}[\,\delta l_{[n+1]}\,] = \\
&\quad = -\int_{\mathcal{F}_{[n]}(\tau)} \left(N'_{\mathcal{F}_{[n]}}[\delta l_{[n+1]}] + \varphi_{[n]}(s,\tau)\right)\,\Delta l_{[n+1]}\,\mathrm{d}s - \frac{1}{2}\int_{\mathcal{F}_{[n]}(\tau)} N'_{\mathcal{F}_{[n]}}[\Delta l_{[n+1]}]\,\Delta l_{[n+1]}\,\mathrm{d}s = \\
&\quad = -\int_{\mathcal{F}_{[n]}(\tau)} \overline{\varphi}_{[n]}\,(\delta w - \delta l_{[n+1]})\,\mathrm{d}s - \frac{1}{2}\int_{\mathcal{F}_{[n]}(\tau)} N'_{\mathcal{F}_{[n]}}[\Delta l_{[n+1]}]\,\Delta l_{[n+1]}\,\mathrm{d}s = \\
&\quad = -\int_{\mathcal{F}_{[n]}(\tau)} \overline{\varphi}_{[n]}\,\delta w\,\mathrm{d}s + \int_{\mathcal{F}_{[n]}(\tau)} \overline{\varphi}_{[n]}\,\delta l_{[n+1]}\,\mathrm{d}s - \frac{1}{2}\int_{\mathcal{F}_{[n]}(\tau)} N'_{\mathcal{F}_{[n]}}[\Delta l_{[n+1]}]\,\Delta l_{[n+1]}\,\mathrm{d}s \geq 0
\end{aligned} \quad (5.14)$$

The first term is non negative, since $\overline{\varphi}_{[n]} \leq 0$ and $\delta w \geq 0$. The second term vanishes in view of Karush-Kuhn-Tucker conditions (5.7). Finally, the last term is non negative under assumption (5.12). The assert is thus proved.

Functional $\chi_{[n]}$ in eq. (5.13) reminds to functional χ defined in formula (2.56) in Section 2.5, but the domains of integrals in the two functionals are different. Theorem 1 descends from consistency condition (2.36) which holds at incipient crack growth conditions ($\varphi = 0$): for this sake, integrals are defined on $\mathcal{F}(t)|_{\varphi=0}$. Theorem 3 descends from the third of conditions (5.7), which holds on the whole crack front.

At iteration n of the Newton Raphson scheme it is still true that $\bar{\mathcal{F}}^o_{[n]}(\tau) \supseteq \bar{\mathcal{F}}_{[n]}(\tau)$ but a definition of $\mathcal{F}^o_{[n]}(\tau)$ is questionable because it would refer to the previous iteration along a different crack front. Furthermore, at each iteration the normal plane, in which elongation is defined, changes, whereas the kinking angle θ keeps vanishing in the assumption of a smooth crack propagation after an initial kink. The amount of external actions remains of course unchanged until convergence is reached and the algorithm ends when a condition is met, eventually in terms of $l(s;t,\tau) = \sum_n \delta l_{[n]}(s;t,\tau)$.

The numerical solution of optimization problems can be achieved with several strategies [153]. Penalty methods replace the minimization of functional (5.13) by a series of unconstrained problems, based on functionals $\chi^{\mathcal{H}}_{[n]}[\delta w(s;t,\tau)]$ that are formed by adding a term $\chi^c_{[n]}[\delta w(s;t,\tau)]$, termed penalty functional, to functional (5.13). Penalty functional consists of a penalty parameter $\epsilon > 0$ multiplied by a measure $\mathcal{H}[\delta w]$ of violation of the constraints, called penetration function. The penetration function vanishes where constraints are not violated, and is chosen to be equal to one elsewhere. The unconstrained form of functional (5.13), will be thus written as:

$$\chi^{\mathcal{H}}_{[n]}[\delta w(s;t,\tau)] = \chi_{[n]}[\delta w(s;t,\tau)] + \chi^c_{[n]}[\delta w(s;t,\tau)] \tag{5.15}$$

where the penalty functional reads:

$$\chi^c_{[n]}[\delta w(s;t,\tau)] = \frac{1}{2}\epsilon \int_{\mathcal{F}_{[n]}(\tau)} \mathcal{H}[\delta w]\, \delta w^2(s;t,\tau)\, ds \tag{5.16}$$

The solution of the Lagrange multiplier method is recovered when $\epsilon \to +\infty$; however, large numbers of ϵ can lead to ill-conditioned problems.
Optimality implies that the Gateaux derivative of functional (5.15), defined as usual by virtue of $\alpha \in \mathbb{R}$ as:

$$\left.\frac{\partial \chi^{\mathcal{H}}_{[n]}[\delta w + \alpha \delta \hat{w}]}{\partial \alpha}\right|_{\alpha=0}$$

vanishes for any admissible function $\delta\hat{w}$ such that $\delta w + \alpha\, \delta\hat{w}$ belongs to the same space of δw:

$$\int_{\mathcal{F}_{[n]}(\tau)} \Big(N'_{\mathcal{F}_{[n]}}[\delta w] + \varphi_{[n]}(s,\tau) - \epsilon\, \mathcal{H}[\delta w]\, \delta w \Big)\ \delta\hat{w}\, ds = 0 \tag{5.17}$$

Let $\delta l^h_{[n+1]}(s;t,\tau)$ be a discrete approximation of the unknown field $\delta l_{[n+1]}(s;t,\tau)$ belonging to the finite dimensional subspace V_h such that:

$$\forall \delta l_{[n+1]}(s;t,\tau),\ \inf_{\delta l^h_{[n+1]} \in V_h} \|\delta l_{[n+1]}(s;t,\tau) - \delta l^h_{[n+1]}(s;t,\tau)\| \to 0 \ \ as \ \ h \to 0 \tag{5.18}$$

for $h > 0$. Denote with $\{\psi_j | j = 1, ..., N_h\}$ a basis of space V_h of finite dimension N_h, with $\psi_i(s_j) = 0$ if $i \neq j$ and $\psi_j(s_j) = 1 \quad \forall\, j = 1, ..., N_h$. The discrete solution $\delta l^h_{[n+1]}(s; t, \tau)$ is the linear combination of shape functions $\psi_j(s)$ and nodal unknowns $\delta l_{j[n+1]}$:

$$\delta l^h_{[n+1]}(s; t, \tau) = \sum_{j=1}^{N_h} \psi_j(s) \delta l_{j[n+1]} \tag{5.19}$$

Exploiting the linearity of operator $N'_{\mathcal{F}_{[n]}}$, the discrete form of eq. (5.17) can be stated as:

$$\sum_{j=1}^{N_h} \int_{\mathcal{F}_{[n]}(\tau)} \psi_i(s) \left(N'_{\mathcal{F}_{[n]}}[\psi_j(s')] - \epsilon \mathcal{H} \left[\sum_{r=1}^{N_h} \psi_r(s) \delta l_{r[n+1]} \right] \psi_j(s) \right) \delta l_{j[n+1]}\, ds =$$
$$- \int_{\mathcal{F}_{[n]}(\tau)} \psi_i(s)\, \varphi_{[n]}(s, \tau)\, ds \tag{5.20}$$

for $i = 1, 2, ..., N_h$. Problem (5.20) is non linear because of the penetration function. Every step n of the Newton-Raphson scheme requires therefore a further, internal, iterative solution scheme, identified by counter k. A Newton-Raphson scheme as well as an Update Linearized scheme have been devised to solve it. The latter leads to:

$$\sum_{j=1}^{N_h} \int_{\mathcal{F}_{[n]}(\tau)} \psi_i(s) \left(N'_{\mathcal{F}_{[n]}}[\psi_j(s')] - \epsilon \mathcal{H} \left[\sum_{r=1}^{N_h} \psi_r(s) \delta l^{(k-1)}_{r[n+1]} \right] \psi_j(s) \right) \delta l^{(k)}_{j[n+1]}\, ds =$$
$$- \int_{\mathcal{F}_{[n]}(\tau)} \psi_i(s) \varphi_{[n]}(s, \tau)\, ds \tag{5.21}$$

for $i = 1, ..., N_h$ until

$$\frac{\| \boldsymbol{\delta l}^{(k)}_{[n+1]} - \boldsymbol{\delta l}^{(k-1)}_{[n+1]} \|}{\| \boldsymbol{\delta l}^{(k)}_{[n+1]} \|} < tol$$

where $\boldsymbol{\delta l}^{(k)}_{[n+1]}$ is the vector of N_h components $\delta l_{j[n+1]}$ at iteration $n+1$ of the crack tracking scheme and iteration k of the internal loop and *tol* is the desired tolerance. To conceptually prove the theory described above, the crack tracking framework is tested on two simple problems in what follows: the axial symmetric example of a penny shape crack subjected to a point tensile action acting in the center of the crack itself, and a penny shape crack loaded by two point forces acting with a certain eccentricity with respect to the center of the crack. Results confirm the potential of the proposed finite-step formulation [128, 130].

5.2 Circular crack axial-symmetric loaded

Consider the circular crack embedded in a continuum linear elastic and isotropic solid Ω depicted in figure 5.1 with radius $a(t) > a(0) > 0$, loaded by two point loads of magnitude $-\kappa(\tau)\mathbf{n}$ acting in the center of the upper and lower crack surfaces. The crack propagation is thus homothetic. The onset of propagation is reached simultaneously at all points along the crack front, and a single scalar characterizes in full the front elongation. Since the shape of the crack remains circular, the smooth increment $\delta a_{[n+1]}(t, \tau)$ of the radius $a(t)$ can be assumed as crack elongation descriptor in place of $\delta l_{[n+1]}(s; t, \tau)$. Spatial discretization (5.19) of the unknown field $\delta a_{[n+1]}(t, \tau)$, namely

$$\delta a^h_{[n+1]}(t, \tau) = \sum_{j=1}^{N_h} \psi_j(s) \delta a_{j[n+1]} \tag{5.22}$$

allows to transform the minimization of functionals (5.10) and (5.13) into a set of algebraic equations with constraints.

Due to the axial-symmetry of the benchmark at hand, it is expected the either the part of $\mathcal{F}_{[n]}(\tau)$ with vanishing elongation $\delta a_{[n+1]}(t,\tau)$ coincides with the whole circular crack front or is empty. As shown in Section 4.2, the former event is only compatible with unloading. If a positive load increment $\delta\kappa > 0$ is taken a priori, minimization of functionals (5.10) and (5.13) leads to a system of unconstrained algebraic equations along the crack front $\mathcal{F}_{[n]}(\tau)$. In the light of this consideration, functional $\chi^{\mathcal{H}}_{[n]}[\delta a(t,\tau)]$ of eq. (5.15) is such that $\chi^{\mathcal{H}}_{[n]}[\delta a(t,\tau)] = \chi_{[n]}[\delta a(t,\tau)]$ because of the vanishing of the penetration function $\mathcal{H}[\delta a(t,\tau)]$ at each iteration n of the Newton-Raphson scheme. After collecting nodal unknowns $\delta a_{j[n+1]}$ in vector $\boldsymbol{\delta a}_{[n+1]}$ the discrete form of functional (5.13) reads:

$$\begin{aligned}\chi_{[n]}[\boldsymbol{\delta a}_{[n+1]}] &= -\frac{1}{2}\sum_{i=1}^{N_h}\sum_{j=1}^{N_h}\int_{\mathcal{F}_{[n]}(\tau)} N'_{\mathcal{F}_{[n]}}[\psi_j(s)]\,\psi_i(s)\,ds\,\delta a_{i[n+1]}\,\delta a_{j[n+1]} \\ &- \frac{1}{2}\sum_{i=1}^{N_h}\int_{\mathcal{F}_{[n]}(\tau)} (K_{1[n]}(s,\tau)\Lambda_{11}K_{1[n]}(s,\tau) - G_C)\,\psi_i(s)\,ds\,\delta a_{i[n+1]}\end{aligned}$$

By means of equations (5.5) referred to the generic step n of the crack tracking scheme and formula (4.54), operator $N'_{\mathcal{F}_{[n]}}[\psi_j(s)]$ writes:

$$\begin{aligned}N'_{\mathcal{F}_{[n]}}[\psi_j(s)] &= \frac{1-\nu^2}{E}K_{1[n]}(s,\tau)\left[\frac{1}{2\pi}\,\text{⨍}_{\mathcal{F}_{[n]}(\tau)}\frac{W^{\mathcal{F}_{[n]}}(s,s')K_{1[n]}(s',\tau)}{D^2(s,s')}\,\psi_j(s')\,ds' + \right. \\ &+ \left.\left(\frac{1}{2}\left.\frac{\partial W^{\mathcal{S}_{[n]}}}{\partial\rho}\right|_{s,s} - \frac{c_{[n]}}{2}\right)K_{1[n]}(s,\tau)\psi_j(s) - \frac{\mu}{1-\nu}\frac{3\sqrt{2\pi}}{8}\Xi_{1[n]}(s)\psi_j(s)\right] \quad (5.23)\end{aligned}$$

In this axial-symmetric case the stationary point for $\chi_{[n]}[\boldsymbol{\delta a}_{[n+1]}]$ is the solution of the linear system

$$\mathbb{A}\,\boldsymbol{\delta a}_{[n+1]} = \mathbf{b} \quad (5.24)$$

with

$$\mathbb{A}_{ij} = -\int_{\mathcal{F}_{[n]}(\tau)} N'_{\mathcal{F}_{[n]}}[\psi_j(s)]\psi_i(s)\,ds \quad (5.25)$$

$$b_i = \frac{1}{2}\int_{\mathcal{F}_{[n]}(\tau)} (K_{1[n]}(s,\tau)\Lambda_{11}K_{1[n]}(s,\tau) - G_C)\,\psi_i(s)\,ds \quad (5.26)$$

Taking into account closed forms (4.56) for the SIF K_1, (4.58) for the 3/2 order coefficient Ξ_1 of the crack opening expansion and (4.69) for the derivative of $W^{\mathcal{S}}$ with respect to ρ, one obtains expressions for the local and non local parts of matrix $\mathbb{A}$, namely:

$$\mathbb{A}^{loc}_{ij} = \frac{1-\nu^2}{E}\frac{(\kappa(t)+\delta\kappa)^2}{(\pi\,a_{[n]})^3}\frac{3}{2}\int_0^{2\pi}\psi_i(\phi)\,\psi_j(\phi)\,d\phi \quad (5.27)$$

$$\mathbb{A}^{nl}_{ij} = -\frac{1-\nu^2}{E}\frac{(\kappa(t)+\delta\kappa)^2}{(\pi\,a_{[n]})^3}\frac{1}{2\pi}\int_{supp(\psi_i)}\psi_i(\phi)\,\text{⨍}_{supp(\psi_j)}\frac{\psi_j(\phi')}{1-\cos(\phi'-\phi)}\,d\phi'\,d\phi \quad (5.28)$$

Evaluation of given terms (5.26) leads to:

$$b_i = \frac{1}{2}\frac{1-\nu^2}{E}\left[\frac{(\kappa(t)+\delta\kappa)^2}{(\pi a_{[n]})^3} - (K_1^C)^2\right]a_{[n]}\int_0^{2\pi}\psi_i(\phi)\,d\phi \quad (5.29)$$

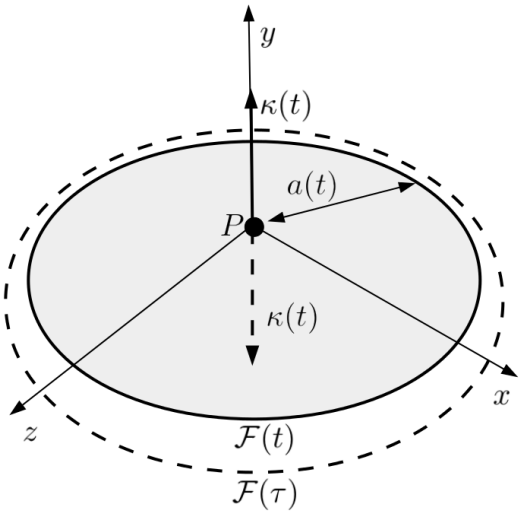

Figure 5.1: *Crack tracking framework described in Section 5.1 is benchmarked against the axial-symmetric problem of a penny shape crack with radius $a(t)$ embedded in an unbounded linear elastic isotropic domain Ω and subject to two point load forces with magnitude $-\kappa(t)\mathbf{n}$ acting in the center of the crack and directed so to open the crack lips. When the load is increased at a value $\kappa(\tau) > \kappa(t)$, configuration $\mathcal{F}(\tau)$ of the crack front is sought as the converged solution of the single load step of the Newton-Raphson scheme.*

If the assumption is made that at time t the condition $\varphi(s,t) = 0$ is reached (either exactly at the beginning or with sufficient accuracy in the iteration process), fracture toughness K_1^C can be related to $\kappa(t)$ in view of (4.56):

$$(K_1^C)^2 = \frac{\kappa^2(t)}{(\pi a_{[0]})^3}$$

If furthermore, for the sake of simplicity, the increment of load $\delta\kappa$ is written as a given percentage of $\kappa(t)$, i.e. $\delta\kappa = \eta\,\kappa(t)$, given terms (5.29) finally hold:

$$b_i = \frac{1}{2}\frac{1-\nu^2}{E}\frac{\kappa(t)^2}{\pi^3}\left[\frac{(1+\eta)^2}{a_{[n]}^3} - \frac{1}{a_{[0]}^3}\right] a_{[n]} \int_0^{2\pi} \psi_i(\phi)\, d\phi$$

Restating $\mathbb{A}_{ij}$ and b_i in the following way:

$$\mathbb{A}_{ij} = -\frac{1-\nu^2}{E}\frac{\kappa(t)^2}{(\pi a_{[n]})^3}(1+\eta)^2\, A_{ij}, \qquad b_i = \frac{1}{2}\frac{1-\nu^2}{E}\frac{\kappa(t)^2}{\pi^3}\left[\frac{(1+\eta)^2}{a_{[n]}^3} - \frac{1}{a_{[0]}^3}\right] a_{[n]}\bar{b}_i \tag{5.30}$$

where A_{ij} and $\bar{b}_i$ are expressed by equations (4.90) and (4.91), respectively ,it comes out immediately

$$\delta a_{i[n+1]} = -(\mathbf{A}^{-1}\mathbf{b})_i\, \frac{1}{2}\left[1 - \frac{a_{[n]}^3}{a_{[0]}^3(1+\eta)^2}\right] a_{[n]} \tag{5.31}$$

The scalar $(\mathbf{A}^{-1}\mathbf{b})_i$, is independent once again on i and on the iteration $[n]$.

By the equality chain:

$$(K_1^C)^2 = \frac{\kappa(t)^2}{(\pi a_{[0]}^3)} = \frac{\kappa(t)^2(1+\eta)^2}{(\pi a_{[n]}^3)}$$

it comes out

$$a_{[n]}^3 = \frac{(1+\eta^2)}{a_{[0]}^3}$$

which is the converged solution of the Newton-Raphson scheme (5.31).

A version of a meta code for a single load increment of the Newton-Raphson scheme can be expressed as follows:

$$\begin{aligned} While\,[\,\delta a_{i[n]} \quad &> \quad a_{[0]}\epsilon_\delta \\ \delta a_{i[n]} \quad &= \quad -(\mathbf{A}^{-1}\mathbf{b})_i \frac{1}{2}\left(1 - \frac{a_{[n]}^3}{a_{[0]}^3(1+\eta)^2}\right) a_{[n]}; \\ \varphi_{[n]} \quad &= \quad \kappa(t)^2 \frac{(1+\eta)^2}{(\pi a_{[n]})^3} - \frac{1}{\pi^3}; \\ a_{[n]} \quad &+= \quad \delta a_{i[n]}; \\ nofit \quad &++ \quad ;\,] \end{aligned}$$

A geometrical condition $\delta a_{i[n]} < a_{[0]}\epsilon_\delta$ is imposed as a test for convergency, at which corresponds a more severe condition on $\varphi < \epsilon_\varphi \ll \epsilon_\delta$.

Take a unit load factor $\kappa(t) = 1$ acting on a given initial crack of unit radius, propagating in a material of $K_1^C = \pi^{-3}$. By assuming a load increment $\eta = 5\%$, the convergence table 5.1 shows that 4 iterations are required to gain an accuracy of 10^{-6} on $\delta a_{i[n]}$ at the first load increment for the Newton-Raphson scheme.

Iteration n	$\delta a_{i[n]}$	$a_{[n]}$	$\varphi_{[n]}$
1	0.0310441	1.03104	0.000189688
2	0.00201305	1.03306	4.0927×10^{-7}
3	4.37737×10^{-6}	1.03306	7.09218×10^{-10}
4	7.5856×10^{-9}	1.03306	1.23502×10^{-12}

Table 5.1: *Convergency table for the proposed Newton-Raphson scheme.*

The load has been further incremented 400 times, to reach a final amount of 21 units load. The final crack radius amounts to $a_{[n]} = 7.61166$, as plotted in figure 5.2, but the features of the Newton-Raphson scheme depicted in table 5.1 remain unaltered in each load step.

5.2.1 The finite difference approach

Estimation of operator $N'_{\mathcal{F}_{[n]}}[\delta l_{[n+1]}]$ and consequently of the operator $\mathbf{K}^{(1)}_{[n]}[s,t;\delta l_{[n+1]}(s';t,\tau)]$ (see eq. (5.5)) by means of the finite difference approach appears to be straightforward at a first sight. Performed numerical experiments show on the contrary that the finite difference approach is not reliable for this sake.

The benchmark of Section 5.2 of a circular crack with unit radius embedded in a continuum body and axial-symmetric loaded by two point load forces, has been studied approximating the first order variation of the SIFs along the crack front $\mathbf{K}^{(1)}_{[n]}[s,t;\delta l_{[n+1]}(s';t,\tau)]$ by:

$$\frac{dK_1}{da} \approx \frac{K_1(a+\delta a) - K_1(a)}{\delta a} \tag{5.32}$$

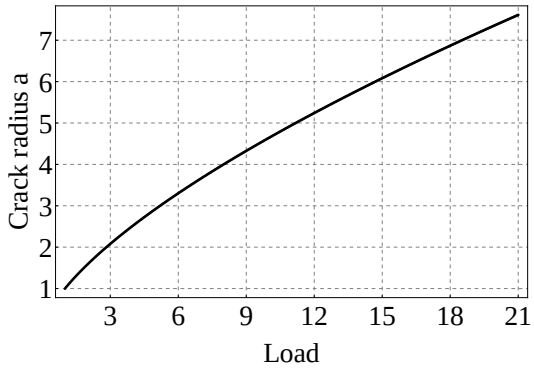

Figure 5.2: *Results of the Newton-Raphson scheme implementation. The radius of the circular crack a goes from* 1 *to* 7.61166 *when the load is increased* 400 *times from a unit value to 21 units.*

Accuracy of formula (5.32) is supposed to increase when the increment of the radius δa becomes smaller and smaller.

Inspired by the solution of the benchmark of Section 5.2, a range of values for δa has been investigated for derivative (5.32), with an upper bound of $\delta a = 0.2$. SIFs before elongation $K_1(a)$ and after elongation $K_1(a + \delta a)$ have been computed by means of the software FRANC3D. Even after using a finer discretization of the crack front $\mathcal{F}$ and surface $\mathcal{S}$, the relative error on the calculation of dK_1/da results extremely high, in the order of 200%, for $\delta a = 10^{-2}$. There is a clear evidence that error does not decrease with δa. Numerical cancellation may explain this behavior. In fact, the exact difference $K_1(a+\delta a)-K_1(a)$ turns out to be much smaller (two orders of magnitude smaller) of any of the two factors $K_1(a + \delta a)$ and $K_1(a)$. In spite having optimized FRANC3D capabilities in SIFs estimation and having refined the discretization, the observed accuracy could not be higher than the two significant digits for the example at hand. Although this accuracy is quite remarkable per se, it reveals to be inadequate for the estimation of dK_1/da because the difference of SIFs results in a severe numerical cancellation. On the other hand, if δa is too large compared to the size of elements mesh, the derivative (5.32) is inaccurate, bringing to the light the same issues described for the stiffness derivative method in Section 3.3.3.

5.3 Circular crack with an eccentric load

A penny shape crack in an unbounded isotropic linear elastic body Ω is subjected to two point load forces $-\kappa(t)\mathbf{n}$ at point P on the crack surface at a distance ρ from the initial crack front $\mathcal{F}(t)$ as depicted in figure 5.3. The location of point P is fixed during crack evolution.
Extension of the benchmark described in Section 5.2 to the more general case of an eccentric load, allows to study the solution of a full Signorini problem, capturing the eventuality of partial crack front elongation having nodes of the discretization of the crack front that are not mobilized.

A fictitious brittle material is considered, with Young's modulus $E = 1$, Poisson's ratio $\nu = 0.3$ and fracture toughness $K_1^C = 0.17$. Exploiting spatial discretization (5.19) of the unknown field $\delta l_{[n+1]}(s;t,\tau)$ and collecting nodal unknowns in vector $\boldsymbol{\delta l}_{[n+1]}$, the discrete form of functional

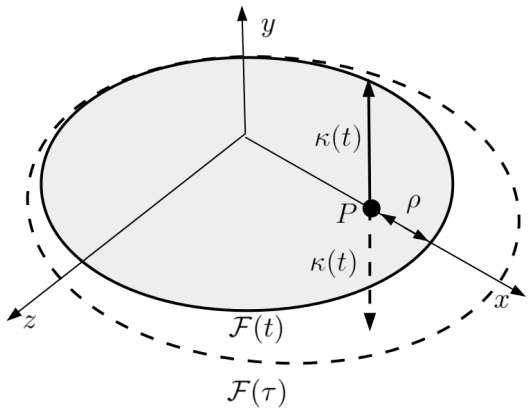

Figure 5.3: *A penny shape crack with radius $a(t)$ embedded in a continuum body is subject to two point load forces with magnitude $k(t)$ acting at a distance ρ from the initial crack front $\mathcal{F}(t)$. Crack tracking framework described in Section 5.1 is therefore benchmarked in the case of partial elongation of the crack front. $\mathcal{F}(\tau)$ represents the solution of the converged Newton-Raphson scheme at the end of the single load step, after the increase of the load at $\kappa(\tau) > \kappa(t)$.*

$\chi^{\mathcal{H}}_{[n]}[\boldsymbol{\delta l}_{[n+1]}]$ (5.15) reads:

$$\begin{aligned}\chi^{\mathcal{H}}_{[n]}[\boldsymbol{\delta l}_{[n+1]}] &= -\frac{1}{2}\sum_{i=1}^{N_h}\sum_{j=1}^{N_h}\int_{\mathcal{F}_{[n]}(\tau)} N'_{\mathcal{F}_{[n]}}[\psi_j(s)]\,\psi_i(s) + \\ &+ \frac{1}{2}\,\epsilon\,\mathcal{H}\left[\sum_{r=1}^{N_h}\psi_r(s)\,\delta l_{r[n+1]}\right]\psi_i(s)\,\psi_j(s)\,ds\,\delta l_{i[n+1]}\,\delta l_{j[n+1]} \\ &- \frac{1}{2}\sum_{i=1}^{N_h}\int_{\mathcal{F}_{[n]}(\tau)}(K_{1[n]}(s,\tau)\Lambda_{11}K_{1[n]}(s,\tau) - G_C)\,\psi_i(s)\,ds\,\delta l_{i[n+1]}\end{aligned}$$

The discretized optimality condition (5.20) has been implemented with penalty parameter $\epsilon = 10^4$. The linear system:

$$(\mathbb{A} + \mathbb{H}^{(k-1)})\boldsymbol{\delta l}^{(k)}_{[n+1]} = \mathbf{b} \tag{5.33}$$

has been solved at each iteration k of the Update Linearized algorithm, with:

$$\mathbb{A}_{ij} = -\int_{\mathcal{F}_{[n]}(\tau)} N'_{\mathcal{F}_{[n]}}[\psi_j(s)]\psi_i(s)\,ds \tag{5.34a}$$

$$\mathbb{H}^{(k-1)}_{ij} = +\epsilon\int_{\mathcal{F}_{[n]}(\tau)} \mathcal{H}[\boldsymbol{\delta l}^{(k-1)}_{[n+1]}]\psi_i(s)\psi_j(s)\,ds \tag{5.34b}$$

$$b_i = +\frac{1}{2}\int_{\mathcal{F}_{[n]}(\tau)}(K_{1[n]}(s,\tau)\Lambda_{11}K_{1[n]}(s,\tau) - G_C)\psi_i(s)\,ds \tag{5.34c}$$

At initial time $t = 0$, $\mathcal{S}(0)$ is the circle of unit radius $a(0) = 1$.
Crack face weight functions are given for such initial geometry as well as $W^{\mathcal{S}}$ and $W^{\mathcal{F}}$. They read:

$$k_{11}(P,s') = \frac{\sqrt{\rho(2a_{[0]}-\rho)}}{\pi\sqrt{\pi a_{[0]}}}\frac{1}{D^2(P,s')} \tag{5.35a}$$

$$W^{\mathcal{S}}(P,s') = \sqrt{\frac{2a_{[0]}-\rho}{2a_{[0]}}} \tag{5.35b}$$

$$W^{\mathcal{F}}(s,s') = 1 \tag{5.35c}$$

Loading conditions are such to enforce a stable mode 1 propagation in the plane that contains the initial configuration of the crack. This circumstance allows using equation (5.23) for operator $N'_{\mathcal{F}_{[n]}}[\cdot]$. Stemming on the definition of crack face weight functions and on formula (5.35a), the mode 1 stress intensity factor along the crack front at time $t = 0$ amounts to:

$$K_1(s,0) = \kappa(0)\frac{\sqrt{\rho(2-\rho)}}{\pi\sqrt{\pi}}\frac{1}{D^2(P,s)} \tag{5.36}$$

and the crack front curvature is $c(0) = -1/2$. In the hypothesis of small eccentricity of the load, coefficients of the crack opening expansion (4.42) can be extrapolated from the closed form solution available for axial-symmetric load for which $\rho \equiv a_{[0]}$, that are expressed in equation (4.58). More generally, high order shape functions must be tailored to numerically capture Ξ_1 in finite or boundary element methods, as seen in Section 3.1.6.

Considering an eccentricity of the load $0.85 \leq \rho < 1$, in the initial equilibrium configuration, all points s along the circular crack front $\mathcal{F}(0)$ of unit radius are in the safe equilibrium domain $\mathbb{E}(s,0)$ (see equation (2.17)) at value $\kappa(0) = 0.65$ of the load factor. To assess this condition SIFs are estimated from the closed form (5.36). The load factor is then increased to $\kappa(\tau) = 1.01$, value at which most of the points along the front exit the safe equilibrium domain in force of the elastic trial (5.1). Figure 5.4 plots $\varphi_{[0]}(s,\tau)$ defined in equation (5.2) for three different values of the eccentricity ρ.

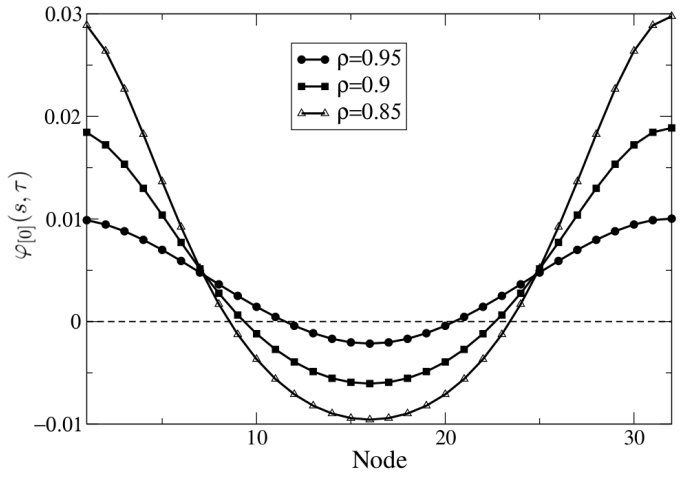

Figure 5.4: $\varphi_{[0]}(s,\tau)$ *along the crack front* $\mathcal{F}_{[0]}(\tau)$ *discretized in* $N_h = 32$ *elements for three different values of the initial eccentricity of the load* $\rho = 0.95, \rho = 0.9$ *and* $\rho = 0.85$ *for a load factor* $\kappa = 1.01$. *The subpart of the front* $\mathcal{F}_{[0]}(\tau)$ *with* $\varphi_{[0]}(s,\tau) \leq 0$ *stay in the safe equilibrium domain* $\mathbb{E}(s,0)$.

A new configuration $\mathcal{F}(\tau)$ in equilibrium at $\kappa(\tau) = 1.01$ is sought for the crack front. Figure

5.5-a plots the front $\mathcal{F}_{[1]}(\tau)$ that evolves from $\mathcal{F}(t)$ by means of the converged solution $\boldsymbol{\delta l}_{[1]}$ of the Update Linearized algorithm (5.33), at a value of the load factor $\kappa = 1.01$.

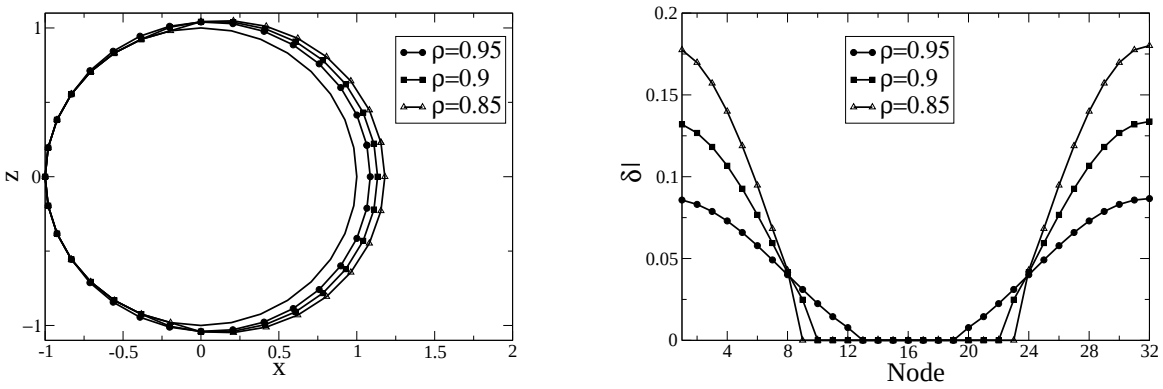

a) b)

Figure 5.5: *a) Converged solution of the Update Linearized algorithm from the initial circular crack (continuous black curve), considering three different locations of the point load $\rho = 0.95$, $\rho = 0.9$ and $\rho = 0.85$. b) Nodal values $\delta l_{[1]}$ along the crack front subdivided into $N_h = 32$ elements, considering three different locations of the point load $\rho = 0.95$, $\rho = 0.9$ and $\rho = 0.85$.*

The nodal values $\boldsymbol{\delta l}_{[1]}$ along the crack front, subdivided into $N_h = 32$ elements, are plotted in figure 5.5-b.

Convergence of the Update Linearized algorithm is detailed in table 5.2. Two iterations are sufficient at each value of ρ in order to have a three digits accuracy:

$$\frac{\|\boldsymbol{\delta l}_{[1]}^{(k)} - \boldsymbol{\delta l}_{[1]}^{(k-1)}\|}{\|\boldsymbol{\delta l}_{[1]}^{(k)}\|} < 10^{-3}$$

	$\rho = 0.95$	$\rho = 0.9$	$\rho = 0.85$
k	$\|\boldsymbol{\delta l}_{[1]}^{(k)}\|$	$\|\boldsymbol{\delta l}_{[1]}^{(k)}\|$	$\|\boldsymbol{\delta l}_{[1]}^{(k)}\|$
1	0.293844	0.431179	0.548453
2	0.293844	0.431179	0.548453

Table 5.2: *Norm of the vector crack front elongation $\boldsymbol{\delta l}_{[1]}^{(k)}$ for each iteration k of the Update Linearized algorithm of the first crack tracking step ($n = 1$) for the three different values of initial ρ, namely $\rho = 0.95$, $\rho = 0.9$, and $\rho = 0.85$.*

The stress intensity factors shall be estimated in order to device which points are in the safe equilibrium domain at configuration $\mathcal{F}_{[1]}(\tau)$, since the geometry has been updated. SIFs have been evaluated numerically at each Newton-Raphson iteration n by the software FRANC3D. They are plotted in figure 5.6 in the initial configuration ($n = 0$) for the case $\rho = 0.95$.

Since the geometry is now rather different from a circumference, fundamental kernels must be updated as well. Figure 5.7 depicts the approximation for FK $W^{\mathcal{F}_{[1]}}(s, s')$ along curvilinear abscissa

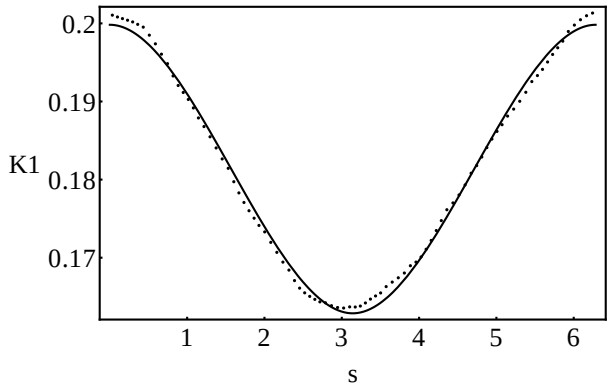

Figure 5.6: *Dots represents the value of SIF $K_{1[0]}(s_i, \tau)$ in the middle node s_i of each crack front element computed in FRANC3D in the initial configuration ($n = 0$) for the case $\rho = 0.95$. Continuous curve shows a cubic spline least square approximation of the discrete data with respect to the curvilinear abscissa s along the crack front $\mathcal{F}_{[0]}(\tau)$.*

s' when two point load forces are applied at a small distance $\bar{\rho}$ from point s of the crack front $\mathcal{F}_{[1]}(\tau)$. It has been achieved by the first order approximation formula (4.100b) of the FK approximation algorithm described in Section 4.3. It is worth noting that discretization of the crack front exploited to compute $W^{\mathcal{F}_{[n]}}(s, s')$ is independent upon the discretization considered in the crack tracking algorithm. The curvature $c_{[1]} = -1/2a_{[1]}$ and the universal quantity $\frac{\partial W^{\mathcal{S}_{[1]}}}{\partial \rho}\Big|_{s,s} = -\frac{1}{4a_{[1]}}$ have been updated at $\mathcal{F}_{[1]}(\tau)$ considering as $a_{[1]}$ a sort of average radius along $\mathcal{F}_{[1]}(\tau)$, namely

$$a_{[1]} = \frac{\sum_{i=1}^{N_h}(a_{[0]} + \delta l_{i[1]})}{N_h}$$

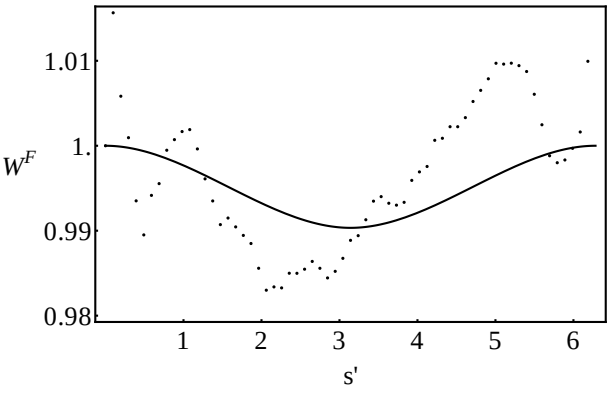

Figure 5.7: *Values of the FK $W^{\mathcal{F}_{[1]}}(s, s')$ by means of the first order approximation formula (4.100b) in the configuration $\mathcal{F}_{[1]}(\tau)$. These latter derive from the case of initial eccentricity of the load $\rho = 0.95$. Continuous curve represents a least square approximation of the discrete data (black dots) deriving from the computation with the software FRANC3D of SIF $K_1(\delta(P); s'_i)$ in the middle node s'_i of each crack front element, due to the application of two point loads $\delta(P)$ in a point P of the crack surface $\mathcal{S}_{[1]}(\tau)$ at a distance $\bar{\rho}$ from $\mathcal{F}_{[1]}(\tau)$.*

The algorithm is iterated, in order to achieve the final configuration $\mathcal{F}(\tau)$ at the end of the first load increment. Three iterations of the Newton-Raphson scheme are necessary to converge up to

the given tolerance 10^{-3} on $\|\boldsymbol{\delta l}_{[n+1]}\|$. Table 5.3 details the evolution of the numerical procedure for the case of an initial $\rho = 0.95$.

$[n+1]$	$\|\boldsymbol{\delta l}_{[n+1]}\|$	$\|\varphi_{[n]}\|$
1	0.293844	0.0127239
2	0.0260217	$9.56499 \cdot 10^{-4}$
3	0.000423446	$3.03741 \cdot 10^{-5}$

Table 5.3: *First load step: iterations of the Newton-Raphson scheme for the case of an initial* $\rho = 0.95$. *Quantity* $\|\varphi_{[n]}\|$ *has been computed as* $\sqrt{\int_{\mathcal{F}_{[n]|\varphi_{[n]}(s,\tau)>0}} \varphi^2_{[n]}(s,\tau)\, ds} \approx \sqrt{\sum_{i=1}^{\hat{N}_h} \bar{\varphi}^2_{[n]}\, l_{\hat{N}_h}}$ *where* $\hat{N}_h$ *are the crack front elements with* $\varphi_{[n]}(s,\tau) > 0$ *and length* $l_{\hat{N}_h}$ *and* $\bar{\varphi}_{[n]}$ *is the average value of* $\varphi_{[n]}(s,\tau)$ *along such elements at iteration* n *of the crack tracking scheme.*

The configuration of the crack front $\mathcal{F}(\tau)$ at the end of the first load step for an initial eccentricity of the load $\rho = 0.95$ is showed in figure 5.8.

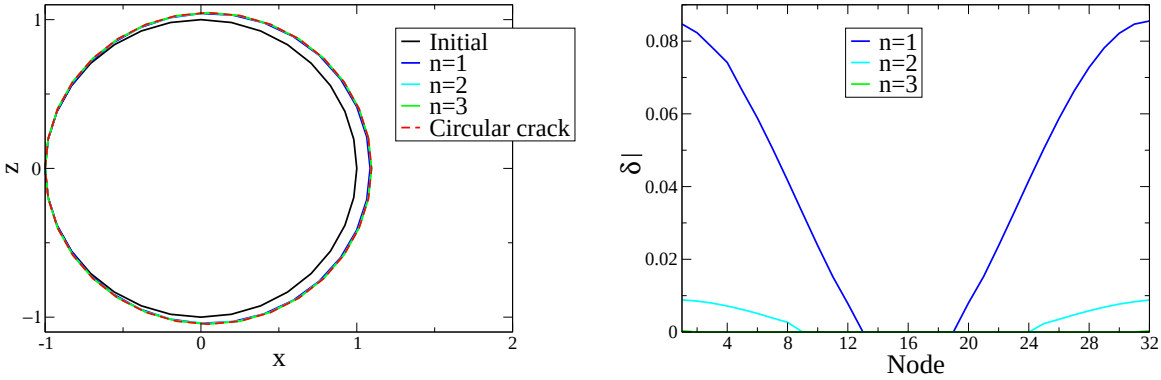

a) b)

Figure 5.8: *a) Obtained converged configurations at each iteration* n *of the crack tracking scheme for the first load step and initial eccentricity* $\rho = 0.95$. *b) Values of the increment of elongation* $\delta l_{[n]}$ *in each node of the crack front, discretized in* $N_h = 32$ *elements, for each iteration* n *of the crack tracking scheme and initial eccentricity* $\rho = 0.95$. *3 iterations are requires to reach the converged solution of the first load step (*$\|\boldsymbol{\delta l}_{[n]}\| < 10^{-3}$*).*

Figure 5.9 plots the onset of propagation $\varphi_{[n]}(s,\tau)$ along the crack front at each iteration of the crack tracking scheme for initial $\rho = 0.95$. Points in incipient propagation condition decrease with the iterations, eventually vanishing. The equilibrium configuration $\mathcal{F}(\tau)$ is therefore reached and only a further increase of the external loads can lead the crack to a further stable propagation.

Intuition suggests that an equilibrium configuration for the problem at hand would be a penny shape fracture centered at the point load. Indeed the configuration $\mathcal{F}(\tau)$ perfectly overlaps a circular front centered at the point load location, plotted in figure 5.8-a with a red dashed curve. Such an equilibrium configuration provides a SIF equal to $K_1(\tau) = 0.169$ according to formula

$$K_1(\tau) = \frac{\kappa(\tau)}{(\pi a(\tau))^{3/2}} \tag{5.37}$$

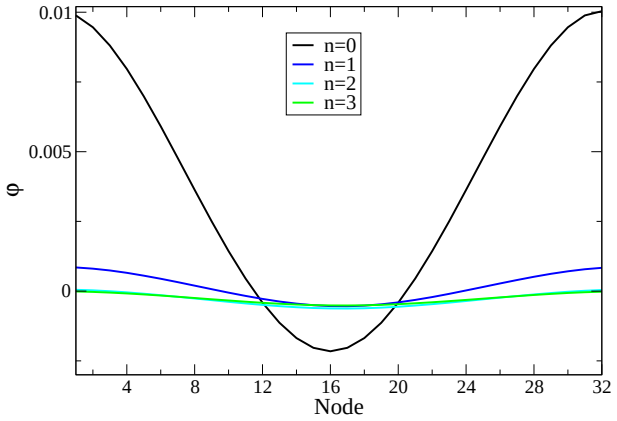

Figure 5.9: *Onset of propagation $\varphi_{[n]}(s,\tau)$ along the crack front for each iteration n of the Newton-Raphson scheme.*

at magnitude $\kappa(\tau) = 1.01$ and radius $a(\tau) = 1.04731$. The distribution of SIFs at iteration $n = 3$ estimated via FRANC3D is printed in figure 5.10 and matches the intuition very well.

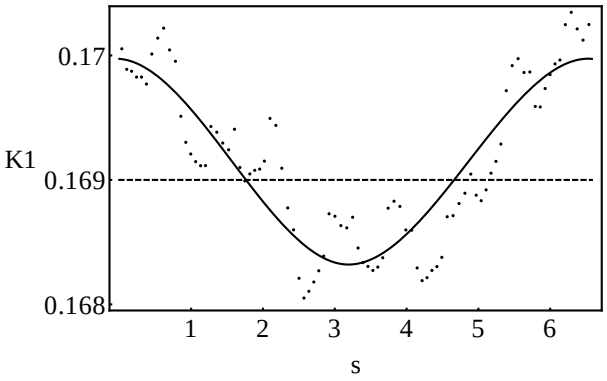

Figure 5.10: *SIF $K_{1[3]}(s,\tau)$ along the crack front computed in FRANC3D at iteration $n = 3$ of the Newthon Raphson scheme (black dots) and least square approximation of the discrete data (continuous black curve). As one can notice, SIFs along $\mathcal{F}(\tau)$ are close to the analytical solution $K_1(\tau) = 0.169$ (dashed black curve) that corresponds to the case of a circular crack of radius $a(\tau) = 1.04731$ axial-symmetrically loaded by two point forces of magnitude $\kappa = 1.01$ acting in the center of the crack according to equation (5.37).*

Chapter 6

Fracture driven by diffusion of species in solids

This Chapter focuses on a germinal model of stable 3D crack growth driven by diffusion of species in solids. In particular the diffusion process investigated involves neutral species in the hypothesis of small displacements and strains.

The fundamental assumption that is made is that guest atoms of the diffusing species in the host material are separated into two different species of solutes, indicated with L and T, which may potentially diffuse in and out of a subpart of the domain. Consequently, each quantity involved in the diffusion process is split in an interstitial part, indicated with the subscript L, and a part indicated with the subscript T that refers to trap sites. Mobility of species T is considered to be zero [69, 136], meaning that species atoms diffuse trough lattice sites and traps sites are filled by lattice diffusion. Traps (i.e. dislocations, grain boundaries, interfaces between phases, voids or cracks) evolve during plastic deformations. Therefore the number of trap sites depends on the deformation level, while the number of lattice sites is constant and depends on the host medium. Only saturable and reversible traps are considered, such as dislocation cores [70].

The diffusion model detailed below [131] is suitable to describe phenomena such as hydrogen embrittlement in metals, intercalation of neutral Lithium in brittle particles in Li-ion batteries, or fracking for shale gas extraction from nano pores in rocks for CO_2 sequestration in brittle material repositories. Although the relevant mechanical constitutive laws are neither linear nor elastic, numerical analyses for real cases of diffusion of species in solids manifest that the response of the material in standard loading conditions is linear elastic almost everywhere apart from areas extremely close to the crack front. Whereas all coupled processes must necessarily account for non linearities in order to properly describe the interstitial diffusion, as for the increment of traps due to plastic flow, evidences show that global inelastic responses are confined in a very narrow zone that appears to correspond to the annulus postulated by the *small scale yielding* description of fracture mechanics. Crack propagation is therefore assumed to take place either in brittle or in completely embrittled environments.

When the description above applies, the process of crack growth can be conveniently described in the LEFM framework, relating the energy release rate to the notion of SIFs. Species diffuses into the crack tip region owing to the energetic driving force created by the chemical potential, which in turn depends on the stresses and concentrations [72] and there is wide evidence that the impurities segregation and enrichment of species around the crack front can greatly modify the fracture processes.

Understanding cracks pattern evolution and predicting quantities of interest has revealed of great

importance in order to increase the safety and improve the mechanical performance of materials and components. In other words: How big can a defect be when the the structural safety, proviso a safety factor, is compromised? The presence of the species dramatically affects the safety in some cases. In other ones, controlled quasi static crack growth can be beneficial, as for hydraulic fracturing in shale gas extraction. Either positive or negative the interpretation of crack growth, the major complexity stands in governing fracture propagation in embrittled materials before unstable propagation takes place.

6.1 Balance laws

6.1.1 Mass balance

The trapping process can be described as a chemical reaction:

$$L \rightleftarrows T \tag{6.1}$$

which portrays the conversion of mobile (L) to trapped (T) species and viceversa by the reaction rate of reaction (6.1), denoted with $\bar{w}$. The rate of the forward and backward reactions (termed $\bar{w}_T$ and $\bar{w}_L$) can be conveniently written in terms of the rate $\bar{w}$ of the reaction (6.1) as:

$$\bar{w}_T = \bar{w}, \qquad \bar{w}_L = -\bar{w} \tag{6.2}$$

Under equilibrium conditions the rate of the forward and backward reactions are equal, and the *equilibrium constant* [1]

$$K_{eq} = \frac{c_T^{eq}}{c_L^{eq}} \frac{c_L^{max} - c_L^{eq}}{c_T^{max} - c_T^{eq}} \tag{6.3}$$

of reaction (6.1) can be established. Equilibrium concentrations of trapped (c_T^{eq}) and mobile (c_L^{eq}) species depend on temperature T, and so does K_{eq} in turn. Differently from Oriani's theory [106] and the papers that it inspired, equilibrium's conditions are not a priori enforced in the present formulation and reaction (6.1) is unbalanced during species diffusion and interstitial species L is either made available or trapped. This results in a mass supply/sink within the mass balance equations, which yields:

$$\frac{\partial c_L}{\partial t} + \operatorname{div}[\,\mathbf{h}_L\,] + \bar{w} = 0 \tag{6.4a}$$

$$\frac{\partial c_T}{\partial t} - \bar{w} = 0 \tag{6.4b}$$

in the assumption that the traps are isolated, i.e. do not form an extended network and the trapped species is immobile (see figure 6.1). This means that the flux of the species $\mathbf{h}$ across the boundary of the domain $\Gamma \equiv \partial\Omega$ is assumed to be purely interstitial (and termed $\mathbf{h}_L$) [72, 73]. Therefore, the trapped species in the bulk do not contribute to species transport and it lacks a mass flux term in eq. (6.4b). Denoting with $\beta = L, T$, symbols in equations (6.4) have the following meaning: c_β is the *molarity* (i.e. the number of moles per unit volume) of a generic species β and c_β^{max} is the correspondent saturation limit; $\mathbf{h}_\beta$ is the mass flux in terms of moles, i.e. the number of moles of species β measured per unit area per unit time, $\bar{w}$ is the reaction rate of the chemical reaction (6.1) pertaining to species β, measured per unit volume per unit time. Concentrations c_β are defined in space $\mathbf{x} \in \Omega$ and time $0 \leq t \leq \tau$, i.e. $c_\beta = c_\beta(\mathbf{x}, t)$. The same holds for $\mathbf{h}_\beta$ and $\bar{w}$. Functional dependence however is specified when necessary only, to favor readability.

[1] Expression (6.3) results by equating chemical potentials μ_L and μ_T after constitutive characterization detailed in Section 6.3.

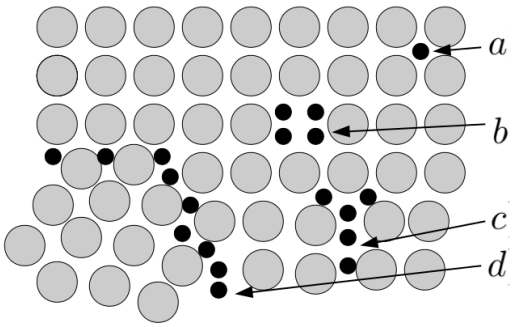

Figure 6.1: *Schematic representation of the presence of impurities, represented by small black dots, inside the crystal lattice of the host medium, represented by big grey dots. Along with the interstitial species L indicated with a, there are trap sites for guest atoms for example at vacancies (b), edge dislocations (c), and grain boundaries (d). Only saturable and reversible traps are considered in the diffusion model presented in this Chapter.*

6.1.2 Balance of momentum

The usual balance of forces:

$$\operatorname{div}[\,\boldsymbol{\sigma}\,] + \mathbf{f} = \mathbf{0} \tag{6.5}$$

and the symmetry of the stress tensor $\boldsymbol{\sigma}$ emanates from the principle of virtual power [50].

6.1.3 Weak form and boundary conditions

The weak formulation of balance equations (6.4, 6.5) results from multiplication by a suitable set of test functions and from an integration upon the domain, exploiting Green's formula to reduce the order of differentiation. Consider the mass balance equation (6.4a):

$$\begin{aligned}
&\int_\Omega \hat{\mu}_L \left\{ \frac{\partial c_L}{\partial t} + \operatorname{div}[\,\mathbf{h}_L\,] + \bar{w} \right\} d\Omega = \\
= &\int_\Omega \hat{\mu}_L \frac{\partial c_L}{\partial t}\, d\Omega + \int_\Omega \operatorname{div}[\,\hat{\mu}_L \mathbf{h}_L\,] - \nabla[\,\hat{\mu}_L\,] \cdot \mathbf{h}_L\, d\Omega + \int_\Omega \hat{\mu}_L \bar{w}\, d\Omega = \\
= &\int_\Omega \hat{\mu}_L \frac{\partial c_L}{\partial t}\, d\Omega - \int_\Omega \nabla[\,\hat{\mu}_L\,] \cdot \mathbf{h}_L\, d\Omega + \int_\Omega \hat{\mu}_L\, \bar{w}\, d\Omega + \int_\Gamma \hat{\mu}_L\, \mathbf{h}_L \cdot \mathbf{n}\, d\Gamma = 0
\end{aligned} \tag{6.6}$$

Within (6.6) a contribution is defined at the boundary Γ. The extension of Neumann boundaries is defined for each field and differs from field to field. In order to enlighten the notation, the field dependence has not been specified in writing Γ^h and has been left backward. Same arguments apply to Dirichlet boundaries. It is not usual to know a priori the amount of mass flux along part of the boundary. It is rather more natural to impose thermodynamic equilibrium between the external species and the one at the boundary of the hosting material. Nevertheless, for the sake of completeness, boundary conditions will be written as:

$$\mathbf{h}_L \cdot \mathbf{n} = \bar{h} \qquad \mathbf{x} \in \Gamma^h$$

The weak form for the mass balance equation (6.4b) can be simply derived as:

$$\int_\Omega \hat{\mu}_T \left\{ \frac{\partial c_T}{\partial t} - \bar{w} \right\} d\Omega = 0 \tag{6.7}$$

Finally, for the equilibrium equation (6.5) one writes in the assumption of vanishing body forces:

$$\int_\Omega \hat{\mathbf{u}} \cdot \operatorname{div}[\,\boldsymbol{\sigma}\,]\, d\Omega = -\int_\Omega \hat{\boldsymbol{\varepsilon}} : \boldsymbol{\sigma}\, d\Omega + \int_\Gamma \hat{\mathbf{u}} \cdot \boldsymbol{\sigma}\, \mathbf{n}\, d\Gamma = 0 \tag{6.8}$$

The boundary condition along Γ^p reads:

$$\boldsymbol{\sigma}\, \mathbf{n} = \bar{\mathbf{p}} \qquad \mathbf{x} \in \Gamma^p$$

A Dirichlet boundary condition (usually homogeneous), for the displacements shall be added along the Dirichlet part of the boundary Γ^u.

In conclusion, the weak form of the balance equations can be written in terms of the potentials in time interval $[0, \tau]$ as:

Find $y \in \mathcal{V}^{[0,\tau]}$ such that

$$\frac{d}{dt} b(\hat{y}, z(t)) + a(\hat{y}, y(t)) = f(\hat{y}) \qquad \forall\, \hat{y} \in \mathcal{V} \tag{6.9}$$

where

$$b(\hat{y}, z(t)) = \int_\Omega \hat{\mu}_L\, c_L + \hat{\mu}_T\, c_T\, d\Omega$$

$$a(\hat{y}, y(t)) = -\int_\Omega \nabla[\,\hat{\mu}_L\,] \cdot \mathbf{h}_L\, d\Omega + \int_\Omega \hat{\boldsymbol{\varepsilon}} : \boldsymbol{\sigma}\, d\Omega + \int_\Omega (\hat{\mu}_L - \hat{\mu}_T)\, \bar{w}\, d\Omega$$

$$f(\hat{y}) = -\int_{\Gamma^h} \hat{\mu}_L\, \bar{h}\, d\Gamma + \int_{\Gamma^p} \hat{\mathbf{u}} \cdot \bar{\mathbf{p}}\, d\Gamma$$

with $z = \{c_L, c_T\}$, $y = \{\mu_L, \mu_T, \mathbf{u}\}$. Columns z and y collect the time-dependent unknown fields. Column $\hat{y}$ collects the steady-state test functions that correspond to the unknown fields in y.

To computationally solve the (either weak or strong) problem, constitutive equations must be specified, and this will be the subject of Section 6.3. The weak form (6.9) acquires the usual meaning of power expenditure: for this reason it is written in terms of chemical potentials $\hat{\mu}_L$ and $\hat{\mu}_T$ rather than concentrations.

6.2 Thermodynamics of fracture in the presence of species

6.2.1 Energy balance

Consider an arbitrary material region $\mathcal{P} \in \Omega \in \mathbb{R}^3$, which is taken as non convecting, in agreement with the assumption of small displacements and strains. The first law of thermodynamics represents the balance of the interplay between the internal energy of $\mathcal{P}$, the power expended on $\mathcal{P}$, the heat transferred in $\mathcal{P}$, and the power due to mass exchanged on $\mathcal{P}$. The energy balance for the problem at hand, for quasi-static interactions, reads:

$$\frac{\partial \mathcal{U}(\mathcal{P})}{\partial t} = \mathcal{W}(\mathcal{P}) + \mathcal{Q}(\mathcal{P}) + \mathcal{T}(\mathcal{P}) \tag{6.10}$$

with $\mathcal{U}$ the net internal energy of $\mathcal{P}$, $\mathcal{W}$ the mechanical external power, $\mathcal{Q}$ the power due to heat transfer, $\mathcal{T}$ the power due to mass transfer. It is assumed that any of these processes is accompanied with its own separate energy contribution in the balance that read:

$$\mathcal{W}(\mathcal{P}) = \int_{\mathcal{P}} \mathbf{f} \cdot \boldsymbol{v}\, d\Omega + \int_{\partial\mathcal{P}} \mathbf{p} \cdot \boldsymbol{v}\, d\Gamma \tag{6.11a}$$

$$\mathcal{Q}(\mathcal{P}) = \int_{\mathcal{P}} s_q \, d\Omega - \int_{\partial\mathcal{P}} \mathbf{q} \cdot \mathbf{n} \, d\Gamma \tag{6.11b}$$

$$\mathcal{T}(\mathcal{P}) = \int_{\mathcal{P}} {}^{u}\mu_L \, s_L + {}^{u}\mu_T \, s_T \, d\Omega - \int_{\partial\mathcal{P}} {}^{u}\mu_L \mathbf{h}_L \cdot \mathbf{n} \, d\Gamma \tag{6.11c}$$

The time variation of net internal energy corresponds to the power expenditure of external agencies: a mechanical contribution due to body forces $\mathbf{f}$ and contact forces $\mathbf{p}$ that spend power against velocities $\boldsymbol{v}$; a heat contribution where the scalar s_q is the heat supplied by external agencies and $\mathbf{q}$ is the heat flux vector; a mass flux contribution with the scalar ${}^{u}\mu_\beta$ denoting the specific energy required to provide a unit supply of mass of species β ($\beta = L, T$), and the scalar s_β stands for the external supply of species (i.e. excluding chemical reaction contributions).

As usual in thermodynamics of continua [50], one can make use of the specific internal energy u:

$$\mathcal{U}(\mathcal{P}) = \int_{\mathcal{P}} u \, d\Omega$$

in small displacements it makes no difference to define specific internal energy per unit mass or per unit volume, since both mass and volume do not change during the process. Standard application of the divergence theorem and of mass balances (6.4) leads from (6.11) to:

$$\mathcal{W}(\mathcal{P}) = \int_{\mathcal{P}} \boldsymbol{\sigma} : \frac{\partial \boldsymbol{\varepsilon}}{\partial t} \, d\Omega \tag{6.12a}$$

$$\mathcal{Q}(\mathcal{P}) = \int_{\mathcal{P}} s_q - \operatorname{div}[\,\mathbf{q}\,] \, d\Omega \tag{6.12b}$$

$$\mathcal{T}(\mathcal{P}) = \int_{\mathcal{P}} {}^{u}\mu_L \frac{\partial c_L}{\partial t} + {}^{u}\mu_L \, \bar{w} - \mathbf{h}_L \cdot \nabla[\,{}^{u}\mu_L\,] \, d\Omega + \int_{\mathcal{P}} {}^{u}\mu_T \frac{\partial c_T}{\partial t} - {}^{u}\mu_T \, \bar{w} \, d\Omega \tag{6.12c}$$

The presence of crack surface $\mathcal{S}$ affects the usual localization procedure of the first principle of thermodynamics. The rate of the internal energy splits in the sum:

$$\frac{\partial}{\partial t}\int_{\mathcal{P}} u \, d\Omega = \frac{\partial}{\partial \mathcal{S}}\int_{\mathcal{P}} u \, d\Omega \, \frac{\partial \mathcal{S}}{\partial t} + \int_{\mathcal{P}} \frac{\partial u}{\partial t} \, d\Omega \Big|_{\mathcal{S}}$$

The first contribution represents the change in internal energy when the fracture surface is changed merely, whereas the second contribution accounts for the change in internal energy when the fracture surface is unchanged. The amount of newly formed fracture surface reads:

$$\frac{\partial \mathcal{S}}{\partial t} = v(s,t)\partial s$$

with the crack front velocity $v(s,t)$ as defined in (2.1). The change in internal energy when nothing but the fracture surface is changed is the *energy release rate*, namely:

$$G(\mathcal{P}) = -\frac{\partial}{\partial \mathcal{S}}\int_{\mathcal{P}} u \, d\Omega$$

Irwin's formula [62]:

$$G = \mathbf{K}^* \cdot \boldsymbol{\Lambda} \mathbf{K}^* \tag{6.13}$$

usually involves the whole volume Ω and the amount $G(\Omega)$ is simply denoted with G. In eq.(6.13) definitions of SIFs vector $\mathbf{K}^*$ and of matrix $\boldsymbol{\Lambda}$ refer to equations (2.3) and (2.12), respectively.

There were no constitutive restrictions on energy release rate G so far and its only exploiting Irwin's formula (6.13) that analysis is restricted to LEFM.

The first principle of thermodynamics results:

$$\begin{aligned} - \quad & G(P)\frac{\partial \mathcal{S}}{\partial t} + \int_{\mathcal{P}} \frac{\partial u}{\partial t}\, d\Omega \Big|_{\mathcal{S}} = \\ = \quad & \int_{\mathcal{P}} \boldsymbol{\sigma} : \frac{\partial \boldsymbol{\varepsilon}}{\partial t} + s_q - \operatorname{div}[\,\mathbf{q}\,] + {}^{u}\mu_L \frac{\partial c_L}{\partial t} + {}^{u}\mu_T \frac{\partial c_T}{\partial t} - \mathbf{h}_L \cdot \nabla[\,{}^{u}\mu_L\,] + ({}^{u}\mu_L - {}^{u}\mu_T)\bar{w}\, d\Omega \end{aligned} \tag{6.14}$$

6.2.2 Entropy imbalance

The following form of the entropy imbalance

$$\frac{\partial}{\partial t}\int_{\mathcal{P}} \eta\, d\Omega + \int_{\mathcal{P}} -\frac{s_q}{T} + \operatorname{div}\left[\,\frac{\mathbf{q}}{T}\,\right] - {}^{\eta}\mu_L s_L + \operatorname{div}[\,{}^{\eta}\mu_L \mathbf{h}_L\,] - {}^{\eta}\mu_T s_T\, d\Omega \geq 0 \tag{6.15}$$

can be derived in terms of the referential entropy η and of the absolute temperature T from the usual entropy balance. The scalar ${}^{\eta}\mu_\beta$ denotes the change in the specific entropy provided by a unit supply of mass[2] of species $\beta = L, T$.

Equation (6.15) stems from the non trivial assumption that mechanics does not contribute to the total entropy flow in the entropy balance equation. The fundamental assumption made is that an extension of fracture surface does not affect the entropy:

$$\frac{\partial}{\partial t}\int_{\mathcal{P}} \eta\, d\Omega = \int_{\mathcal{P}} \frac{\partial \eta}{\partial t} d\Omega$$

A rationale for this assumption can be found in [34]. Although the understanding of the fundamental physics beyond this hypothesis and its long-range impact is not yet fully clear, the timescale of the diffusive process versus the velocity of the crack elongation in real materials seems to play a role. If the velocity of the crack front is much higher than the diffusion velocity, it appears to be reasonable to assume that the entropy of mixing is not influenced by crack elongation and that the entropic redistribution takes place after a new mechanically equilibrated and compatible configuration has been attained. Such a strong assumption is coherent with the assumption made that mechanics does not cause an entropy flux in the entropy imbalance (6.15), and is equivalent to state that the *entropy release rate* is zero. The entropy imbalance thus reads:

$$\int_{\mathcal{P}} \frac{\partial \eta}{\partial t} - \frac{s_q}{T} + \operatorname{div}\left[\,\frac{\mathbf{q}}{T}\,\right] - {}^{\eta}\mu_L s_L + \operatorname{div}[\,{}^{\eta}\mu_L \mathbf{h}_L\,] - {}^{\eta}\mu_T s_T\, d\Omega \;\geq\; 0$$

By noting that

$$\operatorname{div}\left[\,\frac{\mathbf{q}}{T}\,\right] = \frac{1}{T}\operatorname{div}[\,\mathbf{q}\,] - \frac{1}{T^2}\mathbf{q} \cdot \nabla[\,T\,]$$

the entropy imbalance can be rephrased in terms of the internal energy, taking advantage of identity (6.14) and of the sign definiteness of temperature:

$$\begin{aligned} & \int_{\mathcal{P}} T\frac{\partial \eta}{\partial t} - \frac{1}{T}\mathbf{q} \cdot \nabla[\,T\,] - T\,{}^{\eta}\mu_L s_L + T \operatorname{div}[\,{}^{\eta}\mu_L \mathbf{h}_L\,] - T\,{}^{\eta}\mu_T s_T\, d\Omega \\ + \quad & G(\mathcal{P})\frac{\partial \mathcal{S}}{\partial t} - \left\{ \int_{\mathcal{P}} \frac{\partial u}{\partial t} - \boldsymbol{\sigma} : \frac{\partial \boldsymbol{\varepsilon}}{\partial t} - {}^{u}\mu_L \frac{\partial c_L}{\partial t} - {}^{u}\mu_T \frac{\partial c_T}{\partial t} + \mathbf{h}_L \cdot \nabla[\,{}^{u}\mu_L\,] - ({}^{u}\mu_L - {}^{u}\mu_T)\bar{w}\, d\Omega \right\} \geq 0 \end{aligned}$$

[2]The contribution of mass to the flux of entropy in (6.15) is not considered in [50].

By exploiting mass balance equations (6.4) the entropy imbalance becomes

$$\begin{aligned} & G(\mathcal{P})\frac{\partial \mathcal{S}}{\partial t} + \int_{\mathcal{P}} T\frac{\partial \eta}{\partial t} - \frac{\partial u}{\partial t}\, d\Omega + \\ + & \int_{\mathcal{P}} -\frac{1}{T}\mathbf{q}\cdot\nabla\left[T\right] - T\,{}^{\eta}\mu_L\frac{\partial c_L}{\partial t} - T\,{}^{\eta}\mu_T\frac{\partial c_T}{\partial t} + T\,\mathbf{h}_L\cdot\nabla\left[{}^{\eta}\mu_L\right] - T({}^{\eta}\mu_L - {}^{\eta}\mu_T)\,\bar{w}\, d\Omega \\ - & \int_{P} -\boldsymbol{\sigma} : \frac{\partial \boldsymbol{\varepsilon}}{\partial t} - {}^{u}\mu_L\frac{\partial c_L}{\partial t} - {}^{u}\mu_T\frac{\partial c_T}{\partial t} + \mathbf{h}_L\cdot\nabla\left[{}^{u}\mu_L\right] - ({}^{u}\mu_L - {}^{u}\mu_T)\,\bar{w}\, d\Omega \geq 0 \end{aligned}$$

Define the *Helmholtz chemical potential* of species β as

$$\mu_\beta = {}^{u}\mu_\beta - T\,{}^{\eta}\mu_\beta \tag{6.16}$$

and the *affinity of the reaction* (6.1) as:

$$\bar{A} = \mu_T - \mu_L \tag{6.17}$$

in order to write the entropy imbalance as:

$$\begin{aligned} & G(\mathcal{P})\frac{\partial \mathcal{S}}{\partial t} + \int_{\mathcal{P}} T\frac{\partial \eta}{\partial t} - \frac{\partial u}{\partial t}\, d\Omega + \\ + & \int_{\mathcal{P}} -\frac{1}{T}\mathbf{q}\cdot\nabla\left[T\right] + \mu_L\frac{\partial c_L}{\partial t} + \mu_T\frac{\partial c_T}{\partial t} - \mathbf{h}_L\cdot\nabla\left[\mu_L\right] - {}^{\eta}\mu_L\mathbf{h}_L\cdot\nabla\left[T\right] - \bar{A}\,\bar{w} + \boldsymbol{\sigma} : \frac{\partial \boldsymbol{\varepsilon}}{\partial t}\, d\Omega \geq 0 \end{aligned} \tag{6.18}$$

Following [34], a new heat flux:

$$\mathbf{q} = \mathbf{q} + T\,{}^{\eta}\mu_L\mathbf{h}_L \tag{6.19}$$

can be defined, whereby $T\,{}^{\eta}\mu_L\mathbf{h}_L$ represents a heat transfer due to the diffusion of interstitial species in the lattice. $\mathbf{q}$ is the thermodynamic force conjugated to the gradient of temperature, i.e.:

$$\begin{aligned} & G(\mathcal{P})\frac{\partial \mathcal{S}}{\partial t} + \int_{\mathcal{P}} T\frac{\partial \eta}{\partial t} - \frac{\partial u}{\partial t} + \mu_L\frac{\partial c_L}{\partial t} + \mu_T\frac{\partial c_T}{\partial t} + \boldsymbol{\sigma} : \frac{\partial \boldsymbol{\varepsilon}}{\partial t}\, d\Omega \\ + & \int_{\mathcal{P}} -\frac{1}{T}\mathbf{q}\cdot\nabla\left[T\right] - \mathbf{h}_L\cdot\nabla\left[\mu_L\right] - \bar{A}\,\bar{w}\, d\Omega \geq 0 \end{aligned} \tag{6.20}$$

6.2.3 Additive decomposition of strains

As customary in the hypothesis of small strains, the total strain $\boldsymbol{\varepsilon}$ is additively decomposed in four contributions: an elastic recoverable part after unloading $\boldsymbol{\varepsilon}^{el}$, a swelling contribution due to the intercalation of species in the hosting material $\boldsymbol{\varepsilon}^{s}$, an inelastic distorsion, usually of plastic nature $\boldsymbol{\varepsilon}^{in}$, and a thermal distorsion $\boldsymbol{\varepsilon}^{th}$:

$$\boldsymbol{\varepsilon} = \boldsymbol{\varepsilon}^{el} + \boldsymbol{\varepsilon}^{s} + \boldsymbol{\varepsilon}^{in} + \boldsymbol{\varepsilon}^{th} \tag{6.21}$$

The swelling contribution is taken as proportional to the deviation $c_\beta - c_\beta^0$ from the reference concentration c_β^0 by means of factors ω_L and ω_T termed chemical expansion coefficients of the species in the host material and in the traps, which equal one third of the partial molar volumes at a given temperature:

$$\boldsymbol{\varepsilon}^{s} = \omega_L(c_L - c_L^0)\mathbb{I} + \omega_T(c_T - c_T^0)\mathbb{I}$$

with $\mathbb{I}$ the identity matrix.
The thermal strain tensor is assumed to be proportional to the temperature difference $T - T_0$, with T_0 a reference temperature, by means of a factor α termed thermal expansion coefficient:

$$\boldsymbol{\varepsilon}^{th} = \alpha(T - T_0)\mathbb{I}$$

6.2.4 Helmholtz free energy

Different thermodynamic potentials can be considered rather than the internal energy u. The specific *Helmholtz free energy* is defined as:

$$\bar{\psi} = u - T\eta \tag{6.22}$$

and it is used henceforth. It holds:

$$T\frac{\partial \eta}{\partial t} - \frac{\partial u}{\partial t} = -\frac{\partial \bar{\psi}}{\partial t} - \eta\frac{\partial T}{\partial t}$$

to be inserted in (6.20) to derive the entropy imbalance in the final form:

$$\begin{aligned} & G(\mathcal{P})\frac{\partial \mathcal{S}}{\partial t} + \int_{\mathcal{P}} -\frac{\partial \bar{\psi}}{\partial t} - \eta\frac{\partial T}{\partial t}\, d\Omega + \\ + \quad & \int_{\mathcal{P}} \mu_L \frac{\partial c_L}{\partial t} + \mu_T \frac{\partial c_T}{\partial t} + \boldsymbol{\sigma} : \frac{\partial \boldsymbol{\varepsilon}^{el}}{\partial t} + \left(\omega_L \frac{\partial c_L}{\partial t} + \omega_T \frac{\partial c_T}{\partial t}\right) \mathrm{tr}\,[\,\boldsymbol{\sigma}\,] + \boldsymbol{\sigma} : \frac{\partial \boldsymbol{\varepsilon}^{in}}{\partial t} + \\ + \quad & \alpha \frac{\partial T}{\partial t} \mathrm{tr}\,[\,\boldsymbol{\sigma}\,] - \frac{1}{T}\mathbf{q} \cdot \nabla\,[\,T\,] - \mathbf{h}_L \cdot \nabla\,[\,\mu_L\,] - \bar{A}\,\bar{w}\, d\Omega \geq 0 \end{aligned} \tag{6.23}$$

Consider the free energy $\bar{\psi}$ to be function of the temperature T, the concentrations c_L and c_T, the kinematic variables in terms of the small strain elastic tensor $\boldsymbol{\varepsilon}^{el}$, and of some kinematic internal variables $\boldsymbol{\xi}$ that appear with the usual meaning in inelastic constitutive laws. One has therefore:

$$\frac{\partial \bar{\psi}}{\partial t} = \frac{\partial \bar{\psi}}{\partial T}\frac{\partial T}{\partial t} + \frac{\partial \bar{\psi}}{\partial \boldsymbol{\varepsilon}^{el}} : \frac{\partial \boldsymbol{\varepsilon}^{el}}{\partial t} + \frac{\partial \bar{\psi}}{\partial c_L}\frac{\partial c_L}{\partial t} + \frac{\partial \bar{\psi}}{\partial c_T}\frac{\partial c_T}{\partial t} + \frac{\partial \bar{\psi}}{\partial \boldsymbol{\xi}} \cdot \frac{\partial \boldsymbol{\xi}}{\partial t}$$

to be inserted in (6.23). The internal force vector conjugated to $\boldsymbol{\xi}$ is denoted with the symbol $\boldsymbol{\chi}$, i.e.:

$$\boldsymbol{\chi} = -\frac{\partial \bar{\psi}}{\partial \boldsymbol{\xi}}$$

6.2.5 Clausius-Duhem inequality

Entropy imbalance (6.23) can be localized under the usual assumption behind the Colemann-Noll procedure, i.e. (6.23) must be satisfied for every admissible process. Fracturing processes without crack growth are certainly admissible processes, corresponding to condition (2.13). Inequality (6.23) thus implies that:

$$\begin{aligned} & \int_{\mathcal{P}} -\frac{\partial \bar{\psi}}{\partial T}\frac{\partial T}{\partial t} - \frac{\partial \bar{\psi}}{\partial \boldsymbol{\varepsilon}^{el}} : \frac{\partial \boldsymbol{\varepsilon}^{el}}{\partial t} - \frac{\partial \bar{\psi}}{\partial c_L}\frac{\partial c_L}{\partial t} - \frac{\partial \bar{\psi}}{\partial c_T}\frac{\partial c_T}{\partial t} + \boldsymbol{\chi} \cdot \frac{\partial \boldsymbol{\xi}}{\partial t} + \\ - \quad & \eta\,\frac{\partial T}{\partial t} + \mu_L\,\frac{\partial c_L}{\partial t} + \mu_T\,\frac{\partial c_T}{\partial t} + \boldsymbol{\sigma} : \frac{\partial \boldsymbol{\varepsilon}^{el}}{\partial t} + \left(\omega_L \frac{\partial c_L}{\partial t} + \omega_T \frac{\partial c_T}{\partial t}\right) \mathrm{tr}\,[\,\boldsymbol{\sigma}\,] + \alpha\,\frac{\partial T}{\partial t}\mathrm{tr}\,[\,\boldsymbol{\sigma}\,] + \\ + \quad & \boldsymbol{\sigma} : \frac{\partial \boldsymbol{\varepsilon}^{in}}{\partial t} - \frac{1}{T}\mathbf{q} \cdot \nabla\,[\,T\,] - \mathbf{h}_L \cdot \nabla\,[\,\mu_L\,] - \bar{A}\,\bar{w}\, d\Omega \geq 0 \end{aligned} \tag{6.24}$$

Inequality (6.24) must hold for any subregion $\mathcal{P}$, since the latter was arbitrarily taken. Therefore, the following local entropy imbalance, usually termed Clausius-Duhem inequality, yields:

$$\begin{aligned} & \frac{\partial T}{\partial t}\left(\alpha\,\mathrm{tr}\,[\,\boldsymbol{\sigma}\,] - \eta - \frac{\partial \bar{\psi}}{\partial T}\right) + \frac{\partial \boldsymbol{\varepsilon}^{el}}{\partial t} : \left(\boldsymbol{\sigma} - \frac{\partial \bar{\psi}}{\partial \boldsymbol{\varepsilon}^{el}}\right) + \frac{\partial c_L}{\partial t}\left(\mu_L + \omega_L\,\mathrm{tr}\,[\,\boldsymbol{\sigma}\,] - \frac{\partial \bar{\psi}}{\partial c_L}\right) + \\ + \quad & \frac{\partial c_T}{\partial t}\left(\mu_T + \omega_T\,\mathrm{tr}\,[\,\boldsymbol{\sigma}\,] - \frac{\partial \bar{\psi}}{\partial c_T}\right) + \boldsymbol{\sigma} : \frac{\partial \boldsymbol{\varepsilon}^{in}}{\partial t} + \boldsymbol{\chi} \cdot \frac{\partial \boldsymbol{\xi}}{\partial t} - \mathbf{h}_L \cdot \nabla\,[\,\mu_L\,] - \bar{A}\,\bar{w} + \\ - \quad & \frac{1}{T}\mathbf{q} \cdot \nabla\,[\,T\,] \geq 0 \end{aligned}$$

6.2.6 Thermodynamics restrictions

Clausius-Duhem inequality must hold for any value of the time derivative of temperature T, the concentrations c_L and c_T, the small strain elastic tensor $\boldsymbol{\varepsilon}^{el}$. Since they appear linearly in the inequality, the corresponding multiplicative contributions must be zero, otherwise it would be possible to find a value for the time derivatives that make the inequality not to hold. Therefore, the following restrictions apply:

$$\boldsymbol{\sigma} = \frac{\partial \bar{\psi}}{\partial \boldsymbol{\varepsilon}^{el}}, \qquad \eta = -\frac{\partial \bar{\psi}}{\partial T} + \alpha \operatorname{tr}[\boldsymbol{\sigma}], \qquad \mu_L = \frac{\partial \bar{\psi}}{\partial c_L} - \omega_L \operatorname{tr}[\boldsymbol{\sigma}], \qquad \mu_T = \frac{\partial \bar{\psi}}{\partial c_T} - \omega_T \operatorname{tr}[\boldsymbol{\sigma}] \tag{6.25}$$

thus yielding to the inequality:

$$\underbrace{\boldsymbol{\sigma} : \frac{\partial \boldsymbol{\varepsilon}^{in}}{\partial t} + \boldsymbol{\chi} \cdot \frac{\partial \boldsymbol{\xi}}{\partial t}}_{inelastic} - \underbrace{\boldsymbol{h}_L \cdot \nabla[\mu_L]}_{transport} - \underbrace{\bar{A}\,\bar{w}}_{chemical} - \underbrace{\frac{1}{T}\mathbf{q} \cdot \nabla[T]}_{thermal} \geq 0 \tag{6.26}$$

Mechanical, diffusive, chemical and thermal contributions can be devised. The structure of (6.26) is the usual bilinear form, with thermodynamic flows $(\boldsymbol{\sigma}, \boldsymbol{\chi}, \mathbf{h}_L, \bar{w}, \mathbf{q})$ conjugated to thermodynamic variables
$(\frac{\partial \boldsymbol{\varepsilon}^{in}}{\partial t}, \frac{\partial \boldsymbol{\xi}}{\partial t}, \nabla[\mu_L], \bar{A}, \nabla[T])$. The latter vanishes at thermodynamic equilibrium.

Tensors can be decomposed in their volumetric and deviatoric parts:

$$\boldsymbol{\sigma} : \frac{\partial \boldsymbol{\varepsilon}^{in}}{\partial t} = \operatorname{sph}[\boldsymbol{\sigma}] \operatorname{sph}\left[\frac{\partial \boldsymbol{\varepsilon}^{in}}{\partial t}\right] + \operatorname{dev}[\boldsymbol{\sigma}] : \operatorname{dev}\left[\frac{\partial \boldsymbol{\varepsilon}^{in}}{\partial t}\right] = p\,\frac{\partial \operatorname{tr}\left[\boldsymbol{\varepsilon}^{in}\right]}{\partial t} + \operatorname{dev}[\boldsymbol{\sigma}] : \operatorname{dev}\left[\frac{\partial \boldsymbol{\varepsilon}^{in}}{\partial t}\right]$$

with $p = \operatorname{tr}[\boldsymbol{\sigma}]/3$. Inequality (6.26) rewrites accordingly:

$$p\,\frac{\partial \operatorname{tr}\left[\boldsymbol{\varepsilon}^{in}\right]}{\partial t} + \operatorname{dev}[\boldsymbol{\sigma}] : \operatorname{dev}\left[\frac{\partial \boldsymbol{\varepsilon}^{in}}{\partial t}\right] + \boldsymbol{\chi} \cdot \frac{\partial \boldsymbol{\xi}}{\partial t} - \boldsymbol{h}_L \cdot \nabla[\mu_L] - \bar{A}\,\bar{w} - \frac{1}{T}\mathbf{q} \cdot \nabla[T] \geq 0 \tag{6.27}$$

Owing to Curie symmetry principle [34], in inequality (6.27) fluxes and thermodynamic variables of different tensorial character do not couple. Inequality (6.27) thus can be written as[3]

$$\operatorname{dev}[\boldsymbol{\sigma}] : \operatorname{dev}\left[\frac{\partial \boldsymbol{\varepsilon}^{in}}{\partial t}\right] + \boldsymbol{\chi} \cdot \frac{\partial \boldsymbol{\xi}}{\partial t} \geq 0 \tag{6.28a}$$

$$\mathbf{h}_L \cdot \nabla[\mu_L] + \frac{1}{T}\mathbf{q} \cdot \nabla[T] \leq 0 \tag{6.28b}$$

$$p\frac{\partial \operatorname{tr}\left[\boldsymbol{\varepsilon}^{in}\right]}{\partial t} - \bar{A}\,\bar{w} \geq 0 \tag{6.28c}$$

Cross effects, usually termed after Dufour and Soret, emanates from inequality (6.28b). When cross-effects can be neglected, processes act separately and the Coleman-Noll procedure thus applies for which one requires inequality (6.27) to hold for all constitutive processes independently [50, 143]. The following thermodynamic restrictions thus arise:

$$\begin{aligned} &\mathbf{h}_L \cdot \nabla[\mu_L] \leq 0, \quad \mathbf{q} \cdot \nabla[T] \leq 0, \quad p\frac{\partial \operatorname{tr}\left[\boldsymbol{\varepsilon}^{in}\right]}{\partial t} \geq 0 \\ &\bar{A}\bar{w} \leq 0, \quad \operatorname{dev}[\boldsymbol{\sigma}] : \operatorname{dev}\left[\frac{\partial \boldsymbol{\varepsilon}^{in}}{\partial t}\right] + \boldsymbol{\chi} \cdot \frac{\partial \boldsymbol{\xi}}{\partial t} \geq 0 \end{aligned} \tag{6.29}$$

[3] Equation (6.28a) contains terms with different tensorial order. This strategy is adopted since the latter represents the irreversibility due to the inelastic behavior of the host material.

They are usually associated to Clausius and Planck names.

The hypothesis of irreversibility of crack elongation never entered the thermodynamics analysis described thus far. Therefore, the thermodynamic restriction (6.23) is the mere requirement that processes that include crack healing have to satisfy. This intriguing scenario is not investigated in the present work that frames under the assumption of irreversible crack growth, namely $v(s,t) \geq 0 \quad \forall s \in \mathcal{F}$ and

$$G\, v(s,t) \geq 0 \tag{6.30}$$

to add to restrictions (6.29). Inequality (6.30) has been established in Section 2.4, according to [115]. From thermodynamic restriction (6.30) thus descends that the energy release rate G must always be positive, as intuition suggests and Irwin's formula (6.13) states.

6.3 Constitutive theory

All processes are henceforth be assumed to take place under *thermal equilibrium* at temperature T_0, so that the thermodynamic restrictions (6.29) relevant to the temperature and its gradient are a priori satisfied. A more general treatment can be accomplished as in [35].

Guided by the thermodynamic restrictions (6.29) the flux of interstitial species is modeled by Fickian- diffusion, that linearly correlates $\mathbf{h}_L$ to the gradient of its chemical potential:

$$\mathbf{h}_L = -\mathbf{M}_L(c_L)\nabla\left[\,\mu_L\,\right] \tag{6.31}$$

by means of a positive definite mobility tensor $\mathbf{M}_L$. A classical [4] specialization of mobility tensor $\mathbf{M}_L$ for *dilute solutions accounting for saturation* is isotropic yet non linear:

$$\mathbf{M}_L(c_L) = \text{ɬ}_L c_L \left(1 - \frac{c_L}{c_L^{max}}\right)\mathbb{I} \tag{6.32}$$

The amount $\text{ɬ}_L > 0$ is usually termed the *mobility* and represents the average velocity of interstitial species when acted upon by a force of $1N/mol$ independent on the origin of the force. Definition (6.32) represents the physical requirement that both the pure ($c_L = 0$) and the satured ($c_L = c_L^{max}$) phases have vanishing mobilities.

Under the assumption that traps are isolated [106], trapped species does not flow. Assuming that the latter has zero mobility, i.e. $\mathbf{M}_T(c_T) = 0$, is an alternative view of modeling the absence of trapped species flux.

The Helmholtz free energy density $\bar{\psi}$ is decomposed into three separate parts:

$$\bar{\psi}(c_L, c_T, \boldsymbol{\varepsilon}^{el}, \boldsymbol{\xi}) = \bar{\psi}_{diff}(c_L, c_T, \boldsymbol{\xi}) + \bar{\psi}_{el}(\boldsymbol{\varepsilon}^{el}, c_L, c_T) + \bar{\psi}_{in}(\boldsymbol{\xi}) \tag{6.33}$$

The mass transport process is described by $\bar{\psi}_{diff}$, adopting species concentrations as the state variables. Statistical mechanics provides a description of the entropy for isolated systems in terms of the density of states Ɱ, which in the case of two-state systems is the number of possible molecular configurations. Making recourse of Stirling's approximation, combinations formula provides the following number of possible configurations of interstitial species atoms into a crystalline ideal lattice:

$$\text{Ɱ}_L = [\theta_L^{\theta_L}(1-\theta_L)^{(1-\theta_L)}]^{-N_A c_L^{max}} \tag{6.34}$$

having denoted with $N_A = 6.02214129(27)\,10^{23}\,mol^{-1}$ the Avogadro's number and with $\theta_L = c_L/c_L^{max}$. Inserting (6.34) into Boltzmann's equation:

$$\eta_L = k_B\ \ln[\Omega]$$

the following expression of the entropy comes out since the universal constant of gas $R = 8.3144621\,JK^{-1}mol^{-1}$ is the product of Boltzmann constant k_B with Avogadro's number:

$$\eta_L = -R\,c_L^{\max}(\theta_L\ \ln[\theta_L] + (1-\theta_L)\ \ln[1-\theta_L]) \tag{6.35}$$

The η_T counterpart can be derived from Ω_T of the trapped species in terms of $\theta_T = c_T/c_T^{\max}$ where the saturation limit for trapped species $c_T^{\max}(\boldsymbol{\xi})$ depends upon the history of inelastic deformations by means of $\boldsymbol{\xi}$:

$$\eta_T = -R\,c_T^{max}(\boldsymbol{\xi})(\theta_T(\boldsymbol{\xi})\ \ln[\theta_T(\boldsymbol{\xi})] + (1-\theta_T(\boldsymbol{\xi}))\ \ln[1-\theta_T(\boldsymbol{\xi})]) \tag{6.36}$$

Formulas (6.35) and (6.36) allow defining the entropic contributions ${}^{\eta}\mu_L$ and ${}^{\eta}\mu_T$ to the chemical potential, see formula (6.16). From the third and the fourth of thermodynamic equalities (6.25) and definition (6.22), one is naturally lead to define:

$${}^{\eta}\mu_L = \frac{\partial \eta_L}{\partial c_L} = -R\,(\ln[\theta_L] - \ln[1-\theta_L])$$

$${}^{\eta}\mu_T = \frac{\partial \eta_T}{\partial c_T} = -R\,(\ln[\theta_T] - \ln[1-\theta_T])$$

An ideal solution model provides the following free energy density for the ideal continuum approximation to mixing:

$$\bar{\psi}_{diff}(c_L, c_T, \boldsymbol{\xi}) = \mu_L^0 c_L - T\eta_L + \mu_T^0 c_T - T\eta_T \tag{6.37}$$

Specialization (6.37) of Helmholtz's free energy density represents the entropy of mixing of an ideal solution, with no energetic interactions. μ_L^0 and μ_T^0 are reference values of the chemical potential. They are related to the trap binding energy $-\Delta E_T$ (i.e. the opposite of the Gibbs free energy change) with respect to the lattice site, and in turn related to the equilibrium constant K_{eq} of reaction (6.1):

$$-\Delta E_T = \mu_L^0 - \mu_T^0 = RT\ \ln[K_{eq}]$$

Owing to the expression of the stress tensor (6.43) derived below, the chemical potentials result in the form:

$$\begin{aligned}
\mu_L &= \frac{\partial \bar{\psi}_{diff}}{\partial c_L} + \frac{\partial \bar{\psi}_{el}}{\partial c_L} - \omega_L \mathrm{tr}\,[\,\boldsymbol{\sigma}\,] = \\
&= \mu_L^0 + RT(\ln[\theta_L] - \ln[1-\theta_L]) + \frac{1}{2}\frac{\partial \bar{K}(c_L)}{\partial c_L}\mathrm{tr}\left[\,\boldsymbol{\varepsilon}^{el}\,\right]^2 + \frac{\partial \mu(c_L)}{\partial c_L}\left\|\mathrm{dev}\left[\,\boldsymbol{\varepsilon}^{el}\,\right]\right\|^2 \\
&- \omega_L\,\mathrm{tr}\,[\,\boldsymbol{\sigma}\,]
\end{aligned} \tag{6.38a}$$

$$\begin{aligned}
\mu_T &= \frac{\partial \bar{\psi}_{diff}}{\partial c_T} - \omega_T \mathrm{tr}\,[\,\boldsymbol{\sigma}\,] = \\
&= \mu_T^0 + RT(\ln[\theta_T] - \ln[1-\theta_T]) - \omega_T\,\mathrm{tr}\,[\,\boldsymbol{\sigma}\,]
\end{aligned} \tag{6.38b}$$

where $\bar{K}(c_L)$ and $\mu(c_L)$ are the bulk modulus and the shear modulus[4] of the host material, respectively, that are made dependent on c_L, but not on c_T. Even in the simple theory here dealt with, the chemical potential is quite complex and consists in three separate contributions. The first arises from the diffusive part of the free energy, and has a purely entropic nature. The second contribution has a mechanical origin and conveys the effect of the mechanical parameters on the chemical potential. Finally, the last contribution measures the influence of the swelling deformation on the chemical potential.

Defining the *interstitial diffusivity* by $\mathbb{D}_L = \mathbb{k}_L\, RT$, the Fick's law (6.31) becomes:

$$\begin{aligned} \mathbf{h}_L &= -\mathbb{D}_L \nabla\left[\, c_L \,\right] + \omega_L \mathbf{M}_L(c_L) \nabla\left[\, \mathrm{tr}\left[\, \boldsymbol{\sigma} \,\right]\right] + \\ &- \mathbf{M}_L(c_L) \nabla\left[\frac{1}{2} \frac{\partial \bar{K}(c_L)}{\partial c_L} \mathrm{tr}\left[\, \boldsymbol{\varepsilon}^{el} \,\right]^2 + \frac{\partial \mu(c_L)}{\partial c_L} \left\| \mathrm{dev}\left[\, \boldsymbol{\varepsilon}^{el} \,\right] \right\|^2 \right] \end{aligned} \tag{6.39}$$

with the trace of the stress tensor to be evaluated from eq. (6.44) and the elastic strain tensor from decomposition (6.21). By comparing (6.39) with the mass flux formula for infinitely dilute solutions, that can be easily derived by taking $c_L^{\max} \to +\infty$, one concludes that the saturation has no effect on the diffusivity $\mathbb{D}_L$: in fact, the impact of saturation on the mobility tensor (6.32) and on the chemical potential (6.38a) act one against the other and the effects cancel out in the evaluation of diffusivity. Saturation affects the mass transport by mechanical effects, even under the simple assumption that material parameters $\bar{K}$ and μ are not influenced by the interstitial concentration of species.

Similarly to the definition of Fick's law for the mass flux, a classical way to enforce thermodynamic restrictions for affinity of reaction (6.1) is to linearly relate affinity to the reaction rate, by means of a phenomenological coefficient $\bar{L} > 0$:

$$\bar{w} = -\bar{L}\, \bar{A}(c_L, c_T, \boldsymbol{\varepsilon}^{el}, \boldsymbol{\xi}) \tag{6.40}$$

The reaction rate is therefore related to the concentrations of the reactants, in view of the definition (6.17) of the affinity and in view of the chemical potentials derived in (6.38). Some simplifications are generally assumed in order to provide an insightful form for the affinity. It is usually accepted, although on the unsatisfactory basis that there is insufficient information about either from experiments or detailed micro mechanical models, that chemical expansion coefficients ω_L and ω_T are equal. If furthermore the contribution $\frac{\partial \bar{\psi}_{el}}{\partial c_L}$ results negligible with respect to the diffusive parts of the chemical potential in eq. (6.38), for instance because concentration have little influence on the elastic properties, then it comes out:

$$\bar{A}(c_L, c_T, \boldsymbol{\xi}) = \sum_\beta \nu_\beta\, RT \left(ln \left[\frac{c_\beta}{c_\beta^{max} - c_\beta} \right] - ln \left[\frac{c_\beta^{eq}}{c_\beta^{max} - c_\beta^{eq}} \right] \right) \tag{6.41}$$

to be inserted in (6.40). In eq. (6.41) $\beta = L, T$, whereas $\nu_L = -1$ and $\nu_T = 1$. In the proximity of the equilibrium conditions (6.1), easy algebra leads to the following linearized expression for the reaction rate:

$$\bar{w} = -\bar{L} \sum_\beta \nu_\beta \frac{RT}{c_\beta^{eq}} \frac{c_\beta^{\max}}{c_\beta^{max} - c_\beta^{eq}} (c_\beta - c_\beta^{eq}) \tag{6.42}$$

It is remarked in [34] that the linear phenomenological equation (6.40) is not a priori satisfactory for chemical reactions, although there is always a region close to equilibrium where (6.42) holds.

[4] $\mu(c_L)$ represents the shear modulus of the host material depending on the concentration c_L, that has not to be confused with the chemical potentials of the trapped μ_T, and interstitial μ_L species.

The mechanical part of the free energy density $\bar{\psi}_{el}(\boldsymbol{\varepsilon}^{el}, c_L, c_T)$ is the usual quadratic form in $\boldsymbol{\varepsilon}^{el}$

$$\bar{\psi}_{el}(\boldsymbol{\varepsilon}^{el}, c_L, c_T) = \frac{1}{2}\left(\bar{K}(c_L)\,\mathrm{tr}\left[\,\boldsymbol{\varepsilon}^{el}\,\right]^2 + 2\mu(c_L)\,\left\|\mathrm{dev}\left[\,\boldsymbol{\varepsilon}^{el}\,\right]\right\|^2\right)$$

Thermodynamics restrictions (6.25) yield the stress tensor as the gradient of the free energy density with respect to the elastic tensor, namely:

$$\boldsymbol{\sigma} = \bar{K}(c_L)\mathrm{tr}\left[\,\boldsymbol{\varepsilon}^{el}\,\right]\mathbb{I} + 2\mu(c_L)\mathrm{dev}\left[\,\boldsymbol{\varepsilon}^{el}\,\right] \tag{6.43}$$

Owing to the additive decomposition of strains (6.21) and under the assumption of plastic incompressibility $\mathrm{tr}\left[\,\boldsymbol{\varepsilon}^{in}\,\right] = 0$, the identities:

$$\begin{aligned}\mathrm{tr}\left[\,\boldsymbol{\varepsilon}^{el}\,\right] &= \mathrm{tr}\left[\,\boldsymbol{\varepsilon}\,\right] - 3(\omega_L(c_L - c_L^0) + \omega_T(c_T - c_T^0))\\ \mathrm{dev}\left[\,\boldsymbol{\varepsilon}^{el}\,\right] &= \mathrm{dev}\left[\,\boldsymbol{\varepsilon}\,\right] - \mathrm{dev}\left[\,\boldsymbol{\varepsilon}^{in}\,\right]\end{aligned}$$

ensue, to be further inserted into (6.43) to finally derive the stress tensor in terms of the total and plastic strain as well as the concentrations as:

$$\boldsymbol{\sigma} = \bar{K}(c_L)\mathrm{tr}\left[\,\boldsymbol{\varepsilon}\,\right]\mathbb{I} + 2\mu(c_L)\mathrm{dev}\left[\,\boldsymbol{\varepsilon}\,\right] - 3\bar{K}(c_L)[\omega_L(c_L - c_L^0) + \omega_T(c_T - c_T^0)]\mathbb{I} - 2\mu(c_L)\boldsymbol{\varepsilon}^{in} \tag{6.44}$$

Numerical analyses [136, 146] showed that at relatively small values of initial impurity's concentration, the stress distribution is not influenced by the species, being the swelling contribution negligible compared with the mechanical deformation itself.

To capture inelastic effects, any thermodynamically consistent theory that fits well with the experimental evidences is a good candidate. To give an example, a standard J_2 flow theory with isotropic hardening is considered. Accordingly, only one internal variable ξ is used and

$$\bar{\psi}_{in}(\xi) = \frac{1}{2}\bar{K}^{in}\xi^2 \tag{6.45a}$$

It has been taken $\bar{K}^{in} \geq 0$ together with a Von Mises yield criterion:

$$\varphi(\boldsymbol{\sigma}, \tilde{\chi}) = \|\mathrm{dev}\left[\,\boldsymbol{\sigma}\,\right]\| - \sqrt{\frac{2}{3}}\sigma_Y + \chi \tag{6.45b}$$

and normality law:

$$\dot{\boldsymbol{\varepsilon}}^{in} = \frac{\partial\varphi}{\partial\boldsymbol{\sigma}}\,\dot{\lambda}, \qquad \dot{\xi} = \frac{\partial\varphi}{\partial\chi}\,\dot{\lambda} \tag{6.45c}$$

Term σ_Y in equation (6.45b) denotes the yield stress that doesn't depend on c_L [41], while χ has to be meant as

$$\chi = -\frac{\partial\bar{\psi}^{in}}{\partial\xi} \tag{6.45d}$$

Definition (6.45d) and Karush-Kuhn-Tucker conditions

$$\dot{\lambda} \geq 0, \qquad \varphi \leq 0, \qquad \dot{\lambda}\varphi = 0 \tag{6.45e}$$

complete the incremental form of the mechanical constitutive equations.

Owing to definitions (6.36), (6.37) and (6.45d) thermodynamic restriction (6.28a) is rephrased as follows [35]:

$$\boldsymbol{\sigma} : \dot{\boldsymbol{\varepsilon}}^{in} + \chi\dot{\xi} - RT\log(1 - \theta_T)\frac{\partial c_T^{\max}}{\partial\xi}\dot{\xi} \geq 0 \tag{6.46}$$

Adoption of J_2 flow theory with isotropic hardening ensures:

$$\boldsymbol{\sigma} : \dot{\boldsymbol{\varepsilon}}^{in} + \chi\,\dot{\xi} \overset{\varphi=0}{=} (\|\mathrm{dev}\,[\,\boldsymbol{\sigma}\,]\,\| + \chi)\,\dot{\lambda} \overset{\varphi=0}{=} \sqrt{\frac{2}{3}}\,\sigma_Y\,\dot{\lambda} \geq 0$$

and allows to emphasize dependence on c_T^{max} on the equivalent plastic strain

$$\bar{\boldsymbol{\varepsilon}}^{in} = \int_0^t \sqrt{\frac{2}{3}} \|\boldsymbol{\varepsilon}^{in}\|\, d\tau$$

Restriction (6.46) is left with:

$$-\log(1-\theta_T)\frac{\partial c_T^{max}}{\partial \bar{\boldsymbol{\varepsilon}}^{in}}\,\dot{\lambda} \geq 0 \tag{6.47}$$

Term $\log(1-\theta_T)$ is always negative since trap concentration c_T cannot exceed the upper bound set by saturation limit c_T^{max} and thus $0 \leq \theta_T \leq 1$. In view of experimental observations [71] that the number of traps increases with plastic deformation the positiveness of $\frac{\partial c_T^{max}}{\partial \bar{\boldsymbol{\varepsilon}}^{in}}$ is guaranteed and therefore thermodynamic consistency (6.46).

6.3.1 Governing Equations

Under thermal equilibrium assumption, governing equations can be derived by incorporating the constitutive equations (6.39), (6.40), and (6.44) into the balance equations (6.4, 6.5). A new variable μ_L^{mech} that designates the influence of mechanics on the chemical potential μ_L adds to the ones that control the problem evolution, i.e. concentrations c_L and c_T and displacements $\mathbf{u}$. Governing equations are written in a reduced order form in terms of the new field, at all points $\mathbf{x} \in \Omega$:

$$\frac{\partial c_L}{\partial t} - \mathrm{div}\,[\,\mathbb{D}_L\,\nabla\,[\,c_L\,]\,] + \mathrm{div}\left[\,\omega_L \natural_L \mathbf{M}_L(c_L)\,\nabla\left[\,\mu_L^{mech}\,\right]\,\right] - \bar{L}\,\bar{A}(c_L, c_T, \boldsymbol{\varepsilon}^{el}, \boldsymbol{\xi}) = 0 \tag{6.48a}$$

$$\frac{\partial c_T}{\partial t} + \bar{L}\,\bar{A}(c_L, c_T, \boldsymbol{\varepsilon}^{el}, \boldsymbol{\xi}) = 0 \tag{6.48b}$$

$$\mathrm{div}\left[\,\boldsymbol{\sigma}(c_L, c_T, \boldsymbol{\varepsilon}^{el}, \boldsymbol{\varepsilon}^{in}, \boldsymbol{\xi})\,\right] = \mathbf{0} \tag{6.48c}$$

$$\mu_L^{mech} - \overline{\mu_L^{mech}}(c_L, c_T, \boldsymbol{\varepsilon}^{el}, \boldsymbol{\xi}) = 0 \tag{6.48d}$$

defining with:

$$\begin{aligned}
\overline{\mu_L^{mech}}(c_L, c_T, \boldsymbol{\varepsilon}^{el}, \boldsymbol{\xi}) &= \frac{1}{2}\frac{\partial \bar{K}(c_L)}{\partial c_L}\mathrm{tr}\left[\,\boldsymbol{\varepsilon}^{el}\,\right]^2 + \frac{\partial \mu(c_L)}{\partial c_L}\left\|\mathrm{dev}\left[\,\boldsymbol{\varepsilon}^{el}\,\right]^2\right\| - \omega_L \mathrm{tr}\,[\,\boldsymbol{\sigma}\,] = \\
&= \frac{1}{2}\frac{\partial \bar{K}(c_L)}{\partial c_L}\mathrm{tr}\left[\,\boldsymbol{\varepsilon}^{el}\,\right]^2 + \frac{\partial \mu(c_L)}{\partial c_L}\left\|\mathrm{dev}\left[\,\boldsymbol{\varepsilon}^{el}\,\right]^2\right\| + \\
&- 3\,\bar{K}(c_L)\,\omega_L\,(\mathrm{tr}\,[\,\boldsymbol{\varepsilon}\,] - 3(\omega_L(c_L - c_L^0) + \omega_T(c_T - c_T^0)))
\end{aligned}$$

Equations (6.48) are accompanied with non linear evolution equations (6.45) for inelastic strain tensor $\boldsymbol{\varepsilon}^{in}$ and for $\boldsymbol{\xi}$. Boundary conditions

$$\mathbf{h}_L \cdot \mathbf{n} = \bar{h} \qquad \mathbf{x} \in \Gamma^h$$

$$\boldsymbol{\sigma} \cdot \mathbf{n} = \bar{\mathbf{p}} \qquad \mathbf{x} \in \Gamma^p$$

are imposed along Neumann boundaries. To ensure solvability to the problem, Dirichlet boundary conditions have to be enforced along part Γ^u:

$$\mathbf{u} = \bar{\mathbf{u}} \qquad \mathbf{x} \in \Gamma^u \tag{6.50}$$

As assessed in [35], Dirichlet boundary conditions for concentration should not be imposed. The correct boundary condition that enforces equilibrium for dissolved species in the hosting material and the species out of Ω shall be written as an equivalence of chemical potentials.

Initial conditions are usually imposed for concentration of interstitial $c_L(\mathbf{x}, t = 0)$ as well as trapped species $c_T(\mathbf{x}, t = 0)$. To comply with equilibrium thermodynamics they are constant in volume Ω and equal to their equilibrium concentrations with external species. Balance of momentum (6.48c) and the auxialiary condition (6.48d), together with boundary conditions, provide the necessary and sufficient equations to be solved for $\mathbf{u}$ and μ_L^{mech} at t=0.

6.4 Fracture propagation

Denoting as usual with $\Omega \in \mathbb{R}^3$ the spatial domain of problem (6.4, 6.5) with boundary $\partial\Omega \equiv \Gamma$, consider within Ω an existing arbitrarily shaped crack as the one depicted in figure 2.1. The material response to the following quasi-static external actions is sought: tractions $\bar{\mathbf{p}}(\mathbf{x}, t)$ on Γ^p, displacements $\bar{\mathbf{u}}(\mathbf{x}, t)$ on Γ^u, bulk forces $\mathbf{f}(\mathbf{x}, t)$ in Ω, fluxes $\bar{h}(\mathbf{x}, t)$ on Γ^h and potentials $\bar{\mu}_L(\mathbf{x}, t)$ on Γ^μ. In modeling crack elongation, mechanical external actions are all assumed to vary proportionally to the load factor κ and the crack attains its initial length before the beginning of the diffusion process.

It is postulated that the stress-strain fields in the crack tip vicinity are uniquely determined by SIFs vector $\mathbf{K}$. Even if the asymptotic expansion of the SIFs vector $\mathbf{K}(s, \tau)$ at any point s of the crack front at time $\tau > t$ in powers of the elongation $l(s; t, \tau)$ expressed by eq. (2.2) has not been extended to the case of coupled diffusion and mechanics so far, it is assumed that expansion (2.2) still holds at given loads and concentrations and since the material properties may depend upon c_L, so do the SIFs.

The *global incremental quasi-static fracture propagation problem* can therefore be restated as follows in the presence of diffusion of species: given the state of stress, of concentrations and the history of crack propagation, if any, at time t, express the crack propagation rate, if any, of the crack front as a function of the stress, of the concentrations, and of the history. It is made the assumption that the change in geometry is not affecting concentrations, since the time required to reactivate mechanical equilibrium is taken to be much faster than the diffusive time scale. The mathematical expression of the onset of crack propagation eq. (2.11) is now expressed by:

$$\varphi(s, t) = \frac{1}{2}(\mathbf{K}^*(s, t) \cdot \mathbf{\Lambda}\mathbf{K}^*(s, t) - G_c(c_L, c_T))$$

where components of matrix $\mathbf{\Lambda}$ are expressed in eq. (2.12).

Diffusion problem governs the transport of the species to the crack front, whereas mechanic problem accounts for the fracture of the specimen. The coupling between diffusion and mechanics relies in the fact that species transport affects the mechanical properties, decreasing the fracture toughness of the host material, and mechanics affect the diffusion via the stress-field, which appears in the pressure dependence of chemical potentials eq. (6.38).

Perhaps the greatest challenge in the fracture mechanics scenario depicted above is the measurement of the dependence of the fracture energy G_C with the concentrations of the species c_L and c_T. Observed material embrittlement confirms that the fracture energy is highly influenced by

trapped and interstitial species, but it is not so obvious how to define a fracture energy for a material containing mobile species that may move to the surface upon crack formation. Attempts in modeling the evolution of fracture energy $G_C(c_L, c_T)$ have been taken in the framework of cohesive fracture mechanics by Serebrinsky et al. in 2004 [132]. A cohesive law dependent on impurity coverage was calculated from quantum mechanics and afterwards the atomic-level cohesive properties were properly scaled up to the continuum scale in order to embed such a cohesive law into cohesive elements for analysis of the static crack growth.
In the same year Jiang et al. [64] quantitatively assessed the decrease of Fe and Al crystal cohesive energy due to the reduction of the local atomic binding at the crack tip caused by the segregation of hydrogen to the incipient fracture zone inducing embrittlement. A concept closely related to cohesive energy reduction is the decrease of surface energy, whereby the lowering of the surface energy by species increases the driving force to form two new surfaces, i.e. to form a crack. They found that the metal fracture energy decreases almost linearly with increasing hydrogen coverage. Fracture energy computed at an atomistic level was then used as input into higher length scale models for stress corrosion cracking at the continuum level.
The decrease in the surface energy comes from the competition between the propensity for the species to stay on the surface versus remaining in the bulk. Therefore the kinetics of the species segregation to the crack tip on the newly fractured surfaces can govern the cohesion reduction as the crack propagates and may cause a time-delayed cracking behavior, explaining precisely why intermittent crack growth is experimentally observed in continuum modeling of hydrogen embrittlement.

In 2010 Song et al. [134] computed fracture energy as a function of hydrogen concentration in nickel (N_i), exploiting an atomistic model to investigate actual crack tip behavior in the presence of controlled arrays of hydrogen atoms around the crack tip.

Alterations of the fracture toughness and the energy available for crack growth for a solid state diffusion process under chemical and mechanical loadings have been recently described by Haftbaradaran and Qu [51], by means of a chemo-mechanical path-independent J-integral. They proved that the classical J-integral of Rice [114] is path-dependent under combined chemical and mechanical driving forces and developed a path-independent integral for an elastic solid under chemo-mechanical equilibrium with its surrounding, i.e. when long enough time has elapsed or the rate of solute diffusion is much faster in comparison with other kinetic processes in the problem, neglecting the variations in the elastic properties of the host medium caused by solute concentrations. The J-integral represents a balance between the total energy inside the closed contour around the crack tip and the energy passing through the contour line. In the presence of solid state diffusion, the total energy inside the closed contour is higher than just the elastic strain energy since energy associated with species diffusion and distribution must also be taken into account. The chemo-mechanical path-independent integral thus obtained equals the energy release rate via a line integral along any contour which encircles the crack tip.

Assume that the crack front at an arbitrary location s is at the onset of propagation at time t (i.e. $\varphi(s,t) = 0$); stable crack growth may therefore be triggered off.
The system is thus subjected to a variation in the state of deformation $\boldsymbol{\varepsilon}$, a variation in the concentrations c_L and c_T and a potential increment of fracture surface $\partial\mathcal{S}$. Recent investigations [100] conclude that concentrations remain bounded near the crack front. Granted this result, stresses due to swelling (i.e. $-3\bar{K}(c_L)[\omega_L(c_L - c_L^0) + \omega_T(c_T - c_T^0)]\mathbb{I}$) remain bounded and no stress intensity factors emanate from constitutive law (6.44). Nevertheless, a variation of interstitial concentration may affect the bulk and shear modulus and in turn SIFs. This variation can be considered to be small with respect to the variation induced by increment of deformations and neglected, as if

bulk and shear modulus are independent upon c_L. In conclusion therefore, SIFs can be assumed unaffected by concentrations.

The solution of the initial-boundary value problem depicted in the previous Sections describes the evolution of concentrations and displacements with time. The evolution of geometry, i.e. the propagation of cracks, arises from the variational formulation [125, 127] presented in Section 2.5 for LEFM that can be extended to the multi-physics problem at hand.
Propagation is governed at any instant t, by the Karush-Kuhn-Tucker conditions (2.16), namely:

$$\varphi(s,t) \leq 0, \quad v(s,t) \geq 0, \quad \varphi(s,t)\, v(s,t) = 0 \tag{6.51}$$

Referring to the definition of operator N'_v (2.40), variational formulations descending from consistency condition (2.19) read:

Proposition 4: *Under hypothesis of stable crack growth:*

$$N'_v[w]w(s,t) < 0 \quad \forall w(s,t) \geq 0, \;\; s \in \mathcal{F}(t)$$

the crack front velocity $v(s,t)$ that solves the global quasi-static fracture propagation problem at time t minimizes the functional:

$$\chi[w(s,t)] = -\frac{1}{2}\int_{\mathcal{F}(t)|_{\varphi=0}} N'_v[w(s',t)]w(s,t)\, ds - \int_{\mathcal{F}(t)|_{\varphi=0}} \frac{G_C(c_L,c_T)}{\kappa(t)} \left.\frac{\partial \kappa}{\partial t}\right|_t w(s,t)\, ds \tag{6.52}$$

under the constraint $w(s,t) \geq 0 \;\; \forall s \in \mathcal{F}(t)|_{\varphi=0}$

Proposition 5: *Under hypothesis of stable crack growth:*

$$N'_v[w]w(s,t) < 0 \quad \forall w(s,t) \geq 0, \;\; s \in \mathcal{F}(t)$$

the crack front velocity $v(s,t)$ that solves the global quasi-static fracture propagation problem at time t minimizes the functional:

$$\omega[w(s,t)] = -\frac{1}{2}\int_{\mathcal{F}(t)|_{\varphi=0}} N'_v[w(s',t)]w(s,t)\, ds \tag{6.53}$$

under the constraint

$$N'_v[w(s',t)] + \frac{G_C(c_L,c_T)}{\kappa(t)} \left.\frac{\partial \kappa}{\partial t}\right|_t w(s,t) \leq 0 \;\; \forall s' \in \mathcal{F}(t)|_{\varphi=0}$$

Proof of the above theorems does not differ from the one reported in Section 2.5.

6.5 Hydrogen embrittlement

The diffusion model of a neutral species through a solid lattice described above perfectly fits the case of Hydrogen Embrittlement (HE). Atomic hydrogen, being the smallest of gaseous impurities, is a very mobile species that freely diffuses from one interstitial site to another and the presence of hydrogen changes the mechanical properties of the metal, leading to inconsistent and usually degraded structural performances in service. HE in metals has posed serious obstacles to design

strong and reliable structural materials for many decades, and predictive physical mechanisms still are a research subject.

Direct exposure to hydrogen gas can occur in pipelines and in pressure vessels. Indirect exposure to hydrogen can occur from any physical contact of the metal with liquid water or water vapor. In the latter case a chemical reaction between steel and water produces hydrogen gas which subsequently enters and embrittles the metal. Hydrogen can also be introduced into a material during the manufacturing process or by electrochemical charging. Phenomena related to the source of the species and the kinetics of entrance into the host medium are not considered in this Chapter. In any case, HE is a pervasive mode of degradation in many metallic systems that can occur via several mechanisms which may operate simultaneously or separately under certain circumstances. Among them:

- **Hydride-induced embrittlement**
  This mechanism describes the hydrogen-induced phase changes to form metal hydrides ahead of a crack. New hydrides nucleate and growth in the stress field generated by the presence of preexisting hydrides, and finally coalesce. This auto catalytic process of hydride nucleation and growth, together with the brittle nature of them, has been extensively observed experimentally and seems to be the main cause of embrittlement in hydride-forming elements such as V, N_b, T_i or Z_n [149]

- **H-Enhanced DEcohesion (HEDE) mechanism**
  It postulates that H atoms attracted to the crack front lower the fracture energy and favor cleavage-like planar fracture. According to the HEDE mechanisms, hydrogen damage takes place in the crack front process zone, when the local crack front tensile stress exceeds the maximum local atomic cohesion strength, lowered by the presence of H [28, 46, 107, 145]. It was shown [148] that the mobile segregant reduces the cohesion greater than the immobile segregant.

- **H-Enhanced Local Plasticity (HELP) mechanism**
  Transmission electron microscopy observations of changes in dislocations pile-ups with and without H, show high local plastic-like deformations in embrittled materials and formation of slip bands at the crack tips [1, 14, 16, 38, 119, 137]. HELP mechanism suggests that hydrogen in a solid solution reduces the barriers to dislocations motion trough an elastic shielding effect, thereby increasing the amount of plastic deformations that occur in a localized region adjacent to the fracture surface. In this case the term hydrogen-assisted cracking is more descriptive than hydrogen embrittlement, because hydrogen unlocks dislocations and allows them to multiply and move.

The largely observed asymmetry between the kinetics of absorption and the kinetics of evolution of hydrogen in steels, in the sense that absorption proceeds with a larger apparent diffusivity than evolution does, is attributed to trapping of hydrogen atoms at various microstructural trapping sites [35]. Most hydrogen transport models [3, 35, 69], which emanate from the seminal work of Sofronis and McMeeking [136], consider the effect of the hydrostatic stress and trapping on the hydrogen distribution in a plastically deforming steel, assuming that hydrogen diffusion is purely interstitial and that traps sites are filled by lattice diffusion. Krom's model [69] enhances the work of Sofronis and McMeeking [136], that is based on the local equilibrium theory between H in reversible traps and H in the lattice sites presented by Oriani [106], by including a strain rate factor in the H transport equation. Coupled diffusion elastic plastic finite element analyses were carried out in order to investigate the behavior of c_L and c_T near a blunting crack tip under small scale yielding

conditions. Given the material parameters, the strain rate results to have a considerable influence on the hydrogen concentration in lattice sites as a result of the creation and filling of traps sites and at relatively high values of the strain rate the lattice sites can almost be depleted of hydrogen. Krom's model exploits a fit of the number of trap sites versus equivalent plastic strain which is close to experimental observations [71] and to the fit used by Sofronis and McMeeking [136] that reads:

$$\log[N_A c_T^{max}] = 23.26 - 2.33\, e^{-5.5\bar{\boldsymbol{\varepsilon}}^{in}}$$

which satisfies requirement (6.47). Trapped hydrogen is considered as non contributing to the embrittlement mechanism because c_T results fairly independent on strain rate owing to the high binding energy $-\Delta E_T$. This means that a trapped hydrogen must acquire an energy substantially larger than the lattice migration energy to escape the trap and consequently, the mean residence time of a diffusing hydrogen atom is considerably longer in a trap site than in a lattice site.

Krom's model [69] reproduces experimental evidences of Gao et al. [42], who investigated the hydrogen distribution in the vicinity of a crack tip in steel under mixed mode loading using mass spectroscopy, and of Sun et al. [142], who investigated the hydrogen distribution around a crack tip in a fcc single crystal. They found two peaks in the hydrogen distribution ahead of a notch: one peak is in the immediate vicinity of the notch, corresponding to the location of the maximum equivalent plastic strain, and another peak is located at some distance from the notch corresponding to the location of maximum hydrostatic stress.

As already stressed, traps are considered isolated[5], that means that they do not form an extended network. Therefore, in mass balance equation (6.4b) it lacks a flux term $\mathbf{h}_T$ because hydrogen trapped in the bulk doesn't contribute to hydrogen transport by lattice diffusion.

The so called Oriani's approach [106], where the influence of plastic deformations, trapping, and microstructure jointly results in an effective diffusion constant, is used in Krom's model to relate the immobile trapped hydrogen and mobile interstitial lattice one. Indeed Oriani postulated that, within a continuum-level material point, the micostructure affects the local distribution of hydrogen in a manner such that the population of hydrogen in trap sites is always in equilibrium with the population associated with lattice sites trough the equation:

$$c_T = \frac{N_T}{1 + \frac{1}{K_{eq}\theta_L}}$$

where N_T is the trap density, i.e. the number of trap sites per unit volume.

According to [35], the correct boundary condition to add to eq. (6.50) that enforces equilibrium for dissolved hydrogen in the hosting metal and the gaseous hydrogen H_2 out of Ω shall be written as an equivalence in terms of chemical potentials:

$$\mu_L = \frac{1}{2}\mu_{H_2} \tag{6.54}$$

where the chemical potential of the hydrogen gas μ_{H_2} is:

$$\mu_{H_2} = \mu_{H_2}^0 + RT\, \ln\left[\frac{f_{H_2}}{p_{H_2}^0}\right]$$

being $\mu_{H_2}^0$ the chemical potential in a reference state, $p_{H_2}^0$ the reference pressure, and f_{H_2} the fugacity of the hydrogen gas. Fugacity of a real gas is an effective partial pressure that equals the

[5]This assumption is part of the equilibrium theory presented by Oriani [106].

pressure of an ideal gas which has the same chemical potential as the real gas. The fugacity f_{H_2} of the hydrogen molecules in the gas depends on the equation of state of hydrogen and if this latter is taken in the simple Abel-Noble form, then

$$f_{H_2} = p_{H_2} \exp\left(\frac{p_{H_2}\gamma}{RT}\right)$$

where γ is an experimentally measurable constant.

Conventionally $\mu^0_{H_2}$ vanishes at a pressure of $0.101\,MPa$ and a temperature of $298\,K$. Equation (6.54) thus leads to a non linear boundary condition of type:

$$RT\,\ln\left[\frac{c_L}{c_L^{max}-c_L}\right] + \mu_L^{mech} = \frac{\mu^0_{H_2}}{2} - \mu^0_L + RT\,\ln\sqrt{\frac{f_{H_2}}{p^0_{H_2}}} \quad \boldsymbol{x} \in \Gamma^\mu \tag{6.55}$$

that completes the set of governing equations of the diffusion problem described in Section 6.3.1. Contrary to what done imposing constant lattice hydrogen concentration c_L along the Dirichlet boundary of interest, eq. (6.55) allows to take into account that changes in the elastic strain $\boldsymbol{\varepsilon}^{el}$ in μ_L^{mech} during deformation lead to non constant lattice hydrogen concentration c_L on the specimen surface.

Fracture processes are greatly affected by the enrichment of hydrogen around the crack tip. As detailed by Song and Curtin [134, 135], in plastically deforming metals, in order to dissipate energy it exists a competition between the mechanisms of cleavage and of dislocation emission from the crack tip under embrittling species. Solute H can change the fracture mode from ductile rupture to intergranular fracture due to H segregation along grain boundaries with a considerable reduction in ductility. The micromechanics of the Ductile versus Brittle Transition (DBT) under ideal elastic conditions are detailed in [134, 135]. Song and Curtin [135] demonstrated that a HE mechanism operates at the atomic scale in α-iron, in which the accumulation of H around the crack tip, driven by the crack tip stress fields, suppresses crack tip dislocation emission eliminating the material's ability to blunt crack. This favors brittle cleavage failure, followed by slow crack growth. In general, the critical energy release rate for dislocation nucleation from the crack tip and the critical energy release rate for Griffith cleavage decohesion, have to be compared. The nanoscale mechanism presented in [135] is then connected to macroscopic embrittlement allowing to identify the boundary between embrittlement and non embrittlement as a function of H concentration, H diffusion, temperature and mechanical loading rate.
In this regard, under specific conditions, fracture propagation could correctly be described by variational formulations detailed in Section 6.4 and numerical analyses are in progress in order to support this assertion.

Chapter 7

Conclusions

In this thesis the variational formulation for the global incremental quasi-static linear elastic fracture propagation problem, presented by Salvadori and Carini [125] for the two dimensional case, has been extended to three dimensional problems. Laws that describe onset and propagation of cracks fall under the general Griffith theory [49], that puts Linear Elastic Fracture Mechanics (LEFM) in analogy with standard dyssipative systems thermodynamics [87]. The SIFs vector " right after the kink" , if any, $\mathbf{K}^*$ acts as an internal force, conjugated to the internal variable $\mathbf{a}^*$. The latter is related to the crack length and its variation induces a dissipation which must satisfy Clausius-Duhem inequality. A plasticity analogy for LEFM was presented by Salvadori [122]: as expected, it stems from a maximum dissipation principle, the counterpart of the maximum plastic dissipation postulated in the thermodynamics of standard dissipative systems [143]. Griffith's criterion is recovered following a rigorous setting.

The key ingredients for this approach are:

- the SIFs expansion with respect to the crack elongation, provided by Leblond in [82], and Leblond and coworkers in [83]. In the analogy it plays the role of a Colonnetti's decomposition of stress [30, 31].
- the 3D extension of Irwin's formula, that relates the Energy Release Rate to the SIFs. Whereas a formal proof for mixed mode has been provided for 2D in Chambolle et al. [26], a formal 3D derivation seems to be lacking. In this regard, formula (2.11) is taken as a generally accepted result. In the analogy, it is equivalent to the yield function in plasticity and allows the definition of the elastic domain and of its boundary.
- the maximum dissipation principle, whence the normality and the complementarity laws come out.

The rest follows from results of incremental plasticity [24].

Whereas in the 2D case the discrete nature of the number of crack tips makes the formulation simple and the variational formulation a minimum of functions, in the 3D case the presence of a curved crack front requires a detailed investigation of the symmetry property of operator $N_v'[\cdot]$ defined in (2.40). The form (2.6) of non local operator $\mathbf{K}^{(1)}[\cdot]$, does not allow a straightforward proof of symmetry for $N_v'[\cdot]$, and the latter has been provided on the basis of the physical meaning of the operator itself, because of its link with the concept of the energy release rate.

Once the symmetry is provided, two minimum theorems follow. They provide quasi-static velocity in each point along the crack front, based upon the corresponding increment for external loads.

Conditions for stable crack growth and, inherently, for the onset of unstable propagation have been firmly formulated. Such results may reveal of great importance, since the safety of a structural component is usually measured against the stable/unstable crack growth transition, assuming that unstable propagation leads to structural collapse.

Form (2.6) of operator $\mathbf{K}^{(1)}[\cdot]$ originates from the fundamental hypothesis of steady location of a point along the crack front, that was made in the seminal paper of Rice [117] on 3D weight function theory and has been kept afterwards. The purpose of providing a more general form for eq. (2.6), removing in full the hypothesis of steady location, and consequently the ones introduced at a later stage to circumvent the resulting limitations, motivates the reformulation of minimum theorems in terms of weight functions. Such a reformulation brings to the stage the more general concept of finite part of Hadamard in the limit processes to the boundary. In their celebrated paper [83], Leblond and coworkers showed that symmetric operator $\mathbf{K}^{(1)}[\cdot]$ is not universal. Its non local contribution $\mathbf{K}^{(1)}_{nl}[\cdot]$ contains in fact an operator, denoted with $\mathbb{Z}$ in [83], which is intrinsically dependent upon geometry and boundary conditions. Focusing on plane cracks that propagate in their own plane, the first order variation of the SIFs derived, see formula (4.53), contains four alternative constituents of $\mathbf{K}^{(1)}[\cdot]$: the non universal fundamental kernel $\mathbb{W}^{\mathcal{F}}$, the derivative $\partial\mathbb{W}^{\mathcal{S}}/\partial\rho$, the curvature of the crack front, and the 3/2 order term Ξ_1 of the crack opening and sliding expansion. This set of well identified elements has to be evaluated beforehand in order to numerically approximate $\mathbf{K}^{(1)}[\cdot]$. Fundamental kernels are known explicitly for only a few relatively simple crack geometries such as half-plane cracks, and circular cracks (see the review of Lazarus [79]). A general method to approximate fundamental kernels even for finite bodies, based on the definition of weight function itself, is presented in the thesis. In this regard, investigation of crack front shapes different from the circular one is extremely desirable, just as the extension of all the formulation to mixed mode 2 and 3.

As very promisingly done by Bower and Ortiz [19], Lazarus [78] and Favier et al. [37], fundamental kernels $\mathbb{W}^{\mathcal{F}}$ can also be updated incrementally using first and second order [85] techniques. This modus operandi has been applied so far to infinite bodies merely. Boundless is not inborn in Rice's [117] formulation itself, but is a compulsory consequence of the steady location assumption. The final formalism derived in the present thesis has the purpose to extend previous formulations [19, 37, 78] to the case of finite bodies and quasi-static (rather than fatigue) crack growth.
Numerical approximation of the 3/2 order term Ξ_1 has been performed by means of cubic-order singular finite elements along the crack front.

The expression of operator $N'_v[\cdot]$ in terms of weight functions, written in the thesis for the case of mode 1 growth, leads to an easy proof of symmetry property for the operator itself. Its discrete counterpart leads to an effective numerical scheme for the approximation of the velocity of the crack front. It has been benchmarked against an easy problem for fracture mechanics, a penny shaped crack subject to point loads, which in spite of being classical reveals several concerns when dealt with other techniques such as finite differences. The accuracy obtained via the variational characterization is remarkable.

From the approximated crack front velocity field, the formulation of crack tracking algorithms can be devised. An implicit 3D crack tracking algorithm has been detailed in this work (see Section 5.1). It is based on a Newton-Raphson numerical formulation of the Griffith- Maximum Energy Release Rate condition, which is imposed at every iteration starting from an " initial elastic trial". The algorithm shares several features with return mapping algorithms in plasticity, since it is derived essentially from the broader analogy between rigid-plasticity and fracture.

Nevertheless, some differences with plasticity are worth to be remarked. The numerical scheme is here deployed at a " global" level rather than at a constitutive level. The notion therefore of elastic trial can be a bit misleading, as it normally refers to a constitutive equation solution. Here the name was kept motivated by the fact that the global problem is normally elastic, and a trial attempts at a load evolution without changes in geometry. In any case, the elastic trial requires a global analysis.

Triggered off by the elastic trial, the algorithm provides an estimation of the crack front position. Accordingly, the geometry of the problem is updated at each iteration of the Newton-Raphson scheme and a new evaluation of SIFs has to be carried on, again on the global level. The Griffith condition is tested again for the updated SIFs and, if violated, the iteration process is continued up to convergence.
As a major feature of the proposed crack tracking algorithm, it is endowed with a variational formulation within each iteration, where a constrained minimum problem can be solved, which provides a new estimation of the crack front location. The constraint is computationally handled by means of the penalty method, one of the available techniques for constrained optimization. The presence of the penalty term makes any iteration of the Newton-Raphson scheme a non linear problem and for this reason every step of the Newton-Raphson scheme requires a further, internal, iterative solution scheme. An Update Linearized algorithm and an inner Newton-Raphson algorithm have been applied to solve each Newton-Raphson step obtaining coincident results. The solution of a full Signorini's problem is obtained, capturing the eventuality of partial crack front elongation, having nodes of the discretization that are not mobilized. Performed numerical benchmarks confirmed the capability of the proposed algorithm to determine the crack front configurations based upon an increment of the external actions.

The crack tracking algorithm presented in this work revealed to be more accurate, robust, and numerically stable with respect to explicit methods for integration in time, naturally led by the incremental picture of global quasi-static fracture propagation problem. Such explicit type algorithms were formulated in order to allow the step-wise approximation of crack length increment of the crack front. In their simplest formulation these algorithms do not enforce Griffith condition step by step, and may lead to large errors in the estimation of both configuration and critical load, measured at the transition between stable and unstable propagation regimes. The proposed algorithm instead, has the potential to place numerically calculated trajectories on a much firmer basis. Accordingly, industrial applications (for example for ceramic materials, because of their inherent brittleness) may benefit from its implementation in techniques such as standard or eXtended Finite Elements, as well as Boundary Element method in which crack growth direction is usually determined based upon standard criteria [124], but crack growth rate is far less well defined.

The plasticity analogy in which the derived minimum theorems are rooted, allows the interpretation of fracture as a standard dissipative system, being aware that the proposed approach narrows the picture very much with respect to the phase field method. Going out of LEFM, where SIFs are not defined, it does not seem to be obvious. Nevertheless, even within the proposed framework, some extensions can be clearly devised. The issue of environmentally assisted brittle fracture can be included naturally, once the correct driving force is described as done for the increment of external loads. The problem of fracture growth in the presence of diffusion of neutral species in solids is dealt with in the last part of the thesis. Crack propagation is assumed to take place in a completely embrittled environment because of the accumulation of the species at the crack tip, which reduces the cohesive strength of the host material and gives rise to a reduced fracture toughness. For example, high strength steels, when exposed to hydrogen, suffer from a loss of ductility and toughness that may lead to sudden, premature failure. In this case hydrogen induces brittle

intergranular fracture in a manner resembling the failure of polycristalline ceramics.

Governing field equations for species diffusion are described, taking into account the partitioning of the species between the traps and the bulk lattice. Besides cohesive models for fracture growth in the presence of an embrittling species, such as for example that of Serebrinsky et al. [132], the variational formulation derived in this thesis aims at describing fracture growth in the context of LEFM. Minimum theorems give the crack front quasi-static velocity, provided that the dependence of the fracture energy with the concentration of the species can be given. Numerical validations of the proposed model are in progress.

Bibliography

[1] Abraham D.P., Altstetter C.J., *Hydrogen-enhanced localization of plasticity in an austenitic stainless-steel*, Metall. Mater. Trans. A 26: 2859-2871, 1995

[2] Amestoy M., Leblond J.B., *Crack path in plane situations-ii. Detailed form of the expansion of the stress intensity factors*, Int. J. Solids Struct. 29: 465-501, 1992

[3] Anand L., *A thermo-mechanically-coupled theory accounting for hydrogen diffusion and large elastic viscoplastic deformations in metals,* Int. J. Solids Struct. 48: 962-971, 2011

[4] Anand L., *A Cahn-Hilliard-type theory for species diffusion coupled with large elastic-plastic deformations.*, J. Mech. Phys. Solids 60(12): 1983-2002, 2012

[5] Babuška I., Melenk J.M., *The partition of unity method*, Int. J. Num. Meth. Eng. 40(4): 727-758, 1997.

[6] Bank-Sills L., Bortman Y., *Reappraisal of the quarter-point quadrilateral element in linear fracture mechanics*, Int. J. Frac. 25: 169-180, 1984

[7] Bank-Sills L., Einav O., *On singular, nine-noded, distorted, isoparametric elements in linear elastic fracture mechanics*, Computers and Structures 27: 445-449, 1987

[8] Bank-Sills L., *Use of three dimensional finite elements in linear elastic fracture mechanics. Analytical, Numerical and Experimental Aspects of Fracture Processes*, ASME-AMD 91: 89-97, 1988

[9] Bank-Sills L., Sherman D., *On quarter-point three-dimensional finite elements in elastic fracture mechanics*, Int. J. Frac. 41: 177-196, 1989

[10] Bank-Sills L., *Application of the finite element method to linear elastic fracture mechanics*, Appl. Mech. Rev. 44(10): 447-461, 1991

[11] Barsoum R.S., *On the use of isoparametric finite elements in linear elastic fracture mechanics*, Int. J. Num. Meth. Eng. 10: 25-37, 1976

[12] Barsoum R.S., *Triangular quarter-point elements as elastic and perfectly plastic crack tip elements*, Int. J. Num. Meth. Eng. 11: 85-98, 1977

[13] Barenblatt G. I., *On equilibrium cracks forming during brittle fracture (in russian)*, Prikladnaya Matematika i Mekhanika 23: 434-444, 1959

[14] Beacham C.D., *A new model for hydrogen-assisted cracking (hydrogen "embrittlement")*, Metall. Mater. Trans. B 3: 441-455, 1972

[15] Belytschko T., Black T., *Elastic crack growth in finite elements with minimal remeshing*, Int. J. Num. Meth. Eng. 45: 601-620, 1999

[16] Birnbaum C.D., Sofronis P., *Hydrogen-enhanced localized plasticity- a mechanism for hydrogen-related fracture*, Mater. Sci. Eng. A 176: 191-202, 1994

[17] Bourdin B., Francfort G., Marigo J.J., *Numerical experiments in revisited brittle fracture*, J. Mech. Phys. Solids 48(4): 797-826, 2000

[18] Bourdin B., Francfort G., Marigo J.J., *The variational approach to fracture*, Springer, Berlin, 2008

[19] Bower A.F., Ortiz M., *Solution of three-dimensional crack problems by a finite perturbation method*, J. Mech. Phys. Solids 38(4): 443-480, 1990

[20] Budiansky B., Rice J., *Conservation laws and energy release rates*, J. Appl. Mech. 40: 201-203, 1973

[21] Bueckner H.F., *A novel principle for the computation of stress intensity factors*, Zeitschrift fuer Angewandte Mathematik und Mechanik 50: 529-546, 1970

[22] Bui H.D., *Associated path independent J-integral for separating mixed modes*, J. Mech. Phys. Solids 31: 439-448, 1983

[23] Carter B.J., Wawrzynech P.A., Ingraffea A.R., *Automated 3-D crack growth simulation*, Int. J. Num. Meth. Eng. 47: 229-253, 2000

[24] Ceradini G., *Un principio di massimo per il calcolo dei sistemi elasto-plastici*, Rendiconti Istituto Lombardo di Scienze e Lettere A99, 1965

[25] Chambolle A., Francfort G.A., Marigo J.J., *When and how do cracks propagate?*, J. Mech. Phys. Solids 57(9): 1614-1622, 2009

[26] Chambolle A., Francfort G.A., Marigo J.J., *Revisiting energy release rates in brittle fracture*, J. Nonlin. Sci. 20: 395-424, 2010

[27] Chan S.K., Tuba I.S., Wilson W.K., *On the finite element method in linear elastic fracture mechanics*, Eng. Frac. Mech. 2: 1-17, 1970

[28] Chen X. Gerberich W.W., *The kinetics and micromechanics of hydrogen-assisted cracking in Fe_3 pct Si single-crystals*, Metall. Trans. A 22: 59-69, 1991

[29] Citarella R., Soprano A., *Some SIF's evaluations by dual BEM for 3D cracked plates,* J. Achiev. Mater. Manuf. Eng. 19(2): 64-72, 2006

[30] Colonnetti G., *Sul problema delle coazione elastiche*, Rend. Accad. Lincei 5(27): Nota I: 257-270, Nota II: 331-335, 1918

[31] Colonnetti G., *Elastic equilibrium in the presence of permanent set*, Quart. Appl. Math. 7: 353-362, 1950

[32] Davis B., Wawrzynech P.A., Ingraffea A.R., *3-D simulation of arbitrary crack growth using an energy-based formulation- Part I: planar growth*, Eng. Frac. Mech. 115: 204-220, 2014

[33] Davis B., Wawrzynech P.A., Ingraffea A.R., *Simulation of arbitrary mixed-mode crack growth using an energy-based approach*, Conference Proceedings of the Society for Experimental Mechanics Series: 1-9, 2014

[34] De Groot S.R., Mazur P., *Non equilibrium Thermodynamics*, Dover, 1984

[35] Di Leo C., Anand L., *Hydrogen in metals: a coupled theory for species diffusion and large elastic-plastic deformations,* Int. J. of Plasticity 43: 42-69, 2013

[36] Erdogan G., Sih G.C., *On the crack extension in plates under plane loading and transverse shear*, ASME J. Basic Eng. 85: 519-527, 1963

[37] Favier E., Lazarus V., Leblond J.B., *Coplanar propagation paths of 3d cracks in infinite bodies loaded in shear*, Int. J. Solids Struct. 43: 2091-2109, 2006

[38] Ferreira P.J., Robertson I.M., Birnbaum H.K., *Hydrogen effects on the interaction between dislocations*, Acta Mater. 46: 1749-1757, 1998

[39] Francfort G.A., Marigo J.J., *Revisiting brittle fracture as an energy minimization problem*, J. Mech. Phys. Solids 46: 1319-1342, 1998

[40] Freese C.E., Tracey D.M., *The natural isoparametric triangle versus collapsed quadrilateral for elastic crack analysis*, Int. J. Frac. 12: 767-770, 1976

[41] Gangloff R.P., *Hydrogen assisted cracking of high strength alloys*, Comprehensive Structural Integrity 6: 31-101, 2003

[42] Gao H., Cao W., Fang C., and E.R. de los Rios, *Analysis of crack tip hydrogen distribution under I/II mixed mode loads*, Fatigue and Frac. of Eng. Materials and Struct. 17(10): 1213-1220, 1994

[43] Gao H., Rice J.R., *Shear stress intensity factors for a planar crack with slightly curved fronts,* ASME J. Appl. Mech. 53: 774-778, 1986

[44] Gao H., Rice J.R., *Somewhat circular tensile cracks,* Int. J. Frac. 33: 155-174, 1987

[45] Gao H., Rice J.R., *Nearly circular connections of elastic half spaces,* ASME J. Appl. Mech. 54: 627-634, 1987

[46] Gerberich W.W., Oriani R.A., Lii M.J., Chen X., Foeche T., *The necessity of both plasticity and brittleness in the fracture threshold of iron*, Phil. Mag. A 63: 363-376, 1991

[47] Goldstein R.V., Salganik R.L., *Brittle fracture of solids with arbitrary cracks*, Int. J. Frac. 10: 507-523, 1974

[48] Gravouil A., Moës N., Belytschko T., *Non-planar 3D crack growth by the extended finite element and level sets– Part II: level set update*, Int. J. Num. Meth. Eng. 53: 2569-2586, 2002

[49] Griffith A.A., *The phenomena of rupture and flow in solids*, Philos. Trans. R. Soc. 221: 163-198, 1921

[50] Gurtin M.E., Fried E., Anand L, *The Mechanics and Thermodynamics of Continua*, Cambridge University Press, 2010

[51] Haftbaradaran H., Qu J., *A path-independent integral for fracture of solids under combined electrochemical and mechanical loadings*, J. Mech. Phys. Solids 71: 1-14, 2014

[52] Hakim V., Karma A., *Crack path in anisotropic brittle materials*, Phys. Rev. Lett. 95: 235501, 2005

[53] Han W., Reddy B.D., *Plasticity*, Springer, New York, 1999

[54] Hartranft R.J., Sih G.C., *The use of eigenfunction expansions in the general solution of three dimensional crack problems*, J. Math. Mech. 19: 123-138, 1969

[55] Hellen K.T., *On the method of virtual crack extension*, Int. J. Num. Meth. Eng. 9: 187-207, 1975

[56] Henshell R.D., Shaw K.G., *Crack tip finite elements are unnecessary*, Int. J. Num. Meth. Eng. 9: 495-507, 1975

[57] Hibbitt H.D., *Some properties of singular isoparametric elements*, Int. J. Num. Meth. Eng. 11: 180-184, 1987

[58] Hussain M.A., Coffin L.F., Zaleski K.A., *Three-dimensional singular elements*, Computers and Structures 13: 595-599, 1981

[59] Hwang C.G., Wawrzynek P.A., Ingraffea A.R., *On the virtual crack extension method for calculating the derivatives of the energy release rates for a 3D planar crack of arbitrary shape under mode-I loading*, Eng. Frac. Mech. 68: 925-947, 2001

[60] Ichikawa M., Tanaka S., *A critical analysis of the relationship between the energy release rate and the SIFs for noncoplanar crack extension under combined mode loading*, Int. J. Frac. 18: 19-28, 1982

[61] Ingraffea A.R., Manu C., *Stress-Intensity factor computations in three dimensions*, Int. J. Num. Meth. Eng. 15: 1427-1445, 1980

[62] Irwin G., *S. Fluegge (Ed.), Handbuch der Physik, Bd. 6. Elastizitaet und Plastizitaet*, Springer Verlag: 551-590, 1958

[63] Ishikawa H., *A finite element analysis of stress intensity factors for combined tensile and shear loading by only a virtual crack extension*, Int. J. Frac. 16: 243-246, 1980

[64] Jiang D.E., Carter E.A., *First principles assessment of ideal fracture energies of materials with mobile impurities: implications for hydrogen embrittlement of metals*, Acta Mater. 52: 4801-4807, 2004

[65] Kassir M.K., Sih G.C., *Three-dimensional crack problems*, Mechanics of fracture, vol. 2, Noordhoff Int. Publ., Leyden, 1975

[66] Karihaloo B.L., Xiao Q.Z., *Accurate determination of the coefficients of elastic crack tip asymptotic field by a hybrid crack element with p-adaptivity*, Eng. Frac. Mech. 68(15): 1609-1630, 2001

[67] Khoei A.R., Moslemi H., Sharifi M., *Three-dimensional cohesive fracture modeling on non-planar crack growth using adaptative FE technique*, Int. J. Solids Struct. 49: 2334-2348, 2012

[68] Koers R.W.J., *Use of modified standard 20-node isoparametric brick elements for representing stress/strain fields at a crack tip for elastic and perfectly plastic material*, Int. J. Frac. 40: 79-110, 1989

[69] Krom A.H.M., Koers R.W.J., Bakker A., *Hydrogen transport near a blunting crack tip*, J. Mech. Phys. Solids 47: 971-992, 1999

[70] Krom A.H.M., Bakker A., *Hydrogen trapping models in steel*, Metall. and Mat. Trans. B 31: 1475-1482, 2000

[71] Kumnick A.J., Johnson H.H., *Deep trapping states for hydrogen in deformed iron* , Acta Metall. 28: 33-39, 1980

[72] Larche F., Cahn J.W., *Linear theory of thermochemical equilibrium of solids under stress*, Acta Metall. 21(8): 1051-1063, 1973

[73] Larche F., Cahn J.W., *Non linear theory of thermochemical equilibrium of solids under stress*, Acta Metall. 26: 53-60, 1978

[74] Lazarus V., Leblond J.B., Mouchrif S.E., *Crack front rotation and segmentation in mixed mode I + III or I + II + III. Part I: Calculation of stress intensity factors*, J. Mech. Phys. Solids 49: 1399-1420, 2001

[75] Lazarus V., Leblond J.B., Mouchrif S.E., *Crack front rotation and segmentation in mixed mode I + III or I + II + III. Part II: Comparison with experiments*, J. Mech. Phys. Solids 49: 1421-1443, 2001

[76] Lazarus V., Leblond J.B., *In-plane perturbation of the tunnel crack under shear loading I: Bifurcation and stability of the straight configuration of the front*, Int. J. Solids Struct. 39: 4421-4436, 2002

[77] Lazarus V., Leblond J.B., *In-plane perturbation of the tunnel crack under shear loading II: Determination of the fundamental kernel*, Int. J. Solids Struct. 39: 4437-4455, 2002

[78] Lazarus V., *Brittle fracture and fatigue propagation paths of 3d plane cracks under uniform tensile loading*, Int. J. Frac. 122 (1-2): 23-46, 2003

[79] Lazarus V., *Perturbation approaches of a planar crack in linear elastic fracture mechanics*, J. Mech. Phys. Solids 59: 121-144, 2011

[80] Leblond J.B., *Crack paths in plane situations - i. general form of the expression of the stress intensity factors*, Int. J. Solids Struct. 25: 1311-1325, 1989

[81] Leblond J.B., Mouchrif S.E., *The tensile tunnel-crack with a slightly wavy front*, Int. J. Solids Struct. 33: 1995-2022, 1995

[82] Leblond J.B., *Crack paths in three dimensional elastic solids I. Two term expansion of the stress intensity factors. Application to crack path stability in hydraulic fracturing,* Int. J. Solids Struct. 36: 79-103, 1999

[83] Leblond J.B., Lazarus V., Mouchrif S., *Crack paths in three dimensional elastic solids II. Three term expansion of the stress intensity factors – applications and perspectives*, Int. J. Solids Struct. 36: 105-142, 1999

[84] Leblond J.B., Karma A., Lazarus V., *Theoretical analysis of crack front instability in mode I+III*, J. Mech. Phys. Solids 59: 1872-1887, 2011

[85] Leblond J.B., Patinet S., Frelat J., Lazarus V., *Second-order coplanar perturbation of a semi-infinite crack in an infinite body*, Eng. Frac. Mech. 90: 129-142, 2012

[86] Leblond J.B., Lazarus V., *On the strong influence of imperfections upon the quick deviation of a mode I+III crack from coplanarity*, J. Mech. Mat. Struct. 10: 299-316, 2015

[87] Lemaitre J., Chaboche J.L., *Mechanics of solid materials*, Cambridge University Press, Cambridge, 2000

[88] Li F.Z., Shih C.F., Needleman A., *A comparison of methods for calculating energy release rates*, Eng. Frac. Mech. 21: 405-421, 1985

[89] Lin S.C., Abel J.F., *Variational approach for a new direct-integration form of the virtual crack extension method*, Int. J. Frac. 38: 217-235, 1988

[90] Manu C., *Quarter-point elements for curved crack fronts*, Computers and Structures 17: 227-231, 1983

[91] Manu C., *Complete quadratic isoparametric finite elements in fracture mechanics analysis*, Int. J. Num. Meth. Eng. 21: 1547-1553, 1985

[92] Martha L.F., Wawrzynech P.A., Ingraffea A.R., *Arbitrary crack representation using solid modeling*, Eng. Comput. 9: 63-82, 1993

[93] Miehe C., Welschinger F., Hofacker M., *Thermodynamically consistent phase-field models of fractures: variational principles and multi-field FE implementations*, Int. J. Num. Meth. Eng. 83: 1273-1311, 2010

[94] Miehe C., Hofacker M., Welschinger F., *A phase field model for rate-independent crack propagation: robust algorithmic implementation based on operator splits*, Comp. Meth. Appl. Mech. Eng. 199: 2765-2778, 2010

[95] Miehe C., Dal H., Raina A., *A phase-field model for chemo-mechanical induced fracture in lithium-ion battery electrode particles*, Int. J. Num. Meth. Eng., DOI 10.1002, 2015

[96] Mielke A., *Evolution in rate-independent systems.* In: Dafermos C., Feireisl E. (eds) Handbook of differential equations, vol. 2, Elsevier, Amsterdam: 461-559, 2005

[97] Moës N., Dolbow J., Belytschko T., *A finite element method for crack growth without remeshing*, Int. J. Num. Meth. Eng. 46: 131-150, 1999

[98] Moës N., Gravouil A., Belytschko T., *Non-planar 3D crack growth by the extended finite element method and level sets- Part I: Mechanical model*, Int. J. Num. Meth. Eng. 53: 2549-2568, 2002

[99] Moran B., Shih C.F., *A general treatment of crack tip contour integrals*, Int. J. Frac. 35: 295-310, 1987

[100] Morini L., Piccolroaz A., *Boundary integral formulation for interfacial cracks in thermodiffusive bimaterials*, Proc. R. Soc. A 373: 20150284

[101] Movchan A.B., Gao H., Willis J.R., *On perturbations of plane cracks*, Int. J. Solids Struct. 35: 3419-3453, 1998

[102] Nguyen Q.S., *Bifurcation and stability in dissipative media (plasticity, friction, fracture)*, Appl. Mech. Rev. 41(1): 1-30, 1994

[103] Nguyen Q.S., *Stability and nonlinear solid mechanics*, Wiley, New York, 2000

[104] Nikishkov G.P., Atluri S.N., *Calculation of fracture mechanics parameters for any arbitrary three-dimensional crack, by the "equivalent domain integral" method*, Int. J. Num. Meth. Eng. 24: 1801-1827, 1987

[105] Obrezanova O., Movchan A.B., Willis J.R., *Stability of an advancing crack to small perturbation of its path*, J. Mech. Phys. Solids 50: 57-80, 2000

[106] Oriani R.A., *The diffusion and trapping of hydrogen in steel*, Acta Metall. 18(1): 147-157, 1970

[107] Oriani R.A., *A mechanistic theory of hydrogen embrittlement of steels*, Ber. Bunsenges. Phys. Chem. 76: 848-857, 1972

[108] Ortiz M., Pandolfi A., *Finite-deformation irreversible cohesive elements for three- dimensional crack-propagation analysis*, Int. J. Num. Meth. Eng. 44: 1267-1282, 1999

[109] Otsuka A., Mori K., Miyata T., *The condition of fatigue crack growth in mixed mode condition*, Eng. Frac. Mech. 7: 429-439, 1975

[110] Parks D.M., *Stiffness derivative finite element technique for determination of crack-tip stress intensity factors*, Int. J. Frac. 10: 487-502, 1974

[111] Ramamurthy T.S., Krishnamurthy T., Narayana B., Vijayakumar K., Dattaguru B., *Modified crack closure integral method with quarter point elements*, Mech. research Communications 13: 179-186, 1986

[112] Raju I.S., *Calculation of strain-energy release rate with high order and singular finite elements*, Eng. Frac. Mech. 28: 251-274, 1987

[113] Rybicki E.R., Kanninen M.F., *A finite element calculation of stress intensity factors by a modified crack closure integral*, Eng. Frac. Mech. 9: 931-938, 1977

[114] Rice J.R., *A path independent integral and approximate analysis of strain concentration by notches and cracks*, J. Appl. Mech. 32(2): 379-386, 1968

[115] Rice J.R., *Thermodynamics of the quasi-static growth of Griffith cracks*, J. Mech. Phys. Solids, 26: 61-78, 1978

[116] Rice J.R., *First order variation in elastic fields due to variation in location of a planar crack front*, J. Appl. Mech., 52: 571-579, 1985

[117] Rice J.R., *Weight function theory for three-dimensional elastic crack analysis*, in: R.P. Wei, R.P. Gangloff (Eds.), Fracture mechanics: perspectives and directions (20th symposium) vol. 2, ASTM STP 1020, American Society for Testing and Materials, Philadelphia: 29-57, 1989

[118] Riks E., *An incremental approach to the solution of snapping and buckling problems*, Int. J. Solids Struct. 15: 529-551, 1979

[119] Robertson I.M., *The effect of hydrogen on dislocation dynamics,* Eng. Frac. Mech. 68: 671-692, 2001

[120] Salvadori A., *Analytical integrations of hypersingular kernel in 3D BEM problems*, Comput. Methods Appl. Mech. Eng. 190: 3957-3975, 2001

[121] Salvadori A., *Hypersingular boundary integral equations and the approximation of the stress tensor*, Int. J. Numer. Meth. Eng. 72: 722-743, 2007

[122] Salvadori A., *A plasticity framework for (linear elastic) fracture mechanics*, J. Mech. Phys. Solids 56: 2092-2116, 2008

[123] Salvadori A., *Analytical integrations in 3d bem for elliptic problems: evaluation and implementation.*, Int. J. Numer. Meth. Eng. 84: 505-542, 2010

[124] Salvadori A., *Crack kinking in brittle materials*, J. Mech. Phys. Solids 58: 1835-1846, 2010

[125] Salvadori A., Carini A., *Minimum theorems in incremental linear elastic fracture mechanics*, Int. J. Solids Struct. 48: 1362-1369, 2011

[126] Salvadori A., Giacomini A., *The most dangerous flaw orientation in brittle materials and structures*, Int. J. Frac. 183(1): 19-28, 2013

[127] Salvadori A., Fantoni F., *Minimum theorems in 3D incremental linear elastic fracture mechanics* Int J Fract, 184 (1): 57-74,2013

[128] Salvadori A., Fantoni F., *On a 3D crack tracking algorithm and its variational nature*, J. of the European Ceramic Society 34: 2807-2821, 2014

[129] Salvadori A., Fantoni F., *Weight function theory and variational formulations for three dimensional plane elastic crack advancing*, Int. J. Solids Struc. 51(5): 1030-1045, 2014

[130] Salvadori A., Fantoni F., *Fracture propagation in brittle materials as a standard dissipative process: general theorems and crack tracking algorithms*, submitted

[131] Salvadori A., McMeeking R., Grazioli D., Magri M., *A coupled model of transport-reaction-mechanics with application to metal embrittlement by diffusion of species*, unpublished

[132] Serebrinsky S., Carter E.A., Ortiz M., *A quantum-mechanically informed continuum model of hydrogen embrittlement*, J. Mech. Phys. Solids 52: 2403-2430, 2004

[133] Silvester P.P., *Higher order polynomial triangular finite elements for potential problems*, Int. J. Eng. Sci. 7(8): 849-861, 1969

[134] Song J., Soare M., Curtin W.A., *Testing continuum concepts for hydrogen embrittlement in metals using atomistics*, Modelling Simul. Mater. Sci. Eng. 18: 1-16, 2010

[135] Song J., Curtin W.A., *Atomic mechanism and prediction of hydrogen embrittlement in iron*, Nature Materials 12: 145-151, 2013

[136] Sofronis P., McMeeking R.M., *Numerical analysis of hydrogen transport near a blunting crack tip*, J. Mech. Phys. Solids 37: 317-350, 1989

[137] Sofronis P., Robertson I.M., *Transmission electron microscopy observations and micromechanical/continuum models for the effect of hydrogen on the mechanical behavior of metals*, Phil. Mag. A 82: 3405-3413, 2002

[138] Shih C.F., Asaro R., *Elastic-plastic analysis of cracks on bimaterial interfaces; Part I: small scale yielding*, J. Appl. Mech. 55: 299-316, 1988

[139] Sih G.C., *Strain-energy-density factor applied to mixed-mode crack problems*, Int. J. Frac. 10: 305-321, 1973

[140] Sih G.C., Liebowitz H., *Mathematical theories of brittle fracture. In: Liebowitz H. (Ed.)*, Fracture, vol. 2, Academic Press, New York: 67-190, 1968

[141] Strifors H.C., *A generalized force measure of conditions at crack tips*, Int. J. Solids Struct. 10: 1389-1404, 1973

[142] Sun S., Shiozawa J., Gu J., Chen N., *Investigation of deformation field and hydrogen partition around crack tip in fcc single crystal*, Metall. Maters. Tran. A 26: 731-739, 1995

[143] Tadmor E.B., Miller E.R., Elliot R.S., *Continuum Mechanics and Thermodynamics: from fundamental concepts to governing equations*, Cambridge University Press, Cambridge, 2012

[144] Tonti E., *Variational formulation for every nonlinear problem*, Int. J. Eng. Sci. 22: 1343-1371, 1984

[145] Troiano A.R., *The role of hydrogen and other interstitials in the mechanical behavior of metals*, Trans. ASM 52: 54-80, 1970

[146] Villani A., Busso E.P., Ammar K., Forest S., Geers M.G.D., *A fully coupled diffusional-mechanical formulation: numerical implementation, analytical validation, and effects of plasticity on equilibrium*, Archive of Appl. Mech. 84: 1647-1664, 1999

[147] Walters M.C., Paulino G.H., Dodds Jr.R.H., *Interaction integral procedures for 3-D curved cracks including surface tractions*, Eng. Frac. Mech. 72: 1635-1663, 2005

[148] Wang J.S., *The thermodynamics aspects of hydrogen induced embrittlement*, Eng. Frac. Mech. 68: 647-669, 2001

[149] Westlake D.G., *A generalized model for hydrogen embrittlement*, Trans. ASM 62: 1000-1006, 1969

[150] Williams M.L., *On the stress distribution at the base of a stationary crack*, ASME J. Appl. Mech 24 : 109-114, 1957

[151] Willis J.R., *Asymptotic analysis in fracture: an update*, Int. J. Frac. 100: 85-103, 1999

[152] Willis J.R., *Crack front perturbations revisited*, Int. J. Frac. 184: 17-24, 2013

[153] Wriggers P., *Computational Contact Mechanics*, Wiley 2002

[154] Wu C.W., *Maximum-energy release rate criterion applied to a tension-compression specimen with crack*, J. Elasticity 8: 235-257, 1978

[155] Yau J.F., Wang S.S., Corten H.T., *A Mixed-Mode Crack Analysis of Isotropic Solids Using Conservation Laws of Elasticity*, J. Appl. Mech. 47(2): 335-341, 1980

[156] Ying L.A., *A note on the singularity and the strain energy of singular elements*, Int. J. Num. Meth. Eng. 18: 31-39, 1982